

Glacier dynamics in the fjords of Svalbard, inferred from submarine landforms and marine sediment cores

Anne Elina Flink



Thesis for the degree of philosophiae doctor (PhD)
at the University of Bergen

2017

Date of defence: 17-09-19

© Copyright

The material in this publication is protected by copyright law.

Year: 2017

Title: Glacier dynamics in Svalbard fjords, inferred from submarine landforms and marine sediment cores

Author: Anne Elina Flink

Print: AiT Bjerch AS / University of Bergen

Scientific environment



Main supervisor:

Dr. Riko Noormets (The University Centre in Svalbard, Longyearbyen)

Co-supervisor:

Prof. Hafliði Hafliðason (University of Bergen, Bergen)

Acknowledgements

I would like to extend my deepest gratitude to my supervisor Dr. Riko Noormets, without whom this project would not have been possible. Thank you so much for offering me the opportunity to embark on this PhD and for guidance and encouragement during these four years. My deepest thanks to my UNIS officemate and co-worker Oscar Fransner, together with whom I shared hours of field- and labwork. Great thanks to my co-supervisor Prof. Haflidi Haflidason. I am highly indebted to all my colleagues and co-authors, who have contributed with data, discussion and valuable input during this PhD project. I would like to acknowledge the co-authors of my first paper; Prof. Doug Benn, Dr. Harold Lovell and Prof. Adrian Luckman. A special thanks to Dr. Nina Kirchner, not only for her input into the paper, but also for supervision during my Master's thesis. I would like to thank the co-authors of my second paper; Prof. Martin Jakobsson, Dr. Matt O'Regan and Dr. Kelly Hogan. Special thanks to Kelly for introducing me to sediment core logging during the first cruises on Helmer Hanssen. I would also like to acknowledge the staff at the Department of Geology at Stockholm University for their help with laboratory work.

My sincere thanks to all my colleagues and friends at UNIS. I would like to thank Peter Hill, without whom much of the fieldwork would not have been possible. Thank you for awesome field days and brilliant ski trips. I would like to thank Dr. Martin Liira for helping out with the fieldwork and for great discussions. Thanks a lot to Dr. Srikumar Roy and Dr. Teena Chauhan for introducing me to marine geological work at UNIS. Great thanks to all my UNIS geology colleagues, Mark Mulrooney, Hanna-Rosa Hjalmarsson, Dr. Lena Håkansson, Dr. Heidi Sevestre, Alexandra Sikora and many more. Special thanks to my UNIS geo-friends Nina Friis, Dani Röhnert, Andrea Schneider and Richard Hann for the time they spend in the field and for all the scientific discussions on our numerous skiing and kayaking trips. Sincere thanks to Dorothée Vallot and Penny Howe for taking me out on glaciological fieldwork. I would also like to extend my gratitude to all my other friends whom I have met at

UNIS and with whom I have had the pleasure to discover Svalbard, especially Dorota Medrzycka, Niels Weiss, Snowy Haibler, Luise Eichorn, Zoe Burr and Renee Rookus.

Great thanks to all bachelor and master students who came knocking on my door and whom I had the pleasure to meet and teach during these four years. I sincerely thank all my friend and colleagues in the FROZEN and GLANAM networks. Special thanks to Katharina Streuff who joined us for fieldwork in northern Spitsbergen. Finally, I would like to thank my boyfriend Samuel Gauvain, not only for years of patient encouragements, but also for eager help with a multitude of Excel, ArcGIS and programming crisis. You provided diversion from the PhD work during the holidays. Thank you for climbing all the peaks and skiing all the slopes with me.

Live long and prosper

Preface

This thesis is an outcome of a four-year PhD study carried out between 2013-2017 at the Department of Arctic Geology, the University Centre in Svalbard (UNIS) in Longyearbyen. The thesis was undertaken in association with the Department of Earth Sciences, University of Bergen and was financed by the University Centre in Svalbard. Fieldwork in 2015 and 2016 was financed by the Research council of Norway, through the Arctic Field Grant.

One year of the PhD study was assigned to duty work including teaching, outreach and assistance during fieldwork. The candidate participated annually as a teaching assistant in the bachelor's level course AG-211 (Arctic Marine Geology), where she assisted with fieldwork, supervision of sediment core logging, lecturing, teaching sea floor mapping ArcGIS and Fledermaus computer exercises as well as supervising the students' laboratory work and term projects. In 2015 the candidate was a teaching assistant in the Masters and PhD level courses AG-339/839 (Reconstruction of glacial marine sedimentary processes and environments on high-latitude continental margins), where she participated in the cruise, assisted in supervising the students' course projects, was responsible for the terrestrial field-work component and the ArcGIS and Fledermaus computer labs. In 2016, the candidate was a teaching assistant in the Masters and PhD level course AG-348/348 (Late Quaternary Glacial and Marine Environmental History). She participated in the fieldwork and assisted in supervising the marine geology module of the course. The candidate participated in fieldwork with the AG-342/842 (The Marine Cryosphere and its Cenozoic History) course in 2014 and 2016. Besides teaching, the duty work included outreach, assisting UNIS colleagues with fieldwork and assisting in supervision of a UNIS Master student.

The various high-resolution multibeam-bathymetric and sub-bottom data sets used in this PhD thesis have been obtained from different sources. Multibeam data presented in papers I and VI was provided by the Norwegian Hydrographic Service. Geophysical data presented in paper II was partly provided by the Norwegian Hydrographic Service

as well as acquired during a scientific cruise with the R/V Helmer Hanssen in 2012, in which the candidate participated during her master studies. Sediment cores presented in paper II were recovered during the 2012 cruise. Multibeam-data presented in paper III was acquired during a 2013 cruise on the R/V Viking Explorer and the sediment cores were recovered during a winter field-excursion in 2015. Multibeam-data presented in paper IV was provided by the Norwegian Hydrographic Service, while sub-bottom data and sediment cores were obtained during a cruise on R/V Helmer Hanssen in 2016. The geophysical and sedimentological data presented in paper V were recovered on a UNIS cruise in 2011 and 2012.

Altogether, the candidate participated in four cruises with the R/V Viking Explorer, four cruises with the R/V Helmer Hanssen and organised two spring field-excursions to the east coast of Spitsbergen. In 2013, the candidate participated in a two-week cruise to the east coast of Spitsbergen, a one-week cruise to Nordaustlandet with the AG-211 course and a one-week cruise to northern Svalbard with the AG-339/839 course. In 2014 she took part in a week-long cruise to northern Nordaustlandet with AG-211. In 2015 she organised a week-long spring field-excursion to the east coast of Spitsbergen, participated in a five-day field excursion to Billefjorden and a week-long cruise on Isfjorden with the AG-339/839 course. In 2016 the candidate participated in a one-week cruise to the Seven Islands with the AG-342/842 course and a one-week cruise to northern Svalbard with AG-211. She executed a three-day field campaign to Mohnbukta, where an additional sediment core was acquired. Laboratory work was mostly performed at the University Centre in Svalbard, although parts of the laboratory analyses, in particular those presented in papers II and V, were conducted at the Department of Geological Sciences at the Stockholm University.

During her PhD studies, the candidate was associated with the EU Marie Curie Initial Training Network GLANAM (Glaciated North Atlantic Margins) and participated in its workshops and field courses. The candidate was further associated with the FROZEN project (Frozen landscapes in transition: improving predictions of ice sheet stability in a warming world by numerical modelling) at Stockholm University and

participated in its workshops. The candidate participated in several international conferences and the results of this thesis have been presented on the annual PAST Gateways (Paleo-Arctic Spatial and Temporal Gateways) conferences in 2014-2016. Besides scientific papers, this thesis includes a short contribution to the Atlas of Submarine landforms: Modern, Quaternary and Ancient (Flink *et al.* 2016). The results from paper I have also been published in a popular scientific article in Geoforskning.no. The PhD candidate has contributed to two additional papers as a co-author (Lovell *et al.* 2015 and Fransner *et al.* in prep) and to three short contributions in the Atlas of Submarine landforms: Modern, Quaternary and Ancient (Noormets *et al.* 2016a; Noormets *et al.* 2016b; Fransner *et al.* 2016). This doctoral thesis is a synopsis of five research papers and one contribution to the Atlas of Submarine landforms, focusing on the glacial evolution and history of Svalbard fjords.

Abstract

This thesis presents a reconstruction of the late Weichselian, deglacial and Holocene glacial history of the Svalbard fjords, focusing on eastern Svalbard. The study is based on high-resolution multibeam data, shallow acoustic (chirp) data, marine sediment cores, historical maps and aerial- satellite images. During the Last Glacial Maximum the Svalbard Barents Sea ice sheet reached the shelf edge around Svalbard and was drained by large ice streams along its western and northern margins, located in the same areas as the present day cross-shelf troughs. In northeastern Svalbard, fast-flowing ice converged into the Hinlopen Strait ice stream from the surrounding fjords. Submarine landforms indicate that ice flow velocities increased as ice flowed from the inner- to the outer fjords and the shelf. The deglaciation from the northeastern shelf edge proceeded rapidly by ice lift-off in the troughs and deeper parts of the fjords, whereas the shallower areas experienced slower retreat with minor re-advances. The inner fjords around Nordaustlandet were ice free prior to 11.3-10.5 ka BP years.

During early- to mid-Holocene tidewater glaciers in Mohnbukta and Vaigattbogen experienced at least one surge-type advance. These pre-Little Ice Age surges differentiate the east coast glaciers from the west coast glaciers. The early Holocene advance in Mohnbukta has been attributed to rapid climatic and environmental change at the end of the deglaciation, leading to dynamic disequilibrium and an environmentally induced jump into surge-mode. This suggests a more dynamic Holocene glacial history in Svalbard than previously stated, also indicating that the role of climate is more important in the evolution of general surge patterns than previously presumed. Similarly, climatic and environmental changes at the end of the Little Ice Age could explain why many Svalbard glaciers, both on the west and east coasts surged in that time period.

Today, the majority of Svalbard's fjords accommodate tidewater glaciers, of which several have been recorded to surge. Commonly the glaciers have surged at least twice during the Holocene. The surging tidewater glacier landform assemblages share many

similarities and can be used to identify past surges in the geological record. In this study the submarine morphology has been used to identify three new surge-type glaciers in Wahlenbergfjorden. The surge history of the Svalbard glaciers is diverse and even though the landform assemblages share many similarities, they all feature differences, suggesting that local conditions are important in the evolution of glacial surges.

List of publications

Paper I:

Flink, A. E., Noormets, R., Kirchner, N., Benn, D. I., Luckman, A., & Lovell, H. (2015): The evolution of a submarine landform record following recent and multiple surges of Tunabreen glacier, Svalbard. *Quaternary Science Reviews*. Vol. 108: 37-50

Paper II:

Flink, A. E., Noormets, R., Fransner, O., Hogan, A. K., Ó Regan, M., & Jakobsson, M. (2017): Past ice flow in Wahlenbergfjorden and its implications for late Quaternary ice sheet dynamics in northeastern Svalbard. *Quaternary Science Reviews*. Vol. 163: 162-179

Paper III:

Flink, A. E., Hill, P., Noormets, R., & Kirchner, N. (In prep): Glacial evolution of Mohnbukta fjord in eastern Spitsbergen inferred from submarine landform and sediment core records. *Boreas*. Submitted

Paper IV:

Flink, A. E., & Noormets, R. (In prep): The glacial history of Vaigattbogen, eastern Spitsbergen. *Marine Geology*. Submitted

Paper V:

Fransner, O., Noormets, R., Flink, A., Hogan, K., O'Regan, M., Jakobsson, M. (2017): Glacial landforms and their implications for glacier dynamics in Rijpfjorden and Duvefjorden, northern Nordaustlandet, Svalbard. *Journal of Quaternary Science*. Vol. 32(3): 437-455

Paper VI:

Flink, A. E., Noormets, R., & Kirchner, N. (2016): Annual moraine ridges in Tempelfjorden, Spitsbergen. In: Atlas of Submarine glacial landforms: Modern, Quaternary and Ancient. *Geological Society, London, Memoirs*. (46): 75-76

Reprints were made with permission from [Elsevier, Wiley and the Geological Society, London]. All rights reserved.

Contents

1. Introduction

- 1.1. Outline
- 1.2. Regional background and bedrock geology
- 1.3. Glaciological background
 - 1.3.1. A brief summary of the glacial history of Svalbard
 - 1.3.2. Present day glaciers in Svalbard
 - 1.3.3. Surge-type glaciers in Svalbard

2. Motivation

3. Aims and objectives

4. Methods

- 4.4. Geophysical methods
- 4.5. Sedimentological methods

5. Summary of papers

- 5.1. Paper I
- 5.2. Paper II
- 5.3. Paper III
- 5.4. Paper IV
- 5.5. Paper V
- 5.6. Paper VI

6. Synthesis

- 6.1. The LGM and the deglaciation in north eastern Svalbard
- 6.2. Early to mid-Holocene pre-LIA glacier surges in eastern Svalbard
- 6.3. Late Holocene surge activity in Svalbard
- 6.4. Conclusions

7. Future perspectives

Source of data

Research papers I, II, III, IV, V and VI

Glacier dynamics in Svalbard fjords, inferred from submarine landforms and marine sediment cores

1. Introduction

1.1 Outline

Marine ice margins, such as ice shelves, floating ice tongues and tidewater glacier are considered to be one of the largest uncertainties in global climate predictions (IPCC 2014). Their future behavior plays an increasingly important role in a world subjected to global climate change and in particular to sea level rise. Ice sheets and ice caps lose mass mainly by calving along their marine margins and are thus sensitive to changes in climatic and oceanic conditions at their margins (Kleman & Applegate 2014). Marine ice margins act as a buffer for the inland ice, exerting back stress and preventing fast flow and rapid mass wasting (Joughin *et al.* 2014). Therefore, rapid retreat at the marine margins can contribute to greater mass wasting, increased ice flow and enhanced sea level rise (Joughin & Alley 2011; Drews 2015). To understand the connection between climate, sea level rise, oceanographic processes and large-scale ice dynamics it is vital to understand the dynamics of floating ice tongues, ice shelves and tidewater glaciers.

The representation of marine ice-marginal processes in contemporary numerical models is still considered one of the main uncertainties in climate predictions (Kirchner *et al.* 2011; Applegate *et al.* 2012). The beds of contemporary ice sheets are difficult to access and few direct observations of glaciological and sedimentological processes exist from the subglacial environment. Paleo ice sheets can however be used as analogues to modern ice sheets and modern subglacial processes can be better understood by studying the geological and geomorphological records of paleo ice sheets and past glaciers (Jakobsson *et al.* 2011). These geological and geomorphological data are valuable for validating the performance of numerical models (Kirchner *et al.* 2011, 2016; Patton *et al.* 2015). Furthermore, temperature

increase is particularly pronounced in the Arctic (IPCC 2014) and to reliably project future changes, an understanding of past climate variability is imperative.

Surging tidewater glaciers display a characteristic landform assemblage, with lineations indicating fast flow during the active phase (Ottesen *et al.* 2008; Flink *et al.* 2015). Lineations have also been studied at the margins of the Greenland and Antarctic ice sheets as well as at the margins of paleo ice sheets, and been attributed to ice streaming (Ó Cofaigh *et al.* 2002; Andreassen & Winsborrow 2009; Jakobsson *et al.* 2011; Dowdeswell *et al.* 2014). Ice streams are an important dynamical component of the ice sheet and played an important role in the extension of paleo ice sheets (Boulton *et al.* 1977; Andreassen *et al.* 2014). The similarities between the geomorphological records of surging tidewater glaciers and ice streams suggest that they share dynamical similarities. Relatively easily accessible tidewater glacier in Svalbard can thus act as analogues to larger marine terminating glaciers and ice streams. The seafloor in front of Svalbard tidewater glaciers provides an excellent and accessible platform for studying processes at the marine margins. Furthermore, glacial landforms on the seafloor have not been subjected to subaerial processes such as erosion, periglacial activity and weathering, resulting in generally well-preserved morphology (Ottesen & Dowdeswell 2006; Ottesen *et al.* 2008).

1.2 Regional background and bedrock geology

The Svalbard archipelago is located between 74°-81° northern latitude and 10°-35° eastern longitude (Fig. 1a). It consists of a group of islands of which Spitsbergen is the largest, followed by Nordaustlandet and Edgeøya. The west coast of Spitsbergen is indented by several large multi-branched fjord systems, whereas the fjords and bays on the east coast are generally smaller (Fig. 1b). Nordaustlandet, which is separated from Spitsbergen by the Hinlopen Strait, has seven large fjords, such as Wahlenberg-, Ripp- and Duvefjorden (Fig. 2a). Svalbard has a long and diverse geological history, resulting in complex bedrock geology, ranging from, Tertiary rocks to more than 410 million years old basement rocks. The bedrock types range from erosion-resistant metamorphic and crystalline rocks to igneous intrusions and soft sedimentary rocks

(Dallmann *et al.* 2002). Metamorphic and igneous basement rocks are mainly found in northwestern Spitsbergen and Nordaustlandet, while central Spitsbergen is characterized by sedimentary strata. The bedrock is covered by unconsolidated Quaternary deposits, predominantly of glacial origin (Dallmann *et al.* 2002). Contemporary geological processes affecting the islands are dominated by the presence of glaciers and permafrost (Humlum *et al.* 2003). The northern part of the Barents Sea Shelf in eastern Svalbard comprises of Precambrian crystalline rocks from the Hecla Hoek formation, while the southern part is dominated by Mesozoic cherts and sandstones (Hogan *et al.* 2010a; Hogan *et al.* 2010b).

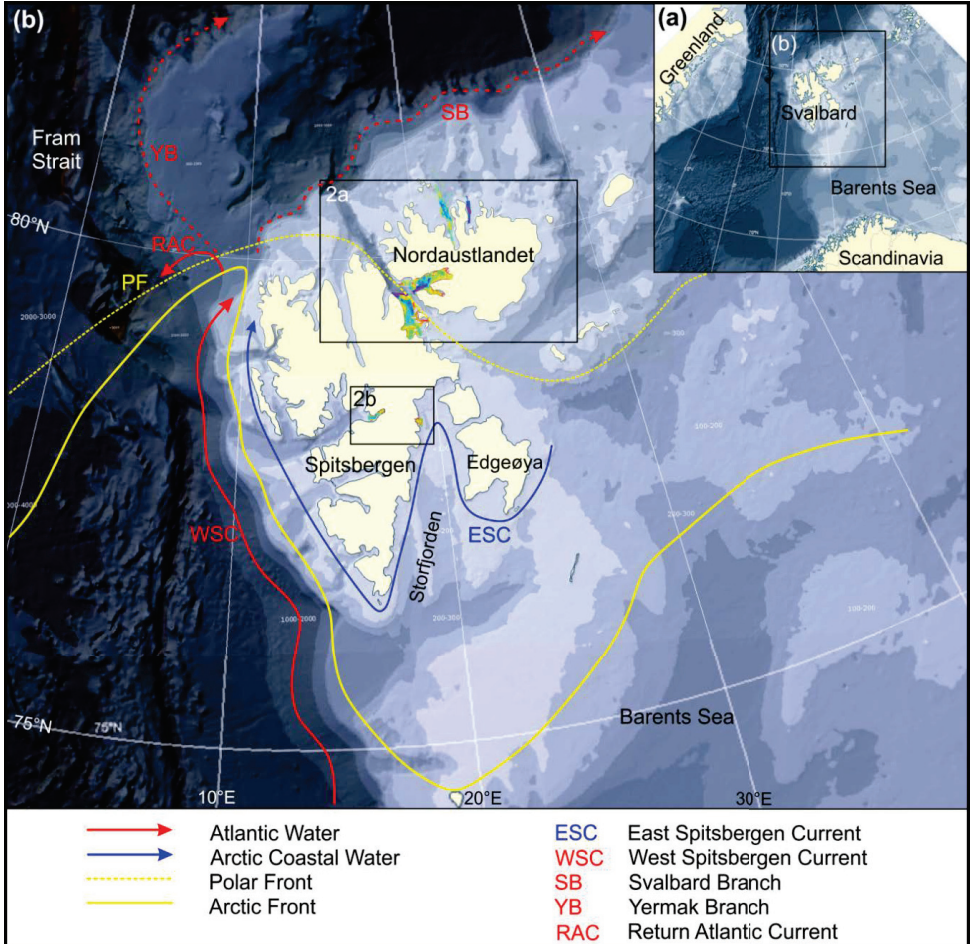


Fig. 1. (a) Overview map of the Barents Sea, showing the location of Svalbard. (b) Map of Svalbard and the NW Barents Sea showing main currents and oceanic fronts. Black

boxes outline the locations of the study areas presented in Figs 2a and b. The figure has been modified after Chauhan et al. (2014). The background shows a map from Svalbardkartet (NPI).

The Svalbard archipelago is located in a climatically sensitive area where air masses and ocean currents of different thermal character meet (Dowdeswell *et al.* 1995). Svalbard has an Arctic climate, even though the temperatures are considerably higher than in other areas on the same latitude. This is mainly due to the West Spitsbergen Current, the northernmost branch of the North Atlantic Drift, which brings warm, highly saline Atlantic waters along the west coast of Spitsbergen to the northern shelf edge, while the east coast of the island is dominated by polar waters, continental climate and the proximity to the polar front (Fig. 1b) (Chauhan *et al.* 2014). These oceanographic and atmospheric differences contribute to different environmental conditions between the moisture-rich maritime west and the drier arctic east Svalbard, both in terms of climate, sea ice distribution, temperatures and snow accumulation (Dowdeswell *et al.* 1995; Benestad *et al.* 2002). Sea ice is a common feature on the east coast of Spitsbergen and in northern Svalbard while the west coast is largely sea ice free with the exception of the inner fjords. Temporal variations in Atlantic water inflow affect the regional climate and sea-ice distribution, particularly in western Spitsbergen and northern Svalbard (Hald *et al.* 2004; Chauhan *et al.* 2014, 2015).

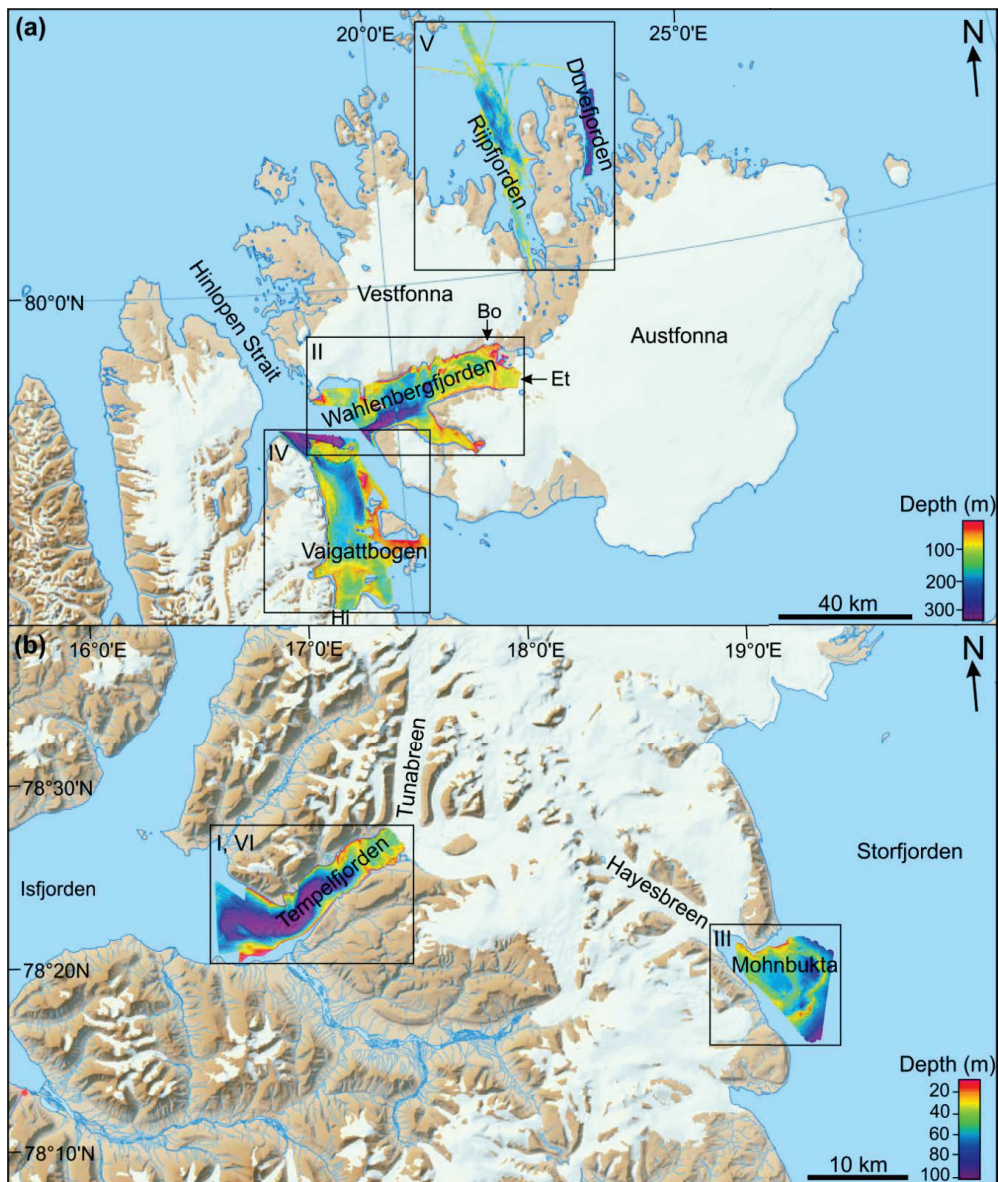


Fig. 2(a) Zoom-in on the study area in north eastern Svalbard. Bo- Bodleybreen, Et- Etonbreen and Hi- Hinlopenbreen. (b) Zoom-in on the study area in Central Spitsbergen. The boxes outline the study areas, presented in the different papers, I= paper 1, II= paper 2, III= paper 3, IV= paper 4, V= paper 5, VI= paper 6. Background maps have been derived from Svalbardkartet (NPI).

1.3 Glaciological background

1.3.1. A brief summary of the glacial history of Svalbard

In the beginning of the 19th century it was first suggested that the climate of Svalbard was much colder prior to the Holocene and the islands was covered a more extensive glacial cover (Lovén 1846; Torrell 1873). In 1900, the Swedish geologist Gerard De Geer was the first to suggest that a large marine-based ice sheet had once covered the Barents Sea, connecting the Scandinavian and Svalbard ice sheets by an extensive cover of thick sea ice (De Geer 1900). During the 1960s, several Swedish geological expeditions were launched to Svalbard. These expeditions confirmed that large parts of the archipelago had indeed been covered by in an ice sheet during the Weichselian (Schytt *et al.* 1968; Hoppe *et al.* 1969; Österholm 1978), but it was not until the 1980s that improvements in marine geophysical techniques provided direct evidence of a marine-based ice sheet in Svalbard and the Barents Sea (Elverhøi & Solheim 1983; Solheim & Kristoffersen 1984; Vorren & Kristoffersen 1986).

To date, abundant geophysical and geological evidence have been acquired suggesting that Svalbard and the adjoining Barents Sea were repeatedly covered by a marine-based ice sheet during the Quaternary (Svendssen *et al.* 2004; Laberg *et al.* 2010; Ingólfsson & Landvik 2013). Small-scale glaciations began sometime during the Plio-Pleistocene period, 3.5-2.4 Ma years ago, during which ice covered only terrestrial areas (Knies *et al.* 2009). The first large-scale glaciation occurred in early- to mid-Pleistocene, around 1.6 Ma years ago, during which the ice sheet reached the shelf edge (Knies *et al.* 2009). Marine evidence indicates that at least eight large-scale glaciations have occurred in the Svalbard-Barents Sea area during the last 0.78 Ma years (Vorren *et al.* 2011). The ice sheet reached its maximum extent during MIS 6, in the late Saalian, around 140 ka years ago (Svendssen *et al.* 2004; Jakobsson *et al.* 2014). The submarine geomorphological record verifies that the Quaternary ice sheets repeatedly reached the continental shelf break of the Norwegian-Svalbard margin during full glacial conditions (Ottesen *et al.* 2005; Ottesen *et al.* 2007; Vorren *et al.* 2011). It has been suggested that the Svalbard Barents Sea Ice Sheet (SBSIS) was a

part of a massive Arctic ice sheet with large ice shelves extending across the Arctic Ocean (Mercer 1970; Hughes *et al.* 1977; Grosswald & Hughes 1999). The prevailing view has been that the ice sheet did not extend further than to the shelf edge during Quaternary glaciations (Svendssen *et al.* 2004). It has even been proposed that the Arctic Ocean was sea ice free during full glacial periods, since a lid of sea ice would have prevented moisture build-up in the atmosphere and decreased ice sheet growth (Donn & Ewing 1966). New evidence support that at least during the Saalian the Arctic ice sheet was more extensive than previously assumed; with large ice shelf complexes reaching the central Arctic Ocean (Jakobsson *et al.* 2014; Jakobsson *et al.* 2016). During the Late Weichselian, between 25-15 ka years ago, the combined British, Fennoscandian and Barents-Kara Sea ice sheets covered Scandinavia, northern Europe, the British Isles, NW Russia, and the Svalbard-Barents and Kara Seas (Svendssen *et al.* 2004; Hughes *et al.* 2016). Temperature reconstructions from the Greenland ice cores show that the Last Glacial Maximum (LGM) temperatures in parts of the Arctic were as much as 20°C lower than today (Miller *et al.* 2009).

During the LGM, the interior of the SBSIS was drained by large ice streams, predominantly located along the same course as present day fjords and submarine cross-shelf troughs (Ottesen *et al.* 2007; Andreassen & Winsborrow 2009; Dowdeswell *et al.* 2010). The fast-flowing ice streams produced a characteristic submarine landform record consisting of streamlined landforms such as mega-scale glacial lineations, crag-and-tails and highly attenuated drumlins, as well as ice flow transverse grounding zone wedges (Batchelor *et al.* 2011; Bjarnadóttir *et al.* 2013; Fransner *et al.* 2017). Streamlined landforms are also found on the troughs east of Svalbard (Hogan *et al.* 2010b; Dowdeswell *et al.* 2010). The ice streams did not only drain ice from the interior of the ice sheet, but also transported large quantities of sediments towards the shelf edge, depositing large through mouth fans (TMFs) at the continental slope (Vorren *et al.* 1998; Dowdeswell *et al.* 2002; Batchelor & Dowdeswell 2014). Several of these prominent cross-shelf troughs with associated TMFs have been mapped along the western continental margins of Svalbard and Scandinavia (Vorren *et al.* 1998; Dowdeswell *et al.* 2002). They form as fast flowing ice streams deposit large amounts of glacial sediments at the continental slope

during subsequent Quaternary glaciations (Vorren *et al.* 1998; Andreassen & Winsborrow 2009). Of the TMFs in the Barents Sea the Bear Island fan is the largest and covers an area of approximately 200 000 km² (Dowdeswell *et al.* 2002). Cross-shelf troughs and TMFs are also present in northern Svalbard, albeit generally much smaller in dimension (Batchelor *et al.* 2011; Fransner *et al.* in prep). TMFs are however not present in front of all Arctic cross-shelf trough, which has been explained by low input of glacial sediments, sediments bypassing the slope or local bedrock geology (Batchelor & Dowdeswell 2014; Fransner *et al.* in prep). The fast-flowing ice streams were bound by inter-ice stream areas, where ice flow velocities were considerably slower (Ottesen & Dowdeswell 2009). The sea floor in the former inter-ice stream areas is dominated by landforms such as hummocky moraines, large retreat moraines and smaller transverse ridges (Ottesen & Dowdeswell 2009).

Jessen *et al.* (2010), suggest that the deglaciation at the western Svalbard shelf edge commenced as early as in 20.5 ka BP. This is a much earlier onset of the deglaciation than the previously suggested 16-17 ka BP (Mangerud *et al.* 1992; Mangerud *et al.* 1998; Landvik *et al.* 1998). The ice sheet started to thin between 25-20 ka BP and retreated from the outer- to the inner shelf between 20.5-16 ka BP (Gjermundsen *et al.* 2013; Hormes *et al.* 2013). In southern Svalbard, at the Storfjorden Trough, ice retreated from the shelf edge prior to 19.7 ka BP (Rasmussen *et al.* 2007), while ice sheet retreat from the shelf edge north of Nordaustlandet begun at 18.5 ka BP (Knies *et al.* 2001). The Svalbard archipelago experienced a rapid step-wise deglaciation (Svendsson *et al.* 1996). The mouth of Isfjorden was ice free around 14.1 ka BP, while the final deglaciation of the inner fjord occurred prior to 11.2 ka BP (Forwick & Vorren 2009). Van Mijenfjorden in the southwest had deglaciated by 11.2 ka BP (Hald *et al.* 2004), while Kongsfjorden in the northwest became ice free in 14.4 ka BP (Henriksen *et al.* 2014). In general, the fjords experienced a more rapid deglaciation compared to the inland areas (Henriksen *et al.* 2014; Flink *et al.* 2017).

Deglaciation ages from northern and eastern Svalbard are scarce. In northern Svalbard, the deglaciation of the Hinlopen Strait begun around 13.7-13.9 ka BP (Koç *et al.* 2002) and the ice sheet had retreated to inner Wahlenbergfjorden prior to 11.3 ka BP (Flink

et al. 2017). The areas south of Kvitøya deglaciated prior to 14.6 ka BP (Kristensen *et al.* 2013), while the inner basin of Storfjorden, on the east coast of Spitsbergen, was ice free around the Younger Dryas-Holocene transition, at 11.7 ka BP (Rasmussen & Thomsen 2015). It has been suggested that the deglaciation was more rapid in the deep troughs and fjords compared to the shallower offshore bank areas (Landvik *et al.* 2005; Kristensen *et al.* 2013). An absence of ice-flow transverse landforms in Wahlenberg- and Rijpfjorden indicate that the deglaciation did proceed more rapidly in the outer and deeper sections of the fjords, where the ice front most likely lifted from the sea floor and became floating during retreat (Fransner *et al.* 2017; Flink *et al.* 2017).

The glaciers in Europe reached their largest post-deglacial extent during the Younger Dryas (YD), between 12.9-11.7 ka BP (Rasmussen *et al.* 2007), but in Svalbard a lack of geomorphological evidence has led to the suggestion that no major glacial regrowth occurred during the YD. Instead the Little Ice Age (LIA) is commonly recognized as the time period when the Svalbard glaciers reached their Holocene maxima (Mangerud *et al.* 1992; Salvigsen *et al.* 1992; Humlum *et al.* 2005; Mangerud & Landvik 2007). According to Mangerud *et al.* (1992) the tidewater glaciers in Isfjorden were located far back in the fjord during YD; while Svendsen *et al.* (1996) suggested that the deglaciation in western Spitsbergen was interrupted by a period of cooling and glacial re-advance around 12.4 ka BP.

Although the ice sheet and glaciers in Svalbard did not experience as pronounced growth as in the rest of Europe, present data seem to agree that a climatic cooling occurred approximately at the time period of the YD. According to Henriksen *et al.* (2014), the tidewater glaciers in Kongsfjorden experienced an advance during the YD or in early Holocene. Data from south of Kvitøya also suggests a cooler climate in northeastern Svalbard during the YD, with perennial sea ice (Kristensen *et al.* 2013). A similar YD cooling with enhanced sea ice has been suggested to occur in Isfjorden (Forwick & Vorren 2009). The lack of glacier growth during the YD has been attributed to reduced precipitation (Mangerud & Landvik 2007).

It is generally agreed that the Early Holocene was a period of relatively warm climate with temperature maxima reached during the Holocene Climate Optimum (HCO) between 10-6 ka BP (Hald *et al.* 2004; Forwick & Vorren 2009; Miller *et al.* 2009; Rasmussen & Thomsen 2015). It has been suggested that the temperatures during the HCO were above present (Kaufman *et al.* 2009). In the Isfjorden area Optimum Holocene climatic conditions with reduced glacier cover occurred between 11.2-9 ka BP (Forwick & Vorren 2009). Svendsen *et al.* (1996) suggested that tidewater glaciers were absent from Isfjorden during this period. In eastern Spitsbergen, in Mohnbukta, optimum Holocene conditions occurred slightly later, between 8-6.5 ka BP (Flink *et al.* in prep). In southwestern Spitsbergen, the warm early Holocene was interrupted by an abrupt cooling at 8.8 ka BP and the overall climate cooled down between 8-4 ka BP (Hald *et al.* 2004).

The temperatures began to fall during the neoglacial around 6 ka BP years (Miller *et al.* 2009; Kaufman *et al.* 2009). In Storfjorden cooler, polar conditions returned around 5 ka BP and were followed by a period of enhanced glacial activity and fluctuating climate (Rasmussen & Thomsen 2015). The neoglaciation culminated in the LIA, which occurred between 1550-1920 in Svalbard (Svendsen & Mangerud 1997). It is widely assumed that the Svalbard glaciers reached their Holocene maxima during the end of the LIA, between the late 19th to the early 20th century (Solheim 1991; Lefauconnier & Hagen 1991). Following the end of the LIA in the 1920s the Svalbard glaciers have experienced increased mass loss, due to a warmer climate with an increase in air temperatures by almost 5°C (Dowdeswell *et al.* 1995; Dowdeswell *et al.* 1997). Over the past 40 years the total mass loss in Svalbard has been estimated to between 5.0-8.4 km³yr⁻¹ water equivalent (w.e.), and has contributed with 0.2 mm yr⁻¹ to global sea-level rise (Hagen *et al.* 2003; Blaszczyk *et al.* 2009). In comparison to other glaciated regions in the Arctic the Svalbard glaciers have experienced a more negative mass balance trend (Nuth *et al.* 2010).

1.3.2. Present day glacier cover in Svalbard

Presently 57% of Svalbard's land area is covered by glaciers (Nuth *et al.* 2013) with the main extent of the glacier-covered area in the north and east of the archipelago. The glaciers range from large ice caps in Nordaustlandet, such as the Aust- and Vestfonna to small cirque and valley glaciers in central Spitsbergen, such as Longyearbreen. The prevailing climate with sparse precipitation, low snow accumulation rates and ice temperatures contribute to generally low ice flow velocities (Lefauconnier & Hagen. 1991). The majority of Svalbard's glaciers are of subpolar type with a polythermal basal regime (Hagen *et al.* 1993; Murray *et al.* 2003) although small, entirely cold-based land-terminating glaciers also exist (Baelum & Benn 2011). Polythermal glaciers contain both cold ice (with temperatures below pressure-melting point) and temperate ice (with temperatures at pressure-melting point) and can display a large variety of thermal structures (Pettersen *et al.* 2004).

The glaciers in Svalbard can be divided into three groups based on their thermal structure (Sevestre *et al.* 2015). 1) Large land-terminating glaciers with temperate ice in the accumulation area and at the base. These glaciers have a cold surface layer which reaches the base at the terminus. 2) Large tidewater glaciers with a core of temperate ice and a cold surface layer which is stripped away by calving at the terminus. 3) Small valley glaciers which are entirely cold based or have a small remnant temperate core. Polythermal glaciers are generally sensitive to changes in external and internal factors, such as geothermal heat flux, climate, overburden pressure and strain heating, since large volumes of their ice exist at or near the phase-transition boundary. Small variations in these factors can result in a phase transition, which in turn can affect the glaciers flow velocity (Benn & Evans 2010).

The majority of Svalbard's fjords accommodate one or several tidewater glaciers. 68% of the glacierised area in Svalbard is drained through tidewater glaciers (Nuth *et al.* 2013). Tidewater glaciers lose the majority of their mass by calving during the summer months. They are the fastest flowing glaciers on Svalbard and some of them can reach velocities of a couple of meters per day (Lefauconnier *et al.* 1994). The tidewater glaciers in Svalbard have grounded margins (Hagen *et al.* 2003). Sea ice influences the tidewater glaciers to a great degree, since it prevents warm ocean

currents from reaching the inner fjords and reduces calving rates during the winter months (Ottesen *et al.* 2008). Sea ice has been shown to be of particular importance for surging glacier dynamics during the quiescent phase since its buttressing effect slows down calving rates, allowing the glacier front to advance (Flink *et al.* 2015).

1.3.3. Surge-type glaciers in Svalbard

Traditionally, a glacial surge has been defined as a cyclical change in the glaciers flow velocity, triggered by internal mechanisms rather than external forcing, such as for example, climate change (Meier & Post 1969). Surge-type glaciers alternate between long periods of slow flow (the quiescent phase) during which the ice flows below its balance velocity and short periods of fast flow (the surge phase) during which ice flow speeds up (Murray *et al.* 2003; Sund *et al.* 2009). The quiescent phase lasts a couple- to several decades, whereas the surge phase last a month- to a few years (Solheim 1991; Dowdeswell *et al.* 1991; Hagen *et al.* 1993; Sund *et al.* 2009). Typically, surging initiates as mass begins to build-up in the upper regions of the glacier (the reservoir area), which commonly corresponds to the accumulation zone, while the lower parts of the glacier experience slow flow (Sund *et al.* 2009). This leads to an imbalance along the glaciers longitudinal profile, which progressively steepens until a surge is triggered (Meier & Post 1969). During the active phase, mass is swiftly transported down-glacier from the reservoir area, resulting in increased flow velocities with up to a factor of ten. As the boundary between fast-and slow flowing ice, (the surge front), moves down-glacier the terminus advances, resulting in stretching and intense crevassing (Clarke *et al.* 1984). In some tidewater glaciers in Svalbard the surge has been observed to initiate at the calving front and propagate up-glacier (Dowdeswell & Benham 2003; Murray *et al.* 2003). The surge stagnates as the glacier surface thins and the system loses potential energy, resulting in reduced flow-velocities (Sund *et al.* 2009). Commonly the glacier experiences steady retreat after surge stagnation. For tidewater glaciers, the steady retreat has been shown to be interrupted by annual re-advances, which occur during winter when calving rates are low (Flink *et al.* 2015; Flink *et al.* 2016).

Up to 90% of Svalbard's glaciers have been inferred to be of surge-type (Lefauconnier & Hagen 1991), whereas others have defined only 13% of Svalbard's glaciers as surge-type glaciers (Jiskoot *et al.* 1998). More recent studies are in agreement that the number is probably closer to the former assumption (Sund *et al.* 2009; Sevestre *et al.* 2015; Sevestre & Benn 2015; Farnsworth *et al.* 2016). Recently, over 400 previously undocumented surge-type glaciers were identified by Farnsworth *et al.* (2016), indicating that not all surge-type glaciers have been recognised to date. The large difference between the suggested numbers can be assigned to the long quiescent phases of the Svalbard glaciers (Sund *et al.* 2009). The average surge cycle in Svalbard is between 60-70 years, although a surge cycle as short as 30 years has been observed for Tunabreen (Hagen *et al.* 1993) while a surge cycle as long as 500 years has been suggested for Bråsvellbreen (Dowdeswell *et al.* 1991). Since many Svalbard glaciers have long quiescent phases they have been observed to surge only once during the historical period (Ottesen *et al.* 2008; Sund *et al.* 2009). According to recent work by Sevestre & Benn (2015) and Sevestre *et al.* (2015), glaciers in a specific climatic envelope can switch from surge-type to non-surge-type and vice versa due to external forcing, which could explain the discrepancy between the numbers of defined surge-type glaciers. A regional scale climatic event, such as the LIA could therefore promote the glaciers in a specific climatic envelope to switch from non-surge to surge-type. It has previously been suggested that the large number of surges at the end of the LIA could be explained by changing external conditions (Liestøl 1969).

During the active phase, surging glaciers are identified by an increase in surface flow velocities, rapid changes in length and/or elevation, intense crevassing or surface features such as foliation and looped moraines (Meier & Post 1969; Clarke *et al.* 1984; Hagen *et al.* 1993; Hamilton & Dowdeswell 1996; Luckman *et al.* 2002; Dowdeswell & Benham 2003; Nuth *et al.* 2010). Surging glaciers produce distinct geomorphological and sedimentological features and past surges can therefore be identified by characteristic landform assemblages, both in terrestrial and marine records (Evans & Rea 1999; Ottesen & Dowdeswell 2006; Ottesen *et al.* 2008; Schomacker *et al.* 2014; Flink *et al.* 2015; Lovell *et al.* 2015). The typical terrestrial surge landform assemblages include some or all of the following elements:

glaciotectonic structures, folding, end-moraines with hummocky moraine, flutes or drumlins, crevasse-squeeze- or -fill ridges, and concertina eskers (Christoffersen *et al.* 2005; Kjær *et al.* 2008; Brynjólfsson *et al.* 2012; Schomacker *et al.* 2014). The sedimentary record is characterized by deformed pre-surge sediments, multiple stacked diamictons and stratified glaciomarine interbedding displaying glaciotectonic folding and deformation (Evans & Rea 1999).

In tidewater glaciers settings glacial lineations form during the active phase of the surge and fjord-floor sediments are pushed in front of the rapidly advancing glacier terminus to form a terminal moraine ridge (Ottesen & Dowdeswell 2006; Ottesen *et al.* 2008; Flink *et al.* 2015; Streuff *et al.* 2015). The terminal moraine ridges mark the maximum extent of the surge and characteristically have debris-flow lobes on their distal slopes. The lobes form continuously during the surge maximum stage or as the surge stagnates and the glacier front begins to retreat, rendering the moraine ridges unstable (Kristensen *et al.* 2009). As the surge stagnates, the glacier front thins and water pressures at the sediment-ice interface nearly exceed the ice overburden pressure enabling soft sediments to be squeezed into basal crevasses, forming a characteristic network of sharply crested crevasse-squeeze ridges (Lovell *et al.* 2015). Small ice-flow transverse retreat moraine ridges form during the quiescent phase as the glacier front experiences minor still-stands or re-advances during general retreat (Flink *et al.* 2015; Flink *et al.* 2016). It is generally agreed that individual landforms cannot be used to infer a former surge with the exception of crevasse-squeeze ridges, which are assumed to form only during surge conditions and are indicative of past surges (Solheim 1991; Ottesen *et al.* 2008; Rea & Evans 2011).

2. Motivation

The motivation behind this study is threefold: firstly, to collect new data from the poorly-studied eastern and northern Svalbard. This includes acquiring high-resolution bathymetric data and collecting sediment cores from these largely unmapped areas. Secondly, to investigate surging tidewater glacier geomorphology and to link geological and geomorphological data to glacier dynamics. Although significant progress has been made in recent years, surging still remains one of the great mysteries

of glaciology. In the paleo-record, one of the main challenges is to separate climatically controlled glacial events from those driven by internal glacier changes. Thirdly, to investigate the late-, de- and post-glacial history of the fjords in eastern and northern Svalbard. This includes providing age constraints for the deglaciation and for Holocene glacial advances in these poorly studied areas and to link morphological data to ice sheet and glacier dynamics. Understanding the dynamics of the marine-based SBSIS during the LGM and the deglaciation is imperative since the SBSIS can serve as an analogue to the modern West Antarctic Ice sheet (WAIS). The paleo-record from the Svalbard-Barents Sea can therefore increase our understanding on the future evolution of the WAIS, and its potential response to the changes in ice sheet and ice shelf dynamics, global temperatures and sea level rise.

3. Aims and Objectives

The aim of the thesis is to investigate the submarine glacial morphology and sedimentology of the fjords in the previously unmapped and poorly-studied eastern and northern Svalbard in order to link the geological records to past glacier and ice sheet dynamics. The thesis addresses the following broad research questions:

- How are late Quaternary and Holocene climatic events, such as the LGM, deglaciation, Holocene Climate Optimum (HCO) and LIA expressed in the geological record of the fjords in eastern Svalbard?
- What was the course of deglaciation in the northeastern Svalbard?
- What were the main factors controlling the glacier activity in the eastern Svalbard?
- Were major glacial events, such as glacial advances, synchronous or asynchronous between the east- and west coasts of Svalbard?
- What are the characteristics of surging tidewater glacier landform assemblages and how can these be used to infer past glacier dynamics?
- What is the role of climate in the evolution of overall surge patterns?

4. Methods

4.1. Geophysical methods

A variety of geophysical data were utilized during this thesis. The data were acquired, between 2010-2016, with the research vessels R/V Helmer Hanssen and R/V Viking Explorer. Swath-bathymetric data for papers II and IV were provided by the Norwegian Hydrographic Service. The R/V Helmer Hanssen uses a hull-mounted Kongsberg-Simrad EM300 multibeam echo-sounder system, which operates at a frequency of 30 kHz. The ship also uses an EdgeTech 3300-HM hull-mounted, sub-bottom profiler (Chirp), which operates at frequencies, between 500 Hz-12 kHz and has a penetration depth of up to 80 m in soft clays and a vertical resolution of 6-10 m. The R/V Viking Explorer uses a Kongsberg EM2040 multibeam echo-sounder which is mounted to the bow of the ship. During each cruise CTD measurements were taken at several locations to calculate the sound velocity profile of the water column.

The QPS Fledermaus v. 7.0 and D-Magic software were used to process and grid the bathymetric data. The data were gridded with different cell sizes depending on seafloor depth. Visual examination and analysis of landforms was conducted in the Fledermaus and ArcGIS software suits, using different angles of sun illumination. ArcGIS was used for mapping the geological features. The Edgetech Discover II Sub-bottom software and Kingdom 8.8 were used to visualize the sub-bottom acoustic profiles. In addition, different sets of aerial and satellite images, and historical maps were used throughout the thesis. The aerial and satellite images were provided by the Norwegian Polar Institute, NASA and NOAA. The aerial and satellite data were georeferenced and integrated with the bathymetric data in ArcGIS.

4.2. Sedimentological methods

The sediment cores presented in papers II, IV and V were recovered during cruises on the R/V Helmer Hanssen in 2012 and 2016. The sediment cores presented in paper III were acquired during snow-scooter field excursion in 2015. The cores were split and analyzed at the University Centre in Svalbard and at the Department of Geological Sciences at Stockholm University. A number of parameters, such as lithology, grain-

size distribution, color, water content, sedimentary texture and structures were logged. Lithofacies coding was adopted from Eyles *et al.* (1983). Standard parameters, such as magnetic susceptibility and shear strength were measured on all cores. The cores presented in paper II and V were also logged using a Multi-Sensor Core Logger (MSCL), which was used to log geophysical properties such as P-wave velocity, gamma density, and magnetic susceptibility. They were also run through an ITRAX micro-X-ray fluorescence core scanner, which was used to obtain radiographic images of the cores. Grain size analysis was conducted on the finer (<1 mm) fraction at 10 cm intervals with a Malvern 3000 laser diffraction particle size analyzer.

All core samples were analyzed for microfossils and foraminifera were picked from samples that contained sufficient amount for radiocarbon dating. The collected samples, consisting of mixed benthic foraminifera or shells/shell fragments, were sent for AMS radiocarbon (^{14}C) dating. Three different AMS laboratories were used for the papers; the AMS laboratory at Lund University, the CRONOS laboratory in Belfast and the Ion Beam Physics laboratory in Zurich. The radiocarbon ages were calibrated with the CALIB 13 software, which has an inbuilt global marine reservoir correction of 405 ± 52 years (Stuiver & Reimer 1993; Reimer *et al.* 2013). A local marine reservoir correction for Spitsbergen with a delta R of 105 ± 24 years was used in the age calibration (Mangerud *et al.* 2006). All reported ages in this thesis are calibrated ages.

5. Summary of papers

5.1. Paper I

Flink, A. E., Noormets, R., Kirchner, N., Benn, D. I., Luckman, A., & Lovell, H., (2015): The evolution of a submarine landform record following recent and multiple surges of Tunabreen glacier, Svalbard. Quaternary Science Reviews. Vol. 108: 37-50.

The aim of this study is to map and analyze the submarine glacial landform record associated with recent surge events of Tunabreen, a tidewater glacier in Tempelfjorden, by combining high-resolution multibeam-bathymetric data, topographic maps, satellite images and aerial photographs. In contrast to most Svalbard surging glaciers, which have long quiescent phases, Tunabreen- has

experienced three surges since the end of the LIA. The landform record in Tempelfjorden is distinguished from previously studied glacier-surge landsystems by containing four well-preserved sets of landform assemblages. These landform assemblages were generated by the LIA advance and three subsequent surges, all of which have partly modified earlier landform records. The submarine retreat moraines in inner Tempelfjorden correlate to glacier terminal positions since the most recent surge in 2004. Glacier surface velocity and ice-front positions derived from high-resolution TerraSAR-X satellite data show minor glacier frontal advances in winter when calving is suppressed by sea ice, demonstrating that the moraines form annually during quiescent phase winter advances as the glacier experiences general retreat. Based on the unique landform record in Tempelfjorden, a new conceptual landsystem model for frequently surging glaciers was put forward improving our understanding of surging glacier dynamics and of how surge-type glaciers can be distinguished from climatically-controlled glaciers in the geological record.

5.2. Paper II

Flink, A. E., Noormets, R., Fransner, O., Hogan, A. K., Ó Regan, M., & Jakobsson, M. (2017): Past ice flow in Wahlenbergfjorden and its implications for late Quaternary ice sheet dynamics in northeastern Svalbard. Quaternary Science Reviews. Vol. 163: 162-179.

The goal of this study is to map the submarine landforms in Wahlenbergfjorden and to link their distribution to past glacial dynamics. High-resolution multibeam-bathymetric and sub-bottom data, as well as sediment cores were used to study the past extent and dynamics of the SBSIS and the glaciers in Wahlenbergfjorden. The submarine landform assemblage in Wahlenbergfjorden consists of landforms characteristic of subglacial, ice marginal and proglacial conditions. Glacial lineations indicate that Wahlenbergfjorden was occupied by fast flowing ice during the LGM and most likely acted as an ice stream onset zone. Westward ice flow in the fjord merged with the northward flowing ice stream in the Hinlopen Strait. Absence of ice recessional landforms in outer Wahlenbergfjorden suggests that the deeper areas deglaciated relatively rapidly, most likely by the glacier front lifting from the sea floor and forming a floating tongue. The inner part of Wahlenbergfjorden and Palanderbukta are

characterized by De Geer moraines, indicating episodic retreat of a grounded glacier front. In Palanderbukta, longer still-stands of the glacier terminus resulted in the formation of larger terminal moraine ridges. The inner part of Wahlenbergfjorden deglaciated prior to 11.3 ka BP. The submarine landform assemblages in front of Bodley-, Eton-, Idun- Frazer- and Aldousbreen confirm that these glaciers have surged at least once during the Holocene.

5.3. Paper III

Flink, A. E., Hill, P., Noormets, R., & Kirchner, N., (In prep): Glacial evolution of Mohnbukta fjord in eastern Spitsbergen inferred from submarine landform and sediment core records. Boreas. Submitted

This study aims to reconstruct the Holocene glacial history of Mohnbukta, a small fjord, located on the east coast of Spitsbergen. Three tidewater glaciers, Heuglin-, Köningsberg- and Hayesbreen calve into Mohnbukta. Hayesbreen surged at the end of the LIA, between 1901 and 1910. The submarine landform assemblage in Mohnbukta contain two large, terminal moraine ridges, with debris-flow lobes on their distal slopes and associated sets of well-preserved crevasse-squeeze ridges proximal to terminal moraines. The crevasse-squeeze ridges suggest that both landform sets were produced during surge-type advances, thus indicating that at least two glacier surges have occurred in Mohnbukta. The 1901 Hayesbreen surge terminal position correlates to the inner terminal moraine ridge suggesting that the outer ridge formed prior to 1901. Marine sediment cores, recovered from the proximity of the inner ridge, display C^{14} ages between 5.7-7.7 ka BP, derived from a clast-rich mud unit. This unit represents pre-surge, unconsolidated Holocene sediments, which were mixed up in front of the glacier terminus during the 1901 surge. The absence of retreat moraines and an aerial image, displaying tabular icebergs calving-off the glacier front during the 1901 surge retreat phase suggests that Hayesbreen was close to flotation during the 1901 surge and therefore did not deposit a consolidated subglacial till. Based on the submarine morphology and the radiocarbon ages we propose that a surge-type advance occurred in Mohnbukta during early Holocene, prior to 7.7 ka BP.

5.4. Paper IV

Flink, A. E., & Noormets, R. (In prep): The glacial history of Vaigattbogen, north eastern Spitsbergen. Marine Geology. Submitted

The aim of this study is to reconstruct the glacial history of the southern Hinlopen Strait and Vaigattbogen, during the last glaciations, deglaciation and the Holocene, by integrating bathymetric- and sub-bottom acoustic data, sediment cores, historical maps and satellite images. During the last glacial, the Hinlopen Strait was occupied by an ice stream, which drained ice towards the northern shelf of Svalbard. Ice flow in Vaigattbogen fed into this ice stream and increased in speed as it moved towards the north. The outer basin of Vaigattbogen deglaciated prior to 9.1 ka BP. Absences of ice-flow transverse landforms indicate that the Hinlopen Strait and the deeper parts of Vaigattbogen deglaciated rapidly, while ice retreat slowed down on the shallower banks. Since the deglaciation, at least two surge-type advances have occurred in Vaigattbogen and deposited two terminal moraine ridges with crevasse-squeeze ridges. Hinlopenbreen surged in the early 1970s and reached the inner terminal moraine ridge. Radiocarbon dates suggest that the outer moraine ridge formed prior to 2.6 ka BP. The radiocarbon ages provide a minimum age indicating that the outer ridge could have formed at any time between 2.6 ka BP and the deglaciation. The outer ridge is double-crested and displays a set of crevasse-squeeze ridges between the ridge crests, suggesting that at least two surge-type advances have occurred prior to 2.6 ka BP and reached approximately the same position.

5.5. Paper V

Fransner, O., Noormets, R., Flink, A. E., Hogan, K. A. O'Regan, M., & Jakobsson, J. (2017): Glacial landforms and their implications for glacier dynamics in Rijpfjorden and Duvefjorden, northern Nordaustlandet, Svalbard. Journal of Quaternary Science. Vol. 32(3): 437-455.

This study integrates high-resolution multibeam, sub-bottom acoustic data, and marine sediment cores in order to investigate the glacial history in the poorly studied Rijp- and Duvefjorden in northern Nordaustlandet. Submarine landforms suggest that the fjords were occupied by topographically controlled ice streams. The ice flow changed directions on the shelf, indicating that ice flow was no longer topographically

controlled. This could be attributed to the absence of well-defined cross-shelf troughs on the northern Nordaustlandet shelf. During the deglaciation, the ice sheet retreated from the shelf edge to the inner fjords in c. 8000 years. Inner Rjipfjorden deglaciated prior to 10.4 ka BP, while central Duvefjorden was ice free in 10.8 ka BP. De Geer moraines in the shallow inner areas of the fjords suggest relatively slow retreat of 100-250 m/year, while the outer, deeper parts of the fjords deglaciated rapidly.

5.6. Paper VI

Flink, A. E., Noormets, R., & Kirchner, N. (2016): Annual moraine ridges in Tempelfjorden, Spitsbergen. In: Atlas of Submarine glacial landforms: Modern, Quaternary and Ancient. Geological Society, London, Memoirs. (46): 75-76

This is a short contribution to the Atlas of submarine glacial landforms, based on the data presented in paper I. The aim of the text is to highlight the correlation between the submarine retreat moraines formed after the 2004 surge of Tunabreen and the annual terminal retreat of the glacier. The correlation between submarine and aerial data sets demonstrates that the retreat moraine ridges have formed annually.

6. Synthesis

6.1. The LGM and the deglaciation in northeastern Svalbard

The dynamics, drainage patterns and deglaciation history of northeastern Svalbard is poorly known. This thesis contributes with new data on ice flow and deglaciation patterns in the fjords around Nordaustlandet. The SBSIS reached the shelf edge during the LGM and was drained by larger ice streams in the Hinlopen, Kvitøya and Albertini troughs (Knies *et al.* 2001; Batchelor *et al.* 2011). In Wahlenbergfjorden, elongated streamlined bedforms, such as glacial lineations, crag-and-tails and glacially sculpted bedrock indicate that the fjord was occupied by fast flowing ice, which was deflected towards the north at the mouth of the fjord and joined the Hinlopen Strait ice stream (Fig. 3a). The Wahlenbergfjorden area has been suggested to represent an ice stream onset zone, where ice flow converged, speeded up and fed into the northward flowing Hinlopen Strait ice stream (Flink *et al.* 2017).

Ice flow in Vaigattbogen was relatively rapid and had a northward direction. Longer glacial lineations in the northern part of the data set suggest that ice flow velocities picked up as the ice flowed towards the north. Relatively fast flowing ice was routed into the Hinlopen Strait ice stream from several of the fjords in southern Hinlopen Strait (Fig. 3). The landform assemblages from Ripp- and Duvefjorden suggest that smaller ice streams drained the northern Nordaustlandet section of the SBSIS. More attenuated bedforms with higher elongation ratios further out on the shelf suggest that ice flow speeded up once it reached the outer fjords and the shelf. Changing directions of the elongated landforms indicate that the ice streams switched directions or were switched on and off, adopting slightly different drainage pathways as they reached the relatively plane shelf. The ice flow on the shelf, north of Nordaustlandet was not confined by deep cross-shelf troughs suggesting that the ice streams might dynamically have acted more like pure ice streams once the ice left the confinements of the fjords. This is supported by sets of lineation with different directions in the Albertini trough, proving that ice streams in the area changed directions depending on varying inflow intensities from different feeding ice flows (Fransner *et al.* 2017). This suggests that the area could have been dynamically similar to, for example, the modern day Siple Coast area in West Antarctica, which is drained by several “pure” ice streams (Rignot *et al.* 2011).

The submarine data support a dynamic, multi-domed ice sheet in northern and eastern Svalbard during the LGM (Fig. 3a). The varying ice flow directions around Nordaustlandet suggest that the SBSIS consisted of multiple domes, which likely migrated with time. Therefore the data is in accordance with several recent studies, which have suggested a multi-domed SBSIS configuration, particularly during the late stages of the LGM (Hormes *et al.* 2011, 2013; Ingólfsson & Landvik 2013; Hogan *et al.* in prep).

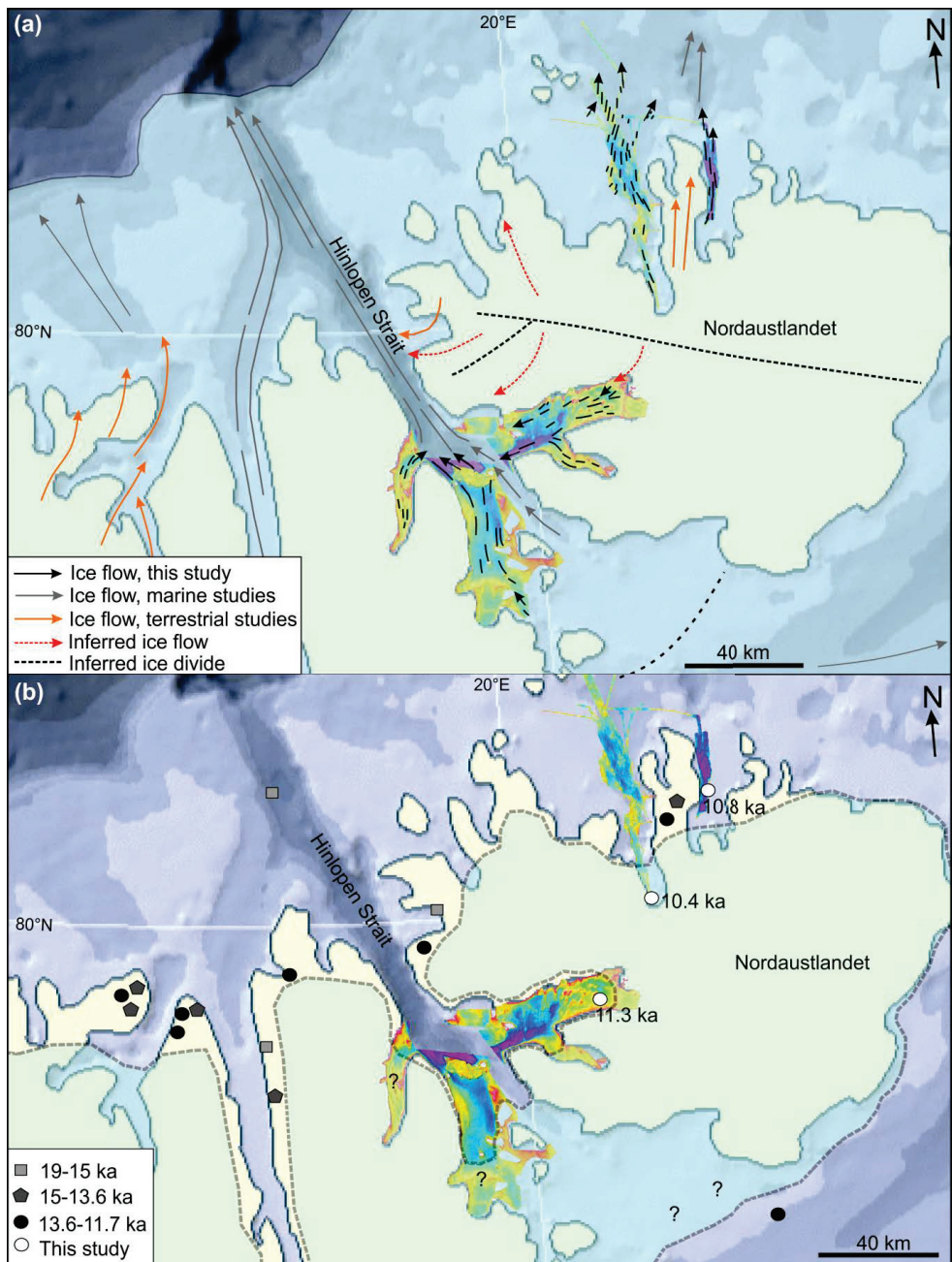


Fig. 3(a) Map of northeastern Svalbard showing the LGM ice extent and the main ice flow drainage pathways. Black arrows are based on mapped submarine landforms. Grey arrows are based on Ottesen et al. (2005); Ottesen et al. (2007) and Dowdeswell et al. 2010. Orange arrows are based on Hormes et al. (2011); Gjermundsen et al.

(2013) and Hormes *et al.* (2013). (b) Reconstruction of the ice sheet extent around 11 ka BP with published deglaciation ages based on Hormes *et al.* (2013). Question-marks outline areas where the timing of the deglaciation is uncertain. Background maps have been derived from Svalbardkartet (NPI).

The onset of the deglaciation in northeastern Svalbard is estimated to 19-16.5 ka BP and commenced by dynamical thinning in the deeper troughs, followed by rapid ice margin retreat by lift-of and substantial calving (Hogan *et al.* in prep). Outer Vaigattbogen deglaciated prior to 9.1 ka BP (Flink & Noormets in prep). Ice flow transverse landforms are absent in the deeper, central and outer parts of Vaigattbogen and Wahlenbergfjorden indicating that the deglaciation of the deeper areas proceeded rapidly, most likely by flotation of the ice front. In difference De Geer moraines on the shallow banks in Vaigattbogen, inner Wahlenbergfjorden and Palanderbukta suggest relatively slow retreat in these areas (Flink *et al.* 2017). It is likely that the islands in Vaigattbogen provided pinning points for the ice sheet terminus and ice remained for longer in these shallower areas. A similar pattern, with De Geer moraines in the shallower areas of the fjords is observed in Ripp-and Duvefjorden, indicating slow retreat, while ice-marginal transverse landforms are absent in the deeper areas suggesting rapid retreat of a floating ice front (Fransner *et al.* 2017). The inner part of Wahlenbergfjorden deglaciated prior to 11.3 ka BP, while inner Rippfjorden had deglaciated prior to 10.4 ka BP and central Duvefjorden prior to 10.8 ka BP (Fig. 3b). This suggests that Hinlopen Strait and the western Nordaustlandet fjords deglaciated prior to the fjords on northern Nordaustlandet, further supporting rapid ice retreat in the deep Hinlopen Strait.

6.2. Early to mid-Holocene pre-LIA glacier surges in eastern Svalbard

It is generally assumed that the Svalbard glaciers reached their post-deglacial maxima in late Holocene; during the end of the LIA (Salvigsen *et al.* 1992; Svendsen & Mangerud 1997; Humlum *et al.* 2005). The data presented in this thesis indicate that this was not the case for all Svalbard glaciers. Radiocarbon ages from sediment cores

in Mohnbukta and Vaigattbogen suggest that a pre-LIA surge-type advance occurred in the fjords in early-mid Holocene (Flink *et al.* in prep; Flink & Noormets. in prep).

The seafloor in Mohnbukta features two surge-type landform assemblages (Fig. 4b). The inner ridge formed during the 1901 surge of Hayesbreen, while the outer ridge is older. Reversed old C¹⁴ ages acquired from a clast rich mud unit and a soft diamicton unit, from two separate cores indicates that the sediments were subjected to reworking during the 1901 surge. The sedimentology of the cores and the C¹⁴ ages suggest that the 1901 surge did not deposit a fully consolidated layer of submarine till, which indicates that Hayesbreen was close to flotation during the surge, with the base of the glacier most likely sliding on a highly pressurized thin film of water. Instead older seafloor sediments were mixed-up during the 1901 surge advance. The C¹⁴ ages fall within an age range of 6-7.7 ka BP, which suggests that a pre-LIA, surge-type advance occurred in Mohnbukta in early Holocene. Similarly to Mohnbukta, at least two surge-type advances have occurred in Vaigattbogen during the Holocene. Radiocarbon ages from the outer ridge in Vaigattbogen indicate that it formed prior to 2.6 ka BP. However, the sediment core did not sample subglacial till and provides only a minimum age for the ridge. It is thus possible that the ridge formed in early Holocene. Crevasse-squeeze ridges between the double crests of the ridge suggest that two surge-type advances could have occurred and reached approximately the same position.

The proposed pre-LIA surges differentiate the east coast glaciers from the west coast glaciers. The main question to ask is what caused the Mohnbukta and Vaigattbogen glaciers to experience surge-type advances in the early-mid Holocene? It is possible that the rapid deglaciation of Storfjorden and Hinlopen Strait led to changes in the east coast glacier systems and subsequent dynamic disequilibrium, resulting in an environmentally induced jump into surge-mode, (cf. Sevestre *et al.*, 2015; Sevestre & Benn 2015). The Mohnbukta and Vaigattbogen data suggest a more dynamic Holocene glacial history in Svalbard than previously presumed. It is possible that other east coast glaciers have experienced similar, early Holocene surge-type advances. The radiocarbon dates provide a minimum age to the outer moraine ridges and it is possible that they formed much earlier and could thus, for example, originate in the YD.

6.3. Late Holocene glacier surge activity in Svalbard

Surging tidewater glaciers can be recognized by their characteristic landform assemblages, which has led to the identification of three previously undocumented surging glaciers in Wahlenbergfjorden, Idun-, Frazer- and Aldousbreen. Even though crevasse-squeeze ridges were not observed, the landform assemblages with glacial lineations, retreat moraines and large terminal moraines with debris-flow lobes, suggest that they formed during surge-type advances. The bathymetric data in front of the glaciers covers only the distal section of the landform assemblages, suggesting that crevasse-squeeze ridges might be present in more proximal settings. Furthermore, crevasse-squeeze ridges are small landforms, easily buried by high sedimentation rates and sometimes difficult to distinguish from recessional moraine ridges. Both the Idun- and Frazerbreen landform assemblages contain at least two larger moraine ridges, suggesting that more than one surge-type advance has occurred during the Holocene.

Tunabreen on the west coast has the to-date shortest recorded surge-cycle in Svalbard, with three surges since the LIA (Fig. 4a). At least two glacier surges have occurred in the majority of the east coast fjords, investigated during this study. Mohnbukta and Vaigattbogen have experienced two surges during the Holocene. The landform assemblage of Etonbreen, in Wahlenbergfjorden suggests that this glacier has also surged at least twice. The Etonbreen landform assemblage contains a large multi-crested terminal moraine ridge with cut-off segments and crevasse-squeeze ridges between the crests, suggesting that the ridge was created during at least two surge-type advances (Flink *et al.* 2017).

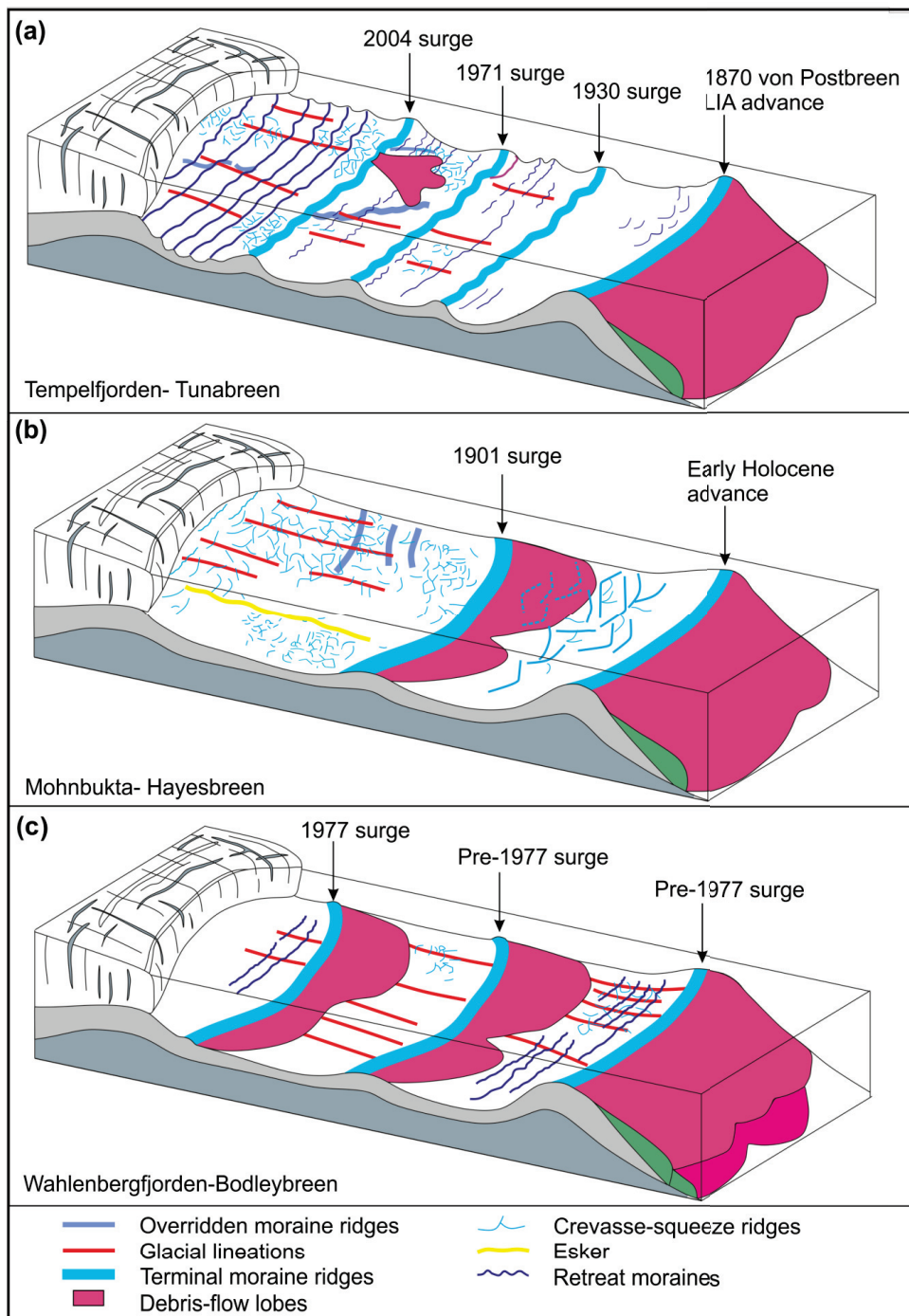


Fig. 4. Conceptual models for surge-type glaciers, based on three different Svalbard

fjords. (a) Tempelfjorden. (b) Mohnbukta (c) Wahlenbergfjorden in front of Bodleybreen.

Tunabreen is not the only tidewater glacier where the landform assemblage suggests that at least three surge-type advances have occurred during the Holocene. Bodleybreen in Wahlenbergfjorden displays three sets of terminal moraine ridges with debris-flow lobes on their distal flanks and glacial lineation and crevasse-squeeze ridges in the two most distal landform sets (Fig. 4c). The maximum terminal position of the 1977 Bodleybreen surge matches the innermost of the submarine ridges, suggesting that the two distal landform sets have formed during earlier surges, prior to the 1970s. The Oslo-Hinlopenbreen glacier system in Vaigattbogen has experienced at least two surge-type advances during the Holocene. Crevasse-squeeze ridges preserved at the center of the double-crested terminal moraine ridge suggest that three surge-type advances could have occurred in the fjord. It is likely that the Holocene maxima of Bodley- and Etonbreen were reached prior to the LIA, as is the case for the glaciers in Mohnbukta and Vaigattbogen.

The extent of the surge and the duration of the active phase seem to be important factors in the shaping of the submarine morphology. For example, the 2004 surge of Tunabreen was rapid, lasting only approximately a year, during which the glacier front advanced merely 2 km. As a result, the terminal moraine ridge of the 2004 surge is much smaller than typical surge terminal moraines in Svalbard and only a small debris-flow lobe exists on its distal slope (Fig. 4a). The thickness and character of the seafloor sediments in front of the glacier margin prior to the surge plays a role in the shaping of the landform assemblage. The LIA surge terminal moraines are most likely so large because thick accumulations of marine sediments had time to settle on the seafloor during the Holocene. Tunabreen, on the other-hand, surged in 1971 which allowed for only 33 years of marine sedimentation prior to the 2004 surge, resulting in a relatively small terminal moraine and the absence of a large debris-flow lobe.

The surging tidewater glacier landform assemblages in Svalbard share many similarities, but there is no such thing as THE surging landform assemblage. They all

feature differences, with some landforms being present in one assemblage and absent in another (Fig. 4). The Etonbreen landform assemblage is the only one which contains eskers and crag-and-tails. The Eton- Bodley- and Hinlopenbreen landform assemblages contain at least two stacked debris-flow lobes distal to the outermost moraine ridges. Small recessional moraine ridges are observed in the majority of the landform assemblages, but are absent in Mohnbukta (Fig. 4b) and in the outer part of the Vaigattbogen landform assemblage. This can be attributed to glacier dynamics during the quiescent phase. The terminus of Hayesbreen was floating or close to flotation after the 1901 surge, thus inhibiting the formation of retreat moraines. If the buttressing effect of sea ice is considered to be the main process, which facilitates terminal advances during winter and the subsequent formation of retreat moraines, changes in sea-ice extent and conditions could determine if small transverse ridges are present in the paleo-record. Eskers are another glacial landform that is indicative of past glacial dynamics, suggesting that subglacial meltwater was drained efficiently through well-established drainage pathways. Eskers are locally present in the Svalbard fjords and have, for example, been mapped in front of Eton- and Hayesbreen.

The Svalbard glaciers have diverse surge histories, ranging from the recent multiple-surges of Tunabreen to the early Holocene surge in Mohnbukta, which has been attributed to rapid climatic and environmental change after the deglaciation. The role of climate appears to be more important in the evolution of general surge patterns than previously presumed. Data from the east coast suggest that glaciers in a region can switch in and out of surge cycling in response to climatic change. Environmental changes during the LIA could similarly explain why many Svalbard glaciers, both on the west and east coasts surged at the end of the LIA. In the case of Tunabreen every successive surge has reached a shorter distance from the ice divide, further suggesting that changes in external factors such as climate affect surge dynamics. This seems to confirm the enthalpy-cycle model put forward by Sevestre & Benn (2015) and Sevestre *et al.* (2015). If surge behavior is modulated by climate we should expect changes in Svalbard glacier dynamics in coincidence with the rapidly changing climatic conditions which occur currently in the Arctic. A recent surge of Tunabreen in 2016/17 supports this conclusion, demonstrating that the length of the surge cycle

follows general climatic trends. It has been suggested that the geometry of a glacier is an important factor in surge mechanisms, with long glaciers being more susceptible to surging (Sevestre & Benn 2015). The long, narrow profile of Tunabreen could explain why the glacier has experienced multiple-surges since the LIA. The differences in Svalbard glacier surge histories and surge styles suggest that local controls, such as subglacial drainage, bed conditions, glacier geometry, thermodynamics and positive feedback mechanisms are ultimately the most important factors in the evolution of glacial surges.

6.4. Conclusions

- During the late glacial fast-flowing ice converged into the Hinlopen Strait ice stream from the surrounding fjords. In Ripp- and Duvefjorden smaller ice streams with changing directions drained the northern Nordaustlandet section of the SBSIS. The ice flow velocities increased as ice reached the outer fjords and the shelf.
- The troughs and deeper sections of the fjords deglaciated rapidly by ice sheet lift-off and calving, whereas shallower areas experienced slower retreat with minor re-advances. The inner fjords around Nordaustlandet were ice free between 11.3-10.5 ka BP years.
- The surging tidewater glacier landform assemblages on the west and east coasts share many similarities and can be used to identify past surges in the geological record. However, they all also feature differences, suggesting that local conditions are important in the evolution of glacial surges and in the shaping of the geological record.
- The main difference between the fjords in east and west Svalbard is the occurrence of pre-LIA surge-type advances on the east coast. The tidewater glaciers in Mohnbukta and Vaigattbogen experienced at least one surge-type advance during early- to mid-Holocene. This suggests a more dynamic Holocene glacial history in Svalbard than previously assumed.
- Glacial surges during periods of environmental and climatic change, such as the onset of the Holocene, LIA and during present times, suggests that the role of climate

is more important in the evolution of general surge patterns than previously presumed. The early Holocene surge in Mohnbukta is suggested to have occurred due to rapid climatic and environmental change at the end of the deglaciation, leading to dynamic disequilibrium and an environmentally induced jump into surge-mode. Climatic change could similarly explain why many Svalbard glaciers, both on the west and east coasts, surged at the end of the LIA. This suggests that glaciers in a region can switch in and out of surge cycling in response to climatic change.

- If surge behavior is modulated by climate the rapidly changing climatic conditions occurring currently in the Arctic should be expected to lead to changes in Svalbard glacier dynamics. A recent surge of Tunabreen in 2016/17 supports this conclusion, demonstrating that the length of the surge cycle follows general climatic trends.

7. Future perspectives

Although this thesis provides new insights into the glacial history of northern and eastern Svalbard, and in particular into tidewater glacier history and dynamics, large areas of the Svalbard-Barents Sea remain unmapped and poorly studied. This holds true particularly for the areas east of Vaigattbogen, around Barents- Edgeøya and in eastern Nordaustlandet/Kvitøya, where detailed timing of maximum ice sheet extent and the style of deglaciations still remain uncertain. The glacial history of the fjords in the southern east coast of Spitsbergen has not been studied. A key question to investigate is if the pre-LIA surge-type advances in Mohnbukta and Vaigattbogen are unique events, or if similar advances have occurred in other fjord on the east coast, particularly in southern Spitsbergen? Another similar question raised during this study is the timing of the surge events in Wahlenbergfjorden.

This thesis focuses on large scale events, such as the deglaciation, LIA and Holocene surges. It would be beneficial to study the fjords presented in this thesis with a wider array of methods, in order to gain higher temporal resolution on past climate variability. Proxy records, such as foraminifera, diatoms, isotopes and biomarkers could be utilized for such purposes. There are yet no studies based on foraminifera

from the smaller east coast fjords. Microfossil studies could shed light on climatic and environmental changes during the Holocene, such as temperature, sea ice and oceanographic changes. Another gap in data is the lack of terrestrial studies in eastern Svalbard, which could provide a possibility for higher resolution, multi-proxy studies, from different environmental records.

The main objective for the future is to investigate the driving mechanisms behind past ice sheet and glacier dynamics. The underlying causes of dynamical ice behavior, such as glacial surges and flow shift in ice streams remain one of the main uncertainties. Interesting questions to be explored are 1) What are the triggering mechanisms behind dynamical events? 2) When and how long were major ice streams active? 3) Did ice streams change pathways through time, and if so, why? 4) Is the evolution of general surge patterns governed by climatic and environmental changes? The landform record provides only a short time slice of the final stages of the SBSIS and of the most recent surge. All previously existing landforms are modified or completely erased by ice flow during the end the ice sheets life cycle, the deglaciation, or the most recent surge cycle. Questions concerning ice dynamics can generally not be answered by geomorphological studies alone and require high-resolution ice sheet models in order to adequately capture past ice dynamics from a single, surging tidewater glacier to a full life cycle of an ice sheet. These models, in turn, are dependent on high-resolution geological and geomorphological data. In order to do validate model output we need to continue filling in the data gaps in the geological record.

Source of data

- Andreassen, K., & Winsborrow, M. (2009): Signature of ice streaming in Bjørnøyarena, Polar North Atlantic, through the Pleistocene and implications for ice-stream dynamics. *Annals of Glaciology*. Vol. 50: 17-26
- Andreassen, K., Winsborrow, M. C. M., Bjarnadóttir, L. R., & Rüther, D. C. (2014): Ice stream retreat dynamics inferred from an assemblage of landforms in the northern Barents Sea. *Quaternary Science Reviews*. Vol. 92: 246-257
- Applegate, P. J., Kirchner, N., Stone, E. J., Keller, K., & Greve, R. (2012): An assessment of key model parametric uncertainties in projections of Greenland Ice Sheet behavior *The Cryosphere*. Vol. 6: 589–606
- Batchelor, C. L., Dowdeswell, J. A., & Hogan, K. A. (2011): Late Quaternary ice flow and sediment delivery through Hinlopen Trough, Northern Svalbard margin: Submarine landforms and depositional fan. *Marine Geology*. Vol. 284: 13-27
- Batchelor, C. I., & Dowdeswell, J. A. (2014): The physiography of high Arctic cross-shelf troughs. *Quaternary Science Reviews*. Vol. 92: 68-96
- Bjarnadóttir, L. R., Rüther, D. C., Winsborrow, M. C. M., & Andreassen, K. (2013): Grounding-line dynamics during the last deglaciation of Kveithola, W Barents Sea, as revealed by seabed geomorphology and shallow seismic stratigraphy. *Boreas*. Vol. 42: 84-107
- Benestad, R. E., Hanssen-Bauer, I., Skaugen, T. E., & Førland, E. J. (2002): Associations between sea-ice and the local climate on Svalbard. *Report No 07/02, Norwegian Meteorological Institute*. 1-7
- Benn, D. I., & Evans, D. J. (2010): *Glaciers and glaciation*. Hodder Education. London
- Blaszczyk, M., Jania, J. A., & Hagen, J. O. (2009): Tidewater glaciers of Svalbard: Recent changes and estimates of calving fluxes. *Polish Polar Research*. Vol. 30: (2) 85-142
- Boulton, G. S., Jones, A. S., Clayton, K. M., & Kenning, M. J. (1977): A British Ice Sheet model and patterns of glacial erosion and deposition in Britain. In: Shotton, F.W., eds. *British Quaternary Studies*, Oxford, Clarendon Press. 231-246
- Brynjólfsson, S., Ingólfsson, Ó., & Schomacker, A. (2012): Surge fingerprinting of cirque glaciers at the Tröllaskagi peninsula, North Iceland, *Jökull*. Vol. 62: 151-166
- Bælum, K., & Benn, D. I. (2011): Thermal structure and drainage system of a small valley glacier (Tellbreen, Svalbard), investigated by ground penetrating radar. *The Cryosphere*. Vol. 5: 139-149
- Chauhan, T., Rasmussen, T. L., Noormets, R., Jakobsson, M., & Hogan, K. A. (2014): Glacial history and paleoceanography of the southern Yermak Plateau since 132 ka BP. *Quaternary Science Reviews*. Vol. 92: 155-169

- Chauhan, T., Rasmussen, T. L., & Noormets, R. (2015): Palaeoceanography of the Barents Sea continental margin, north of Nordaustlandet, Svalbard, during the last 74 ka. *Boreas*. Vol. 45: 76-99
- Christoffersen, P., Piotrowski, J. A., & Larsen, N. K. (2005): Basal processes beneath an Arctic glacier and their geomorphic imprint after a surge, Elisebreen, Svalbard. *Quaternary Research*. Vol. 64: (2) 125-37
- Clarke, G. K. C., Collins, S. G., & Thompson, D. E. (1984): Flow, thermal structure, and subglacial conditions of a surge-type glacier. *Canadian Journal of Earth Sciences*. Vol. 21: (2) 232-240
- Dallmann, W. K., Ohta, Y., Elvevold, S., & Blomeier, D. (2002): Bedrock map of Svalbard and Jan Mayen. *Norsk Polarinstitutt Temakart*. (Norwegian Polar Institute) No. 33
- De Geer, G. (1900): Om östra Spetsbergens glaciation under istiden. *Geologiska Föreningens i Stockholm Förhandlingar*. Vol. 22 (5): 427-36
- Donn, W. L., & Ewing, M. (1966): A theory of ice ages III. *Science*. Vol. 152: 1706-1712
- Dowdeswell, J. A., Hamilton, G. S., & Hagen, J. O. (1991): The duration of the active phase on surge-type glaciers: contrasts between Svalbard and other regions. *Journal of Glaciology*. Vol. 37: 388-400
- Dowdeswell, J. A., Hodgkins, R., Nuttall, A-M., Hagen, J. O., & Hamilton, G. S. (1995): Mass balance change as a control on the frequency and occurrence of glacial surges in Svalbard, Norwegian High Arctic. *Geophysical Research Letters*. Vol. 22. (No. 21): 2909-2912
- Dowdeswell, J. A., Hagen, J. O., Björnsson, H., Glazovsky, A. F., Harrison, W. D., Holmlund, P., Jania, J., Koerner, R. M., Lefauconnier, B., Ommanney, C. S. L., & Thomas, R. H. (1997): The mass balance of circum-arctic glaciers and recent climate change. *Quaternary Research*. Vol. 48: 1-14
- Dowdeswell, J. A., Ó Cofaigh, C., Taylor, J., Kenyon, N. H., Mienert, J., & Wilken, M. (2002): On the architecture of high-latitude continental margins: the influence of ice-sheet and sea-ice processes in the Polar North Atlantic. *Geological Society, London, Special Publications*. Vol. 203: 33-54
- Dowdeswell, J. A., & Benham, T. J. (2003): A surge of Perseibreen, Svalbard, examined using aerial photography and ASTER high-resolution satellite imagery. *Polar Research*. Vol. 22 (2): 373-83
- Dowdeswell, J. A., Hogan, K. A., Evans, J., Noormets, R., Ó Cofaigh, C., & Ottesen, D. (2010): Past ice-sheet flow east of Svalbard inferred from streamlined subglacial landforms. *Geology*. Vol. 38: 163-166
- Dowdeswell, J. A., Hogan, K. A., Ó Cofaigh, C., Fugelli, E. M. G., & Noormets, R. (2014): Late Quaternary ice flow in a West Greenland fjord and cross-shelf trough system: submarine landforms from Rink Isbrae to Uummannaq shelf and slope. *Quaternary Science Reviews*. Vol. 92: 292-309

- Drews, R. (2015): Evolution of ice-shelf channels in Antarctic ice shelves. *The Cryosphere*. Vol. 9: 1169–1181
- Elverhøi, A., & Solheim, A. (1983): The Barents Sea ice sheet—a sedimentological discussion. *Polar Research*. Vol. 1(1): 23–42
- Eyles, N., Eyles, C. H., & Miall, A. D. (1983): Lithofacies types and vertical profile models; an alternative approach to the description and environmental interpretation of glacial diamict and diamict sequences. *Sedimentology*. Vol. 30: 393–410
- Evans, D. J. A., & Rea, B. R. (1999): Geomorphology and sedimentology of surging glaciers: a land-systems approach. *Annals of Glaciology*. Vol. 28 (1): 75–82
- Farnsworth, W. R., Ingólfsson, Ó., Retelle, M., & Schomacker, A. (2016): Over 400 previously undocumented Svalbard surge-type glaciers identified. *Geomorphology*. Vol. 264: 52–60
- Flink, A. E., Noormets, R., Kirchner, N., Benn, D. I., Luckman, A., & Lovell, H. (2015): The evolution of a submarine landform record following recent and multiple surges of Tunabreen glacier, Svalbard. *Quaternary Science Reviews*. Vol. 108: 37–50
- Flink, A. E., Noormets, R., & Kirchner, N. (2016): Annual moraine ridges in Tempelfjorden, Spitsbergen. In: Atlas of Submarine glacial landforms: Modern, Quaternary and Ancient. *Geological Society, London, Memoirs*. (46): 75–76
- Flink, A. E., Noormets, R., Fransner, O., Hogan, A. K., Ó Regan, M., & Jakobsson, M. (2017): Past ice flow in Wahlenbergfjorden and its implications for late Quaternary ice sheet dynamics in northeastern Svalbard. *Quaternary Science Reviews*. Vol. 163: 162–179
- Flink, A. E., Hill, P., Noormets, R., & Kirchner, N. (in prep): Glacial history of Mohnbukta fjord, east Spitsbergen; inferred from submarine morphology and marine sediment cores. *Boreas*. Submitted
- Flink, A. E., & Noormets, R. (in prep). The glacial history of Vaigattbogen, eastern Spitsbergen. *Marine Geology*. Submitted
- Forwick, M., & Vorren, T. O. (2009): Late Weichselian and Holocene sedimentary environments in Isfjorden, Spitsbergen. *Palaeogeography, Palaeoclimatology, Palaeoecology*. Vol. 280: 258–274
- Fransner, O., Noormets, R., Flink, A. E., & Hohan, K. A. (2016): Crag-and-tail landforms in outer Rijpfjorden, Nordaustlandet, Svalbard. In: Atlas of Submarine glacial landforms: Modern, Quaternary and Ancient. *Geological Society, London, Memoirs*. (46): 57–58
- Fransner, O., Noormets, R., Flink, A. E., Hogan, K. A., O'Regan, M., & Jakobsson, J. (2017): Glacial landforms and their implications for glacier dynamics in Rijpfjorden and Duvefjorden, northern Nordaustlandet, Svalbard. *Journal of Quaternary Science*. Vol. 32(3): 437–455

- Fransner, O., Noormets, R., Flink, A. E., Hogan, K. A., & Dowdeswell, J. A. (in prep): Sedimentary processes on the continental slope off Kvitøya and Albertini troughs north of Nordaustlandet, Svalbard – the importance of structural-geological setting in trough-mouth fan development. *Marine Geology*. Submitted
- Gjermundsen, E. F., Briner, J. P., Akçar, N., Salvigsen, O., Kubik, P., Gantert, N. & Hormes, A. (2013): Late Weichselian local ice dome configuration and chronology in Northwestern Svalbard: early thinning, late retreat. *Quaternary Science Reviews*. Vol. 72: 112-27
- Grosswald, M. G., & Hughes, T. J., (1999): The case for an ice shelf in the Pleistocene Arctic Ocean. *Polar Geography*. Vol. 23: 23-54
- Hagen, J. O., Liestøl, O., Roland, E. & Jørgensen, T. (1993): Glacier atlas of Svalbard and Jan Mayen. *Meddelelser 129*. Oslo: Norsk Polarinstitutt. 141
- Hagen, J. O., Kohler, J., Melvold, K. & Winther, J.G. (2003): Glaciers in Svalbard: mass balance, runoff and freshwater flux. *Polar Research*. Vol. 22 (2): 145-59
- Hald, M., Ebbesen, H., Forwick, M., Godtliebsen, F., Khomenko, L., Korsun, S., Ringstad Olsen, L., & Vorren, T. O. (2004): Holocene paleoceanography and glacial history of the West Spitsbergen area, Euro-Arctic margin. *Quaternary Science Reviews*. Vol. 23: 2075–2088
- Hamilton, G. S. & Dowdeswell, J. A. (1996): Controls on glacier surging in Svalbard. *Journal of Glaciology*. Vol. 42 (140): 157-68
- Henriksen, M., Alexanderson, H., Landvik, J. Y., Linge, H., & Peterson, G. (2014): Dynamics and retreat of the Late Weichselian Kongsfjorden ice stream, NW Svalbard. *Quaternary Science Reviews*. Vol. 92: 235-245
- Hogan, K. A., Dowdeswell, J. A., Noormets, R., Evans, J., Ó Cofaigh, C., & Jakobsson, M. (2010a): Submarine landforms and ice-sheet flow in the Kvitøya Trough, northwestern Barents Sea. *Quaternary Science Reviews*. Vol. 29: 3545-3562
- Hogan, K. A., Dowdeswell, J. A., Noormets, R., Evans, J., & Ó Cofaigh, C. (2010b): Evidence for full-glacial flow and retreat of the Late Weichselian Ice Sheet from the waters around Kong Karls Land, eastern Svalbard. *Quaternary Science Reviews*. Vol. 29: 3563-3582
- Hogan, K. A., Dowdeswell, J. A., Hillenbrand, C-D., Ehrmann, W., Noormets, R., & Wacker, L. (in prep). Subglacial sediment pathways and deglacial chronology of the northern Barents Sea Ice Sheet. *Boreas*. Accepted
- Hoppe, G., Schytt, V., Häggblom, A., & Osterholm, H. (1969): The glacial history of Hopen. *Geografiska Annaler*. Vol. 5: 185-192
- Hormes, A., Akçar, N., & Kubik, P. W. (2011): Cosmogenic radionuclide dating indicates ice-sheet configuration during MIS 2 on Nordaustlandet, Svalbard. *Boreas*. Vol. 40: 636-649

- Hormes, A., Gjermundsen, E. F., & Rasmussen, T. L. (2013): From mountain top to the deep sea – Deglaciation in 4D of the northwestern Barents Sea ice sheet. *Quaternary Science Reviews*. Vol. 75: 78-99
- Hughes, T., Denton, G. H., & Grosswald, M. G. (1977): Was there a late-Wurm Arctic ice sheet? *Nature*. Vol. 266: 5603
- Hughes, A. L., Gyllencreutz, R., Lohne, S., Mangerud, J. & Svendsen, J. I. (2016): The last Eurasian ice sheets--a chronological database and time-slice reconstruction, DATED-1. *Boreas*. Vol. 45(1): 1-45
- Humlum, O., Instanes, A., & Sollid, J. L. (2003): Permafrost in Svalbard: a review of research history, climatic background and engineering challenges. *Polar research*. Vol. 22(2): 191-215
- Humlum, O., Elberling, B., Hormes, A., Fjordheim, K., Hansen, O. H., & Heinemeir, J. (2005): Late-Holocene glacier growth in Svalbard, documented by subglacial relict vegetation and living soil microbes. *The Holocene*. Vol. 15: 396-407
- Ingólfsson, Ó., & Landvik, J. Y. (2013): The Svalbard Barents Sea ice-sheet e Historical, current and future Perspectives. *Quaternary Science Reviews*. Vol. 64: 33-60
- IPCC. (2014): *Synthesis Report. Contribution of Working Groups I, II and III to the Fifth Assessment Report of the Intergovernmental Panel on Climate Change* [Core Writing Team, R.K. Pachauri and L.A. Meyer (eds.)]. IPCC, Geneva, Switzerland.
- Jakobsson, M., Anderson, J.B., Nitsche, F. O., Dowdeswell, J. A., Gyllencreutz, R., Kirchner, N., Mohammad, R., O'Regan, M., Alley, R. B., Anandakrishnan, S., Eriksson, B., Kirshner, A., Fernandez, R., Stollendorf, T., Minzoni, R., & Majewski, W. (2011): Geological record of ice shelf break-up and grounding line retreat, Pine Island Bay, West Antarctica. *Geology*. Vol. 39(7): 691-4
- Jakobsson, M., Andreassen, K., Bjarnadóttir, L. R., Dove, D., Dowdeswell, J. A., England, J. H., Funder, S., Hogan, K., Ingólfsson, Ó., Jennings, A., Krog Larsen, N., Kirchner, N., Landvik, J. Y., Mayer, L., Mikkelsen, N., Möller, P., Niessen, F., Nilsson, J., O'Regan, M., Polyak, L., Nørgaard-Pedersen, N., & Stein, R. (2014): Arctic Ocean glacial history. *Quaternary Science Reviews*. Vol. 92: 40-67
- Jakobsson, M., Nilsson, J., Anderson, L., Backman, J., Björk, G., Cronin, T. M., Kirchner, N., Koshurnikov, A., Mayer, L., Noormets, R., O'Regan, M., Stranne, C., Ananiev, R., Barrientos Macho, N., Cherniykh, D., Coxall, H., Eriksson, B., Flodén, T., Gemery, L., Gustafsson, Ö., Jerram, K., Johansson, C., Khortov, A., Mohammad, R. & Semiletov, I. (2016): Evidence for an ice shelf covering the central Arctic Ocean during the penultimate glaciation. *Nature communications*. Vol. 7: doi:10.1038/ncomms10365
- Jessen, S. P., Rasmussen, T. L., Nielsen, T., & Solheim, A. (2010): A new Late Weichselian and Holocene marine chronology for the western Svalbard slope 30,000-0 cal years BP. *Quaternary Science Reviews*. Vol. 29(9): 1301-12
- Jiskoot, H., Boyle, P., & Murray, T. (1998): The incidence of glacier surging in Svalbard: evidence from multivariate statistics. *Computers & Geosciences*. Vol. 24(4): 387-99

- Joughin, I., & Alley, R. B. (2011): Stability of the West Antarctic ice sheet in a warming world. *Nature Geoscience*. Vol. 4(8): 506-13
- Joughin, I., Smith, B. E. & Medley, B. (2014): Marine ice sheet collapse potentially under way for the Thwaites Glacier Basin, West Antarctica. *Science*. Vol. 344: 735–738
- Kaufman, D. S., Schneider, D. P., McKay, N. P., Ammann, C. M., Bradley, R. S., Briffa, K. R., Miller, G. H., Otto-Bliesner, B. L., Overpeck, J. T., & Vinther, B. M. (2009): Recent warming reverses long-term Arctic cooling. *Science*. Vol. 325(5945): 1236-9
- Kirchner, N., Hutter, K., Jakobsson, M., & Gyllencreutz, R. (2011): Capabilities and limitations of numerical ice sheet models: a discussion for Earth-scientists and modelers. *Quaternary Science Reviews*. Vol. 30: 3691-3704
- Kirchner, N., Ahlkrona, J., Gowan, E. J., Lötstedt, P., Lea, J. M., Noormets, R., von Sydow, L., Dowdeswell, J. A., & Benham, T. (2016): Shallow ice approximation, second order shallow ice approximation and full Stokes models: A discussion of their roles in palaeo-ice sheet modelling and development. *Quaternary Science Reviews*. Vol. 135: 103-114
- Kjær, K. H., Korsgaard, N. J., & Schomacker, A. (2008): Impact of multiple glacier surges - a geomorphological map from Brúarjökull, East Iceland. *Journal of Maps*. Vol. 4(1): 5-20
- Kleman, J., & Applegate, P. J. (2014): Durations and propagation patterns of ice sheet instability events. *Quaternary Science Reviews*. Vol. 92: 32-39
- Knies, J., Kleiber, H-P., Matthiessen, J., Muller, C., & Nowaczyk, N. (2001): Marine ice-rafted debris records constrain maximum extent of Saalian and Weichselian ice-sheets along the northern Eurasian margin. *Global and Planetary Change*. Vol. 31: 45-64
- Knies, J., Matthiessen, J., Vogt, C., Laberg, J. S., Hjelstuen, B. O., Smelror, M., Larsen, E., Andreassen, K., Eidvin, T., & Vorren, T. O. (2009): The Plio-Pleistocene glaciation of the Barents Sea–Svalbard region: a new model based on revised chronostratigraphy. *Quaternary Science Reviews*. Vol. 28: 812-829
- Koç, N., Klitgaard-Kristensen, D., Hasle, K., Forsberg, K. F., & Solheim, A. (2002): Late glacial palaeoceanography of Hinlopen Strait, northern Svalbard. *Polar Research*. Vol. 21: 307-314
- Kristensen, L., Benn, D. I., Hormes, A., & Ottesen, D. (2009): Mud aprons in front of Svalbard surge moraines: Evidence of subglacial deforming layers or proglacial glaciotectonics? *Geomorphology*. Vol. 111(3-4): 206-21
- Kristensen, D. K., Rasmussen, T. L., & Koç, N. (2013): Palaeoceanographic changes in the northern Barents Sea during the last 16 000 years - new constraints on the last deglaciation of the Svalbard-Barents Sea Ice Sheet. *Boreas*. Vol. 42(3): 798-813
- Laberg, J. S., Andreassen, K., Knies, J., Vorren, T. O., & Winsborrow, M. (2010): Late Pliocene–Pleistocene development of the Barents Sea Ice Sheet. *Geology*. Vol. 38(2): 107-110

- Landvik, J. Y., Bondevik, S., Elverhøi, A., Fjeldskaar, W., Mangerud, J., Salvigsen, O., Siegert, M. J., Svendsen, J.-I., & Vorren, T. O. (1998): The last glacial maximum of Svalbard and the Barents Sea area: ice sheet extent and configuration: *Quaternary Science Reviews*. Vol. 17: 43-75
- Landvik, J. Y., Ingólfsson, Ó., Mienert, J., Lehman, S. J., Solheim, A., Elverhøi, A., & Ottesen, D. (2005): Rethinking Late Weichselian ice sheet dynamics in coastal NW Svalbard. *Boreas*. Vol. 34: 7-24
- Lefauconnier, B., & Hagen, J. O. (1991): Surging and calving glaciers in eastern Svalbard. *Nor. Polarinst. Medd (Norwegian polarinstitute)*. Vol. 116: 1-130
- Lefauconnier, B., Hagen, J. O., & Rudant, J. P. (1994): Flow speed and calving rate of Kongsbreen glacier, Svalbard, using SPOT images. *Polar Research*. Vol. 13: 59-65
- Liestøl, O. (1969): Glacier surges in West Spitsbergen. *Canadian Journal of Earth Sciences*. Vol.6(4): 895-897
- Lovell, H., Fleming, E. J., Benn, D. I., Hubbard, B., Lukas, S., Rea, B. R., Noormets., R & Flink, A. E (2015): Debris entrainment and landform genesis during tidewater glacier surges. *Journal of Geophysical Research*. Vol. 120(8): 1574-1595
- Lovén, S. (1846): Några anmärkningar öfver de skandinaviska hafsmolluskernas geografiska utbredning. *Kungliga Vetenskaps Akademiens Handlingar*. 252-274
- Luckman, A., Murray, T., & Strozzi, T. (2002): Surface flow evolution throughout a glacier surge measured by satellite radar interferometry. *Geophysical Research Letters*. Vol. 29(23): doi:10.1029/2001GL014570
- Mangerud, J., Bolstad, M., Elgersma, A., Helliksem, D., Landvik, J. Y., Lonne, I., Lycke, A. K., Salvigsen, O., Sandahl, T., & Svendsen, J. I. (1992): The last glacial maximum on Spitsbergen, Svalbard. *Quaternary Research*. Vol. 28: 1-31
- Mangerud, J., Dokke, N. T., Hebbeln, D., Heggen, B., Ingólfsson, Ó., Landvik, J., Mejdahl, V., Svendsen, J. I., & Vorren, T. O. (1998): *Quaternary Science Reviews*. Vol. 17: 11-42
- Mangerud, J., Bondevik, S., Gulliksen, S., Hufthammer, K. A., & Hoisaeter, T. (2006): Marine 14C reservoir ages for 19th century whales and molluscs from the North Atlantic. *Quaternary Science Reviews*. Vol. 25: 3228-3245
- Mangerud, J., & Landvik, J. Y. (2007): Younger Dryas cirque glaciers in western Spitsbergen: smaller than during the Little Ice Age. *Boreas*. Vol. 36(3): 278-85
- Meier, M. F., & Post, A. (1969): What are glacier surges? *Canadian Journal of Earth Sciences*. Vol. 6(4): 807-17
- Mercer, J. H. (1970): A former ice sheet in the Arctic Ocean? *Palaeogeography, Palaeoclimatology, Palaeoecology*. Vol. 8(1): 19-27
- Miller, G. H., Brigham-Grette, J., Anderson, L., Bauch, H., Douglas, M. A., Edwards, M. E., Elias, S., Finney, B., Funder, S., Herbert, T., Hinzman, L., Kaufman, D. K.,

- MacDonald, G., Robock, A., Serreze, M., Smol, J., Spielhagen, R., Wolfe, A. P., & Wolff, E. (2009): Temperature and precipitation history of the Arctic. In: *Past Climate Variability and Change in the Arctic and at High Latitudes*. A report by the U.S. Climate Change Science Program and Subcommittee on Global Change Research. U.S. Geological Survey, Reston, VA. 31-90
- Murray, T., Luckman, A., Strozzi, T. & Nuttall, A.M. (2003): The initiation of glacier surging at Fridtjovbreen, Svalbard. *Annals of Glaciology*. Vol 36(1): 110-6
- Noormets, R., Kirchner, N., & Flink, A. E. (2016a): Medial moraines in Hambergbukta, south-eastern Spitsbergen. In: Atlas of Submarine glacial landforms: Modern, Quaternary and Ancient. *Geological Society, London, Memoirs*. (46): 61-62
- Noormets, R., Kirchner, N., Flink, A. E., & Dowdeswell, J. A. (2016b): Possible iceberg-produced terraces in Hambergbukta, Spitsbergen. In: Atlas of Submarine glacial landforms: Modern, Quaternary and Ancient. *Geological Society, London, Memoirs*. (46): 102-102
- Nuth, C., Moholdt, G., Hagen, J. O., & Kääh, A. (2010): Svalbard glacier elevation changes and contribution to sea level rise. *Journal of Geophysical Research*. Vol. 115: doi:10.1029/2008JF00122
- Nuth, C., Kohler, J., König, M., von Deschwenden, A., Kääh, A., Moholdt, G., & Pettersson, R. (2013): Decadal changes from a multi-temporal glacier inventory of Svalbard. *The Cryosphere*. Vol. 7: 1603-1621
- Ó Cofaigh, C., Pudsey, C. J., Dowdeswell, J. A., & Morris, P. (2002): Evolution of subglacial bedforms along a paleo-ice stream, Antarctic Peninsula continental shelf. *Geophysical Research Letters*. Vol. 29(8): doi:10.1029/2001GL01448
- Ottesen, D., Dowdeswell, J. A., & Rise, L. (2005): Submarine landforms and the reconstruction of fast-flowing ice streams within a large Quaternary ice sheet: The 2500-km-long Norwegian-Svalbard margin (57-80 N). *Geological Society of America Bulletin*. Vol. 117(7-8): 1033-50
- Ottesen, D., & Dowdeswell, J. A., (2006): Assemblages of submarine landforms produced by tidewater glaciers in Svalbard. *Journal of Geophysical Research, Earth Surface*. Vol.111: 1-16
- Ottesen, D., Dowdeswell, J. A., Landvik, J. Y., & Mienert, J. (2007): Dynamics of the Late Weichselian ice sheet on Svalbard inferred from high-resolution sea-floor morphology. *Boreas*. Vol. 36: 286-306
- Ottesen, D., Dowdeswell, J. A., Benn, D. I., Kristensen, L., Christiansen, H. H., Christensen, O., Hansen, L., Lebesbye, E., Forwick, M., & Vorren, T. O. (2008): Submarine landforms characteristic of glacier surges in two Spitsbergen fjords. *Quaternary Science Reviews*. Vol. 27: 1583-1599
- Ottesen, D., & Dowdeswell, J.A. (2009): An inter-ice-stream glaciated margin: Submarine landforms and a geomorphic model based on marine-geophysical data from Svalbard. *Geological Society of America Bulletin*. Vol. 121: 1647-1665

- Patton, H., Andreassen, K., Bjarnadóttir, L. R., Dowdeswell, J. A., Winsborrow, M. C. M., Noormets, R., Polyak, L., Auriac, A., & Hubbard, A. (2015): Geophysical constraints on the dynamics and retreat of the Barents Sea Ice Sheet as a palaeo-benchmark for models of marine ice-sheet deglaciation. *Reviews of Geophysics*. Vol. 53: 1051-1098
- Petterson, R., Jansson, P., & Blatter, H. (2004): Spatial variability in water content at the cold-temperate transition surface of the polythermal Storglaciären Sweden. *Journal of Geophysical Research*. Vol. 109: doi:10.1029/2003JF000110
- Rasmussen, T. L., Thomsen, E., Ślubowska, M. A., Jessen, S., Solheim, A. & Koç, N. (2007): Paleoceanographic evolution of the SW Svalbard margin (76°N) since 20,000 14C yr BP. *Quaternary Research*. Vol. 67(1): 100-14
- Rasmussen, T. L., & Thomsen, E., (2015): Palaeoceanographic development in Storfjorden, Svalbard, during the deglaciation and Holocene: evidence from benthic foraminiferal records. *Boreas*. Vol. 44: 24-44
- Rea, B. R., & Evans, D. J. A., (2011): An assessment of surge-induced crevassing and the formation of crevasse squeeze ridges. *Journal of Geophysical Research*. Vol. 116: doi:10.1029/2011JF001970.
- Reimer, P. J., Bard, E., Bayliss, A., Beck, J. W., Blackwell, P. G., Bronk Ramsey, C., Buck, C. E., Cheng, H., Edwards, R. L., Friedrich, M., Grootes, P. M., Guilderson, T. P., Hafliðason, H., Hajdas, I., Hattel, C., Heaton, T. J., Hoffmann, D. L., Hogg, A. G., Hughen, K. A., Kaiser, K. F., Kromer, B., Manning, S. W., Niu, M., Reimer, R. R., Richards, D. A., Scott, M. E., Southon, J. R., Staff, R. A., Turney, C. S. M., van der Plicht, J. (2013): INTCAL13 and Marine13 Radiocarbon age calibration curves, 0-50,000 years cal BP. *Radiocarbon*. Vol. 55: 1869-1887
- Rignot, E., Mouginot, J., & Scheuchl, B. (2011): Ice flow of the Antarctic ice sheet. *Science*. Vol. 333: 1427-1430
- Salvigsen, O., Formann, S. L., & Miller, G. H. (1992): Thermophilous molluscs on Svalbard during the Holocene and their paleoclimatic implications. *Polar Research*. Vol. 11: 1-10
- Schytt, V., Hoppe, G., Blake Jr, W. & Grosswald, M. G. (1968): The extent of the Würm glaciation in the European Arctic. *International Association of Scientific Hydrology*. Vol. 79: 207-16
- Schomacker, A., Benediktsson, O. I., & Ingólfsson, Ó. (2014): The Eyjabakkajökull glacial landsystem, Iceland: Geomorphic impact of multiple surges. *Geomorphology*. Vol. 218: 98-107
- Sevestre, H., Benn, D. I., Hulton, N. R. J., & Baelum, K. (2015): Thermal structure of Svalbard glaciers and implications for thermal switch models of glacier surging *Journal of Geophysical Research: Earth Surface*. Vol. 120(10): 2220-36
- Sevestre, H. & Benn, D. I. (2015): Climatic and geometric controls on the global distribution of surge-type glaciers: implications for a unifying model of surging. *Journal of Glaciology*. Vol. 61(228): 646-62

- Solheim, A. & Kristoffersen, Y. (1984): Sediments above the upper regional unconformity: thickness, seismic stratigraphy and outline of the glacial history. *Norsk Polarinstitutt Skrifter. Oslo.* (179B)
- Solheim, A. (1991): The depositional environment of surging sub-polar tidewater glaciers: A case study of the morphology, sedimentation and sediment properties in a surge affected marine basin outside Nordaustlandet, the Northern Barents Sea. *Norsk Polarinstitutt Skrifter. Oslo.* (194): 5-97
- Streuff, K., Forwick, M., Szczuciński, W., Andreassen, K. & Ó Cofaigh, C. (2015): Submarine landform assemblages and sedimentary processes related to glacier surging in Kongsfjorden, Svalbard. *Arktos.* Vol. 1(14): 10.1007/s41063-015-0003-y
- Stuiver, M., & Reimer, P. J. (1993): Extended 14C database and revised CALIB radiocarbon calibration program. *Radiocarbon.* Vol. 35: 215-230
- Sund, M., Eiken, T., Hagen, J.O., & Kääb, A. (2009): Svalbard surge dynamics derived from geometric changes, *Annals of Glaciology.* Vol. 50(52): 50-60
- Svendsen, J. I., Elverhøi, A., & Mangarud, J. (1996): The retreat of the Barents Sea Ice Sheet on the western Svalbard margin. *Boreas.* Vol. 25(4): 244-56
- Svendsen, J. I., & Mangerud, J. (1997): Holocene glacial and climatic variations on Spitsbergen, Svalbard. *The Holocene.* Vol. 7(1):45-57
- Svendsen, J. I., Alexanderson, H., Astakhov, V. I., Demidov, I., Dowdeswell, J. A., Funder, S., Gataullin, V., Henriksen, M., Hjort, C., Houmark-Nielsen, M., Hubberten, H. W., Ingólfsson, Ó., Jakobsson, M., Kjær, K.H., Larsen, E., Lokrantz, H., Lunkka, J. P., Lyså, A., Mangerud, J., Matiouchkov, A., Murray, A., Möller, P., Niessen, F., Nikolskaya, O., Polyak, L., Saarnisto, M., Siegert, C., Siegert, M. J., Spielhagen, R. F., & Stein, R. (2004): Late Quaternary ice sheet history of northern Eurasia. *Quaternary Science Reviews.* Vol. 23: 1229-1271
- Torell, O. (1873): Undersökningar över istiden 2. *Öfversikt af Kongliga Vetenskapsakademiens Handlingar.* 47-64
- Vorren, T. O., & Kristoffersen, Y. (1986): Late Quaternary glaciation in the south western Barents Sea. *Boreas.* Vol. 15(1): 51-9
- Vorren, T. O., Laberg, J. S., Blaume, F., Dowdeswell, J. A., Kenyon, N. H., Mienert, J., Rumohr, J., & Werner, F. (1998): The Norwegian Greenland Sea continental margins: morphology and late Quaternary sedimentary processes and environment. *Quaternary Science Reviews.* Vol. 17: 273-302
- Vorren, T. O., Landvik, J. Y., Andreassen, K., & Laberg, J. S. (2011): Quaternary Glaciations – Extent and Chronology, A Closer Look. *Developments in Quaternary Science.* Vol. 15: 361-72
- Österholm, H. (1978): The Movement of the Weichselian Ice Sheet over Northern Nordaustlandet, Svalbard. *Geografiska Annaler, Series A, Physical Geography.* (6): 189-208

Research papers



The evolution of a submarine landform record following recent and multiple surges of Tunabreen glacier, Svalbard



Anne Elina Flink^{a,*}, Riko Noormets^a, Nina Kirchner^{b,c}, Douglas I. Benn^{a,d},
Adrian Luckman^{a,f}, Harold Lovell^{e,a}

^a Departments of Arctic Geology and Arctic Geophysics, University Centre in Svalbard, 9170 Longyearbyen, Norway

^b Department of Physical Geography and Quaternary Geology, Stockholm University, 106 91 Stockholm, Sweden

^c Bolin Centre for Climate Research, Stockholm University, 106 91 Stockholm, Sweden

^d Department of Geography and Sustainable Development, University of St Andrews, KY169AL, St Andrews, Scotland, UK

^e School of Geography, Queen Mary University of London, E14NS, London, UK

^f Department of Geography, College of Science, Swansea University, SA2 8PP, UK

ARTICLE INFO

Article history:

Received 15 April 2014

Received in revised form

7 November 2014

Accepted 11 November 2014

Available online

Keywords:

Submarine landforms

Tidewater glacier

Glacier surges

Multibeam-bathymetric data

Remote sensing

Svalbard

ABSTRACT

This study focuses on the glacial landform record associated with recent surge events of Tunabreen – a calving tidewater glacier in Tempelfjorden, Spitsbergen. Submarine geomorphology and recent terminal fluctuations of Tunabreen's glacier front were studied using high-resolution multibeam-bathymetric data and a range of published and remote-sensing sources, including topographic maps, satellite images and aerial photographs. The retreat moraines in the inner part of Tempelfjorden have been correlated with glacier terminus positions during retreat from the 2004 surge maximum. Glacier surface velocity and ice-front positions derived from high-resolution TerraSAR-X satellite data show ice movements at the glacier front during minor advances of the front in winter when calving is suppressed. This suggests that the moraines have formed annually during quiescent phase winter advances.

Tunabreen has experienced three surges since the Little Ice Age (LIA). This is in contrast with most Svalbard surging glaciers which have long quiescent phases and have typically only undergone one or two surges during this time. The landform record in Tempelfjorden is distinguished from previously studied glacier-surge landsystems by four, well-preserved sets of landform assemblages generated by the LIA advance and three subsequent surges, all of which partly modify earlier landform records. Based on the unique landform record in Tempelfjorden, a new conceptual landsystem model for frequently surging glaciers has been put forward improving our understanding of the dynamics of the surging glaciers and, most importantly, how they can be distinguished from the climatically-controlled glaciers in the geological record.

© 2014 Elsevier Ltd. All rights reserved.

1. Introduction

Glaciers are sensitive indicators of climate change, and sequences of moraines demarcate glacial retreat or readvance that can often be used as proxies for past climatic fluctuations. However, major glacier advances known as surges, can also occur in response to internal dynamical processes which are largely thought to be unrelated to climatic variations (Meier and Post, 1969; Fowler et al.,

2001). Glacier surges in the High-Arctic archipelago of Svalbard are characterized by long periods of quiescence (100–150 years) punctuated by short phases of increased ice velocities, usually accompanied by terminus advance. These surge events, or active phases, typically last for ~3–10 years (Dowdeswell et al., 1991; Murray et al., 2003). To avoid misinterpretation, it is important to distinguish glacial landforms formed during surges from those created by climatically-controlled advances.

Conceptual descriptions of glacial landform records, known as landsystem models, have been developed for both, terrestrial and fjord-terminating surging glaciers (e.g. Evans and Rea, 1999, 2003; Ottesen and Dowdeswell, 2006; Ottesen et al., 2008; Benediktsson et al., 2010; Brynjólfsson et al., 2012). However, it is likely that the

* Corresponding author. University Centre in Svalbard, PO Box 156, 9171, Longyearbyen, Norway.

E-mail address: AnneF@unis.no (A.E. Flink).

examples described to date encompass only part of the range of variation. There is a particular need for studies of glacial landform records that can be directly linked to observed surge events, to provide benchmarks for the interpretation of geomorphological data where the glacial history is not independently known.

In this paper, we present detailed observations of the glacial landform record of Tunabreen, a tidewater surge-type glacier in central Spitsbergen (Fig. 1). The glacier is known to have surged in c.1930, 1971 and 2003–2005. Glacier behavior during and following the 2003–2005 event is particularly well known (e.g. Fleming et al. 2013). Using a combination of multibeam echosounding mapping of the fjord floor, remote-sensing data, and ground-based observations of the glacier we show how the geomorphological record in Tempelfjorden expresses key glaciological processes which have been active during multiple surge cycles.

2. Geological and glaciological setting

Tunabreen is an outlet glacier of the Lomonosovfonna ice cap that terminates at the head of Tempelfjorden, the easternmost branch of Isfjorden, Spitsbergen (Fig. 1). Tempelfjorden is about 14 km long, up to 5 km wide, and has a surface area of nearly 57 km². The maximum water depth is 110 m. The sedimentary environment in Tempelfjorden has been influenced mainly by Tunabreen, its neighboring glacier von Postbreen, and the Sassenelva River during the late- and post-glacial period. Changes in the sediment sources and sedimentation conditions have been suggested to reflect the multiple advances and retreats of the glacier fronts during the Holocene (Forwick et al., 2010).

During the early and mid-Holocene between 10 and 5 ka BP, tidewater glaciers were most likely absent from the Isfjorden area or at least reduced in size (Mangerud et al., 1992; Svendsen and Mangerud 1992; Forwick and Vorren, 2009). They re-advanced

into the fjord during the late Holocene around 4 ka BP, and reached their most recent maxima during the Little Ice Age (LIA) advance around 1850 AD (Svendsen et al., 1996; Plassen et al., 2004; Forwick and Vorren, 2009). The confluent von Postbreen and Tunabreen glacier system reached its late Holocene maximum position in the 1870s, probably at the culmination of a surge (Plassen et al., 2004). This event produced a large terminal moraine with debris-flow lobes on its distal slope, similar to those observed in front of other tidewater surging glaciers in Svalbard (Plassen et al., 2004; Ottesen and Dowdeswell, 2006; Ottesen et al., 2008).

After the 1870 advance, von Postbreen appears to have been quiescent and in continuous retreat, and is now entirely land-based. Tunabreen remained in contact with the fjord floor and underwent general retreat interrupted by surges in the 1930s, 1970s and the early 2000s, with each subsequent surge being less extensive than the previous one. During its most recent surge in 2003–2005, Tunabreen advanced about 2 km. The rather regular 40-year surge cycle of Tunabreen is the shortest known in Svalbard; many of Svalbard's glaciers have surge cycles of over one hundred years (Dowdeswell et al., 1991). The short surge cycle of Tunabreen and the diverse observational record for this glacier, therefore, provides a unique opportunity to study the imprint of repeated surge events on the seafloor morphology.

3. Datasets and methods

Mapping and analysis of the submarine landforms and the terminus positions of Tunabreen in the inner part of Tempelfjorden is based on multibeam-bathymetric, remote-sensing, and published data, including ice-marginal positions and their chronology. The multibeam-bathymetric data were acquired with a Kongsberg EM3002, a 300 kHz multibeam echosounder system by the Norwegian Hydrographic Service from 3rd to 7th July, 2011. The data

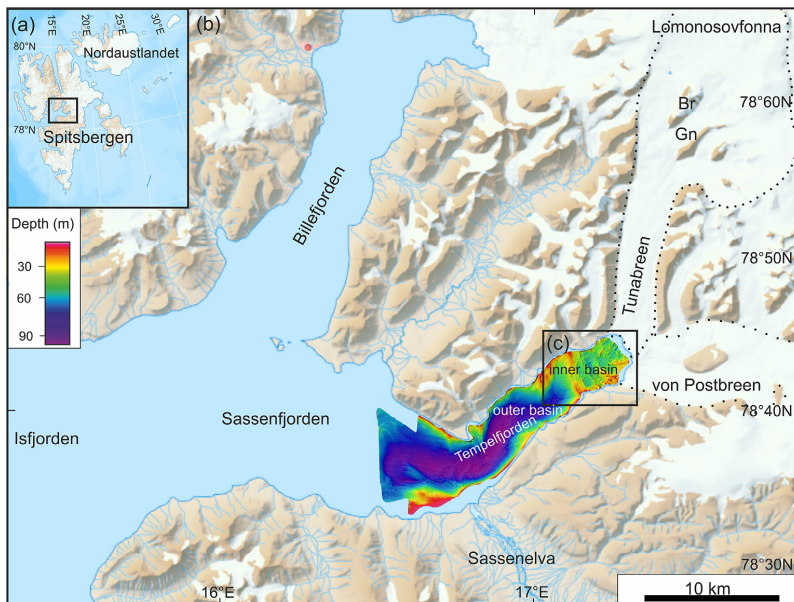


Fig. 1. Site map. (a) The location of the Isfjorden fjord system in central Spitsbergen. (b) Location of Tunabreen, von Postbreen and Tempelfjorden. Dashed lines outline the glacier systems of Tunabreen and von Postbreen. Br and Gn mark the locations of Bromsfjella and Gnomfjella, respectively. (c) The black rectangle shows the main study area in the inner part of Tempelfjorden (Fig. 4). Background maps are from Svalbardkartet (Norwegian Polar Institute, NPI).

were processed by applying optimal sound–velocity profiles to determine accurate water depths and gridded into an isometric grid with cell size of 5×5 m in the Caris and QPS Fledermaus softwares. The UTM 33N projection was used with the WGS 84 datum.

Satellite images (Landsat, ASTER, Envisat and TerraSAR-X), aerial photographs, and topographic maps were used for establishing the glacier margin positions between the 1970s and 2012. Terminus positions prior to the 1970s are based on published data (De Geer, 1910; Liestøl, 1969; Plassen et al., 2004; see Table 1 for a summary of data sources). All images were georeferenced or reprojected to the UTM 33N projection (WGS84 datum) in order to facilitate correlation with the multibeam-bathymetric data. The Landsat data contain images collected during the summer months as well as in the winter months (Table 1). The ASTER images were all obtained during the summer months, June–September. The wide-swath-mode SAR images of the Tunabreen area were taken by the European Space Agency (ESA) Envisat satellite during late summer.

By analyzing images taken during different periods of the year (summer and winter) and by combining data from different sources, a quasi-continuous record of glacier terminus fluctuations has

been obtained. Additionally, high spatial resolution data were obtained during 2013 and early 2014 on the annual cycle of ice-front activity of Tunabreen using TerraSAR-X data. Feature tracking a pair of TerraSAR-X images provides glacier surface velocities by detecting the movement of identifiable objects, speckle patterns or phase changes in the image samples. Ice margins and submarine landforms were tracked and digitized in ArcGIS. Cloud free images taken during the summer months were chosen for tracking the ice margins and crevasse positions.

4. Results

4.1. History of terminus fluctuations in Tempelfjorden

Tidewater margin fluctuations in Tempelfjorden from 1870 to 2012, encompassing the surges of Tunabreen and von Postbreen, are shown in Fig. 2. The westernmost mapped margin, located 4.5 km from the Tunabreen marginal position in 2012 is the LIA maximum of von Postbreen in 1870 as mapped by De Geer (1910) (Fig. 2). This represents the maximum glacier extent in Tempelfjorden during the Holocene and the culmination of LIA glacier regrowth following an extended period of stepwise retreat after the Last Glacial (Forwick et al., 2010). The maximum extent of von Postbreen could either reflect a surge event or a period of strong positive mass balance. The position of the von Postbreen terminus was also mapped in 1882, 1896 and 1908 by De Geer (1910), indicating a retreat of 2 km in 40 years (Fig. 2).

Glacier retreat in Tempelfjorden continued until 1930, when Tunabreen surged to a position 1 km upfjord from the 1870 position of von Postbreen. The switch of the dominant flow unit from von Postbreen to Tunabreen during this advance is clear in oblique photographs published by Liestøl (1969), which show a small, pinched-out Tunabreen comprising <25% of the coalescent terminus and a deflected medial moraine in 1924. This contrasts with the situation in 1932, where Tunabreen made up over a third of the advanced coalescent terminus and a straightened medial moraine is evident. Following the 1930s surge, Tunabreen retreated around 3 km during 36 years until the next mapped position in 1966, by which time von Postbreen had retreated onto land. Between 1966 and 1970, Tunabreen began to surge again and had advanced 2 km by 1971 (Hodgkins and Dowdeswell, 1994). The 1971 surge terminated 1 km upfjord from the 1930s surge maximum (Fig. 2). The retreat of the margin following the 1970s surge is well documented in satellite and aerial images and shows a stepwise retreat of 3 km in 31 years up to 2002 (Fig. 2).

Between June 2002 and August 2003, the Tunabreen margin began to advance, providing the first visible signs of the most recent surge (Fig. 3). The heavily-splayed 2004 margin delimits the surge maximum, recording a margin advance of 2 km to a position 1 km up-fjord from the 1971 surge maximum. Up-glacier propagation of crevasses has been observed during the surge cycle, starting with crevasses only at the front of the glacier in 2002. In 2004 the crevasses had propagated along the entire length of the glacier (Fig. 3). The surge terminated sometime between July 2004 and June 2005. After 2005 the terminus underwent a stepwise retreat of 1.5 km to its 2012 position at rates of $100\text{--}300 \text{ m a}^{-1}$.

Fig. 2 demonstrates that each surge of Tunabreen has been characterized by an advance of 2 km and has reached a maximum position 1 km up-fjord from the previous surge limit. Furthermore, Fig. 2 suggests that Tunabreen has a remarkably short, and over the time period where data is available, consistent surge-cycle length in the context of Svalbard surge-type glaciers (only Blomstrandbreen at c. 47 years is comparable; Mansell et al., 2012).

Table 1
Summary of data types and sources used for mapping the terminal position of Tunabreen.

Data type and details	Terminus position data acquired (dd/mm/yy) or (mm/yy) or (yyyy)	Source
Published data		
Liestøl (1969)	1924–1932	Mapped photogrammetrically
Hodgkins and Dowdeswell (1994)	1966–1971	Aerial photographs
Plassen et al. (2004)	1870 1882 1896 1908 1930 1966 1971 1990	Topographic maps and aerial image from the Norwegian polar institute. Maps by De Geer (1910).
Norwegian Polar Institute (NPI) maps (1:100,000 scale)	1993	
Satellite imagery		
Landsat MSS (80 m pixel resolution)	09/04/75 18/07/76 24/07/79 19/10/82	USGS Earth Explorer (https://earthexplorer.usgs.gov)
Landsat TM (30 m pixel resolution)	26/06/88 27/07/06	Global Land Cover Facility (www.landcover.org)
Landsat ETM+ (30 m pixel resolution)	09/07/99 17/06/01 18/08/11 19/07/12	USGS Earth Explorer (https://earthexplorer.usgs.gov)
ASTER (15 m pixel resolution)	13/06/02 12/07/03 25/07/04 16/06/05 01/08/10	Land Processes Distributed Active Archive Center (http://LPDAAC.usgs.gov)
ENVISAT SAR (150 m resolution)	2007/10 2008/10	European Space Agency
TerraSAR-X (2 m resolution)	03/13–02/14	DLR (German Space Agency)
Aerial photographs		
NPI aerial photographs (1:50,000 scale)	20/08/95 27/07/04 02/08/09	Norwegian Polar Institute (NPI)

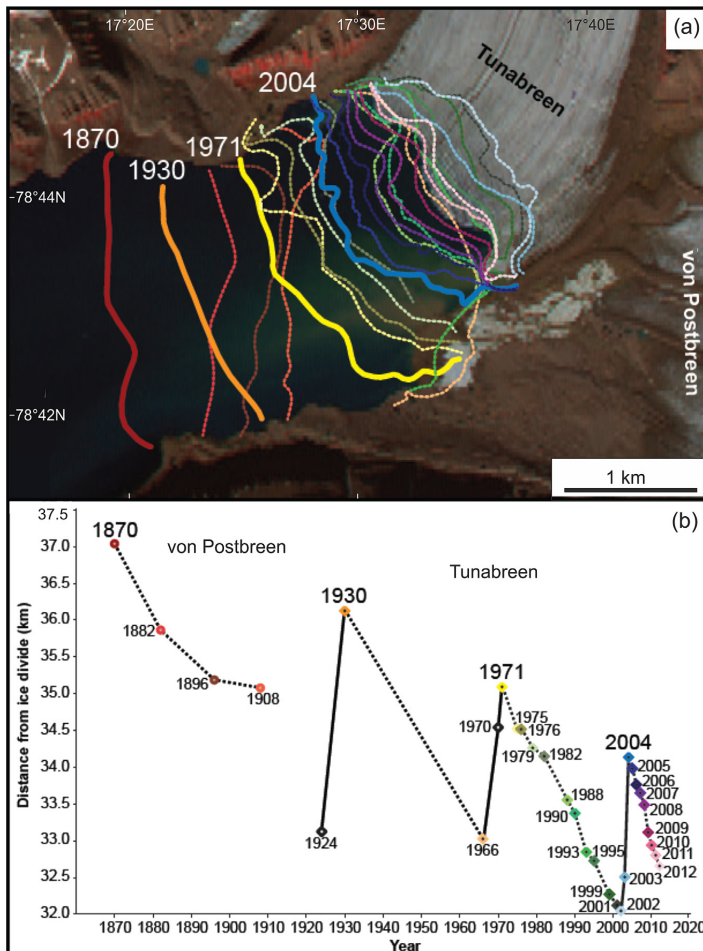


Fig. 2. Glacier terminus fluctuations in Tempelfjorden between 1870 and 2012. (a) Terminus positions derived from a range of data sources (see Table 1) overlain on a 2009 aerial image (NPI). Thicker lines show surge maximums. (b) Terminus positions plotted as distance along a centre line from Lomonosovfonna ice divide (derived from Hagen et al., 1993). The 1924, 1970 positions are not mapped limits but are relative positions based on observations in Liestøl (1969) and Hodgkins and Dowdeswell (1994).

4.2. Description and interpretation of submarine landforms

Tempelfjorden comprises of two basins, a larger outer basin and a smaller inner basin (Fig. 1). The outer basin has a maximum depth of 110 m, whereas the inner basin is 60 m deep at its maximum. The von Postbreen terminal moraine ridge, deposited at its LIA maximum extent in the 1870s (Fig. 2), separates the two basins. The landforms in the outer part of Tempelfjorden have been described in previous studies (Plassen et al., 2004; Forwick et al., 2010). These landforms include the von Postbreen terminal moraine and two debris-flow lobes on its distal slope. The surface of the stratigraphically lower debris-flow lobe has been deformed into thrust moraines (De Geer, 1910; Plassen et al., 2004; Forwick et al., 2010). In this study, we focus on the geomorphological features in the previously unexplored inner part of Tempelfjorden (Fig. 4).

4.2.1. Elongate streamlined bedforms: glacial lineations

4.2.1.1. Description. Elongate, streamlined bedforms, oriented parallel to the fjord axis, occur in several places on the seafloor in Tempelfjorden down to water depths of 50 m (Fig. 4). The elongation ratio of the ridges is 5:1. Typically, these bedforms rise between 1 and 3 m above the surrounding seafloor (Fig. 5a and e). Ridge width varies between 50 and 150 m and they are usually around 500 m long. However, some of the ridges closest to Tunabreen are up to 1000 m in length. The distance between the crests and troughs of these bedforms is typically 50–100 m. Some of the streamlined bedforms are superimposed on large streamlined mounds which are up to 10 m high. We have identified streamlined bedforms in front of the present glacier terminus, west of the 2004 surge maximum, and in the area between the 1930s and 1970s surge limits (Fig. 4). Adjacent to the present glacier front, one of the

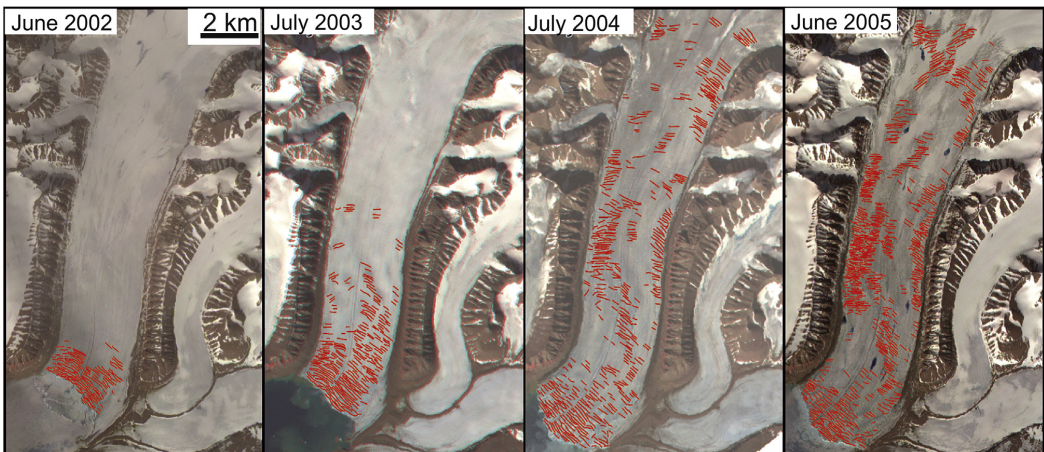


Fig. 3. Landsat satellite images showing up-glacier propagation of crevasses during the most recent surge of Tunabreen between 2002 and 2005.

streamlined bedforms appears to be coincident with the debris-rich medial moraine of Tunabreen, pointed out with a black arrow (Fig. 4a).

4.2.1.2. Interpretation. The elongated, streamlined bedforms are interpreted as glacial lineations produced by soft-sediment deformation at the glacier-bed interface. The lineations form parallel to ice flow, in the presence of a saturated deformable till (King et al., 2009). Glacial lineations are typical of fast-flowing glacier ice (Stokes and Clark, 2002; Ottesen and Dowdeswell, 2006; King et al., 2009), and are therefore consistent with a surge advance of Tunabreen.

Adjacent to the present glacier front, one of the streamlined bedforms appears to be coincident with the debris-rich medial moraine of Tunabreen (Fig. 4a). The unusually large size of the ridge suggests that it is not a pure glacial lineation, but could be an overridden medial moraine.

4.2.2. Large transverse ridges: surge terminal moraines

4.2.2.1. Description. Four NW–SE aligned, large cross-fjord ridges occur on the seafloor of the inner Tempelfjorden and are oriented transverse to the fjord axis. The innermost ridge, R1, is located 1.4 km from the 2012 glacier front and curves across the entire, 3 km-wide fjord (Fig. 4). The ridge is 6–8 m high and 50 m wide. The second ridge, R2, is located 2.2 km from the 2012 glacier front, is 10–15 m high, 50–100 m wide and 3 km long. The third ridge, R3, is located 3 km from the 2012 glacier front. The ridge has a width of 150–200 m, extends 3.5 km across the entire fjord and has an average height of 10 m. The fourth ridge, R4 is 3.5 km long and 1 km wide. It is maximum 70 m high and contains multiple crestlines. Large debris-flow lobes are present on the distal side of the R4 ridge. The ridge and the debris-flow lobes are described in further detail by Hagen et al. (1993), Plassen et al. (2004) and Forwick et al. (2010). In general, the large transverse ridges are asymmetric, with 10°–20° steep ice-proximal slopes, and distal slopes between 5° and 10°. The R4 ridge has significantly gentler slopes of 2°–6°. The ridges are typically multi-crested along their entire lengths. The exception is the R1 ridge, which is mainly single-crested, but has some multi-crested sections.

4.2.2.2. Interpretation. The locations of the large ridges correlate well with the ice-terminus positions of Tunabreen as mapped from remote-sensing and published data (Fig. 2). The easternmost ridge, R1, displays a strong spatial correlation with the maximum position of the glacier front in 2004 (Fig. 4). The glacier position during the 1970's surge according to Plassen et al. (2004) correlates well with the position of the second large submarine moraine, R2, and the position of R3 correlates with the mapped position of the glacier front during the 1930s (Plassen et al., 2004). We therefore interpret the ridges R3, R2 and R1 as terminal moraines formed during the surge maxima in 1930, 1971 and 2004, respectively.

The westernmost large transverse ridge, R4, is contiguous with the subaerial moraines on both sides of Tempelfjorden, which together are interpreted as the latero-terminal moraine system formed by von Postbreen during its LIA maximum (De Geer, 1910; Hagen et al., 1993; Plassen et al., 2004). The R4 ridge with multiple crestlines, large debris-flows lobes and numerous dislocated sediment blocks on its distal slope is morphologically similar to terminal moraines formed by surges in other Svalbard fjords (cf. Ottesen and Dowdeswell, 2006; Ottesen et al., 2008). Kristensen et al. (2009) have argued that this type of moraine forms by bulldozing of marine mud in front of the surging glacier with quasi-continuous failure of weak, saturated sediments on the moraine front. In contrast, large debris-flow lobes are not present on the distal slopes of ridges R1–R3, although the asymmetric, multi-crested form of these ridges indicates that they were also likely formed by ice push (cf. Boulton et al., 1996). We suggest that the absence of large debris-flow lobes adjacent to the R1–R3 ridges reflects lower sediment availability because of the relatively short surge interval of only 40–60 years, during which there would have been little time for accumulation of mud on the fjord floor between the surge events. Furthermore, much of the pre-existing soft sediment (sediment that accumulated on the sea floor pre-1870) had been pushed up into the LIA moraine, which helps to explain the size of the 1870 moraine (R4) when compared to the R1–R3 moraines.

The large transverse ridges in Tempelfjorden are in general smaller, in both height and width, than surge terminal moraines mapped elsewhere in Svalbard (Ottesen and Dowdeswell, 2006; Ottesen et al., 2008). The von Postbreen LIA moraine, which is up to 1 km wide, is most similar to the surge moraines described

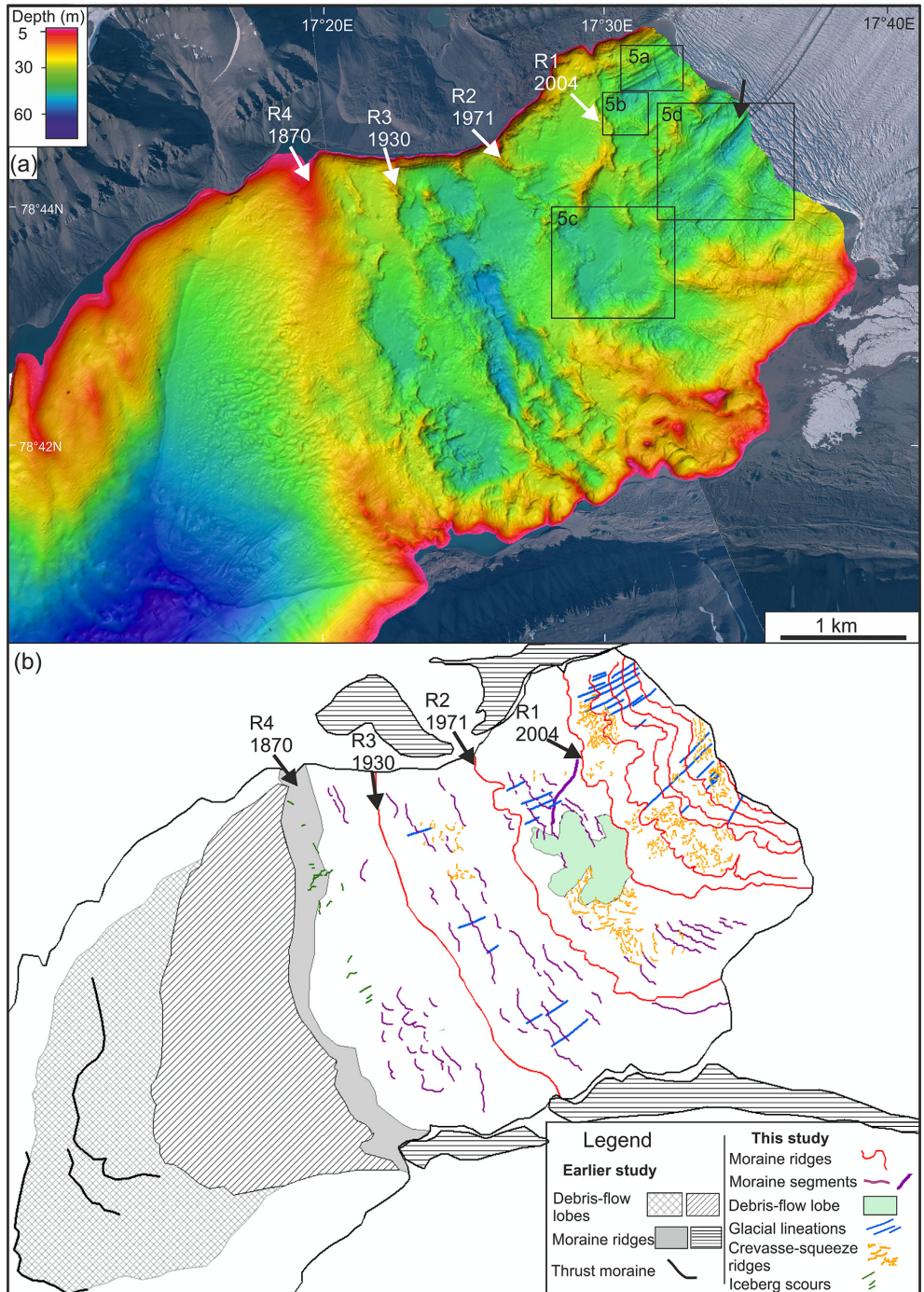


Fig. 4. The glacial landform record in Tempelfjorden. (a) Multibeam-bathymetric image showing the geomorphology in the inner part of Tempelfjorden, superimposed on a NPI aerial image from 2009. Black rectangles show the location of the images in Fig. 5. Black arrow points towards glacial lineation which corresponds with the medial moraine of the glacier. (b) Map of interpreted submarine landforms. Mapping of the R4 ridge, subaerial moraine ridges, older debris-flow lobes and thrust moraines is based on Plassen et al. (2004) and Forwick et al. (2010).

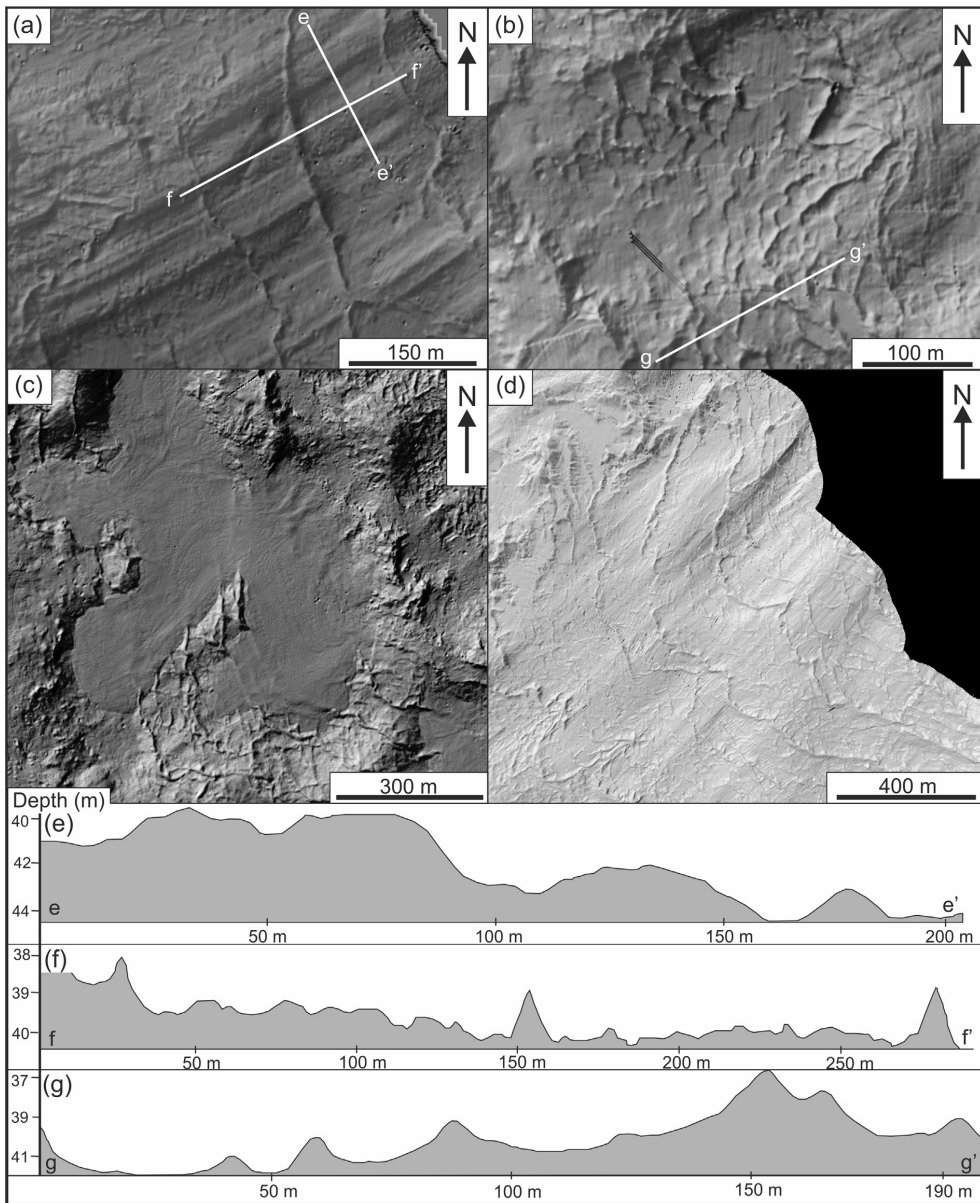


Fig. 5. Examples of the landforms in Tempelfjorden. (a) Glacial lineations. (b) Crevasse-squeeze ridges. (c) Debris-flow lobe, covering older crevasse-squeeze ridges. (d) Annual retreat moraines superimposed on glacial lineations. (e) Seafloor profile of the glacial lineations. (f) Seafloor profile of annual retreat moraines. (g) Seafloor profile of crevasse-squeeze ridges.

in Rindersbukta and Van Keulensfjorden in southern Spitsbergen (Ottesen et al., 2008). The surge moraines of Borebreen located on the northern side of Isfjorden display similar characteristics, although with slightly larger dimensions than the innermost ridges (R1–R3) in Tempelfjorden (Ottesen and Dowdeswell, 2006).

4.2.3. Sediment lobe at the 2004 ice margin: debris-flow lobe

4.2.3.1. Description. No large debris-flow lobes were observed on the distal sides of ridges R1–R3.

A small sediment lobe can, however, be observed distal to the terminal moraine R1 (Fig. 5c). The lobe has a maximum length of 0.7 km and a width of 0.9 km. It comprises three lobe-shaped

protuberances at its front. It is located in 30–50 m water depth adjacent to the moraine ridge. The sediment lobe covers a small depression in the fjord bathymetry and partly overrides older ridges. The surface of the lobe has a smooth appearance, but the overridden ridges are clearly visible in the southern section of the sediment lobe.

4.2.3.2. Interpretation. The sediment lobe on the distal side of R1 has been interpreted as a debris-flow lobe based on its shape as well as on the fact that the lobe onlaps onto small moraine ridges. The short duration of the 2004 surge and sedimentation rates of 3800 cm ka⁻¹ near the present glacier front (Forwick et al., 2010) further indicates that the sediment lobe originated as a debris-flow from the ridge itself rather than due to gradual sediment accumulation. Similar glacialic debris-flow lobes have been discovered in front of marine-terminating surge-type glaciers in Svalbard (Ottesen and Dowdeswell, 2006; Ottesen et al., 2008). These lobes are, however, much larger, having similar dimensions as the debris-flow lobe originating from the von Postbreen LIA moraine (Ottesen et al., 2008).

4.2.4. Geometrical ridge networks: crevasse-squeeze ridges

4.2.4.1. Description. There are several areas in the inner part of Tempelfjorden where small, symmetrical sediment ridges form dense, cross-cutting networks (Fig. 4). The ridge networks are most widespread inside the 2004 surge moraine (R1), although an extensive, double-arcuate shaped network is also found between R1 and R2 on a bathymetric high. No ridge networks have been observed down-fjord of the 1930s surge limit. The individual ridges are commonly up to 3 m high, but can be less than 1 m high, and are between 5 and 10 m wide (Fig. 5b and g). The ridges are commonly between 10 and 20 m long; however the larger ones can be up to 100 m long. Many of the ridges are oriented approximately parallel

or at right angles to former ice-front positions, although oblique ridges are also common. In places, intersecting ridges with two dominant directions form rhombic patterns (Fig. 5b).

4.2.4.2. Interpretation. The crosscutting network of ridges has been interpreted as crevasse-squeeze ridges. The ridge network between the R1 and R2 ridge consist of a combination of crevasse-squeeze ridges and fjord-transverse ridges (see Section 4.2.6). Networks of small, sharp-crested ridges also occur on land, particularly on the foreland of von Postbreen (Fig. 6a and b). In addition, numerous debris-rich structures are exposed in ice-cliff sections at the margins of Tunabreen (Fleming et al., 2013; Lovell et al., in preparation, Fig. 6c). The structures extend upwards from the bed and are infilled with basal till. In some instances, continuity can be demonstrated between till-filled structures and low ridges of till exposed by ice retreat (Fig. 6d). The ridge networks are similar to those described previously from the forelands of other surging glaciers in Svalbard (e.g. Bennett et al., 1996; Ottesen and Dowdeswell, 2006).

The close similarity of the ridge networks on the fjord floor to those on land, and the association between terrestrial examples and debris-rich structures in the ice of Tunabreen, demonstrates that they form by injection of debris into basal fractures and subsequent melt-out. During glacier surges, basal crevasses can form in regions of longitudinal extension (Rea and Evans, 2011) and/or in regions of intense compression near surge fronts (Lawson et al., 2000; Kristensen and Benn, 2012). In both cases, basal fracturing and the upward injection of till are encouraged by subglacial water pressures close to the ice overburden pressure. It is difficult to determine which of these is most applicable to the Tempelfjorden ridges based solely on their geometric characteristics and location. However, the surface crevasse pattern at the splayed glacier front in 2004 (see Fig. 11a in Fleming et al., 2013) (Fig. 7) supports the

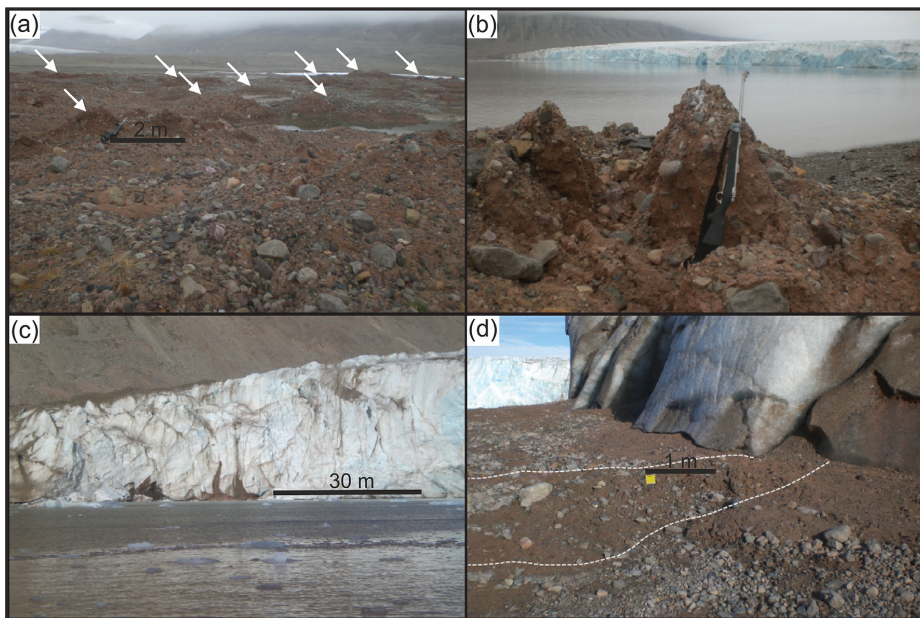


Fig. 6. Examples of terrestrial ridges and englacial debris-rich structures in August 2011. (a) Part of the ridge network on the southern side of Tempelfjorden. Individual ridges are arrowed. View is towards von Postbreen. (b) Detail of an individual sharp-crested ridge within the network on the southern side of Tempelfjorden (rifle for scale). (c) Vertical debris-rich structures within Tunabreen ice cliff. (d) Low ridge melting out from the englacial debris-rich structure in Tunabreen ice cliff. White dashed lines denote the ridge.

presence of a complex stress regime, as it shows both large transverse crevasses (indicative of longitudinal extension) and, at the very front, oblique crevasses (indicative of transverse extension). This pattern of surface crevasses (Fig. 7b) shows close correspondence with that of the ridge networks in the central part of the fjord, indicating that the latter reflect predominantly extensional stresses (longitudinal and transverse) during the 2004 surge. The mapped crevasses (Fig. 7b) show close correspondence to the position of mapped submarine crevasse-squeeze ridges. The crevasse-squeeze ridges are commonly present in the same areas as complex patterns of transverse, longitudinal and oblique surface crevasses.

4.2.5. Small transverse ridges: annual retreat moraines

4.2.5.1. Description. A number of relatively closely-spaced, sub-parallel cross-fjord ridges can be observed within the 2004 surge limit. The ridges are aligned approximately perpendicular to the fjord axis and extend into the shallow-water areas along the fjord margins. They are 2–4 m high and 10–20 m wide, with an average spacing of 100–300 m. The ridges are curvi-linear in planform and asymmetric in cross-profile. The average proximal slope angle is 10° , while the average distal slope angle is 8° . The ridges are superimposed on the glacial lineations in front of the current glacier front (Fig. 5d and f).

4.2.5.2. Interpretation. The transverse ridges can be matched with annual positions of the front of Tunabreen determined from satellite imagery, equating to one ridge for each year between 2005 and 2009, which marks the inner limit of our survey data (Fig. 8). Therefore, the ridges can be confidently interpreted as annual moraines, corroborating previous interpretations of similar transverse ridges in other Svalbard fjords (e.g. Solheim, 1991; Ottesen and Dowdeswell, 2006; Ottesen et al., 2008). The moraines are however much more lobate than the glacier margin delineations, indicating that the grounding line has a different form from the top of the glacier. The indentations of the grounding line are likely related to subglacial conduits and/or bathymetric deepenings.

The formation of annual moraine ridges in front of quiescent tidewater surge-type glaciers has been attributed to winter still-stands or minor re-advances (Solheim, 1991; Ottesen and Dowdeswell, 2006; Ottesen et al., 2008). At Tunabreen, surface velocity and ice-front position data derived from TerraSAR-X satellite images demonstrate that the glacier front re-advances during winter and spring, when calving rates are very low. Fig. 9 shows an annual retreat of 150 m which includes a winter advance of 20 m. Velocity data for early February 2014 are shown in Fig. 10, and indicate that ice located a few hundred metres behind the calving front exhibits extending flow, with velocities at the terminus of up to 0.5 m day^{-1} . The main trunk of the glacier, however, has no detectable motion, consistent with its quiescent state. This type of velocity pattern persists throughout the image series (January 2013–March 2014), with short-term variations in frontal speed relating to sea-ice extent and the buttressing effects of sea ice.

During the summer and autumn months, calving rates exceed the rate of ice flow, and the glacier retreats. During winter, calving rates are very small, allowing the front to advance a few tens of metres. Therefore, for fjord-terminating surge-type glaciers winter push moraines can form even during quiescent phases. This is in contrast with the situation for terrestrial surge-type glaciers, the tongues of which downwaste *in situ* with no annual readvances of the front. The asymmetric cross-profile of the ridges further indicates that they have formed through ice push (cf. Boulton et al., 1996). Minor winter readvances may also be responsible for the buckling of sea ice in front of the glacier margin (e.g. Marchenko et al., 2012).

4.2.6. Transverse to semi-transverse ridge segments: retreat moraines

4.2.6.1. Description. Segments of small fjord-transverse ridges can be found between the R1 and R2 ridges (Fig. 4). The ridges are up to 1 km long, between 1 and 3 m high and 3–10 m wide. The ridges are not continuous across the fjord floor and are most visible on the southern side of the fjord as well as on the topographic highs in its central part. The spacing between the ridges on the SW side of the

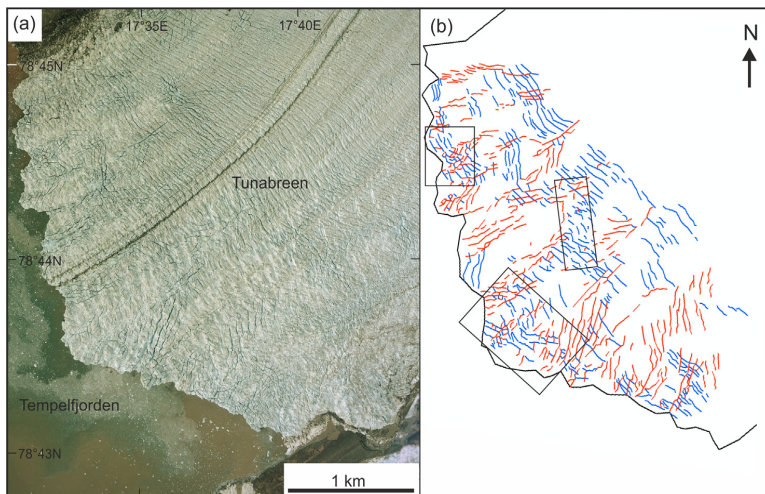


Fig. 7. The terminus of Tunabreen during the 2004 surge. (a) Aerial photomosaic (NPI), showing the heavily crevassed glacier front. (b) Mapped crevasses at the glacier front: transverse crevasses in blue, longitudinal and oblique crevasses in red. Black boxes outline main areas of crevasse-squeeze ridges. (For interpretation of the references to color in this figure legend, the reader is referred to the web version of this article.)

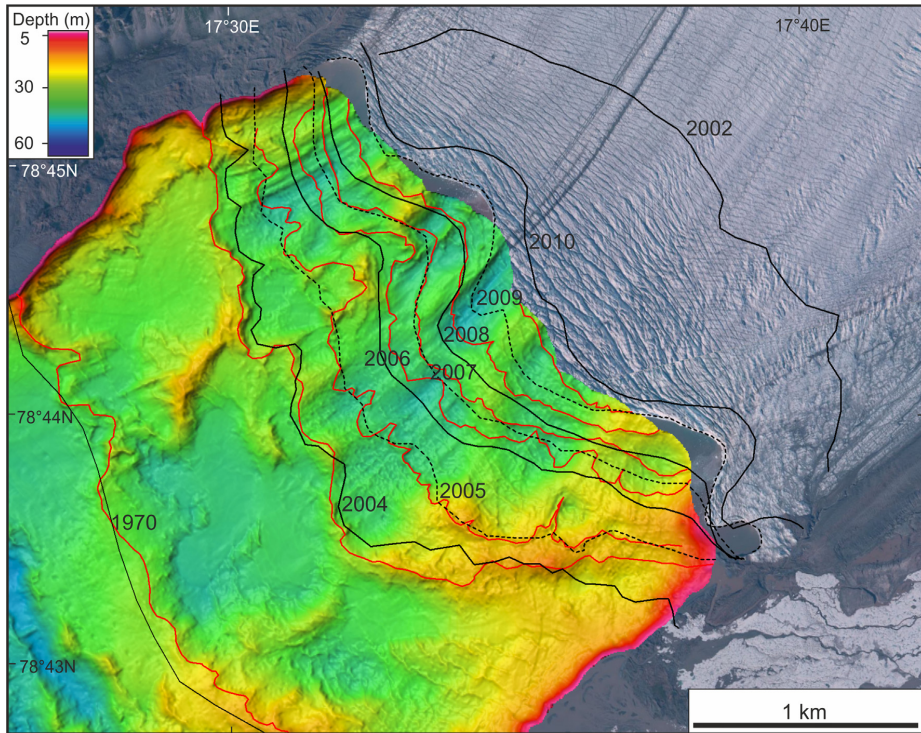


Fig. 8. Terminus positions from 2002 to 2010 (black lines) in relation to the submarine moraines (red lines). The terminal positions have been mapped from ASTER/Landsat and SAR images. The background shows an aerial image from 2009 (NPI).

fjord is fairly regular, between 80 and 100 m. The ridges are mainly asymmetric in cross-profile, with steeper proximal sides, which distinguishes them from a network of crevasse-squeeze ridges, which are also present in the same area. Segments of transverse ridges also exist between the R2 and R3 ridges, as well as between the R3 and R4 ridges.

Subdued large-scale ridges are also present in the inner part of Tempelfjorden. These ridge segments are up to 15 m high, 150 m wide and 600 m long. They are oblique to the fjord and have been overprinted by glacial lineations, crevasse-squeeze ridges and retreat moraines.

4.2.6.2. *Interpretation.* The fjord-transverse ridges are similar to the annual retreat moraines proximal to the R1 ridge. They match the ice margin form of R1 and R2 (Fig. 2) and have therefore been interpreted as segments of small retreat moraines, formed after the 1970's surge. The rhombohedral pattern of some of the ridges in the area suggests that the ridge network consists of a mixture of retreat moraines and crevasse-squeeze ridges.

It is likely that the transverse ridges are continuous across the entire fjord, but the debris-flow lobe and sediment infill during the 2004 surge has buried parts of the ridges. Due to the close spacing and similarity of these ridges to the post-2004 annual retreat

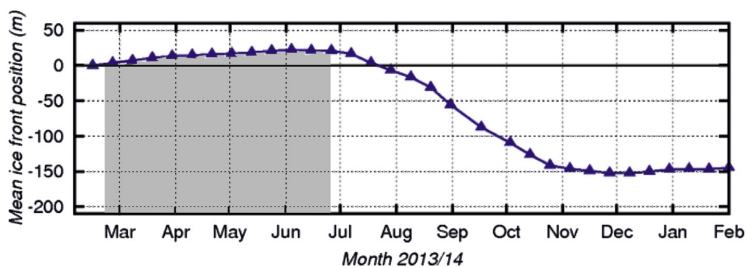


Fig. 9. Mean relative position of the terminus of Tunabreen during 2013 and early 2014. Note annual retreat of c. 150 m and winter advance of c. 20 m. Gray area shows the period of fast sea ice in the inner part of Tempelfjorden (Norwegian meteorological institute).

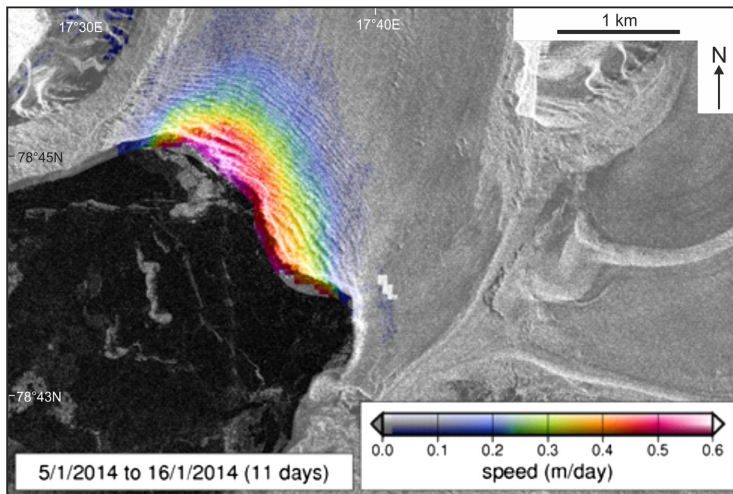


Fig. 10. Surface speed of the terminus of Tunabreen during January 2014 derived from feature tracking a pair of TerraSAR-X images.

moraines these ridges were most likely formed annually. Due to the incompleteness of the geomorphological record this interpretation is somewhat ambiguous.

The transverse ridges between the R2 and R3 terminal moraines are similar to the ridges between the R1 and R2 moraines. The ridge segments distal to the R3 ridge are however larger in scale, being up to 10 m high and 30 m wide, suggesting that they have formed during longer still-stands of the glacier front or during shorter glacier advances.

The underlying large-scale ridges have been interpreted as overridden terminal moraines. They are similar to overridden terminal moraines described by Ottesen and Dowdeswell (2006). These ridges have most likely formed by ice marginal processes during the older retreat phases of the glacier front. One of the ridges, just distal to the 2004 surge terminal moraine coincides with the position of the glacier front in 1908. It is therefore likely that these ridge segments have formed by the retreating glacier front of von Postbreen after the 1870 LIA maximum. The front of the glacier has most likely experienced periods of longer still stands, or shorter advance phases during general retreat.

5. Discussion

Detailed data on the recent behavior of Tunabreen, including annual and seasonal variations in glacier extent, velocities, and observations of sea ice and glacial debris structures, have been studied together with high-resolution seabed morphology in inner Tempelfjorden. Direct links have been drawn between the observations of the recent glacier dynamics and newly formed submarine landforms. In particular, the observed changes in glacier dynamics since the 2004 surge have been directly linked to the submarine landforms. Furthermore, we have been able to correlate discrete winter advances of the glacier terminus with annual push moraine formation by using feature tracking in TerraSAR-X imagery.

The 40 m freeboard (height of the ice cliff above the water line) of Tunabreen in 2011 (Marchenko et al., 2012) suggests that the glacier was grounded during and following the 2004 surge event. Significant thinning of the glacier front (up to 30 m) would be necessary for Tunabreen to become floating in the shallow inner

part of Tempelfjorden. Therefore, the best preserved glacial lineations in the innermost part of Tempelfjorden most likely result from the latest, 2004 surge event. Figs. 4a and 8 illustrate the link between the debris-rich belt in the glacier and one of the streamlined bedforms in front of the modern glacier margin that most likely represents a medial moraine. This particular medial moraine has its origin approximately 17 km up-glacier where the Tunabreen and Gnombreen glaciers converge south of the nunatak mountain of Bromsfjället (Fig. 1). The deposition of the debris incorporated into the glacier by glacial erosion and slope processes at Bromsfjället forms the medial moraine at the glacier margin.

With increasing distance from the 2012 ice front, the glacial lineations are less common in the geomorphological record, most likely due to reworking by subsequent surge events. Evidence of landform burial can be seen in the foreland of the 2004 surge, where post-1970 retreat landforms have been buried by a small debris-flow lobe emanating from the 2004 terminal moraine (Fig. 5c). This provides evidence for the modification of pre-existing glacial surge landform records by subsequent surges.

The landform assemblage observed in inner Tempelfjorden is unique in terms of three consecutive surges having modified the geomorphological record, creating a multiple surge landscape with landforms partially preserved from different surges. This has led to the construction of a more complex surging glacier landsystem model (Fig. 11). The observed landforms, however, are rather similar to those described from other Svalbard fjords where surges are known or have been inferred to occur (cf. Ottesen and Dowdeswell, 2006; Ottesen et al., 2008; Kristensen et al., 2009). The main characteristics and glaciological significance of the submarine landforms in inner Tempelfjorden are described below.

Glacial lineations were formed during the fast ice-flow phase of each surge by molding of soft fjord-floor sediments into flow-parallel ridges and grooves. It is generally accepted that glacial lineations reflect fast basal ice motion (e.g. Stokes and Clark, 2002; King et al., 2009), although it has rarely been possible to quantify either the ice velocities or the length of time required for their formation. Assuming that the lineations on the proximal side of the 2004 surge moraine were formed solely during the 2003–2005 surge, the duration and rate of terminus advance suggest that the

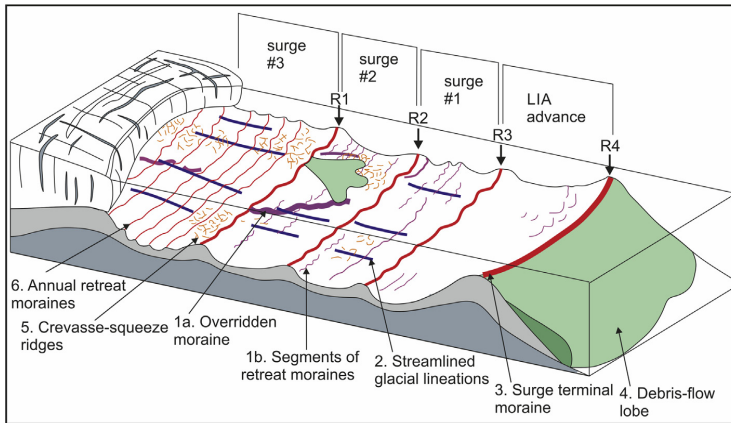


Fig. 11. Multiple surge glacial landsystem model based data from Tempelfjorden.

lineations were formed during a fast-flow (with average speed of at least 1 km a^{-1}) phase lasting <24 months. However, the assumption that all lineations were generated during the 2004 surge should be taken with reservations as some of them could be inherited from earlier surges. Also, the glacier flow-velocity estimate should be considered as a minimum value because of unknown calving loss at the glacier front. This value differs somewhat from the modern ice flow-velocities in Antarctica (c. 800 m a^{-1} ; Joughin et al., 2002), implying that the formation of glacial lineations in Tempelfjorden could have been relatively fast. The glacial lineations in Tempelfjorden are, however, smaller (c. 500 m long) than the several km long ones associated with LGM glaciers (Ottesen and Dowdeswell, 2009).

The terminal moraines record the location of the glacier front during successive surge maxima. The distal slope of the outermost (1870) terminal moraine is covered by lobe-shaped debris-flow deposits (Plassen et al., 2004) and numerous dislodged blocks of sediment (Fig. 4). Following Kristensen et al. (2009), we interpret the 1870 moraine and associated debris-flow deposits as evidence of bulldozing of soft fjord-floor sediments during the surge, with quasi-continuous failure of the advancing moraine front. Evidence for such a process has been observed by the authors during the recent surge of Nathorstbreen in southern Svalbard, where large mass of low shear strength fluid mud emerged in front of the glacier as it advanced along Van Keulenfjorden (Lovell, unpublished).

Commonly, large debris-flow lobes have been observed on the distal slopes of submarine surge terminal moraines in Svalbard (Ottesen et al., 2008). However, large debris-flow lobes do not occur in front of the inner, R1–R3 terminal moraines, even though a small debris-flow lobe is emanating from the distal slope of the 2004 surge moraine. This is uncommon in the geomorphological record of surge-type glaciers, although the same pattern (i.e. an outer ridge with debris-flow deposits and three inner ridges without debris-flow lobes) has been observed earlier in Borebukta (Ottesen and Dowdeswell, 2006). The scarceness of debris-flow deposits may reflect insufficient time for sediment accumulation due to the short surge cycle of 40 years. The sedimentation rates near the present glacier front have been estimated to 3800 cm ka^{-1} (Forwick et al., 2010). This gives an average annual sedimentation rate of 3.8 cm a^{-1} . It is likely that sedimentation rates during the active phase of the surge are much higher. However the short duration (only one to two years) of the active surge phase limits the sediment delivery to the glacier terminus leading to lower surge

terminal moraines which are less likely to experience slope failure. This is demonstrated by the smaller dimensions of the R1–R3 ridges in comparison with the larger R4 ridge.

Networks of small ridges are widespread inside the 2004 surge limit, and locally also inside the 1970s surge moraine. The geometry and location of the networks east of the 2004 moraine, the patterns of crevasses on the glacier surface during the 2003–2005 surge (Fleming et al., 2013) (Fig. 7) and comparison with the landforms exposed by the retreating present-day ice front (Fig. 6) suggest that the networks of ridges were formed by squeezing of water-saturated basal debris into fractures, which developed in zones dominated by extensional stretching (Rea and Evans, 2011). The surface crevasse pattern at the surge maximum in 2004 (Fig. 7) shows both, large transverse and longitudinal to oblique crevasses, indicative of fracturing due to longitudinal and transverse extension, respectively. Where crevasses are open at the bed, till can be injected to heights of up to several tens of metres aided by high basal water pressures (e.g. Fig. 6c). The crevasse-squeeze ridge pattern within the limits of the 2004 surge resembles closely that of earlier described submarine crevasse-squeeze ridge fields (Ottesen and Dowdeswell, 2006; Ottesen et al., 2008). The ridge pattern within the 1970 surge limit is however distinctly different from earlier described crevasse-squeeze ridge networks. We have interpreted these ridges as a combination of crevasse-squeeze ridges and ice-marginal retreat moraines. Due to the relatively small dimensions of crevasse-squeeze-ridges these are easily overprinted by sediment accumulation during or following a surge event (Fig. 5c).

The transverse annual moraines are the youngest landforms in the surge landform record. They have formed by ice push during winter re-advances of the grounded glacier margin, during the post-surge retreat phase. Although the main trunk of Tunabreen has no detectable motion during the present quiescence phase, the terminal zone of the glacier undergoes longitudinal extension in response to the force imbalance at the calving front, resulting in ice velocities of up to 0.5 m day^{-1} . These velocities are sufficient to allow re-advances of a few tens of metres in the winter months, when calving rates are very small due to suppression by sea ice. The close correlation between the presence of fast sea ice (between the 25th of February to the 27th of June, 2013) and the period of terminal winter advance in inner Tempelfjorden implies that sea ice is an important mechanism in the formation of the annual retreat moraines (Fig. 9).

Similar retreat moraines can be observed distal to the 1970s surge moraine. The main difference between these and the post-2004 retreat moraines is that the former are not continuous across the fjord, due to later erosion and overprinting. Sections of retreat moraine-like features can also be observed between the 1970–1930, as well as between the 1930–1870 surge limits. These ridge segments are incomplete and do not occur in swarms. Due to the similarities in shape and dimensions, they probably represent modified and partly overprinted retreat moraines.

The main difference between the Tempelfjorden landsystem model (Fig. 11) and earlier submarine surge landsystem models is that multiple surges have been recorded in Tempelfjorden, leading to a modified and overprinted glacier surge landform record. The landform record produced by the 2004 surge event is similar to the landform records produced by other Svalbard surge glaciers (Ottesen et al., 2008). However a continuous set of retreat moraines can only be found proximal to the 2004 surge moraine. Debris-flow lobes are not present distal to the R2 and R3 ridges and crevasse-squeeze ridges can only be found very locally. Glacial lineations are lacking distal to the 1930s surge limit (Fig. 11).

The incomplete landform records related to the older surges can be attributed to poor preservation or burial of landforms due to the multiple surges. Sedimentation rates of 3.8 cm a^{-1} in the vicinity of the present glacier front (Forwick et al., 2010) give a sediment accumulation of around 3 m during 80 years. This is enough to (at least partly) bury smaller landforms, such as crevasse-squeeze ridges and retreat moraines. Overridden, partially eroded and superimposed ridge segments further indicate that the landform record has been modified. The position of the large overridden ridge between the 2004 and 1970s surge moraines (Figs. 4 and 11) matches the glacier terminal position in 1908, indicating that this is a modified retreat ridge. The lack of glacial lineations, crevasse-squeeze ridges and distinct retreat moraines, distal to the 1930s surge moraine suggests that the 1870 event was not a surge, but rather reflects a glacial advance due to changed climatic conditions during the LIA cold period.

Terrestrial surge landsystem models differ from the Tempelfjorden model as they do not include retreat moraine ridges or debris-flow lobes. However, they do include eskers, outwash plains and hummocky moraines (Schomacker et al., 2014). The main similarity between the models is the presence of crevasse-squeeze ridges and glacial lineations.

6. Conclusions

The post-Little Ice Age (LIA) dynamics of Tunabreen, a tidewater surge-type glacier in Tempelfjorden, has been reconstructed by combining published data, remote sensing (satellite images and aerial photographs) and high-resolution multibeam-bathymetric data.

The well preserved glacial landform record in the inner part of Tempelfjorden has been directly linked to the observed 2004 surge event showing with confidence that the retreat moraines have formed annually.

Ice-front positions and velocity data from feature tracking TerraSAR-X imagery has been used to correlate discrete terminal winter advances with the formation of the annual retreat moraines. The correlation between the period of the terminal winter advances and the presence of sea ice in inner Tempelfjorden suggest that sea ice is an important factor in the formation of the annual retreat ridges.

The landform record in Tempelfjorden, consisting of glacial lineations, large terminal moraines, debris-flow lobes, crevasse-squeeze ridge networks and small annual retreat moraines, shares many similarities with surge glacier landsystem models

based on other Svalbard tidewater glaciers (e.g. Ottesen and Dowdeswell, 2006; Ottesen et al., 2008). Landforms particularly characteristic of the inner Tempelfjorden include segments of retreat moraines and large overridden ridges.

The landform record in Tempelfjorden (Fig. 11) is distinguished from previously proposed glacier surge landsystem models by including four sets of landform assemblages associated with the LIA advance and three subsequent surges which have partly modified the earlier landform records.

The landform records of the 1930s and 1970s surges are lacking debris-flow lobes suggesting that these are not an integral part of a glacier surge landsystem model. The presence of debris-flow lobes is most likely related to the length of the active surge phase.

The landform record of the von Postbreen LIA advance differs from the surge landform record by lacking glacial lineations, crevasse-squeeze ridges and distinct retreat moraines. This might be due to poor preservation of the landform record. Alternatively, the von Postbreen advance was not a surge-related process but rather a climatically controlled one.

Acknowledgments

Permission for presenting the bathymetric data was granted by the Norwegian Hydrographic Service (permission nr. 13/G706). Landsat satellite images were acquired from USGS Earth Explorer and the Global Land Cover Facility. ASTER satellite images were acquired from the NASA Land Processes Distributed Active Archive Center (LPDAAC). Envisat data were provided by ESA through project AOCRY2676. TerraSAR-X data were provided by DLR through project OCE1503, and funded by the ConocoPhillips-Lundin Northern Area Program project CRIOS (Calving Rates and Impact on Sea Level). The topographic maps and aerial photographs were obtained from the Norwegian Polar Institute (NPI). Aerial photos were provided by NERC Earth Observation Data Centre. H. Lovell was funded by a NERC PhD studentship (NE/I528050/1), the Queen Mary Postgraduate Research Fund and the Arctic Field Grant program of the Research Council of Norway. UNIS logistics is thanked for fieldwork support. Parts of this work benefitted from discussions with Ed Fleming and Sven Lukas, and we would also like to thank Sarah Greenwood at Stockholm University as well as Teena Chauhan, Srikumar Roy and Oscar Fransner from UNIS for commenting on the early draft. We would also like to thank Henry Patton and an anonymous reviewer for providing valuable feedback on the manuscript.

References

- Benediktsson, Schomacker, A., Lokrantz, H., Ingólfsson, O., 2010. The 1890 surge end moraine at Eyjabakkajökull, Iceland: a re-assessment of a classic glaciotectonic locality. *Quat. Sci. Rev.* 29, 484–506.
- Bennett, M., Hambrey, M.J., Huddart, D., Ghiene, J.F., 1996. The formation of a geometrical ridge network by the surge-type glacier Kongsvegen, Svalbard. *J. Quat. Sci.* 11 (No. 6), 437–449.
- Boulton, G.S., Van Der Meer, J.J.M., Hart, J., Beets, D., Ruegg, G.H.J., Van Der Wateren, F.M., Jarvis, J., 1996. Till and moraine emplacement in a deforming bed surge—An example from a marine environment. *Quat. Sci. Rev.* 15, 961–987.
- Brynjólfsson, S., Ingólfsson, O., Schomacker, A., 2012. Surge fingerprinting of cirque glaciers at the Tröllaskagi peninsula, North Iceland. *Jökull* 62, 151–166.
- De Geer, G., 1910. Guide de l'excursion au Spitsberg. Excursion A1. (Guide to excursions on Spitsbergen A1). Stockholm: XI International Geological Congress.
- Dowdeswell, J.A., Hamilton, G.S., Hagen, J.O., 1991. The duration of the active phase on surge-type glaciers: contrasts between Svalbard and other regions. *J. Glaciol.* 37 (127), 388–400.
- Evans, D.J.A., Rea, B.R., 1999. Geomorphology and sedimentology of surging glaciers: a landsystem approach. *Ann. Glaciol.* 28, 75–82.
- Evans, D.J.A., Rea, B.R., 2003. Surging glacial landsystems. In: Evans, D.J.A. (Ed.), *Glacial Landsystems*, pp. 259–288. Arnold, London.
- Fleming, E., Lovell, H., Stevenson, C., Petronis, M., Benn, D.I., Hambrey, M., Fairchild, I., 2013. Magnetic fabrics in basal ice of a surge-type glacier. *J. Geophys. Res.* 118, 2263–2278.

- Forwick, M., Vorren, T.O., 2009. Late Weichselian and Holocene sedimentary environments in Isfjorden, Spitsbergen. *Palaeogeogr. Palaeoclimatol. Palaeoecol.* 280, 258–274.
- Forwick, M., Vorren, T.O., Hald, M., Korsun, S., Roh, Y., Vogt, C., Yoo, K.-C., 2010. Spatial and Temporal Influence of Glaciers and Rivers on: the Sedimentary Environment in Sassenfjorden and Tempelfjorden, Spitsbergen. In: Geological Society of London, Special Publications, vol. 44, pp. 163–183.
- Fowler, A.C., Murray, T., Ng, F., 2001. Thermally controlled glacier surging. *J. Glaciol.* 47, 527–538.
- Hagen, J.O., Liestøl, O., Roland, E., Jorgensen, T., 1993. *Glacier Atlas of Svalbard and Jan Mayen*, vol. 129. Norwegian Polar Institute, Meddelelser, pp. 1–169.
- Hodgkins, R., Dowdeswell, J.A., 1994. Tectonic processes in Svalbard tide-water glacier surges: evidence from structural glaciology. *J. Glaciol.* 40 (136), 553–560.
- Joughin, I., Tulaczyk, L., Bindschadler, R., Price, S.F., 2002. Changes in west Antarctic ice stream velocities: observations and analysis. *J. Geophys. Res.* 107.
- King, E.C., Hindmarsh, R.C.A., Stokes, C.R., 2009. Formation of mega-scale glacial lineations observed beneath a West Antarctic ice stream. *Nat. Geosci.* 2, 585–588.
- Kristensen, L., Benn, D.I., 2012. A surge of Skobreen/Paulabreen, Svalbard, observed by time-lapse photographs and remote sensing data. *Polar Res.* 31, 1–9.
- Kristensen, L., Benn, D.I., Hormes, A., Ottesen, D., 2009. Mud aprons in front of Svalbard surge moraines: evidence of subglacial deforming layers or proglacial tectonics? *Geomorphology* 111 (3–4), 206–221.
- Lawson, W.J., Sharp, M.J., Hambrey, M.J., 2000. Deformation histories and structural assemblages of glacier ice in a non-steady flow regime. In: Maltman, A.J., Hubbard, B., Hambrey, M.J. (Eds.), *Deformation of Glacial Materials*, Geological Society, London, Special Publication, vol. 176, pp. 55–96.
- Liestøl, O., 1969. Glacier surges in west Spitsbergen. *Can. J. Earth Sci.* 6, 895–897.
- Lovell, H., Fleming, E.J., Benn, D.I., Hubbard, B., Lukas, S., Flink, A.E., Noormets, R., 2014. Debris Entrainment during Tidewater Glacier Surges and Implications for Landform Genesis at Tunabreen, Svalbard (in preparation).
- Mangerud, J., Bolstad, M., Elgersma, A., Helliøsem, D., Landvik, J.Y., Lonne, I., Lycke, A.K., Salvigsen, O., Sandahl, T., Svendsen, J.I., 1992. The last glacial maximum on Spitsbergen, Svalbard. *Quat. Res.* 28, 1–31.
- Mansell, D., Luckman, A., Murray, T., 2012. Dynamics of tidewater surge-type glaciers in northwest Svalbard. *J. Glaciol.* 58 (207), 110–118.
- Marchenko, A.V., Morozov, E.G., Muzylev, S.V., 2012. A tsunami wave recorded near a glacier front. *Nat. Hazards Earth Syst. Sci.* 12, 415–419.
- Meier, M.F., Post, A.S., 1969. What are glacier surges? *Can. J. Earth Sci.* 6, 807–819.
- Murray, T., Strozzi, T., Luckman, A., Jiskoot, H., Christakos, P., 2003. Is there a single surge mechanism? Contrasts in dynamics between glacier surges in Svalbard and other regions. *J. Geophys. Res.* 108 (B5), 1–15.
- Ottesen, D., Dowdeswell, J.A., 2006. Assemblages of submarine landforms produced by tidewater glaciers in Svalbard. *J. Geophys. Res. Earth Surf.* 111, 1–16.
- Ottesen, D., Dowdeswell, J.A., 2009. An inter-ice-stream glaciated margin: submarine landforms and a geomorphic model based on marine-geophysical data from Svalbard. *Geol. Soc. Am. Bull.* 121 (11–12), 1647–1665.
- Ottesen, D., Dowdeswell, J.A., Benn, D.I., Kristensen, L., Christiansen, H.H., Christensen, O., Hansen, L., Lebesbye, E., Forwick, M., Vorren, T.O., 2008. Submarine landforms characteristic of glacier surges in two Spitsbergen fjords. *Quat. Sci. Rev.* 27 (15–16), 1583–1599.
- Plassen, L., Vorren, T.O., Forwick, M., 2004. Integrated acoustic and coring investigation of glacial deposits in Spitsbergen fjords. *Polar Res.* 23, 89–110.
- Rea, B., Evans, D.J.A., 2011. An assessment of surge-induced crevassing and the formation of crevasse-squeeze ridges. *J. Geophys. Res. Earth Surf.* <http://dx.doi.org/10.1029/2011JF001970>.
- Schomacker, A., Benediktsson, O.I., Ingólfsson, O., 2014. The Eyjabakkajökull glacial landsystem, Iceland: geomorphic impact of multiple surges. *Geomorphology* 218, 98–107.
- Solheim, A., 1991. The Depositional Environment of Surging Sub-polar Tidewater Glaciers, vol. 194. Norsk polarinstitutt skrifter, (Norwegian polarinstitute), pp. 1–97.
- Stokes, C., Clark, C.D., 2002. Are long subglacial bedforms indicative of fast ice flow? *Boreas* 31, 239–249.
- Svendsen, J.I., Mangerud, J., 1992. Paleoclimatic inferences from glacial fluctuations on Svalbard during the last 2000 years. *Clim. Dyn.* 6, 213–220.
- Svendsen, J.I., Elverhøi, A., Mangerud, J., 1996. The retreat of the Barents Sea ice sheet on the western margin. *Boreas* 25, 244–256.



Contents lists available at ScienceDirect

Quaternary Science Reviews

journal homepage: www.elsevier.com/locate/quascirev

Past ice flow in Wahlenbergfjorden and its implications for late Quaternary ice sheet dynamics in northeastern Svalbard



Anne E. Flink ^{a,*}, Riko Noormets ^a, Oscar Fransner ^a, Kelly A. Hogan ^b, Matthew ÓRegan ^c, Martin Jakobsson ^c

^a Department of Arctic Geology, University Centre in Svalbard, 9170 Longyearbyen, Norway

^b British Antarctic Survey, Madingley Road, High Cross, Cambridge, UK

^c Department of Geological Sciences, Stockholm University, 10691 Stockholm, Sweden

ARTICLE INFO

Article history:

Received 22 February 2016

Received in revised form

20 March 2017

Accepted 21 March 2017

Keywords:

Submarine glacial landforms

Ice flow

Deglaciation

Surging glaciers

Multibeam-bathymetric data

ABSTRACT

Wahlenbergfjorden is a fjord situated in the western part of Nordaustlandet in northern Svalbard. It leads into the 400 m deep Hinlopen Strait located between Nordaustlandet and Spitsbergen. High-resolution multibeam bathymetric and sub-bottom data, as well as sediment cores are used to study the past extent and dynamics of glaciers in Wahlenbergfjorden and western Nordaustlandet. The submarine landform assemblage in Wahlenbergfjorden consists of landforms characteristic of subglacial, ice marginal and proglacial conditions. Glacial lineations indicate that Wahlenbergfjorden was occupied by streaming ice during the LGM and most likely acted as an ice stream onset zone. Westward ice flow in the fjord merged with the ice stream in Hinlopen Strait. Absence of ice recessional landforms in outer Wahlenbergfjorden suggests relatively fast deglaciation, possibly by flotation of the glacier front in the deeper parts of the fjord. The inner part of Wahlenbergfjorden and Palanderbukta are characterized by De Geer moraines, indicating episodic retreat of a grounded glacier front. In Palanderbukta, longer still stands of the glacier terminus resulted in the formation of larger terminal moraine ridges. The inner part of Wahlenbergfjorden was deglaciated prior to 11.3 ± 55 Cal. ka BP. The submarine landform assemblages in front of Bodleybreen, Etonbreen, Idunbreen, Frazerbreen and Aldousbreen confirm that these glaciers have surged at least once during the Holocene.

© 2017 Elsevier Ltd. All rights reserved.

1. Introduction

Expansion and retreat of ice sheets during Quaternary glacial-interglacial periods is recorded by a wide range of submarine landforms in the Barents Sea (e.g. Ottesen and Dowdeswell, 2009; Bjarnadóttir et al., 2012). The submarine glacial geomorphology is used to reconstruct the ice sheet configurations and dynamics in fjords as well as on the continental shelf (Ottesen et al., 2007, 2008a; Robinson and Dowdeswell, 2011; Andreassen et al., 2008; Ottesen and Dowdeswell, 2009; Ruther et al., 2011). Marine geophysical data confirm that the entire Barents Sea area was covered by a grounded ice sheet during the Last Glacial Maximum (LGM) (Solheim et al., 1990; Svendsen et al., 2004; Dowdeswell et al., 2010). According to glacial isostatic adjustment

reconstructions based on terrestrial data, the Svalbard Barents Sea Ice Sheet (SBSIS) was centered on Kong Karls Land in northeastern Svalbard (Ingólfsson et al., 1995; Lambeck, 1995; Landvik et al., 1998; Svendsen et al., 2004; Ingólfsson and Landvik, 2013). Recently published submarine landform records, suggest that a local ice dome was located in the southern Hinlopen Strait area (Dowdeswell et al., 2010; Hogan et al., 2010a). It is therefore likely that the SBSIS consisted of more than one local dome during at least periods of the last glacial cycle (Dowdeswell et al., 2010; Hormes et al., 2013; Ingólfsson and Landvik, 2013). The timing and dynamics of these domes is, however, unknown.

During LGM, the western sector of the SBIS was divided into fast-flowing ice streams separated by inter-ice stream areas dominated by slow-flowing ice (Ottesen and Dowdeswell, 2009). The ice-sheet configuration and dynamics in eastern Svalbard are less well-known, mainly because of the relative inaccessibility of the area due to more persistent sea-ice cover. Recent work south and east of Nordaustlandet and in the Kvitøya Trough have

* Corresponding author. University Centre in Svalbard, PO Box 156, 9171 Longyearbyen, Norway.

E-mail address: AnneF@unis.no (A.E. Flink).

indicated easterly and northerly ice-flow directions, respectively (Hogan et al., 2010a, 2010b; Dowdeswell et al., 2010). Bathymetric data southeast of Nordaustlandet also indicates eastward ice flow (Robinson and Dowdeswell, 2011). Mega-scale glacier lineation like features and drumlins on the continental shelf, and stacked debris flows in the form of a trough-mouth fan on the continental slope, suggest that the Hinlopen Strait was occupied by a fast, northwards flowing ice stream during the LGM. Ice-flow at the mouth of Wahlenbergfjorden was deflected towards the north and coalesced with the flow in Hinlopen Strait. (Ottesen et al., 2007; Batchelor et al., 2011). The timing of these ice flows is uncertain.

This study provides a comprehensive analysis of the submarine landform assemblage in the previously poorly known Wahlenbergfjorden and Palanderbukta in order to reconstruct the ice-sheet configuration, dynamics and the deglaciation of the western Nordaustlandet area during the last deglaciation. Data from the inner part of Wahlenbergfjorden also provides insight into more recent glacier dynamics. Two sediment cores collected from Wahlenbergfjorden shed light on the sedimentary environment and provide a time constraint for deglaciation in the fjord.

2. Study area

The 50-km long Wahlenbergfjord is located in western Nordaustlandet. It terminates in the Hinlopen Strait - an up to 400-m deep water divide between Nordaustlandet and Spitsbergen (Fig. 1). The Hinlopen Strait continues northward into the Hinlopen Trough, which terminates with a slide scar at the shelf edge. A mega slide took place around 30 ka BP at the shelf edge (Winkelmann and

Stein, 2007) and a post-slide sediment fan has been deposited during the LGM (Vanneste et al., 2006; Batchelor et al., 2011; Hogan et al., 2013). Wahlenbergfjorden can be divided into two branches, the E-W trending main fjord and the smaller S-E trending Palanderbukta (Fig. 1). Wahlenbergfjorden is 9.5 km wide and has a maximum water depth of 290 m (Fig. 2a). The 20-km long and 6.3 km wide Palanderbukta has a maximum water depth of 120 m (Fig. 2a).

The Wahlenbergfjorden area displays a complex bedrock geology, which is dominated by clastic sedimentary and carbonate rocks (Fig. 1b). Metasedimentary and metavolcanic rocks, as well as Caledonian granites and migmatites are also common in the area. Many of the islands in Hinlopen Strait are comprised of resistant dolerites from the Diabasodden suite (Dallmann et al., 2002). Dolerite usually occurs as dykes or sills and is common in the outer part of Wahlenbergfjorden, where it occurs on Guldenøyane and Iduneset (Fig. 1b). The Hinlopen Strait area is dominated structurally by reverse faults running in north-south directions. A normal fault with an east-west orientation is located in the inner part of Wahlenbergfjorden (Fig. 1b).

Today, the Wahlenbergfjorden area is partially glacierised with outlet glaciers of Idunbreen, Frazerbreen, Aldousbreen, Bodleybreen, Etonbreen and Palanderbreen calving into the fjord (Fig. 1). A number of the outlet glaciers in Nordaustlandet have surged since the 1930s (Dowdeswell et al., 1999; Bamber et al., 2004; Robinson and Dowdeswell, 2011). Etonbreen is believed to have surged in 1938 (Bamber et al., 2004; Mothold et al., 2010). Bodleybreen surged between 1976 and 1981 (Dowdeswell, 1986). Of the glaciers terminating into Palanderbukta, Palanderbreen is believed to have surged sometime prior to 1969, while Clasebreen

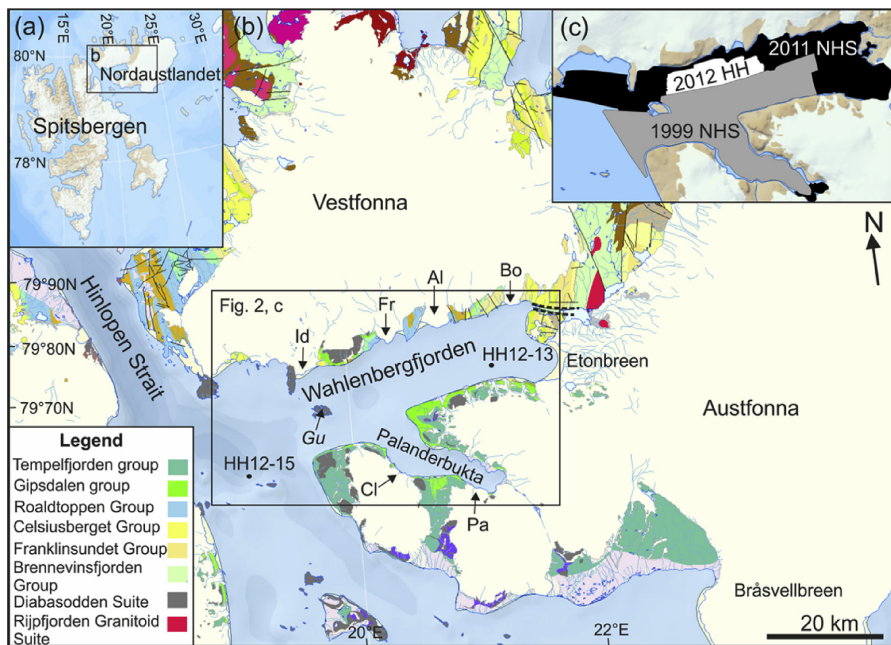


Fig. 1. (a) The location of Spitsbergen and Nordaustlandet. (b) Geological map of Wahlenbergfjorden and Palanderbukta. The black rectangle shows the location of Fig. 2. Gu marks the location of Guldenøyane. Id, Fr, Al, Bo, Cl and Pa mark the locations of Idunbreen, Frazerbreen, Aldousbreen, Bodleybreen, Clasebreen and Palanderbreen, respectively. Black indexed dots show the locations of the two sediment cores and black dashed lines outline the normal fault immediately east of the fjord. The legend highlights the most common bedrock types (for more info, see, Flood et al. (1969)). (c) Map showing the boundaries between the different multibeam-data sets. Background maps are from Svalbardkartet, (Norwegian Polar Institute (NPI)).

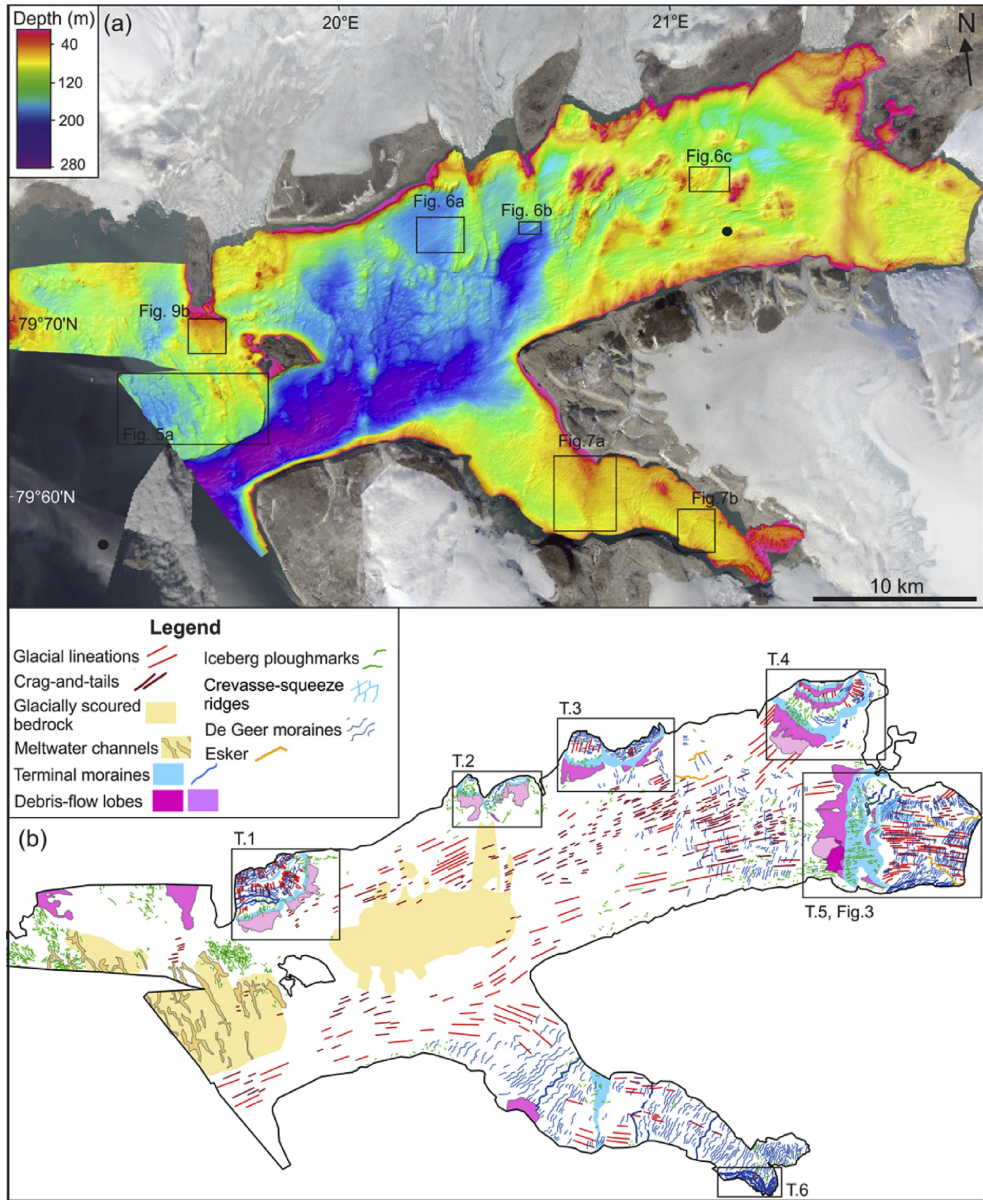


Fig. 2. (a) Shaded and color-coded multibeam-bathymetric image of Wahlenbergfjorden. Rectangles mark the locations of Fig. 5a–7 and 9b. Black dots mark the core locations. The background shows a mosaic of aerial photos from 2010 to 2011 (NPI) (For photo IDs see Appendix 1). (b) Geomorphological map of submarine landforms. Rectangles mark the locations of the tidewater glacier landform assemblages T.1–T.6 formed during Holocene terminal maxima and the location of Fig. 3. Different color-nuances represent different generations of debris-flow lobes.

surged between 1938 and 1939 (Lefauconnier and Hagen, 1991). Idunbreen, Frazerbreen and Aldousbreen are believed to have reached their maximum positions prior to 1938 and their maximum Holocene extents are not known (Lefauconnier and Hagen, 1991).

3. Methods

3.1. Geophysical data

Marine-geophysical data from Wahlenbergfjorden were

acquired from two different sources (Fig. 1c). The bathymetric data provided by the Norwegian Hydrographic Service were acquired with a Kongsberg EM-1002 single head and EM-3002 dual head systems in 1999 and 2011, respectively (grey and black areas, respectively in Fig. 1c). In addition, bathymetric data from the northern part of the fjord were collected during a cruise on the research vessel R/V Helmer Hanssen in 2012 (white area in Fig. 1c). These data were collected with a Kongsberg EM-300 multibeam

swath bathymetric system with a $1 \times 1^\circ$ beam configuration. All three datasets were merged into a grid with isometric cell size of 5 m in UTM33N projection and using sea chart zero (lowest astronomical tide level) as a vertical reference (Figs. 2 and 3). The combined dataset covers the entire fjord. Additional data collected during the 2012 cruise consist of chirp sonar sub-bottom profiles (Fig. 4a), acquired with a 4 kW, 2–16 kHz, EM3300 hull-mounted sub-bottom profiler. Depths for the sub-bottom profiles were

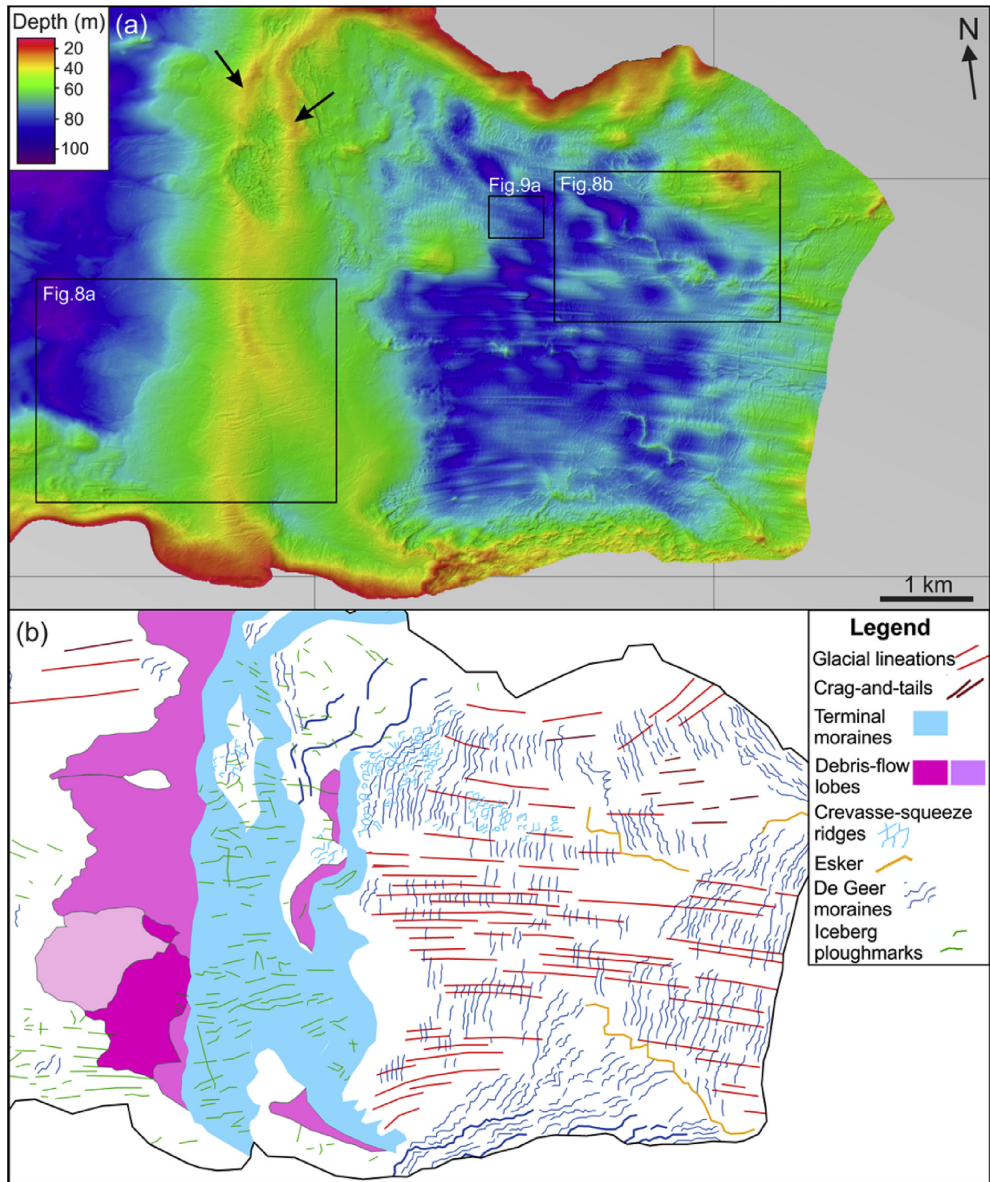


Fig. 3. (a) Zoom-in on the tidewater glacier landform assemblage (T5) in front of Etonbreen. Rectangles mark the locations of Fig. 8 and 9a. Arrows point to the multi-crested terminal moraine ridge. (b) Map of the interpreted landforms.

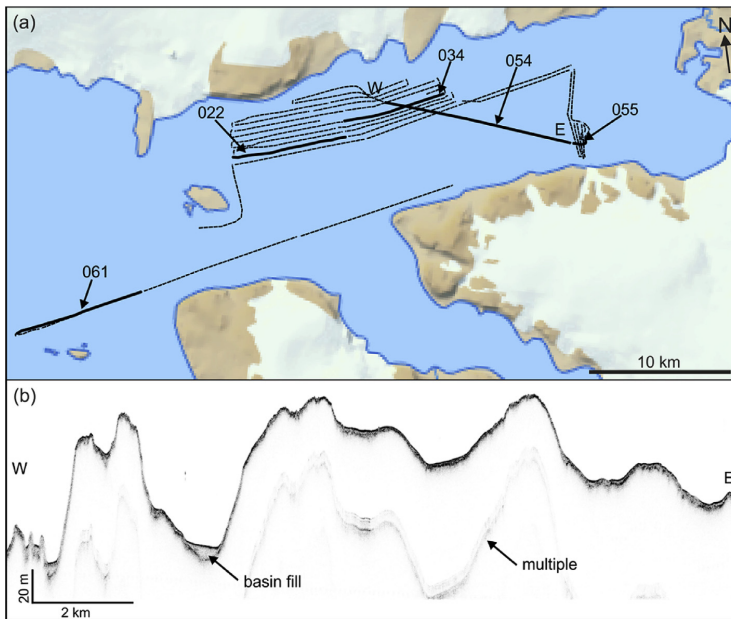


Fig. 4. (a) Dashed lines show the coverage of the chirp data. Bold lines show the location of profiles discussed in the article. (b) Example of a representative chirp profile, 054, along Wahlenbergfjorden.

calculated assuming a sound wave velocity of 1500 m s^{-1} through the water column and the sediments. The acquired multibeam data were analyzed and visualized in the QPS Fledermaus and ArcGIS software suites, using different angles of sun illumination. Sub-bottom profiles were visualized in the Discover and Kingdom software suites.

3.2. Sediment cores

Two sediment cores were recovered in Wahlenbergfjorden during the 2012 cruise on R/V Helmer Hanssen using a gravity corer (Fig. 1b). The cores were split, logged and sub-sampled at the Department of Geological Sciences, Stockholm University. The following parameters were logged: lithology, grain-size distribution, color, sedimentary texture and structure, and clast shape. Lithofacies coding was adopted from Eyles et al. (1983). A Multi Sensor Core Logger (MSCL) was used to measure geophysical properties such as P-wave velocity, bulk density, and magnetic susceptibility at 1 cm intervals. P-wave velocities with values outside of $1400\text{--}2300 \text{ m s}^{-1}$ and amplitudes less than 80% were cleaned away. Bulk density values outside $1.2\text{--}2.2 \text{ g cm}^{-3}$ and clear spikes in MS data were also cleaned away.

Shear strength was measured with a fall-cone instrument at a down-core resolution of 5 cm. Additional measurements were taken to capture variations across obvious lithological boundaries. An ITRAX micro-X-ray fluorescence core scanner was used to obtain radiographic images of the cores. Grain-size analyses were conducted on the finer fraction ($<1 \text{ mm}$), at 10 cm intervals and additionally on both sides of every visually-obvious lithological boundary. A Malvern 3000 laser diffraction particle size analyzer was used to determine the grain-size distribution (cf. Shevenell et al., 1996). Radiocarbon (^{14}C) dates were obtained with an accelerator mass spectrometer from samples consisting of mixed

benthic foraminifera at the AMS laboratory at Lund University. Calibration of the radiocarbon ages was performed with the CALIB 14 software using the MARINE13 calibration curve which has an inbuilt global marine reservoir correction of 440 ± 52 years (Stuiver and Reimer, 1993; Reimer et al., 2013). A local marine reservoir correction for Spitsbergen (ΔR) of 105 ± 24 years (Mangerud et al., 2006), was used in the age calibration. Radiocarbon ages are reported with a two sigma error.

4. Description and interpretation of submarine landforms

4.1. Channels: subglacial meltwater channels

4.1.1. Description

A plateau, located approximately 80 m higher than the seafloor in the adjacent trough, is present in the outer part of Wahlenbergfjorden (Fig. 2a). The relief of the plateau and the presence of outcropping dolerites on shore (cf. section 2; Dallmann et al., 2002) suggest that it consists of more resistant bedrock in comparison to the adjacent glacially-scoured trough. Glacially-eroded dolerites have also been shown to be present in the modern seafloor morphology in other Svalbard fjords (Senger et al., 2013; Roy et al., 2014, 2015). Deep N-S trending channels are cut into the surface of the plateau (Fig. 5a). The channels are up to 400 m wide, 40 m deep and 2 km long. The width and depth of the channels varies along their course and occasionally they intersect each other. They are U-shaped in cross-section and in general, one of their banks is higher than the other (Fig. 5b). There is no apparent spatial trend in this asymmetric shape. The channels are partly infilled with sediment.

4.1.2. Interpretation

The shape and size of the channels in Wahlenbergfjorden suggests that these are subglacial meltwater channels or tunnel

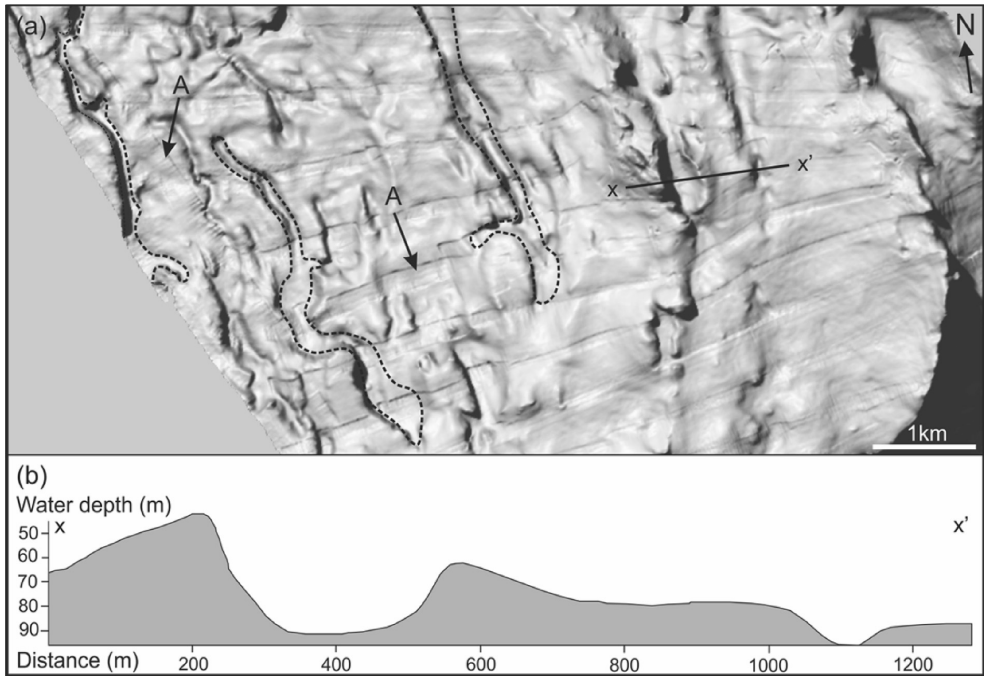


Fig. 5. (a) Subglacial meltwater channel system in Wahlenbergfjorden. Arrows labeled A point to geophysical artefacts. Dashed lines outline some of the meltwater channels. (b) Cross-profile showing the characteristic U-shape of the meltwater channels. For the location see Fig. 2.

valleys. Tunnel valleys trend roughly parallel to ice-flow directions and drain water towards the ice margin. They can be up to 4 km wide, 500 m deep and 100 km long (e.g. Graham et al., 2009; Janszen et al., 2012). In cross-section they exhibit steep-sided, U-shaped flanks similar to fjord walls (Lowe and Anderson, 2003). In general, they form anastomosing patterns and have irregular longitudinal profiles without consistent downstream deepening and abrupt terminations, which suggest that they have formed by erosion of pressurized subglacial water (Lowe and Anderson, 2003; Janszen et al., 2012).

Lowe and Anderson (2003) suggested that subglacial meltwater channels can form in areas where thick, cold-based or relatively slow-sliding ice rests over impermeable and rugged crystalline bedrock. During catastrophic discharge events the base of the ice sheet is separated from the bedrock as high amounts of pressurized meltwater is expelled through channels, leading to subglacial erosion. The channels in Wahlenbergfjorden are somewhat smaller compared to observed tunnel valleys in other areas (Lowe and Anderson, 2003; Janszen et al., 2012) and trend almost perpendicular to the fjord long-axis and past ice flow. Their shape however suggests that they, like tunnel valleys, have formed as a result of subglacial erosion by pressurized meltwater, possibly during catastrophic events. Therefore, we suggest that thick, relatively slow moving ice covered the rugged topography of the bedrock plateau resulting in channelized flow of pressurized basal meltwater confined by the overlying ice. To the south, in the adjacent trough meltwater was probably incorporated into the sedimentary substrate forming water-saturated deformation tills which are thought to support faster ice flow and possibly ice streaming (Lowe and Anderson, 2003). It is also possible that

subglacial meltwater was sourced from the N side of the fjord and drained into the deeper trough on the southern side of the fjord. Differences in the pressure and routing of the subglacial meltwater could explain the partly discontinuous shape of the channels, since water is sometimes pressed through and does not erode the bed. Due to the considerable erosion needed to excavate these large features, it is possible that the subglacial meltwater channel system in Wahlenbergfjorden is, to some extent, inherited from previous glaciations.

4.2. Streamlined bedforms: glacial lineations

4.2.1. Description

Fjord-parallel streamlined bedforms are observed in both, Wahlenbergfjorden and Palanderbukta. In Wahlenbergfjorden, the streamlined bedforms are up to 2.5 km long, 80–250 m wide and 3–8 m high (Fig. 6a and b). This yields maximum elongation ratios ($E = l/w$) of 10:1. In Palanderbukta, they are 0.5–1.5 km long, 100–400 m wide and 3–5 m high, having maximum elongation ratio of 3.75:1. The streamlined bedforms are in general irregularly spaced, with average crest-to-crest spacing of 120–500 m. In outer Palanderbukta, the streamlined bedforms are curvilinear and deflected towards the west (Fig. 2b). In many areas they have been overprinted by small moraine ridges and debris-flow lobes. Groups of streamlined bedforms are further found in the tidewater glacier land systems, T.1–T.5 (Fig. 2b). Their lengths range from a couple of 100 m to 2.5 km and they are commonly overprinted by small moraine ridges. In the tidewater glacier land system, T.5, the average crest-to-crest spacing is 100–150 m (Fig. 3).

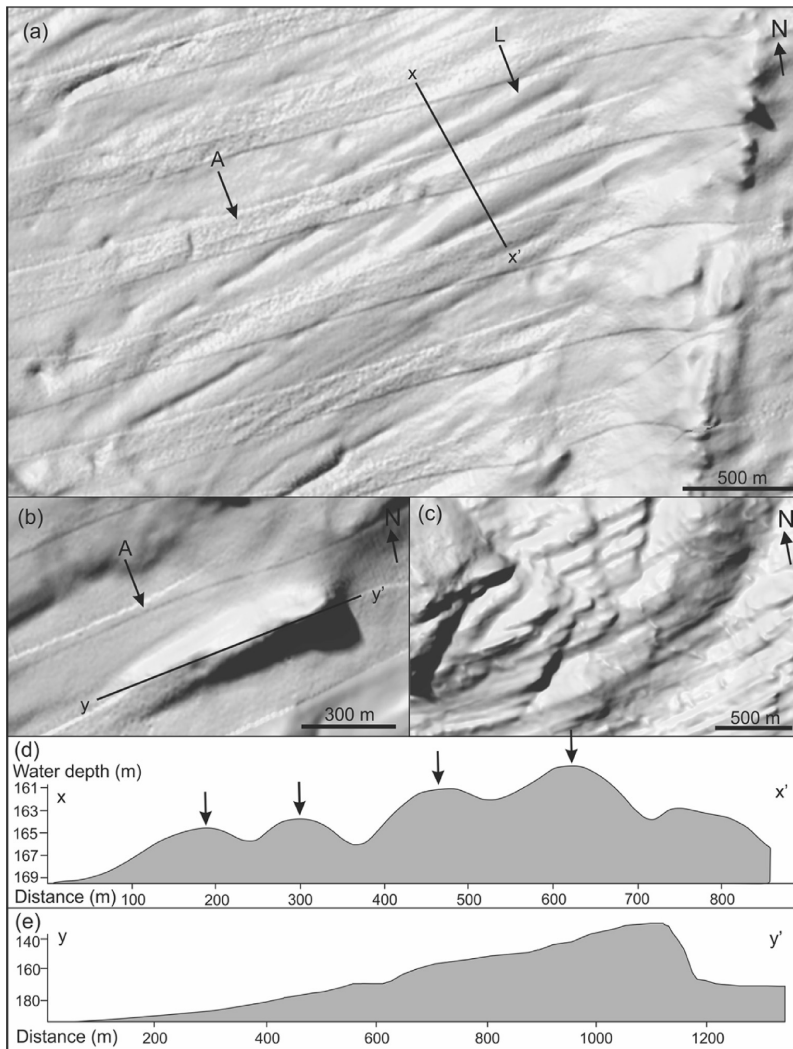


Fig. 6. (a) Glacial lineations in Wahlenbergfjorden. Arrows labeled “A” point to geophysical artefacts, formed due to refraction in the outer beams as a result of mismatch in the sound speed profiles. The arrow with “L” points towards the lineations. (b) A single crag-and-tail. (c) A group of crag-and-tails. (d) Cross-profile of the glacial lineations. Arrows point to lineation ridges. (e) Long-profile of the single crag-and-tail. For the locations see Fig. 2.

4.2.2. Interpretation

The streamlined landforms are interpreted as glacial lineations, which have formed subglacially in deformable till (Stokes and Clark, 2002; King et al., 2009; Robinson and Dowdeswell, 2011). The westward deflected lineations in outer Palanderbukta (Fig. 2b) imply that the ice flow in outer Palanderbukta was affected by the main ice flow from Wahlenbergfjorden. In the inner part of Wahlenbergfjorden, merging lineations indicate confluent ice flow. In the tidewater glacier landsystems the streamlined bedforms radiate out towards the large terminal ridges indicating diverging ice flow during their formation at the termini of the tidewater glaciers. The lineations in the T.5 landsystem most likely formed during the Etonbreen surge event in 1938 (Lefauconnier and Hagen,

1991). The glacial lineations in the T.1, T.3 and T.4 landsystems suggest that these glaciers have also experienced advances with relatively fast flow.

4.3. Streamlined bedforms with bedrock cores: crag-and-tails

4.3.1. Description

Streamlined bedforms with wider and higher heads and narrower and lower tails are found across the entire Wahlenbergfjorden (Fig. 2). The heads clearly have steeper stoss sides and more gently-sloping lee sides. They are aligned parallel to the fjord axis and occur both individually and in groups (Fig. 6b and c). The landforms have varying dimensions and their elongation ratios

range between 3:1 and 6:1. The largest ones are 10–25 m high and 300–500 m long, but can be up to 1 km long (Fig. 6e). The smaller ones are 5–10 m high, 100–200 m long, 100–150 m wide and are closely spaced (80–100 m apart).

4.3.2. Interpretation

These landforms are interpreted as crag-and-tails due to their characteristic shapes with steep stoss sides and elongated lee sides. Similar landforms are reported from formerly glaciated areas in many high-latitude regions (Benn and Evans, 2010). Crag-and-tails consist of a bedrock core with a tail of sediment on the lee side. The crag-and-tails in Wahlenbergfjorden are mainly found in areas where sub-bottom profiles indicate that bedrock is outcropping at the seafloor. This suggests that most of the crag-and-tails indeed have bedrock cores. Crag-and-tails are aligned with the direction of ice flow confirming that ice flowed from east to west in Wahlenbergfjorden. In some locations the crag-and-tails have been overprinted by small ice flow-transverse ridges indicating that the ridges post-date the crag-and-tails (Fig. 6c).

4.4. Large fjord-transverse ridges: terminal moraines

4.4.1. Description

Large submarine ridges are observed in Palanderbukta and near the present tidewater glacier fronts (Figs. 2 and 3). In Palanderbukta, these fjord transverse ridges are c. 10 m high, 200 m wide and 4 km long. They extend across the fjord and have proximal and distal slope angles of 4–5° and c. 3.5°, respectively. One

ridge in central Palanderbukta is 30 m high and up to 2 km wide (Fig. 7c). The ridge is wider on its northeastern part (Fig. 7a) and has gentle slope angles of around 2°. It is multi-crested and superimposed by small transverse ridges. In the inner part of Wahlenbergfjorden single or multiple large transverse ridges are found in front of modern tidewater-glacier termini (Fig. 2). The ridges are larger than those in Palanderbukta and vary in both width and height. The ridges are 0.5–1 km wide and 15–25 m high. They are mostly multi-crested and have gentle slopes between 2° and 4°, which are slightly steeper on the ice-proximal sides. The T.5 ridge is the largest with a maximum width of 3 km and a height up to 40 m (Fig. 3). The T.1 landsystem contains two large ridges with a ridge-spacing of approximately 1.5 km. The T.4 landsystem contains three large ridges with a spacing of around 1.5 km between the outermost ridge crests and 800 m between the innermost crests (Fig. 2).

4.4.2. Interpretation

The large transverse ridges are interpreted as terminal moraines (Fig. 2b), formed by bulldozing of marine muds and subglacial sediments in front of an advancing glacier terminus or by sediment accumulation during periods of longer terminal still stands (Boulton et al., 1996). Smaller ridges superimposed on the large terminal moraine ridge in the central part of Palanderbukta, indicate that this ridge was overridden by one or several glacier advances (Fig. 7). This could explain the difference in the morphology of the southwestern and northeastern sides of the ridge as well as the very gentle slope gradients of the terminal moraines. The ridges in inner Wahlenbergfjorden have similar shape and dimensions as

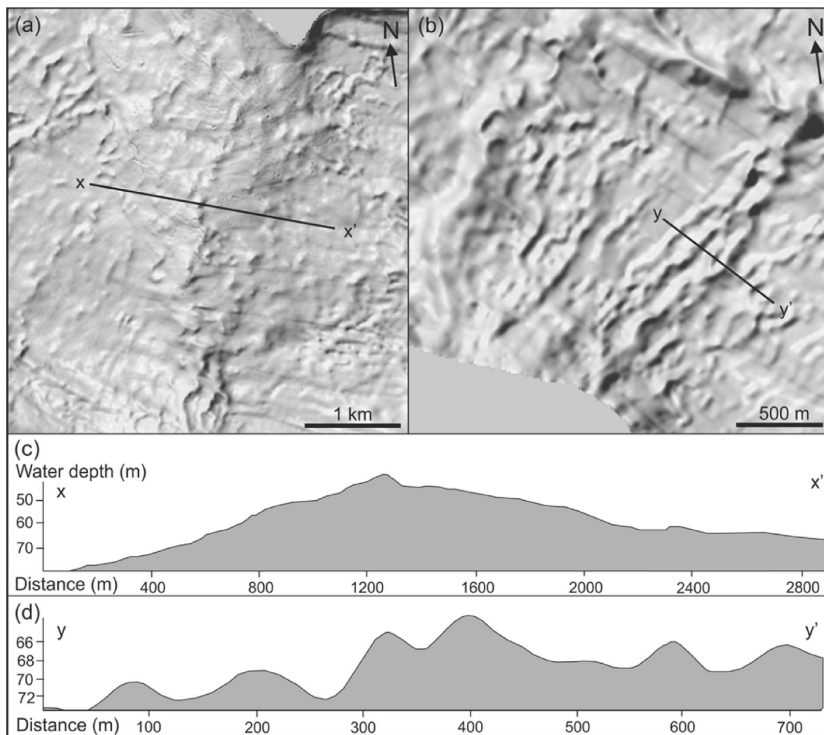


Fig. 7. (a) Large terminal moraine in central Palanderbukta. (b) De Geer moraines in the inner part of Palanderbukta. (c) Profile of the large terminal moraine. (d) Profile of the De Geer moraines. For the location see Fig. 2.

earlier studied terminal moraine ridges associated with surging glaciers in Svalbard fjords (Figs. 2 and 3), (Ottesen and Dowdeswell, 2006; Ottesen et al., 2008a; Flink et al., 2015). The T.4 and T.5 ridges are located in front of tidewater glaciers which have been recorded to surge (Lefauconnier and Hagen, 1991; Bamber et al., 2004), indicating that these ridges formed during surge maxima. The three sets of terminal moraine ridges in the T.4 landsystem imply that Bodleybreen most likely has surged three times, with each successive surge being less extensive, possibly indicating a similar pattern of general retreat interrupted with temporary surge-driven ice margin advances, as is observed in western Svalbard (Flink et al., 2015). The large width of the T.5 moraine and the presence of small ridges between the crests suggest that the moraine consists of at least two ridges (multiple crests are shown with arrows in Fig. 3). This indicates that at least two, but most likely three glacier advances have extended almost to the same position forming a complex terminal moraine system in front of Etonbreen. Since the surge terminal position matches well with the position of the submarine moraine ridge, we can with confidence state that the T.5 terminal ridge has been created, or at least modified, by the 1938 surge of Etonbreen (Lefauconnier and Hagen, 1991).

4.5. Small fjord-transverse ridges: De Geer moraines

4.5.1. Description

Series of sub-parallel and ice flow-transverse ridges occur in the inner part of Wahlenbergfjorden and across the entire Palanderbukta (Fig. 2). They are superimposed on crag-and-tails and glacial lineations. The ridges are closely spaced and have curvilinear plan forms (Fig. 7b and d). They are commonly discontinuous along their length across the fjord and vary from 150 m to 1.8 km. In Palanderbukta, the ridges are 40–100 m wide and 2–5 m high. Ridge-spacing varies between 80 and 250 m, but is typically c. 140 m. In Wahlenbergfjorden, the ridges are somewhat less distinct and continuous than in Palanderbukta. They are generally less than 100–500 m long, 20–60 m wide and 2–4 m high. The spacing between the ridges is 130–200 m and they are only observed in the inner, shallower part of the fjord. The ridges associated with the T.1–T.6 landsystems, however, display closer crest-to-crest spacing of 100–150 m, and locally even as little as 50 m. The shape of the ridges in cross-profile varies, but in general they display somewhat steeper proximal (3° – 7°) than distal (3° – 5°) slopes.

4.5.2. Interpretation

The ice flow-transverse ridges are interpreted as De Geer moraines, based on their dimensions, large number, fairly regular spacing and superposition on glacial lineations (De Geer, 1940; Linden and Möller, 2005; Benn and Evans, 2010; Todd et al., 2007). They are interpreted to form at, or close to the grounded margin of water-terminating glaciers (Benn and Evans, 2010; Todd et al., 2007). The less distinct morphology of the De Geer moraines in the inner Wahlenbergfjorden suggests that these ridges might have been partially buried by later marine sedimentation. The original ridges were possibly higher and more continuous.

The small ridges in the T.4 and T.5 surge glacier landsystems formed during still stands or small re-advances of the glacier front during the quiescent (non-surge) phase, when the glaciers experience general retreat. The ridges in the T.1, T.2 and T.3 landsystems display similar characteristics as the T.4 and T.5 ridges, suggesting that these also formed by surging glaciers during the quiescent phase. The De Geer moraines in Palanderbukta and the T.1–T.5 ridges are similar in shape, dimensions and spacing, to retreat moraines in surging glacier settings, which are inferred to form annually during winter terminal still-stands or minor re-advances when calving rates are low (Ottesen and Dowdeswell, 2006; Flink et al., 2015). This

indicates that the formation mechanism of De Geer moraines and retreat moraines in surging glacier settings may be similar, implying that the buttressing effects of sea ice might also be an important factor in the formation of De Geer moraines in fjords. If the ridges have formed annually in these tidewater glacier landsystems, the retreat rate of the glacier fronts is estimated to c. 100–150 m⁻¹ a.

4.6. Sediment lobes: debris-flow lobes

4.6.1. Description

Large, lobate accumulations of sediment are observed at the distal slopes of the terminal moraine ridges in inner Wahlenbergfjorden (Figs. 2 and 3). The sediment accumulations have maximum widths of 6 km along the distal side of the moraines and comprise of several lobe-shaped protuberances, which have run-out distances of up to 2.5 km from the moraine ridge crests. In general, they extend from 50 to 100 m water depth. The surfaces of the lobes show dislocated blocks and flow structures (Fig. 8a). In particular, the T.1 and T.4 sediment lobes contain clearly visible downslope-oriented flow structures. The sediment lobes overprint glacial lineations and De Geer moraines. Three generations of stacked lobes are distinguished in the T.5 landsystem (Fig. 8a and c). In the T.3 and T.4 landsystems, two stacked sediment lobes are observed. Two similar large lobate sediment accumulations are also observed on the northwestern slope of Wahlenbergfjorden (Fig. 2). These have runout distances of 2.5 km and cannot be directly linked to terminal moraine ridges.

4.6.2. Interpretation

The sediment lobes are interpreted as debris-flow lobes based on their shape and location on the distal flanks of the terminal moraine ridges. The debris-flow lobes comprise of glacial sediments, which are brought to the terminal moraine ridge subglacially by the glacier, and occasionally material moves downslope as the ridge becomes unstable due to high sediment input (Ottesen et al., 2008a; Kristensen et al., 2009). Submarine debris-flow lobes are common in Svalbard fjords and often occur on the lee side of the submarine Little Ice Age moraines (Plassen et al., 2004; Ottesen and Dowdeswell, 2006; Ottesen et al., 2008a). Debris-flow lobes are also common in surging glacier settings where large amounts of glacial sediments are brought to the glacier front during the active phase. The lobes have been suggested to form during the active phase as continuously failing sediments are pushed in front of the advancing glacier front (Kristensen et al., 2009) or during surge stagnation, when the glacier front stops advancing, the moraine ridges become unstable and prone to mass movements (Ottesen et al., 2008a). At least two stacked debris-flow lobes are present on the distal slopes of the moraine ridges in the T.3 to T.5 landsystems. The lobes indicate high sediment input, likely due to a high subglacial sediment flux, possibly related to glacier surges. The debris lobes on the northwestern slope of Wahlenbergfjorden (Fig. 2) cannot be directly linked to terminal moraine ridges, but they are located downslope from the glacier fronts of Gimlebreen and Bragebreen. Just like the other tidewater glacier in Wahlenbergfjorden, both of these glaciers had larger extents in the past (Lefauconnier and Hagen, 1991), suggesting that the debris-flow lobes are linked to advances of these glaciers. The debris-flow lobe in Palanderbukta (Fig. 2) could be related to the Claserbreen surge between 1938 and 1939 (Lefauconnier and Hagen, 1991), but it could also originate from a down-slope mass movement at a later time.

4.7. Sinuous ridges: eskers

4.7.1. Description

Sinuous ridges are observed in two areas in the inner part of Wahlenbergfjorden (Figs. 2 and 8b). The ridges are between 2 and

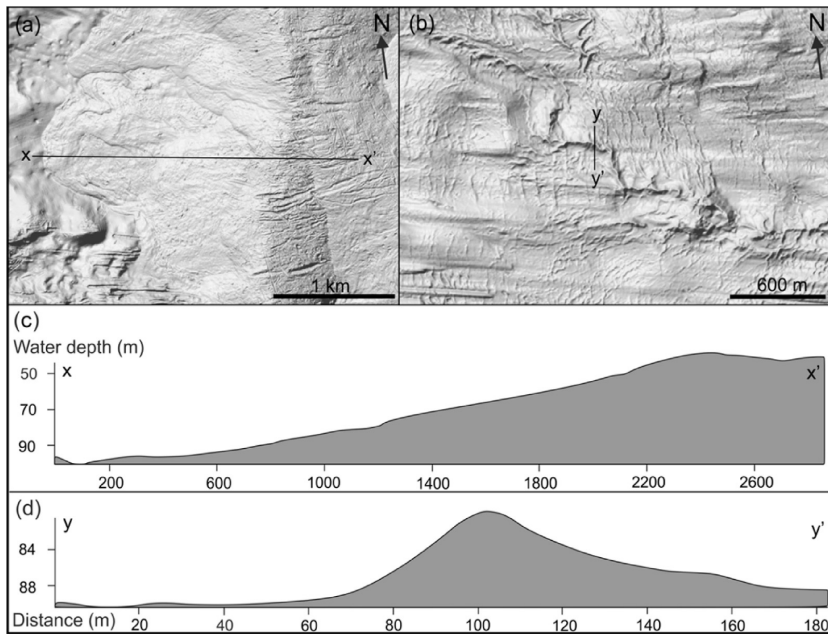


Fig. 8. (a) Debris-flow lobes at the distal slope of the T.5 terminal moraine. (b) Esker in front of Etonbreen. (c) Cross-profile of the terminal moraine and the debris-flow lobes. (d) Cross-profile of the esker. For the locations see Fig. 3.

4 km long, 60–80 m wide and 10–15 m high (Fig. 8d). They are sinuous in planform and generally oriented parallel to the fjord axis (Fig. 8b). The ridges are symmetric or nearly symmetric in cross-section and are superimposed on glacial lineations. They usually follow the deeper parts of the fjord.

4.7.2. Interpretation

The sinuous ridges are interpreted as eskers that formed in subglacial conduits by sediment infill (Ottesen *et al.* 2008a; Kristensen *et al.*, 2009). The position and shape of the eskers in front of the modern glacier terminus of Etonbreen suggest that subglacial streams are present under the glacier. The eskers are superimposed on the glacial lineations indicating that they formed after the glacier advance. According to Kamb *et al.* (1985) and Murray *et al.* (1998) eskers are indicative of an efficient subglacial drainage system and therefore suggested to form after surge stagnation. During the active phase of the surge, the subglacial drainage system is assumed to be inefficient and drainage of meltwater occurs across large areas of the glacier bed and not through single large conduits. The inefficient subglacial drainage system contributes to high basal water pressures and rapid ice flow velocities during the surge (Kamb *et al.*, 1985; Benn *et al.*, 2009). Because eskers are indicative of an efficient drainage system, they likely formed after the surge of Etonbreen.

4.8. Geometrical ridge networks: crevasse-squeeze ridges

4.8.1. Description

The T.5 landsystem contains several sets of small ridges oriented in different directions that often cross-cut each other to form

geometrical ridge networks (Fig. 3). The ridge networks are found near the terminal moraine ridge (Fig. 3). The individual ridges in the networks are 1–3 m high, 10 m wide and 30–100 m long (Fig. 9a and c). They are symmetrical in cross-profile and the majority of the ridges are oriented at low angles, i.e. are sub-parallel, to the terminal moraine ridge.

4.8.2. Interpretation

Their similar dimensions and geometrical pattern of the ridges in the T.5 landsystem to earlier described crevasse-squeeze ridges (Ottesen and Dowdeswell, 2006; Ottesen *et al.*, 2008a; Flink *et al.*, 2015; Lovell *et al.*, 2015) allows us to interpret these as the same submarine landforms. In the T.5 landsystem the crevasse-squeeze ridges intersect with retreat moraines, making it sometimes difficult to distinguish these ridges from each other. The crevasse-squeeze ridges, however, differ from the retreat moraines by being smaller in size and more often symmetrical in cross-profile. Crevasse-squeeze ridges form in the thin, highly-crevassed margin of a surge lobe, by the upward injection of debris into basal crevasses, when subglacial water pressures are close to the ice overburden pressure (Lovell *et al.*, 2015). This supports the conclusion that the T.5 landsystem has formed by a glacier surge.

Crevasse-squeeze ridges are not observed in the other tidewater glacier landsystems in the study area. This could be explained by the older age of these landsystems or higher sedimentation rates near the glacier termini, which has resulted in the burial of the crevasse-squeeze ridges. Alternatively, these ridges were not formed or preserved as a result of local glacier dynamics. In order to preserve crevasse squeezed ridges, they must form just at the very

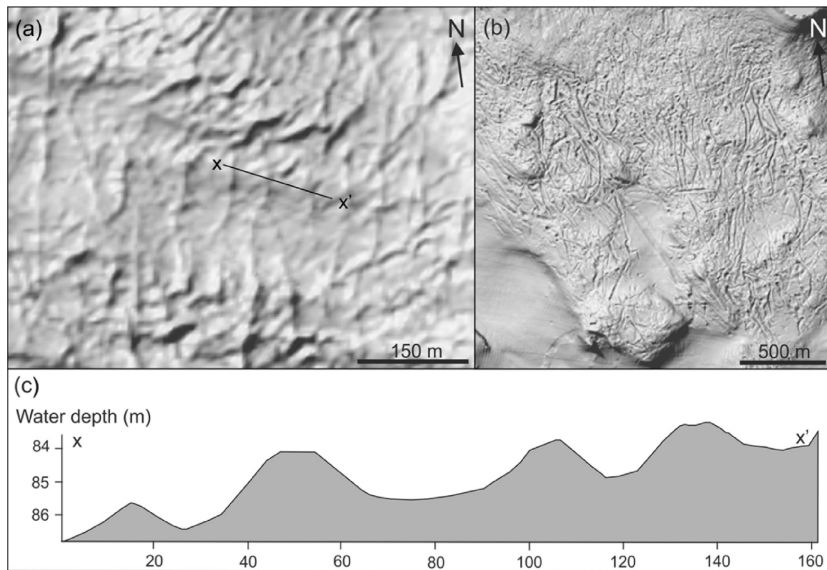


Fig. 9. (a) Crevasse-squeeze ridges in inner Wahlenbergfjorden; in the T5 landsystem. (b) Iceberg ploughmarks and pits in outer Wahlenbergfjorden. (c) Cross-profile of the crevasse-squeeze ridges. For the locations see Figs. 2 and 3.

last moment before the ice front lift of the ground and break up, since they are very small features and any ice movement over them should remove them.

4.9. Randomly oriented linear to curvilinear grooves: Iceberg ploughmarks and pits

4.9.1. Description

Linear to curvilinear grooves are present in the shallow inner part and on the sides of the fjord, and on the bedrock plateau in the outer fjord. They are particularly abundant on the crests of the terminal moraine ridges (Fig. 3). The grooves are variably oriented but the dominant orientation is parallel to the long axis of the fjord. The grooves in Wahlenbergfjorden were recorded in the areas with water depth of 100 m and shallower. In Palanderbukta, they are present down to water depths of 60 m. The depressions are in general 100–200 m long, 0.5–3 m deep and 30–50 m wide (Fig. 9a and c). In cross-section they have U- or V-shaped profiles and locally have small berms on one or both sides. Some grooves have larger, isometric depressions at one end.

4.9.2. Interpretation

Linear to curvilinear grooves with V- or U-shaped cross-profiles are characteristic of iceberg ploughmarks (cf. Dowdeswell and Ottesen, 2013). Due to these characteristics, the randomly oriented linear to curvilinear grooves are interpreted as iceberg ploughmarks (Fig. 9b). The grooves form when the keels of icebergs plough through seafloor sediments, often producing small berms along their sides (Robinson and Dowdeswell, 2011). The isometric depressions are interpreted as iceberg pits on the basis that they occur in areas with iceberg ploughmarks. The pits

imply that icebergs have touched down and been grounded on the seafloor. The size of the icebergs is linked to the height of the tidewater cliffs of glaciers terminating into the fjord system. In Wahlenbergfjorden and Palanderbukta, the depth of the ploughmarks is related to the size of the icebergs produced in respective fjord.

5. Acoustic sub-bottom facies of Wahlenbergfjorden

Chirp sonar sub-bottom data were collected in Wahlenbergfjorden (Fig. 4a) during the R/V Helmer Hanssen cruise in 2012. Wahlenbergfjorden is covered by a thin sediment drape, which is typically 5 m thick and consists of fine grained marine muds with occasional dropstones (Fig. 10). Locally the sediment drape is only a couple of meters thick or completely absent. However, in depressions and in the central, deeper part of the fjord sediment thickness can reach 10–20 m (Fig. 4b).

The acoustic sub-bottom facies in Wahlenbergfjorden can be divided into three different facies, F.1–F.3 (Fig. 10). Acoustic facies F.1 is generally 1–5 m thick and covers most of the area mapped by chirp data. The F.2 facies is found locally and usually occurs below the F.1 facies. The F.3 facies is more common in the inner part of the fjord. The lack of acoustic penetration suggests that the F.3 facies consists of a hard substrate, such as bedrock or glacial till.

6. Description and interpretation of the sediment core data

6.1 Gravity core HH12-13

6.1.1. Description

The 2.26 m-long HH12-13 core was recovered from the inner part of Wahlenbergfjorden in a water depth of 76 m (Fig. 1). The

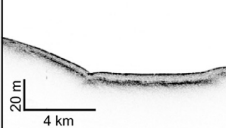
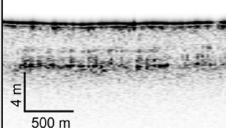
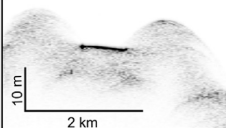
Acoustic facies	Chirp example	Description	Interpretation
F.1		Acoustically homogenous, transparent sediments draping the seafloor. 1–5 m thick, with a strong, continuous top reflector and locally discontinuous bottom reflector (chirp line 022).	Fine grained Holocene muds formed by distal sedimentation (cf. Hogan et al. 2011). Correlates to the lithological unit Fmd.
F.2		Parallel or sub-parallel, often diffuse multiple sub-bottom reflectors. Commonly less than 1 m thick and found below the F.1 facies (chirp line 034).	Laminated muds, formed through ice proximal glaciomarine sedimentation. Represents early deglaciation phase (cf. O Cofaigh et al. 2001; Hogan et al. 2011). Correlates with the Flw unit.
F.3		Strong upper reflector, diffuse on slopes with acoustically transparent underlying signal. Common in areas with steep irregular topography (chirp line 054).	Acoustically impenetrable facies consisting of coarse grained sediments, such as subglacial till or bedrock (cf. Hogan et al. 2011). Correlates to the Dmm unit.

Fig. 10. Acoustic sub-bottom facies identified from chirp data in the northern part of Wahlenbergfjorden.

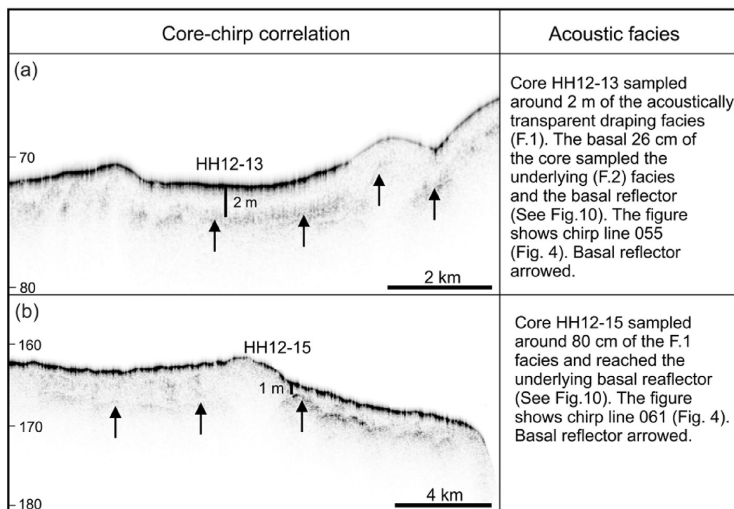


Fig. 11. Chirp sonar sub-bottom profiles from the core sites in Wahlenbergfjorden. (a) Profile 005 and core HH12-13. (b) Profile 061 and core HH12-15. The black bars show the locations and approximate penetration depth of the two gravity cores. Depths in m, displayed on the y-axis, were calculated assuming a sound wave velocity of 1500 m s^{-1} through the water column and the sediments. For the locations of chirp profiles see Fig. 4; for acoustic sub-bottom facies descriptions and interpretations see Fig. 10.

core was acquired from an area dominated by crag-and-tails and small transverse ridges (Fig. 11a). The core is divided into four units, represented by lithological facies codes, Dmm (massive matrix-supported diamicton), Fmd (massive mud with dropstones), Flw (diffusely laminated mud) (Eyles et al. 1983), (Fig. 12a). The upper Dmm unit consists of a continuous 5 cm thick diamicton layer. The diamicton contains subangular gravel-sized particles and sands in a fine mud matrix (Fig. 12a). Unit Fmd covers the interval of 5–200 cm and consists of reddish brown, massive mud with outsized clasts (Figs. 12a and 13). The texture of the mud is silty-clay with a mean grain size (D50) of 5–20 μm (very fine to medium silt). A peak of medium to coarse

silt occurs at 60–80 cm depth and at the transition to the Flw unit. Unit Fmd contains shell fragments and foraminifera, from which ^{14}C ages were obtained (Table 1). Sub-angular to sub-rounded outsized clasts and sandy-gravelly lenses are present through the unit.

The Flw unit is 20 cm thick and consists of laminated mud (Fig. 12a). The laminations are parallel, 5–30 mm thick and continuous across the core (Fig. 13). They are defined by changes in sediment color rather than grain size differences. Two sand layers (Sm) are incorporated into the Flw unit. Shear strength values display a peak of 8 kPa at 210 cm, which corresponds to the sand layers (Fig. 12a). The basal Dmm unit consists of an unsorted

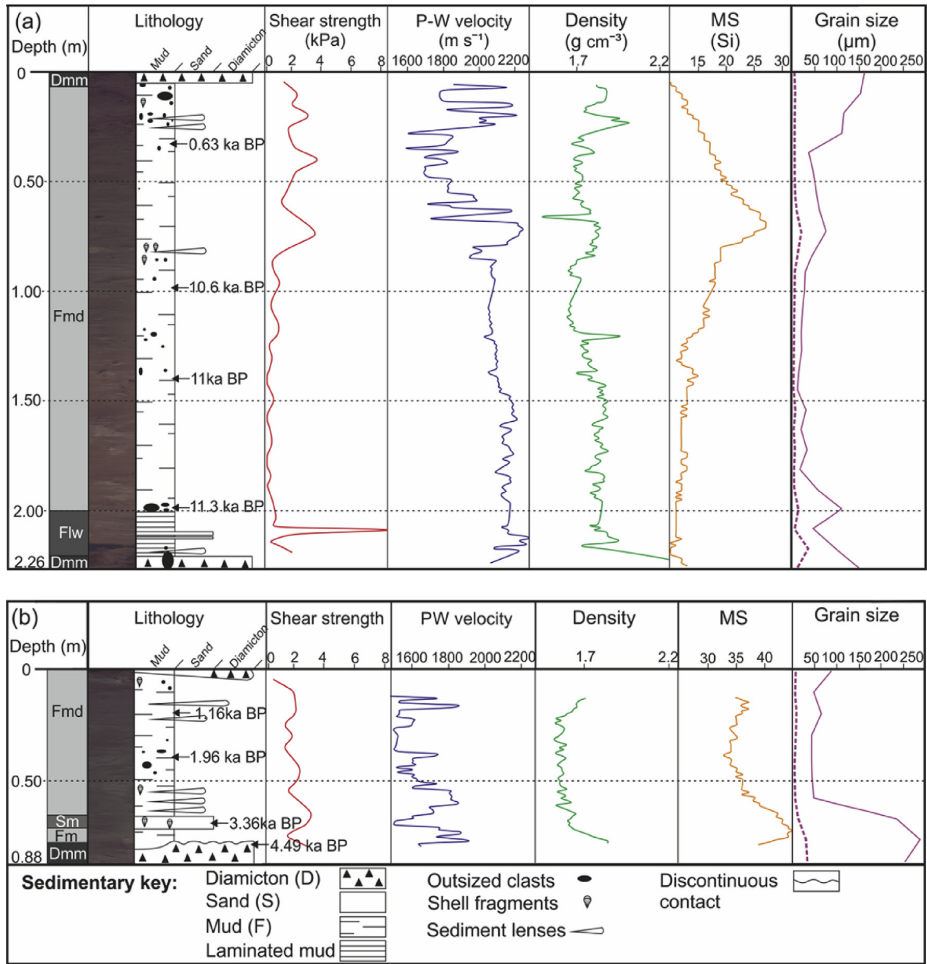


Fig. 12. Composite logs of the Wahlenbergfjorden cores. (a) HH12-13 and (b) HH12-15, showing lithology, undrained shear strength, P-wave velocity, density, magnetic susceptibility and grain-size distribution on the <1 mm fraction. In the grain size column, dashed lines show the D50 (mean grain size) and continuous lines the D90. Black arrows point to the depths where samples for ¹⁴C dating were retrieved. The ages are reported as calibrated ¹⁴C BP ages.

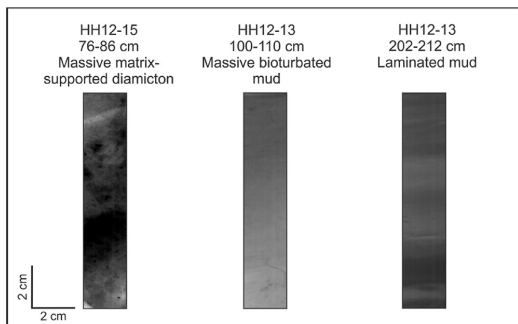


Fig. 13. X-Radiographic images of the main lithological facies in the cores HH12-13 and HH12-15 (Dmm, Fm, Flw).

diamicton facies (Fig. 12a). The contact between the diamicton and the overlying Flw unit is sharp. The basal Dmm unit consists of up to pebble-sized, sub-rounded to sub-angular clasts in a mud-supported matrix with a high content of sand.

P-wave (P-W) velocities in the core range between 1600 and 2300 m s⁻¹ with high variability in the upper 80 cm. In the lower part of the core the values remain fairly constant at around 2100 m s⁻¹ with a maximum of 2300 m s⁻¹ at 210 cm. The P-W values are relatively high and several measurement with amplitudes less than 80% were cleaned away in the lower part of the core. The bulk density is between 1.5 and 2.2 g cm⁻³ with a peak of 2.3 g cm⁻³ at the base of the core, corresponding to the basal Dmm unit (Fig. 12a). Most of the values fall near the estimated average density of 1.7 g cm⁻³ for marine sediments (Tenzer and Gladkikh, 2014). Magnetic susceptibility (MS) values display a peak at 70 cm.

Table 1

¹⁴C ages for the cores HH12-13 and HH12-15. ¹⁴C ages are reported as calibrated BP mean ages with two sigma uncertainty. Sedimentation rates have been calculated for the respective depth ranges shown in column "Depth range".

Samples	Depth (cm)	C ¹⁴ age BP	Uncertainty ±	Cal. age BP two sigma	Cal. Mean BP	Depth range (cm)	Sed. Rate (cm kyr ⁻¹)	Sample type
HH12-13								
HH12-13-A	34	1175	40	540–710	630	0–34	54	Mixed benthic forams
HH12-13-B	99	9830	50	10480–10790	10640	34–99	6	Mixed benthic forams
HH12-13-C	140	10180	60	10870–11220	11040	99–140	101	Mixed benthic forams
HH12-13-D	199	10380	55	11130–11560	11350	140–199	193	Mixed benthic forams
HH12-15								
HH12-15-A	20	1705	40	1050–1260	1160	0–20	17	Mixed benthic forams
HH12-15-B	40	2440	40	1840–2090	1960	20–40	25	Mixed benthic forams
HH12-15-C	70	3590	45	3220–3500	3360	40–70	22	C.lobatulus
HH12-15-D	79	4450	40	4350–4630	4490	70–79	8	Mixed benthic forams

6.1.2. Interpretation

Since the upper unit consists of diamicton (Dmm) and is found at the top of the core it is interpreted to form through iceberg or sea-ice sedimentation. The deposition of the diamicton together with a higher amount of outsized clasts at the top of the core might indicate a regrowth of the tidewater glacier during the late-Holocene. Unit Fmd consists of fine grained silty mud and corresponds to acoustic sub-bottom facies F.1 (Figs. 10 and 11a) indicating that the unit formed in a distal glaciomarine environment by continuous accumulation of suspended sediment settling through the water column. The outsized clasts suggest that the core location was influenced by sea ice and iceberg-rafted debris during the deposition of unit Fmd. The outsized clasts, sand and gravel lenses may have formed by iceberg dumping, by sea ice transported sedimentation (Nurnberg et al., 1994) or by sediment mass flows. Fluctuations in the P-W velocity together with a higher amount of outsized clasts at the top of the core might indicate pulses of released icebergs related to increased calving of the tidewater glaciers in the fjord. P-W velocity values are closely related to grain size, where coarser grains give higher P-W velocities (Weber et al., 1997). High P-W velocities and bulk density values trough out the core suggest that the mud matrix has relatively high silt/sand content. The increase in MS values does not correspond with a visible grain-size change (Fig. 12a) and might, therefore, indicate a change in rock type and sediment source area (Robinson et al., 1995).

The laminated unit Flw indicates a more ice-proximal setting (cf. Ó Cofaigh et al., 2001) and correlates to acoustic sub-bottom facies F.2, which is interpreted as an ice-proximal acoustic facies (cf. Hogan et al., 2011, Fig. 10). The Flw unit overlies the basal Dmm unit, possibly forming a deglacial sediment sequence, which records progressively more ice-distal deposition during the retreat of a nearby ice-margin. Unit Dmm consists of a mix of grain sizes with sub-angular gravel-sized clasts, and it is overlain by the Flw unit, suggesting that the basal diamicton could possibly be a subglacial till, which is supported by the high bulk density of the unit, reflecting both a reduced porosity from subglacial loading and shear, as well as a coarsening of the sediment matrix. The radio-carbon age HH12-13D (Table 1), derived from the top of the laminated mud (Fig. 12a) further support that the Flw and Dmm units represent a deglacial sequence.

6.2 HH12-15

6.2.1. Description

The HH12-15 core is 0.87 m long and was recovered near the crest of a subdued ridge (Fig. 11b) in the outer part of the fjord at a water depth of 166 m (Fig. 1). The core is divided into four

lithological units, Fmd, Sm (massive sand), Fm and Dmm (Fig. 12b). The main unit, Fmd consists of massive, homogenous olive grey mud, with randomly oriented outsized clasts and organic matter in the form of shell fragments and foraminifera. A gravel-rich lens and sand lenses are present throughout the Fmd unit. A 9-cm thick unit of massive sand, Sm, with shell fragments occurs between the Fmd and Fm units. The contact between the units is sharp. An increase in grain size diameter occurs at around 60 cm, implying that 10% of the matrix consists of grains >250 µm, i.e. above the medium sand fraction (Fig. 12b). The basal unit (Dmm) consists of massive, matrix-supported diamicton, with sub-rounded to sub-angular clasts (Fig. 13). The contact between the two units is erosive, sub-horizontal and marked by a distinct color change from olive grey to reddish brown (Fig. 12b). Shear strength and P-W velocity values vary throughout the core. Density values stay below 1.5 g cm⁻³, indicative of a matrix dominated by terrigenous clay sized particles, except for peaks at the top and base of the core. MS values are higher than in core HH12-13, with the highest values close to the base (Fig. 10b).

6.2.2. Interpretation

Units Fmd and Fm were deposited in a similar environment as the Fmd unit in core HH12-13 and can be correlated to acoustic sub-bottom facies F.1 (Fig. 10). The gravel lens at the top of the core was likely deposited as an iceberg dump. Iceberg dumps generally form mound shaped lenses of coarser sediments (Thomas and Connell, 1985). The relatively young ¹⁴C age derived from the boundary between units Fm and Dmm, above the basal diamicton, indicates that this is likely not a subglacial diamicton, but rather a mass flow or an iceberg dump facies. However, sample D was derived from the top of the Dmm unit (Fig. 12b, Table 1) at the boundary to the Fm unit. The boundary between the Dmm and the overlying Fm unit is diffuse, and may indicate an erosional episode. The sediments composing the Dmm unit might therefore be much older than indicated by the ¹⁴C age from sample D. The core was retrieved from a submarine high (Fig. 11b) suggesting that early Holocene sediments could have been subjected to disturbances, such as mass movements. This might explain why early Holocene sediments are not present in the core and possibly also why no deglacial, laminated acoustic sub-bottom facies (F.2) is present. Unfortunately no reliable geophysical values were obtained from the Dmm facies.

7. Discussion

7.1. Ice-sheet dynamics

The submarine landform record in Wahlenbergfjorden (Fig. 2) indicates that the fjord acted as a conduit for fast flowing ice. The

orientation of the elongated landforms show that ice flowed westwards, towards the Hinlopen Strait. This suggests that ice flow in Wahlenbergfjorden was deflected towards the north at the head of the fjord where it joined the northerly flow of the Hinlopen Strait ice stream. The submarine landform assemblage in Wahlenbergfjorden is similar to the landform assemblage on the inner shelf of the Hinlopen Strait, which also contains glacially-scoured bedrock, crag-and-tails and glacial lineations (Ottesen et al., 2007; Batchelor et al., 2011). It is therefore plausible that similar ice-flow conditions existed in Wahlenbergfjorden as in the inner Hinlopen Strait. The elongation ratios of the glacial lineations in Wahlenbergfjorden are; however, lower than the 10:1 ratio for MSGs. The difference in elongation ratios between the lineations in the two fjords (Wahlenberg and Palanderbukta) suggests that ice streaming occurred for a longer time period, or was faster, in Wahlenbergfjorden.

Elongated bedforms, such as glacial lineations, drumlins, and crag-and-tails, together with hard crystalline bedrock and rock drumlins, are commonly found in ice-stream onset zones (Stokes and Clark, 1999; De Angelis and Kleman, 2008; Ottesen et al., 2008b). Therefore, Wahlenbergfjorden could have acted as an ice-stream onset zone. This interpretation is further supported by the patterns of submarine landforms indicating convergent ice flow in inner Wahlenbergfjorden, and the coalescing tributary ice flow from Palanderbukta, since ice-stream onset zones are commonly characterized by convergent flow patterns (Joughin et al., 2002; De Angelis and Kleman, 2008).

The glacially-scoured bedrock in Wahlenbergfjorden (Fig. 2) indicates that glacial scouring as well as large amounts of meltwater production played an important role in the sculpting of these bedrock highs. Production of large amounts of meltwater and meltwater-related landforms have also been suggested to be indicative of ice-stream onset zones (Ó Cofaigh et al., 2002; Lowe and Anderson, 2003), further supporting the hypothesis that Wahlenbergfjorden has acted as an ice-stream onset zone. It is possible that the submarine sills and plateaus consisting of resistant bedrock (see section 2, Fig. 1b) were overlain by slower flowing or even cold-based ice. This can be inferred from the meltwater channels (Fig. 2). Therefore, it is plausible that the fast-flowing ice in the fjord was bordered by slower flowing ice, located on the crystalline bedrock highs at the sides of the fjord. This would indicate spatially changing thermal bed conditions, with warm based ice located in the deeper part of the fjord and possibly cold-based ice located on the bedrock highs. Alternatively the fast-flowing ice in the deeper parts of the fjord might be a response to elevated pore water pressures in the subglacial sediments/tills, which are absent on the bedrock highs and allow stronger frictional coupling between the ice base and the bed.

Ice-stream onset zones are commonly associated with changes in the thermal state of the bed, from frozen to melted (De Angelis and Kleman, 2008). Based on the submarine landform record, Wahlenbergfjorden and Palanderbukta can both be described as topographically controlled ice-stream onset zone tributaries characterized by coalescence of topographically constrained ice flow (cf. Joughin et al., 2002). The outer fjord and Hinlopen Strait acted as a transitional ice-stream zone, where flow velocities accelerated to full ice-stream velocities. This has been inferred from submarine landforms, with mega-scale glacial lineation like features and highly elongated drumlins in the middle-shelf of the Hinlopen Strait and bedrock drumlins and less elongated lineation in the inner-shelf and at the mouth of Wahlenbergfjorden (Ottesen et al., 2007; Batchelor et al., 2011). The confluent ice-flow in inner Wahlenbergfjorden could suggest the presence of ice domes

centered approximately at the present positions of Austfonna and Vestfonna during the late glacial period.

7.2. Deglaciation

The submarine data indicates that the deglaciation of Wahlenbergfjorden, particularly in its outer part, proceeded rapidly, since no evidence for longer still stands, in the form of grounding-zone wedges, debris-flow lobes or large terminal moraines are observed there. Deglaciation probably occurred by flotation of the glacier front in the deepest parts of the fjord in response to ice-sheet thinning and sea level rise (Lambeck et al., 2002). In the shallower inner part of the fjord, ice retreat slowed down. This is suggested by the occurrence of De Geer moraines in the inner fjord. The oldest ^{14}C date from core HH12-13 was obtained from the top of the laminated mud unit, interpreted as a deglacial ice-proximal facies, and indicates that the core site became ice-free some time prior to 11.3 ± 55 Cal. ka BP. This age is in agreement with other studies in northern Svalbard, suggesting deglaciation ages of the straits around Nordaustlandet at 14–10 ka BP (Hogan et al., 2010a, 2010b; Fransner et al. 2017). ^{14}C dates from the Hinlopen Strait indicate that the ice sheet retreated from there around 13.7–13.9 ka BP (Koç et al., 2002). This suggests that the ice sheet retreated from the Hinlopen Trough to inner Wahlenbergfjorden in approximately 2.5 kyr.

In Palanderbukta, ice flow-transverse landforms are common, indicating slow and episodic retreat of the ice margin (cf. Dowdeswell et al., 2008; Linden and Möller, 2005). The fairly regular spacing between the crests of the De Geer moraines in Palanderbukta suggests that the terminus of the ice sheet retreated with a steady speed, assuming that the ridges formed annually or semi-annually (as interpreted in other Svalbard fjords (cf. Ottesen and Dowdeswell, 2006; Flink et al., 2015)). This would indicate ice sheet retreat rates of approximately $130\text{--}200$ m yr^{-1} and implies slightly slower terminal retreat rates in Wahlenbergfjorden compared to estimated ice-margin retreat rates in, for example, northern Sweden, where De Geer moraines and varve chronology indicate approximate rates of 400 m yr^{-1} (Linden and Möller, 2005). The large terminal moraines in Palanderbukta suggest that the slow retreat was interrupted by several longer still-stands. The difference in deglaciation pattern between Wahlenbergfjorden and Palanderbukta can most likely be attributed to the difference in seafloor depth. Wahlenbergfjorden is 290 m deep in its outer part, whereas Palanderbukta is typically less than 120 m deep. Global sea-level rise of up to 15 mm yr^{-1} between 16 and 12.5 ka BP and $11.5\text{--}0.9$ ka BP (Lambeck et al., 2002) could have contributed to the fast deglaciation of Wahlenbergfjorden by promoting flotation of the ice in deeper marine areas.

^{14}C ages indicate that the uppermost lithological units (Dmm and Fmd in HH12-13 and Fmd in HH12-15 cores) are of Holocene age. The ^{14}C ages (C and D) from core HH12-13, derived from the lower part of Fmd and the top of the Flw unit, indicate high sedimentation rates, of up to 193 cm kyr^{-1} in the early Holocene (Table 1). Sedimentation rates in Svalbard fjords have in general been estimated to between 10 and 40 cm kyr^{-1} (Plassen et al., 2004; Fransner et al. 2017). The high sedimentation rates between the early Holocene samples (C and D) and the base of core HH12-13 suggest considerably faster accumulation of sediments during deglaciation. The late Holocene sedimentation rate of 54 cm kyr^{-1} is also relatively high in core HH12-13 (Table 1). Higher sedimentation rates in the inner Wahlenbergfjorden might be explained by tidewater glacier advances bringing more coarser-grained sediments to the inner fjord area during late Holocene or

by increased surge events. Modern sedimentation rates near surging glacier termini are estimated to be as high as 3800 cm kyr⁻¹ (Forwick et al., 2010).

The ¹⁴C ages from the HH12-15 core are much younger indicating late Holocene marine sedimentation. The lower sedimentation rates of around 20 cm kyr⁻¹ might be explained by the fact that the core is located farther away from the tidewater glaciers in the inner fjord (Forwick et al., 2010). Since the Wahlenbergfjorden catchment area contains carbonate rocks (See section 2) it cannot be excluded that the radiocarbon ages have been contaminated by older carbon, possibly from a detrital source. The presence of carbonate rocks in the catchment area could lead to apparently older ¹⁴C ages due to the hard water effect (Shotton, 1972).

7.3. Late Holocene glacier dynamics

The T.4 and T.5 landform assemblages are interpreted as surging glacier landform assemblages, because they contain a set of landforms characteristic of glacier surges (cf. Flink et al., 2015), and because these glaciers are known to have surged during recent times (Dowdeswell, 1986; Bamber et al., 2004). Crevasse-squeeze ridges have, however, only been observed as part of the T.5 landform assemblages. This could be explained by burial of the relatively small ridges due to high sedimentation rates near the tidewater-glacier termini. The T.4 landsystem includes three large terminal moraines (Fig. 2), with debris-flow lobes emanating from each ridge indicating that Bodleybreen has advanced at least three times, most likely during surge events. During its most recent surge the terminus of Bodleybreen only reached the position of the most proximal submarine ridge, which must have formed during the 1977 surge. This confirms that the glacier extended further than the most proximal ridge prior to 1977 (Lefauconnier and Hagen, 1991). During its most recent surge in 1938, the terminus of Etonbreen reached the position of the large submarine moraine ridge some km 7 from the present-day glacier margin. The occurrence of small ridges between the multiple crests of the large terminal moraine indicates that the glacier front reached approximately the same position earlier (See section 4.4.2, Fig. 3). The occurrence of three stacked debris flow-lobes and the multi-crested terminal ridge with small ridges in between, indicates that Etonbreen most likely surged to approximately the same position two or possibly three times. It is not possible from our data to determine when the glacier previously extended to this position and it is possible that the outermost terminal ridges formed during a Little Ice Age advances or earlier, and was only modified by the 1938 surge.

The submarine landform assemblage T.6 does not display the characteristics of a typical glacier surge landform assemblage, since there is no single large terminal moraine or debris-flow lobe present on the seafloor. Palanderbreen likely surged just prior to 1969, but the exact surge limit has not been recorded and the surge has only been inferred from a depressed upper glacier basin and heavy crevasing in the ablation area based on aerial photos (Lefauconnier and Hagen, 1991). The outermost moraine ridge displays a hummocky character, more similar to glaciotectonic end-moraines formed by terrestrial glacier surges (Schomacker et al., 2014). It is possible that the shallow water depth in front of Palanderbreen (approximately 10 m below present sea level) has led to different glacier dynamics during the active surging phase, leading to the formation of an atypical landform assemblage. Since the maximum position of the Palanderbreen surge is not known it is also possible that the glacier did not reach the area covered by the bathymetric data and the ridges (Fig. 2) are closely spaced De Geer moraines.

Idunbreen, Frazerbreen and Aldousbreen are previously believed to be of non-surge type and there are no historical records

indicating surging from these glaciers (Dowdeswell, 1986; Lefauconnier and Hagen, 1991). The T.1, T.2 and T.3 landsystems, however, display many similarities to the T.4 and T.5 landsystems suggesting that they have formed in similar conditions (Fig. 2). Large terminal moraine ridges with debris-flow lobes, glacial lineations and small retreat moraines are all present in these landsystems, suggesting that surging of these glaciers cannot be ruled out. The outermost ridges in the T.1, T.2 and T.3 landsystems could also have formed during climatically induced glacier advances, for example during the Little Ice Age. It is however likely that the Svalbard tidewater glaciers in the Nordaustlandet area have experienced a similar climatically-forced shift to surge conditions during the Little Ice Age as has been suggested for terrestrial glaciers (Sevestre et al., 2015; Sevestre and Benn, 2015). Both increased sedimentation rates in the inner fjord during late Holocene and evidence of nearly simultaneous surge activity during the Little Ice Age support the hypothesis that glaciers in an intermediate climatic envelope can experience climatically induced switches to- and from a surge mode (Sevestre and Benn, 2015).

7. Conclusions

- Streamlined bedforms indicate that Wahlenbergfjorden was occupied by streaming ice. The converging pattern of the streamlined landforms in the inner fjord implies that Wahlenbergfjorden has acted as an ice stream onset zone.
- The westerly ice flow along Wahlenbergfjorden indicates that some time during the last glacial, local ice domes were centered over Austfonna.
- Radiocarbon dates from the inner part of Wahlenbergfjorden indicate that the fjord was deglaciated prior to 11.3 ± 55 ka BP.
- The deglaciation was different in Wahlenbergfjorden and Palanderbukta: in the deeper part of Wahlenbergfjorden, deglaciation proceeded rapidly, possibly by flotation of the ice terminus, whereas the deposition of De Geer moraines in Palanderbukta suggests a gradual retreat of a grounded glacier margin. Based on the De Geer moraines, retreat rate of the ice terminus was estimated to 130–200 m yr⁻¹.
- High sedimentation rates of up to 193 cm kyr⁻¹ occurred in the inner part of Wahlenbergfjorden during early Holocene.
- The landform assemblages in front of Bodleybreen and Etonbreen suggest that the glaciers have experienced more than one surge event during the Holocene.
- The landform assemblages T.1-T.3 suggest that the tidewater glaciers Idunbreen, Frazerbreen and Aldousbreen are of surge-type.
- Increased sedimentation rates in the inner fjord during late Holocene and evidence of surge activity suggests that the glaciers in the Wahlenbergfjorden area experience a climatically induced switch to- and from a surge mode during the Little Ice Age.

Acknowledgements

Permission for presenting the bathymetric data was granted by the Norwegian Hydrographic Services (permission nr. 13/G706). Aerial photographs were used and presented by the courtesy of the Norwegian Polar Institute (NPI), photo series: 13831 and 13832. The crew of Helmer Hanssen is thanked for fieldwork support. We would also like to thank the Department of Geology at Stockholm University for the use of geophysical instruments and valuable support during core logging. Special thanks to Carina Johansson for all her help with the core logging.

Appendix 1. Aerial image photo IDs

ID/year	13831/2011	25161/2011
3	116	374
5	118	376
7	120	460
9	122	462
11	124	464
13	126	
15	130	
17	132	
19	134	
21	135	
23	137	
25	139	
27	141	
29	143	
76	145	
83	151	
85	153	
87	189	
89	191	
90	193	
	195	
	197	
	199	
	201	
	203	
	205	
	208	
	210	
	212	
	214	
	216	
	218	
	220	
	222	
	809	
	811	
	813	
	815	
	817	
	819	
	820	
	822	
	824	
	833	
	835	
	837	

References

- Andreassen, K., Laberg, J.S., Vorren, T.O., 2008. Seafloor geomorphology of the SW Barents Sea and its glaci-dynamic implications. *Geomorphology* 97, 157–177.
- Bamber, J., Krabill, W., Raper, V., Dowdeswell, J.A., 2004. Anomalous recent growth of part of a large Arctic ice cap: Austfonna, Svalbard. *Geophys. Res. Lett.* 31 <http://dx.doi.org/10.1029/2004GL019667>.
- Bjarnadóttir, L.R., Rütther, D.C., Winsborrow, M.C.M., Andreassen, K., 2012. Grounding-line dynamics during the last deglaciation of Kveithola, W Barents Sea, as revealed by seabed geomorphology and shallow seismic stratigraphy. *Boreas*. <http://dx.doi.org/10.1111/j.1502-3885.2012.00273>.
- Batchelor, C.L., Dowdeswell, J.A., Hogan, K.A., 2011. Late Quaternary ice flow and sediment delivery through Hinlopen Trough, Northern Svalbard margin: submarine landforms and depositional facies. *Mar. Geol.* 284, 13–27.
- Benn, D.I., Kristensen, L., Gouzel, J.D., 2009. Surge propagation constrained by a persistent subglacial conduit, Bakaininbreen-Paulabreen, Svalbard. *Ann. Glaciol.* 50, 81–86.
- Benn, D.I., Evans, D.J., 2010. *Glaciers and Glaciation*. Hodder Education, London.
- Boulton, G.S., Van Der Meer, J.J.M., Hart, J., Beets, D., Ruegg, G.H.J., Van Der Wateren, F.M., Jarvis, J., 1996. Till and moraine emplacement in a deforming bed surge—An example from a marine environment. *Quat. Sci. Rev.* 15, 961–987.
- Dallmann, W.K., Ohta, Y., Elvevold, S., Blomeier, D., 2002. Bedrock Map of Svalbard and Jan Mayen. Norsk Polarinstutt Temakart (Norwegian polarinstitute) No. 33.
- De Angelis, H., Kleman, J., 2008. Paleo-ice stream onsets: examples from the north-eastern Laurentide ice sheet. *Earth Surf. Process. Landforms* 33, 560–572.
- De Geer, G.F., 1940. *Geochronologia suecica principes*. Kungliga svenska vetenskapsakademiens handlingar, Ser. III 18, 1–89.
- Dowdeswell, J.A., 1986. Remote sensing of ice cap outlet glacier fluctuations on Nordaustlandet, Svalbard. *Polar Res.* 4, 25–32.
- Dowdeswell, J.A., Unwin, B., Nuttall, A.M., Wingham, D.J., 1999. Velocity structure, flow instability and mass flux on a large Arctic ice cap from satellite radar interferometry. *Earth Planet. Sci. Lett.* 167, 131–140.
- Dowdeswell, J.A., Ottesen, D., Evans, J., Ó Cofaigh, C., Anderson, J.B., 2008. Submarine glacial landforms and rates of ice-stream collapse. *Geology* 36, 819–822.
- Dowdeswell, J.A., Hogan, K.A., Evans, J., Noormets, R., ÓCofaigh, C., Ottesen, D., 2010. Past ice-sheet flow east of Svalbard inferred from streamlined subglacial landforms. *Geology* 38, 163–166.
- Dowdeswell, J.A., Ottesen, D., 2013. Buried iceberg ploughmarks in the early Quaternary sediments of the central North Sea: a two-million year record of glacial influence from 3D seismic data. *Mar. Geol.* 344, 1–9.
- Eyles, N., Eyles, C.H., Miall, A.D., 1983. Lithofacies types and vertical profile models: an alternative approach to the description and environmental interpretation of glacial diamict and diamict sequences. *Sedimentology* 30, 393–410.
- Flink, A.E., Noormets, R., Kirchner, N., Benn, D.I., Luckman, A., Lovell, H., 2015. The evolution of a submarine landform record following recent and multiple surges of Tunabreen glacier, Svalbard. *Quat. Sci. Rev.* 108, 37–50.
- Flood, B., Gee, D.G., Hjelle, A., Siggerud, T., Winsnes, T.S., 1969. The geology of Nordaustlandet, northern and central parts. *Nor. Polarinst. Skr.* 146, 1–140.
- Forwick, M., Vorren, T.O., Hald, M., Korsun, S., Roh, Y., Vogt, C., Yoo, K.-C., 2010. Spatial and temporal influence of glaciers and rivers on: the sedimentary environment in Sassenfjorden and Tempelfjorden, Spitsbergen. *Geol. Soc. Lond. Spec. Publ.* 44, 163–183.
- Fransner, O., Noormets, R., Flink, A.E., Hogan, K.A., 2017. Glacial Landforms and Their Implications for Glacial Dynamics in Rjipfjord and Dufvefjord, Northern Nordaustlandet Svalbard. *J. Quat. Sci.* <http://dx.doi.org/10.1002/jqs.2938>.
- Graham, A.G.C., Larter, R.D., Gohl, K., Hillenbrand, C.-D., Smith, J.A., Kuhn, G., 2009. Bedform signature of a West Antarctic paleo-ice stream reveals a multi-temporal record of flow and substrate control. *Quat. Sci. Rev.* 28, 2774–2793.
- Hogan, K.A., Dowdeswell, J.A., Noormets, R., Evans, J., Ó Cofaigh, C., 2010a. Evidence for full-glacial flow and retreat of the late weichselian ice sheet from the waters around Kong Karls Land, eastern Svalbard. *Quat. Sci. Rev.* 29, 3563–3582.
- Hogan, K.A., Dowdeswell, J.A., Noormets, R., Evans, J., Ó Cofaigh, C., Jakobsson, M., 2010b. Submarine landforms and ice-sheet flow in the Kvitøya Trough, north-western Barents Sea. *Quat. Sci. Rev.* 29, 3545–3562.
- Hogan, K.A., Dix, J.K., Lloyd, J.M., Long, A.J., Cotterill, C.J., 2011. Seismic stratigraphy records the deglacial history of Jakobshavn Isbrae, West Greenland. *J. Quat. Sci.* 26, 757–766.
- Hogan, K.A., Dowdeswell, J.A., Mienert, J., 2013. New insights into slide processes and seafloor geology revealed by side-scan imagery of the massive Hinlopen Slide, Arctic Ocean Margin. *Geo Marine Lett.* 33, 325–343.
- Hormes, A., Gjermundsen, E.F., Rasmussen, T.L., 2013. From mountain top to deep sea—Deglaciation in 4D of the northwestern Barents Sea ice sheet. *Quat. Sci. Rev.* 75, 78–99.
- Ingólfsson, Ó., Rögnvaldsson, F., Bergsten, H., Hedenäs, L., Lemdahl, G., Lirio, J.H., Sejrup, H.P., 1995. Late quaternary glacial and environmental history of Kong-saya, Svalbard. *Polar Res.* 14, 123–139.
- Ingólfsson, Ó., Landvik, J.Y., 2013. The Svalbard Barents Sea ice-sheet e Historical, current and future Perspectives. *Quat. Sci. Rev.* 64, 33–60.
- Janszen, A., Spaak, M., Moscarriello, A., 2012. Effects of the substratum on the formation of glacial tunnel valleys: an example from the Middle Pleistocene of the southern North Sea Basin. *Boreas* 41, 629–643.
- Joughin, I., Tulaczyk, S., Bindshadler, R., Price, S.F., 2002. Changes in West Antarctic ice stream velocities: observation and analysis. *J. Geophys. Res.* 107 <http://dx.doi.org/10.1029/2001JB001029>.
- Kamb, B., Raymond, C.F., Harrison, W.D., Engelhardt, H., Echelmeyer, K., Humphrey, N., Brugman, M.M., Pfeffer, T., 1985. Glacier surge mechanism: 1982–1983 surge of Variegated Glacier, Alaska. *Science* 227, 469–479.
- King, E.C., Hindmarsh, R.C.A., Stokes, C.R., 2009. Formation of mega-scale glacial lineations observed beneath a West Antarctic ice stream. *Nat. Geosci.* 2, 585–588.
- Koç, N., Kiltgaard-Kristensen, D., Hasle, K., Forsberg, K.F., Solheim, A., 2002. Late glacial palaeoceanography of Hinlopen Strait, northern Svalbard. *Polar Res.* 21, 307–314.
- Kristensen, L., Benn, D.I., Hormes, A., Ottesen, D., 2009. Mud aprons in front of Svalbard surge moraines: evidence of subglacial deforming layers or proglacial glaciotectonics? *Geomorphology* 111, 206–221.
- Lambeck, K., 1995. Constraints on the late Weichselian ice sheet over the Barents Sea from observations of raised shorelines. *Quat. Sci. Rev.* 14, 1–16.
- Lambeck, K., Yokoyama, Y., Purcell, T., 2002. Into and out of the Last Glacial Maximum: sea-level change during Oxygen isotope stage 3 and 2. *Quat. Sci. Rev.* 21, 343–360.
- Landvik, J.Y., Bondevik, S., Elverhøi, A., Fjeldskaar, W., Mangerud, J., Salvgisen, O., Stegert, M.J., Svendsen, J.-I., Vorren, T.O., 1998. The last glacial maximum of Svalbard and the Barents Sea area: ice sheet extent and configuration. *Quat. Sci. Rev.* 17, 43–75.
- Lefauconnier, B., Hagen, J.O., 1991. Surging and calving glaciers in eastern Svalbard.

- Nor. Polarinst. Medd. Nor. Polarinst. 116.
- Linden, M., Möller, P., 2005. Marginal formation of De Geer moraines and their implications to the dynamics of grounding-line recession. *J. Quat. Sci.* 20, 113–133.
- Lovell, H., Fleming, E.J., Benn, D.I., Hubbard, B., Lukas, S., Rea, B.R., Noormets, R., Flink, A.E., 2015. Debris Entrainment and landform genesis during tidewater glacier surges. *J. Geophys. Res.* 120, 1574–1595.
- Lowe, A., Anderson, J.B., 2003. Evidence for abundant subglacial meltwater beneath the paleo-ice sheet in Pine Island Bay, Antarctica. *J. Glaciol.* 49, 125–138.
- Mothold, G., Hagen, J.O., Eiken, T., Schuler, T.V., 2010. Geometric changes and mass balance of the Austfonna ice cap, Svalbard. *Cryosphere* 4, 21–34.
- Mangerud, J., Bondevik, S., Gulliksen, S., Hufthammer, K.A., Høisaeter, T., 2006. Marine 14C reservoir ages for 19th century whales and molluscs from the North Atlantic. *Quat. Sci. Rev.* 25, 3228–3245.
- Murray, T., Dowdeswell, J.A., Drewry, D.J., Frearson, I., 1998. Geometric evolution and ice dynamics during a surge of Bakaninbreen, Svalbard. *J. Glaciol.* 44, 263–272.
- Nürnberg, D., Wollenburg, L., Dethleff, D., Eicken, H., Kassens, H., Letzig, T., Reimnitz, E., Thiede, J., 1994. Sediments in Arctic sea ice—implications for entrainment, transport and release. *Mar. Geol.* 119, 185–214.
- Ó Cofaigh, C., Pudsey, C.J., Dowdeswell, J.A., Morris, P., 2002. Evolution of subglacial bedforms along a paleo-ice stream, Antarctic Peninsula continental shelf. *Geophys. Res. Lett.* 29.
- Ó Cofaigh, C., Dowdeswell, J.A., Grobe, H., 2001. Holocene glacial marine sedimentation, inner Scoresby Sund, East Greenland: the influence of fast-flowing ice-sheet outlet glaciers. *Mar. Geol.* 175, 103–129.
- Ottesen, D., Dowdeswell, J.A., 2006. Assemblages of submarine landforms produced by tidewater glaciers in Svalbard. *J. Geophys. Res.* Earth Surf. 111, 1–16.
- Ottesen, D., Dowdeswell, J.A., Landvik, J.Y., Mienert, J., 2007. Dynamics of the Late Weichselian ice sheet on Svalbard inferred from high-resolution sea-floor morphology. *Boreas* 36, 286–306.
- Ottesen, D., Dowdeswell, J.A., Benn, D.I., Kristensen, L., Christiansen, H.H., Christensen, O., Hansen, L., Lebesbye, E., Forwick, M., Vorren, T.O., 2008a. Submarine landforms characteristic of glacier surges in two Spitsbergen fjords. *Quat. Sci. Rev.* 27 (15–16), 1583–1599.
- Ottesen, D., Stokes, C.R., Rise, L., Olsen, L., 2008b. Ice-sheet dynamics and streaming along the coastal parts of northern Norway. *Quat. Sci. Rev.* 27, 922–940.
- Ottesen, D., Dowdeswell, J.A., 2009. An inter-ice-stream glaciated margin: submarine landforms and a geomorphic model based on marine-geophysical data from Svalbard. *Geol. Soc. Am. Bull.* (11–12), 1647–1665.
- Plassen, L., Vorren, T.O., Forwick, M., 2004. Integrated acoustic and coring investigation of glacialic deposits in Spitsbergen fjords. *Polar Res.* 23, 89–110.
- Reimer, P.J., Bard, E., Bayliss, A., Beck, J.W., Blackwell, P.G., Bronk Ramsey, C., Buck, C.E., Cheng, H., Edwards, R.L., Friedrich, M., Grootes, P.M., Guilderson, T.P., Hafflidason, H., Hajdas, I., Hattel, C., Heaton, T.J., Hoffmann, D.L., Hogg, A.G., Hughen, K.A., Kaiser, K.F., Kromer, B., Manning, S.W., Niu, M., Reimer, R.R., Richards, D.A., Scott, M.E., Southon, J.R., Staff, R.A., Turney, C.S.M., van Plicht, J., 2013. INTCAL13 and Marine13 Radiocarbon age calibration curves, 0–50,000 years cal BP. *Radiocarbon* 55, 1869–1887.
- Robinson, S.G., Maslin, M.A., McCave, N., 1995. Magnetic susceptibility variations in upper Pleistocene deep-sea sediments of the NE Atlantic: implications for ice rafting and paleocirculation at the last glacial maximum. *Paleoceanography* 10, 221–250.
- Robinson, P., Dowdeswell, J.A., 2011. Submarine landforms and the behavior of a surging ice cap since the last glacial maximum: the open-marine setting of eastern Austfonna, Svalbard. *Mar. Geol.* 286, 82–94.
- Roy, S., Senger, K., Braathen, A., Noormets, R., Hovland, M., Olausson, S., 2014. Fluid migration pathways to seafloor seepage in inner Isfjorden and Adventfjorden, Svalbard. *Nor. J. Geol.* 94, 99–119.
- Roy, S., Hovland, M., Noormets, R., Olausson, S., 2015. Seepage in Isfjorden and its tributary fjords, West Spitsbergen. *Mar. Geol.* 363, 146–159.
- Ruther, D.C., Mattingsdal, R., Andreassen, K., Forwick, M., Husum, K., 2011. Seismic architecture and sedimentology of a major grounding zone system deposited by the Bjørnøyrenna Ice Stream during Late Weichselian deglaciation. *Quat. Sci. Rev.* 30, 2776–2792.
- Schomacker, A., Benediktsson, O.L., Ingólfsson, Ó., 2014. The Eyjabakkajökull glacial landsystem, Iceland: geomorphic impact of multiple surges. *Geomorphology* 218, 98–107.
- Senger, K., Roy, S., Braathen, A., Buckley, S.J., Bælum, K., Gernogon, L., Mjelde, R., Noormets, R., Ogata, O., Olausson, S., Planke, S., Ruud, B.O., Tveranger, J., 2013. Geometries of doleritic intrusions in central Spitsbergen, Svalbard: an integrated study of an onshore-offshore magmatic province with implications for CO₂ sequestration. *Nor. J. Geol.* 93, 143–166.
- Sevestre, H., Benn, D.I., 2015. Climatic and geometric controls on the global distribution of surge-type glaciers: implications for a unified model of surging. *J. Glaciol.* 61, 646–662.
- Sevestre, H., Benn, D.I., Hulton, N.R.J., Bælum, K., 2015. Thermal Structure of Svalbard Glaciers and implications for thermal switch models of glacier surging. *J. Geophys. Res.* Accepted.
- Shevenell, A., Domack, E.W., Kernan, G.M., 1996. Record of Holocene palaeoclimate change along the Antarctic Peninsula: evidence from glacial marine sediments, Lallemand fjord. *Pap. Proc. R. Society Tasmania* 130, 55–64.
- Shotton, F.W., 1972. An example of hard-water error in radiocarbon dating of vegetable matter. *Nature* 240, 460–461.
- Solheim, A., Russwurm, L., Elverhøi, A., Nyland Berg, M., 1990. Glacial geomorphic features in the northern Barents Sea: direct evidence for grounded ice and implications for the pattern of deglaciation and late glacial sedimentation. *Geol. Soc. Spec. Publ.* 53, 253–268.
- Stokes, C., Clark, C.D., 1999. Geomorphological criteria for identifying Pleistocene ice streams. *Ann. Glaciol.* 28, 67–74.
- Stokes, C., Clark, C.D., 2002. Are long subglacial bedforms indicative of fast ice flow? *Boreas* 31, 239–249.
- Stuiver, M., Reimer, P.J., 1993. Extended 14C database and revised CALIB radiocarbon calibration program. *Radiocarbon* 35, 215–230.
- Svendsen, J.I., Alexanderson, H., Astakhov, V.I., Demidov, I., Dowdeswell, J.A., Funder, S., Gataullin, V., Henriksen, M., Hjort, C., Houmark-Nielsen, M., Hubberten, H.W., Ingólfsson, O., Jakobsson, M., Kjær, K.H., Larsen, E., Lokrantz, H., Lunkka, J.P., Lyså, A., Mangerud, J., Matiouchkov, A., Murray, A., Möller, P., Niessen, F., Nikolskaya, O., Polyak, L., Saarnisto, M., Siegert, C., Siegert, M.J., Spielhagen, R.F., Stein, R., 2004. Late Quaternary ice sheet history of northern Eurasia. *Quat. Sci. Rev.* 23, 1229–1271.
- Tenzen, R., Gladkikh, V., 2014. Assessment of density variations of marine sediments with ocean and sediment depths. *Sci. Worldjournal*. <http://dx.doi.org/10.1155/2014/823296>.
- Thomas, G.S.P., Connell, R.J., 1985. Iceberg drop, dump and grounding structures from Pleistocene glacio-lacustrine sediments, Scotland. *J. Sediment. Petrol.* 55, 0243–0249.
- Todd, B.J., Valentine, P.C., Longva, O., Shaw, J., 2007. Glacial landforms on German bank, scotian shelf: evidence for late wisconsinan ice-sheet dynamics and implications for the formation of De geer moraines. *Boreas* 36, 148–169.
- Vanneste, M., Mienert, J., Bunz, S., 2006. The Hinlopen Slide: a giant, submarine slope failure on the northern Svalbard margin, Arctic Ocean. *Earth Planet. Sci. Lett.* 245, 373–388.
- Weber, M.E., Niessen, F., Kuhn, G., Wiedicke, M., 1997. Calibration and application of marine sedimentary physical properties using multi-sensor core loggers. *Mar. Geol.* 136, 151–172.
- Winkelmann, D., Stein, R., 2007. Triggering of the Hinlopen/Yermak Megaslide in relation to paleoceanography and climate history of the continental margin north of Spitsbergen, Arctic Ocean. *Geochem. Geophys. Geosystems* 8, Q06018. <http://dx.doi.org/10.1029/2006GC001485>.

Glacial history of Vaigattbogen, northeastern Spitsbergen

Anne E. Flink^{1*}, Riko Noormets¹

¹Department of Arctic Geology, University Centre in Svalbard, 9170 Longyearbyen, Norway

*Corresponding author. University Centre in Svalbard, PO Box 156, 9171 Longyearbyen, Norway.

E-mail address: AnneF@unis.no

Abstract

Vaigattbogen is located in northern Svalbard. The area is currently extensively glaciated with several tidewater glaciers. This study uses multibeam-, sub-bottom acoustic data, and four sediment cores to reconstruct the Late Weichselian and Holocene glacial history in Vaigattbogen. During the last glacial, ice flowed northwards through Vaigattbogen and fed into the Hinlopen Strait ice stream. Streamlined bedforms indicate relatively fast ice flow in the area and their increasing elongation ratios towards the north suggest increasing flow velocities. A sediment core recovered from the northern section of the study area suggests that the north basin deglaciated prior to 9.1 ka BP. De Geer moraines in the shallower parts of Vaigattbogen suggest slower ice retreat in these areas. In the south basin, two large moraine ridges with networks of crevasse-squeeze ridges suggest that at least two surge-type advances occurred during the Holocene. The Hinlopenbreen glacier surged in the early 1970s and deposited the inner (R.2) of the two large moraine ridges. Radiocarbon ages from a sediment core recovered from the crest of the outer (R.1) ridge yield a basal age of 2.6 ka BP. However, the core did not sample subglacial diamict and the age of the ridge could be anything between 2.6 ka BP. to early Holocene. The R.2 ridge formed prior to the Little Ice Age (LIA), supporting that at least on the east coast of Spitsbergen more than one tidewater glacier has experienced a pre-LIA surge. The R.1 ridge is double-crested with crevasse-squeeze ridges between the crests suggesting that more than one surge-type advance probably occurred during the Holocene and reached approximately the same distance from the present glacier front.

Keywords: Multibeam data; Glacier dynamics; Submarine morphology; Surging glaciers; fjord; Svalbard

1. Introduction

Ice shelves and tidewater glaciers are important components of polar ice sheets and ice caps, since the majority of their mass is lost by calving at the marine margins. Rapid climatic and oceanographic change at the marine margins can lead to draw-down of inland ice, changes in ice dynamics, increased mass loss and subsequent sea level rise (Joughin *et al.* 2014). It is thus imperative to understand how future global climate change will affect these dynamic components of the ice sheets and caps (IPCC 2014). Geological imprint of paleo ice sheets and past glaciers can provide clues regarding the links between past and future ice dynamics and their climatic and oceanographic controls.

In recent years, several articles have been published, based on multibeam-bathymetric data from the fjords in northeastern Svalbard and Nordaustlandet (Ottesen *et al.* 2007; Fransner *et al.* 2016; Noormets *et al.* 2016a; Noormets *et al.* 2016b; Flink *et al.* 2017; Flink *et al.* in prep; Streuff *et al.* in review). These studies have provided new knowledge on glacier dynamics in eastern Svalbard during and after the Last Glacial Maximum (LGM). It has, for example, been suggested that a surge-type advance took place in Mohnbukta in eastern Spitsbergen during early Holocene, and that similar early Holocene advances

could have occurred in other fjords on eastern Svalbard, thus indicating a more dynamic early Holocene than previously presumed (Flink *et al.* in prep). High-resolution data from the fjords in eastern and northern Svalbard are however still few compared to western Svalbard (Ottesen & Dowdeswell 2006; Ottesen *et al.* 2008; Blaszczyk *et al.* 2009; Vieli *et al.* 2002; Kristensen *et al.* 2009; Flink *et al.* 2015; Streuff *et al.* 2015; Sobota *et al.* 2016).

In this study, we map and analyse submarine glacial landforms in Vaigattbogen in order to study the Late Weichselian and Holocene history of the fjord and to compare this with recently published data from other fjords in eastern and northern Svalbard. The study aims to provide a broader context for understanding the surge history of Svalbard glaciers and the role of climatic events, such as the deglaciation, Holocene Climate Optimum (HCO) and the Little Ice Age (LIA) on regional glacier dynamics. An important question to be answered is: was the pre-LIA surge in Mohnbukta a unique event or do we see evidence for similar advances in other parts of eastern and northern Svalbard? This study extends the knowledge base on the glacial history in eastern Svalbard in the context of major regional climate events.

2. Study area

Vaigattbogen is an open fjord, located between northeastern Spitsbergen and Nordaustlandet (Fig. 1a, b). It is connected to the southern part of the Hinlopen Strait, which separates Spitsbergen from Nordaustlandet. Submarine landforms indicate that the Hinlopen Strait was occupied by an ice stream during the last glacial (Batchelor *et al.* 2011). Inner Vaigattbogen is a two-branched fjord with a larger south basin and a smaller NW basin, which are constrained by large submarine ridges, R.1 and R.3, respectively. The ridges create natural sills between the south and NW basins and the deeper north basin (Fig. 2a). The maximum depths of the south and NW basins are 146 m and 116 m, respectively. Vaigattbogen is surrounded by several small islands, comprising of resistant dolerite sill and dyke intrusions of the Diabasodden suite (Fig. 1b) (Dallmann *et al.* 2002). Dolerites are also present along the mountainsides and coastlines in northeastern Spitsbergen. The dominant bedrock geology in the Vaigattbogen area consists of soft Mesozoic sedimentary rocks, such as shales, sand- and siltstones of the Tempelfjorden and Gipsdalen Groups (Fig. 1b). Carbonates from the Akademikerbreen and Polarisen Groups are present further inland (Dallmann *et al.* 2002). Quaternary unconsolidated glacial, glaci-fluvial and marine deposits drape the shorelines.

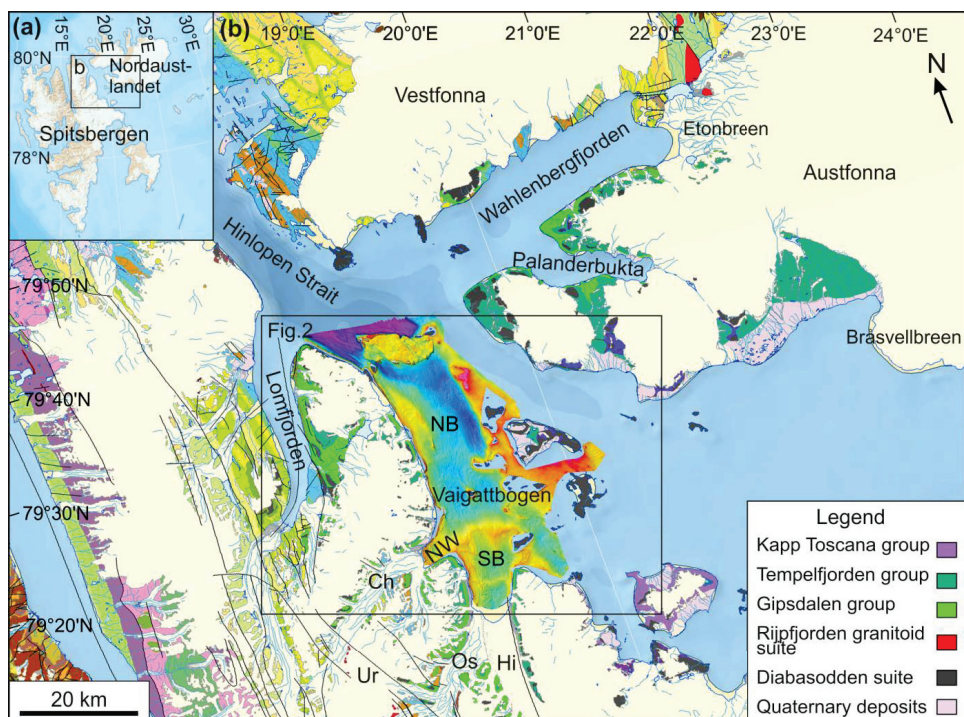


Fig. 1. (a) The location of Svalbard. Area within black box is shown in (b). (b) Bedrock map of northeastern Svalbard. Black box outlines the area shown in Fig. 2. Abbreviations indicate the locations of: Hi-Hinlopenbreen, Os-Oslobreen, Ch-Chydeniusbreen, Ur-Ursafonna, NB-north basin and SB-south basin and NW-northwest basin. Maps were derived from Svalbardkartet (NPI).

Three glaciers, Hinlopen-, Oslo- and Hønerbreen, terminate into the south basin with a joint tidewater cliff (Fig. 3a). Hinlopenbreen, which drains ice towards the east coast from the Kongsfonna ice cap in Olav V Land, is the largest of these glaciers. The glacier is 68.5 km long at its center line and covers an area of approximately 1250 km² (Hagen *et al.* 1993). Oslobreen is the second largest glacier draining into the south basin (Fig. 2). The glacier is located west of Hinlopenbreen and has a drainage area towards the southwest (Fig. 1b). Hønerbreen is a small glacier, wedged in between Oslobreen and the west coast of the south basin (Fig. 3a). Several small glaciers, such as Veite-, Loder- and Vellebreen terminate with tidewater cliffs into the south basin (Fig. 3a). Two tidewater glaciers, Polaris- and Chydeniusbreen flow into the NW basin. Polarisbreen drains the Ursafonna ice cap and flows northwards into Vaigattbogen (Fig. 1b). Chydeniusbreen has a large drainage area, extending towards the southwest and is fed by several tributary glaciers during its course northwards. Two tidewater glaciers, Kosterbreen and Sven Ludvigbreen, terminate into the north basin (Figs 2a and 3a).

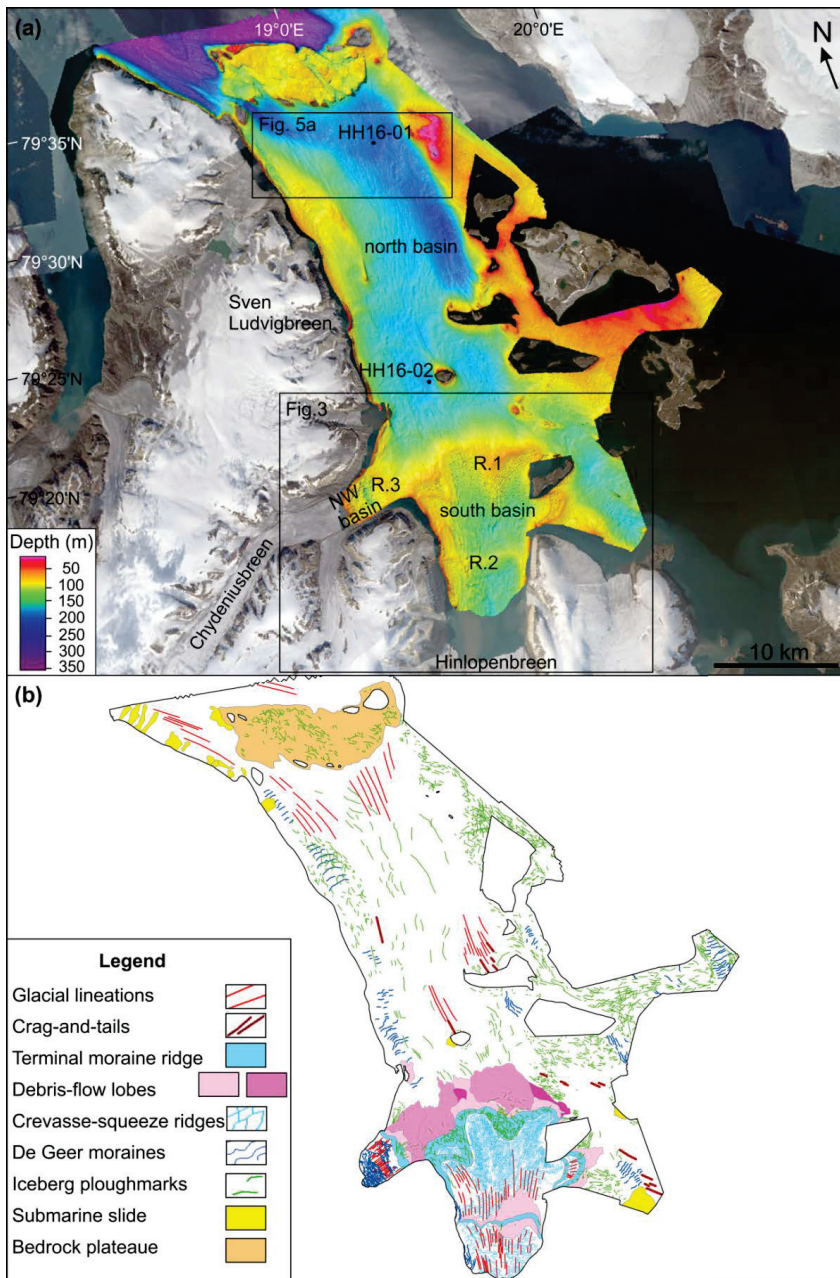


Fig. 2. (a) Bathymetry of Vaigattbogen. Boxes show locations of Figs 3 and 5a. Background displays a satellite image from 2013 (NPI). (b) Mapped submarine landforms in Vaigattbogen.

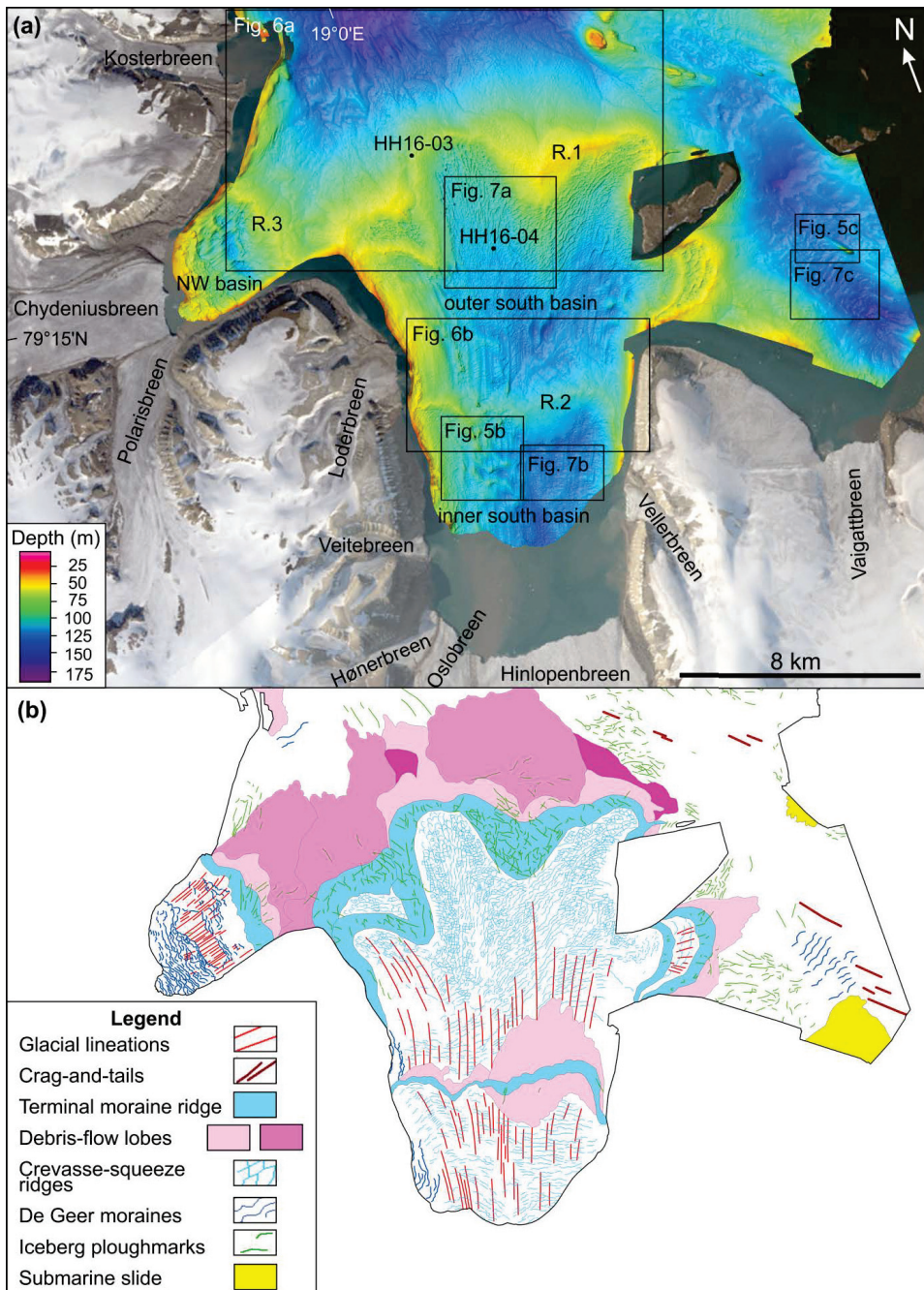


Fig. 3. (a) Zoom-in on the bathymetry in the south and NW basins. Boxes show locations of Figs 5b, 6 and

7. Background satellite image by the courtesy of NPI. (b) Mapped submarine landforms in the south and NW basins.

3. Glaciological background

The earliest maps of Vaigattbogen were produced in 1901 (Vassiliev 1907; De Geer 1923). Both maps show a straight glacier front situated at approximately the same location (Fig. 4). After 1901, the glacier experienced continuous retreat. In 1956 the front was located far back in the fjord, only 2 km from its present position (Fig. 4). The earliest aerial images from 1938 display sinuous moraines on Oslobreen, indicating that the glaciers were more active prior to 1901 and possibly had a larger extent. Hinlopenbreen surged in the early 1970s. The surge initiated in 1969 and lasted for at least three years (Lefauconnier & Hagen 1991). The glacier reached its maximum in 1971, when it had advanced 7 km from its previously known 1956 position (Fig. 4). Between 1970 and 1971 the glacier advanced approximately 2.5 km and experienced flow speeds of 8-12 m per day (Lefauconnier & Hagen 1991). Aerial images show that the ice cliff of Hinlopenbreen was between 25-50 m high during the surge, which gives an ice thickness of 115-160 m at the glacier terminus. The exact time of surge stagnation cannot be determined, since there are no aerial images immediately after 1971. After the early 1970s the glacier front continued to retreat and has presently retreated around 8 km from the surge maximum position (Fig. 4).

Loderbreen, which is located north of Hinlopenbreen (Fig. 3a), reached its maximum extent during the LIA, when it developed a lobe into the fjord according to the 1901 map (De Geer 1923). In 1901, the joint front of Polarisbreen and Chydeniusbreen was located approximately 4.3 km from their present terminal position and the glaciers have experienced retreat since then (Fig. 4). Since 1936, the front of Chydeniusbreen has been situated approximately at its current location and no surges have been recorded. Lefauconnier & Hagen (1991) suggest that the glaciers reached their maximum extent prior to 1901 based on lateral moraines that reach further out than the 1901 extent. Kosterbreen, located north of Polaris- and Chydeniusbreen, reached its maximum Holocene extent prior to 1901 based on the morphology of the lateral moraines (Fig. 4). The front of Kosterbreen has been nearly stationary since 1901, experiencing only slow retreat. The glacier has not been recorded to surge, but a highly crevassed surface suggests that surges could have occurred in 1936 and between 1956 and 1970 (Lefauconnier & Hagen 1991). Sven Ludvigbreen reached its maximum extent in 1901 and has experienced constant retreat since the end of the LIA with no recorded surges (Lefauconnier & Hagen 1991) (Fig. 2a).

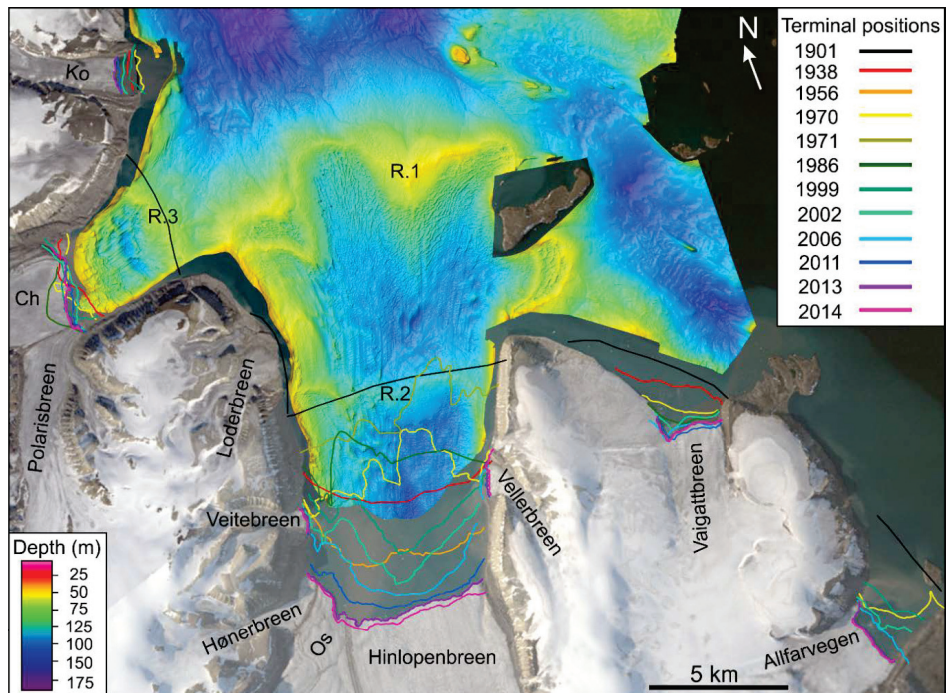


Fig. 4. (a) Glacial terminal positions in Vaigattbogen shown on top of the multibeam bathymetric data. Abbreviations indicate the locations of Ch-Chydeniusbreen, Ko-Kosterbreen and Os-Oslobreen. Background shows and satellite image from 2013 (NPI).

4. Methods

4.1. Geophysical methods

Marine geophysical data from Vaigattbogen was provided by the Norwegian Hydrographic Service. The data were acquired in 1999 with Kongsberg EM1000 and EM100 Swath-bathymetric systems, both of which operate at a frequency of 95 kHz. The bathymetric data were gridded to a resolution of 10 m. The data were visualized and interpreted in the QPS Fledermaus and ArcGIS software suites. Bathymetric data and aerial/satellite data were combined in ArcGIS, where the submarine landforms and the glacier terminal positions were mapped. Glacier terminal positions were mapped from historical maps, aerial/satellite images and maps from the Norwegian Polar Institute (NPI) as well as Landsat images from the U. S. Geological Survey (USGS). For a detailed description of source data see Appendix 1. Shallow acoustic sub-bottom (chirp) data were collected in 2016 during a cruise with the R/V Helmer Hanssen with the EdgeTech 3300-HM sub-bottom profiler. The two-way travel time (TWT) was converted to meters using sound velocity of 1500 m/s. The data were analyzed in the EdgeTech Discover II software.

4.2. Sediment core methods

Four sediment cores, HH16-01, HH16-02, HH16-03 and HH16-04 were collected from Vaigattbogen during the cruise with R/V Helmer Hanssen in 2016. The cores were photographed, logged and subjected to preliminary lithological analysis onboard. Magnetic susceptibility was measured on whole cores with a loop sensor at 2 cm intervals and on split cores with a point sensor at 1 cm intervals using the Bartington MS2 magnetic susceptibility system. Shear strength was measured every 5 cm with a Geonor fall cone instrument. The cores were logged for lithology, color, grain size, textures, structures and clast size. Lithofacies codes applied from Eyles *et al.* (1983) were assigned to different units. The cores were shipped to the University Centre in Svalbard where they were subsampled from each lithological unit. The samples were analyzed for water content, grain size and microfossil content. Grain sizes were determined by wet sieving at 63 μ m, 100 μ m and 1mm. Microfossils were picked from cores HH16-01 and HH16-03 and sent for radiocarbon dating to the Ion Beam Physics AMS laboratory in Zürich, Switzerland. Radiocarbon ages were calibrated using the CALIB calibration curve, which has a global marine reservoir correction of 440 \pm 52 yr (Stuiver *et al.* 2017). A local delta R of 105 \pm 24 yr for Spitsbergen was applied (Mangerud *et al.* 2006).

5. Submarine landforms in Vaigattbogen

5.1 Streamlined bedforms without and with a bedrock core: glacial lineations and crag-and-tails

5.1.1. Description

Groups of streamlined bedforms can be observed in the north, south and NW basins of Vaigattbogen (Fig. 2). They are parallel to the fjord and follow fjord topography. In the south basin the streamlined bedforms are 80-100 m wide and commonly between 800-1500 m long with a maximum length of 3.9 km (Figs 3, 5b and 5d). In the north basin, the bedforms are longer, with maximum lengths of 4.5 km and widths between 100-400 m (Figs 2 and 5a). The elongation ratio of the bedforms is on average 10:1 in the south and NW basins and 25:1 in the north basin, where the elongation ratios increase towards the north. In the south basin, the bedforms are fairly regularly spaced, with a crest-to-crest spacing of 100-400 m and a regular crest-to crest spacing of 150 m in the NW basin (Fig. 3). The elongated bedforms are overprinted by small fjord-transverse ridges. A few of the streamlined bedforms in Vaigattbogen have steep stoss-sides and adjoining lower sedimentary tails. The largest of these bedforms are up to 20-40 m high on the stoss-side with shallower, 1-2 m high, tails of sediment on their lee-side. The bedforms are 1-2 km long and 200-400 m wide with decreasing widths along the tail, which yields an average elongation ratio of 5:1 (Figs 2 and 5c, e). They are common on the lee-side of small islands which are abundant in Vaigattbogen and consist mainly of resistant dolerite bedrock (Fig. 1b).

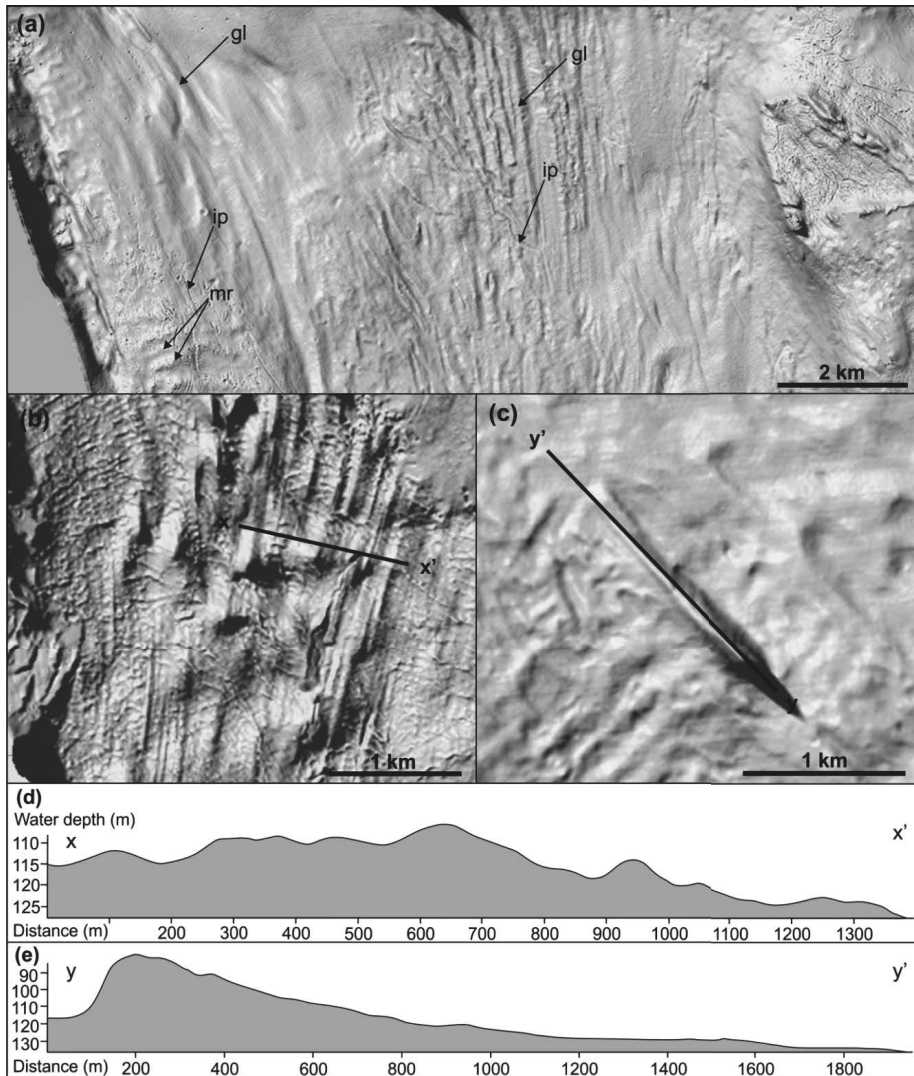


Fig. 5. (a) Glacial lineation in the north basin. Arrows point to: *gl*-glacial lineation, *ip*-iceberg ploughmark, *mr*-moraine ridge. (b) Glacial lineations in the inner south basin (c) A single crag-and-tail. (d) Cross-profile of the glacial lineations. (e) Long-profile of the crag-and-tail. For location of figures see Figs 2a and 3a.

5.1.2. Interpretation

The fjord-parallel elongated bedforms are interpreted as glacial lineations based on their streamlined characteristics and elongation ratios. The streamlined bedforms with a higher stoss-side are interpreted as crag-and-tails, based on their high stoss-sides and low tails which extend in the down ice direction. Similar submarine glacial lineations and crag-and-tails are common features in other Svalbard fjords and submarine troughs (Ottesen *et al.* 2008; Hogan *et al.* 2010a, b; Fransner *et al.* 2016; Flink *et al.* 2017).

The elongation ratios of the lineations fall within the minimum 10:1 ratio characteristic of mega-scale glacial lineations (MSGs). MSGs have been interpreted to form below fast flowing ice streams, but they are typically 100-200 km long and can be up to a couple of km wide (Stokes & Clark 2002; Dowdeswell *et al.* 2008; Andreassen *et al.* 2014). The dimensions of the lineations in Vaigattbogen do not fit these criteria and the bedforms should therefore not be described as classic MSGs. However, their high elongation ratios indicate that they formed by fast flowing ice in soft deformation tills (Boulton *et al.* 1976; Ó Cofaigh *et al.* 2002; Stokes & Clark 2002; King *et al.* 2009). The glacial lineations in the north basin are interpreted to have formed subglacially at the base of the Svalbard Barents Sea Ice Sheet (SBSIS), while the glacial lineations in the south and NW basins have formed at the base of Hinlopen/Oslobreen and Chydeniusbreen as they flowed out to the fjord. The occurrence of crag-and-tails is typically associated with outcropping crystalline, erosion-resistant bedrock or a substrate of mixed bedrock types (Ó Cofaigh *et al.* 2002; Evans *et al.* 2004). Both these conditions are most likely present in Vaigattbogen, explaining why both, glacial lineations and crag-and-tails are present (Fig. 1b).

5.2. Large transverse ridges and lobe-shaped deposits: Terminal moraine ridges and debris-flow lobes

5.2.1. Description

Three large submarine ridges are present in Vaigattbogen (Fig. 2). They are oriented transverse to inferred ice flow from the Hinlopen- and Chydeniusbreen glaciers. The ridges have large lobate sediment accumulations partially covering their distal slopes. The south basin is divided into an outer and inner basin by the R.2 ridge (Fig. 3a). The R.1 ridge is around 20 km long and distinctly lobate in planform (Fig. 6a). It is located approximately 14 km from the present front of Hinlopenbreen. The ridge is double crested in its western and eastern parts with small ridges present between the crests (Fig. 6a). It is 20-30 m high and between 1-3 km wide, including its double-crested sections. The individual ridge width at the double crested section is 0.5-1 km. The ridge has a steeper proximal side with slope angle of 0.01°-0.06°. On the distal flank, large sediment lobes emanate from the ridge crest and several lobes overprint each other (Fig. 6a). The sediment lobes have a hummocky surface and a maximum run-out distance of 5 km. The ridge crest is overprinted by multiple linear to curvilinear grooves with varied orientations.

The R.2 ridge is located 8.5 km from the present glacier front. It is between 15-25 m high and 500 m wide, excluding the sediment lobes on the distal and proximal flanks of the ridge. Together with the sediment lobes the ridge has a maximum width of 3.8 km (Fig. 6b, d). The sediment lobes are more prominent on the eastern side of the fjord. On the western side, they can only be observed on the distal slope of the R.2 ridge (Fig. 6b). They have a smoother surface than the R.1 lobes and clearly overprint glacial lineations and moraine ridges. The R.2 ridge has proximal slope angles between 0.03°-0.08° and a uniform distal slope angle of 0.02°. The ridge is less lobate in planform and located at a deeper water depth than the R.1 ridge. Curvilinear to linear grooves are uncommon on the crest of the R.2 ridge. The R.3 ridge is oriented transverse to inferred ice flow from Chydeniusbreen (Fig. 3a). The ridge is 20-25 m high and 600 m wide. It is located approximately 4 km from the present front of Chydeniusbreen and has proximal and distal slope angles of 2.5°-4.5° and 1.2°-2°, respectively. Two sediment lobes extend 3.7 km seaward from the crest of the ridge (Fig. 6a). The surface of the ridge is hummocky and overprinted by linear to curvilinear grooves. The grooves are between 0.5-2 m deep, 100-600 m long and 10-40 wide. They are V-to-U shaped in cross-profile and located on the ridge crests and in shallow parts of the fjord, at maximum water depths of 80 m in the south basin and 190 m in the north basin (Figs 2, 3).

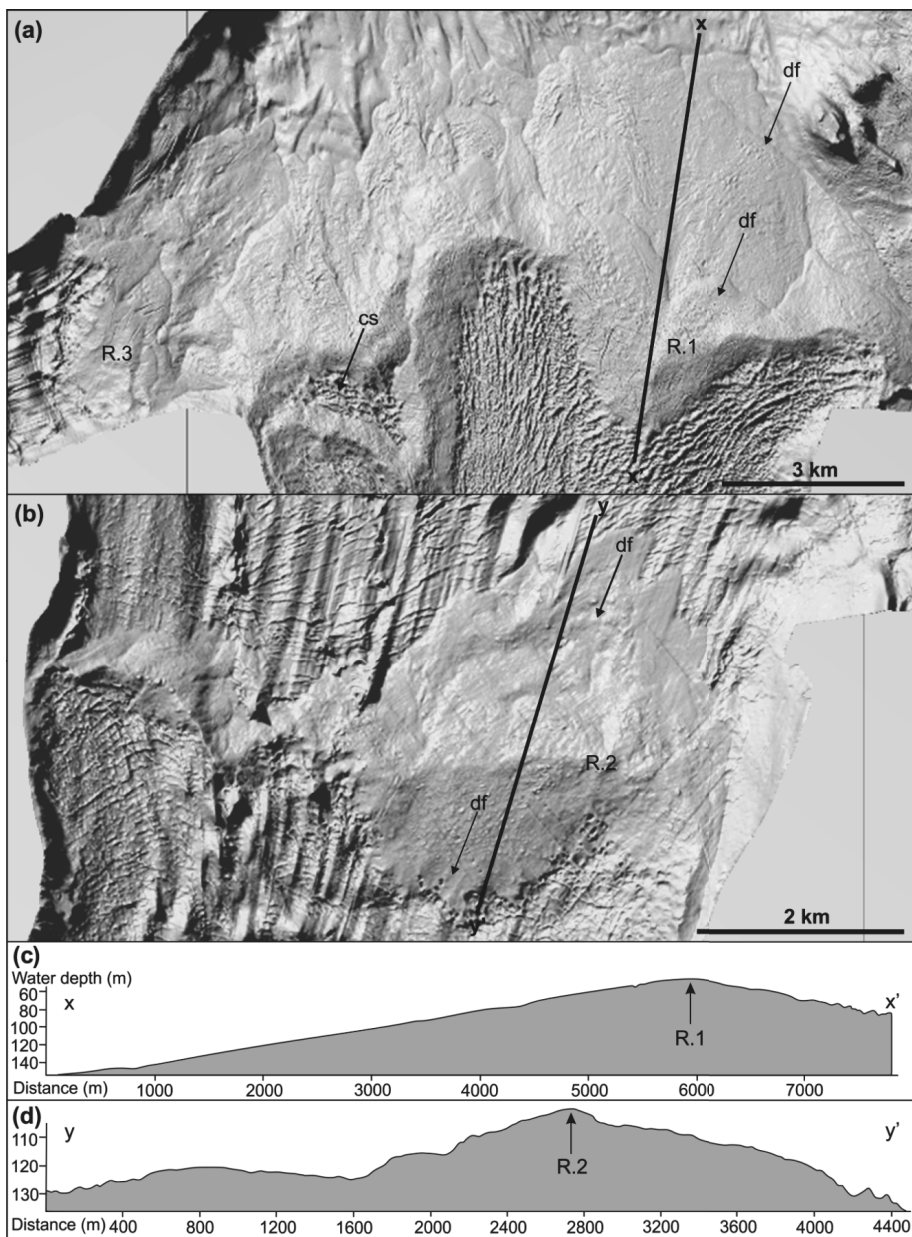


Fig. 6. (a) The R.1 and R.3 ridges and debris-flow lobes. Arrows point to: cs- crevasse-squeeze ridges and df-debris-flow lobe. (b) The R.2 ridge and debris-flow lobes. (c) Cross-profile of the R.1 ridge. (d) Cross-profile of the R.2 ridge. For location of figures see Fig. 3a.

5.2.2. Interpretation

The large transverse ridges are interpreted as terminal moraine ridges based on their shape, dimensions and similarity to previously described submarine terminal moraine ridges from Svalbard fjords (Ottesen & Dowdeswell 2006; Ottesen & Dowdeswell 2009; Kristensen *et al.* 2009; Streuff *et al.* 2015; Flink *et al.* 2017). The ridges have formed at the tidewater front as the glaciers experienced an advance and pushed up marine, sub- and proglacial sediments in front of their terminus or as sediments were brought to the terminus during a longer still-stand (Boulton *et al.* 1999; Kristensen *et al.* 2009). Terminal moraine ridges are common within a few kilometers of present tidewater termini in Svalbard fjords and record the maximum Holocene glacier extent. Most often these advances have been associated with the LIA (Plassen *et al.* 2004; Ottesen & Dowdeswell 2009) or with later surge events (Ottesen *et al.* 2008; Flink *et al.* 2015; Streuff *et al.* 2015). The sediment lobes are inferred to be debris-flow lobes, which are common features on the distal slopes of many Svalbard terminal moraine ridges and form as glacigenic sediments at the terminus become unstable and flow downslope (Plassen *et al.* 2004; Ottesen & Dowdeswell 2006; Ottesen *et al.* 2008) or as subglacially sourced outwash during or after the maximum surge extent (Boulton *et al.* 1996; Kristensen *et al.* 2009; Streuff *et al.* 2015).

The R.1 ridge has a larger dimension, consist of multiple lobes and is located further out in the fjord than most submarine terminal moraine ridges observed in Svalbard (Ottesen & Dowdeswell 2006; Ottesen *et al.* 2008; Kristensen *et al.* 2009; Burton *et al.* 2015). Crevasse-squeeze ridges and the lobate shape of the R.1 ridge suggest that it formed during a surge-type advance. The double crested nature of the ridge, the multiple stacked debris-flow lobes and the preserved crevasse-squeeze ridges between the crests (Fig. 6a) suggest that at least two surge-type advances formed the R.1 ridge. Crevasse-squeeze ridges also indicate that the R.2 ridge has formed during a surge-type advance, suggesting that at least three glacier surges have occurred in the south basin. The grooves on the ridge crests and in the fjord are interpreted as iceberg ploughmarks based on their linear-to curvilinear character, variable directions and U- and V-shaped cross-profiles (Dowdeswell & Forsberg 1992; Dowdeswell & Ottesen 2013).

5.3. Transverse ridges: De Geer moraines/Annual retreat moraines

5.3.1. Description

Small fjord-transverse ridges are present in the NW basin. Some of the ridges can be traced across the entire basin, but most of them occur as shorter, 100-600 m long segments. The ridges are 30-60 m wide and commonly 1-2 m high, with a maximum height of 8 m. They have a fairly regular crest-to-crest spacing of 60-80 m and sometimes cross-cut each other. Ridges with similar dimensions occur in the south basin transverse to the Veitebreen glacier front (Fig. 3). Fjord transverse ridges also occur in the north basin along its western side and near the islands (Figs 2 and 3). Some of the ridges between the islands have W-E orientations instead of being transverse to overall fjord topography. Most of the ridges are subdued and have been partly buried by marine sediments (Fig. 7c). They are a couple of meters high, between 80-200 m wide and 0.1-1 km long (Fig. 7g). The crest-to-crest spacing varies from 200-400 m between the different sets of ridges.

5.3.2. Interpretation

The fjord transverse ridges are interpreted as retreat or De Geer moraines, formed by small readvances of an ice sheet or a glacier front during general retreat. The ridges in the NW basin have similar shape, characteristics and crest-to-crest spacing as earlier described annual retreat moraines in Svalbard and other parts of the world (Sharp 1984; Ottesen & Dowdeswell 2006; Ottesen *et al.* 2008; Flink *et al.* 2015) which suggests that they have formed annually. This would indicate an annual glacier retreat of 60-80 m yr⁻¹ in the inner part of the basin. It is also possible that some of the ridges in the NW basin have

crevasse-squeeze origin. Similarly shaped, partly intersecting, transverse ridges have previously been interpreted as De Geer moraines and assigned either an annual, semi-annual or crevasse-squeeze origin (Streuff *et al.* 2015). Sub-bottom data suggests that many of the ridges have been partially or entirely buried by subsequent sedimentation. The absence of annual push-ridges in the south basin could indicate an absence of sea ice, which prevented the glacier front from stabilising during winter (Boulton 1986; Flink *et al.* 2015). It could also relate to internal glacier dynamics leading to exceptionally fast retreat with no readvances. It is likely that the ridges, particularly in the inner south basin, consist of both retreat moraines and crevasse-squeeze ridges (Fig. 7b).

The small transverse ridges in the north basin are interpreted as De Geer moraines based on their dimension and morphology (De Geer 1940; Linden & Möller 2005). De Geer moraines form subaquatically by either sediment squeeze into basal crevasses (Zilliakcus 1989; Beadry & Prichonnet 1991) or as push moraines near the grounding line of a retreating ice sheet or glacier (De Geer 1940; Boulton 1986; Blake 2000). They have been suggested to form annually or semi-annually (De Geer 1940; Boulton 1986; Flink *et al.* 2017). Based on the similarity between the moraine ridges in the NW and the north basins, we suggest that the De Geer moraines have formed as push moraines. It is therefore possible that the De Geer moraines in the north basin record annual retreat of the SBSIS during the deglaciation.

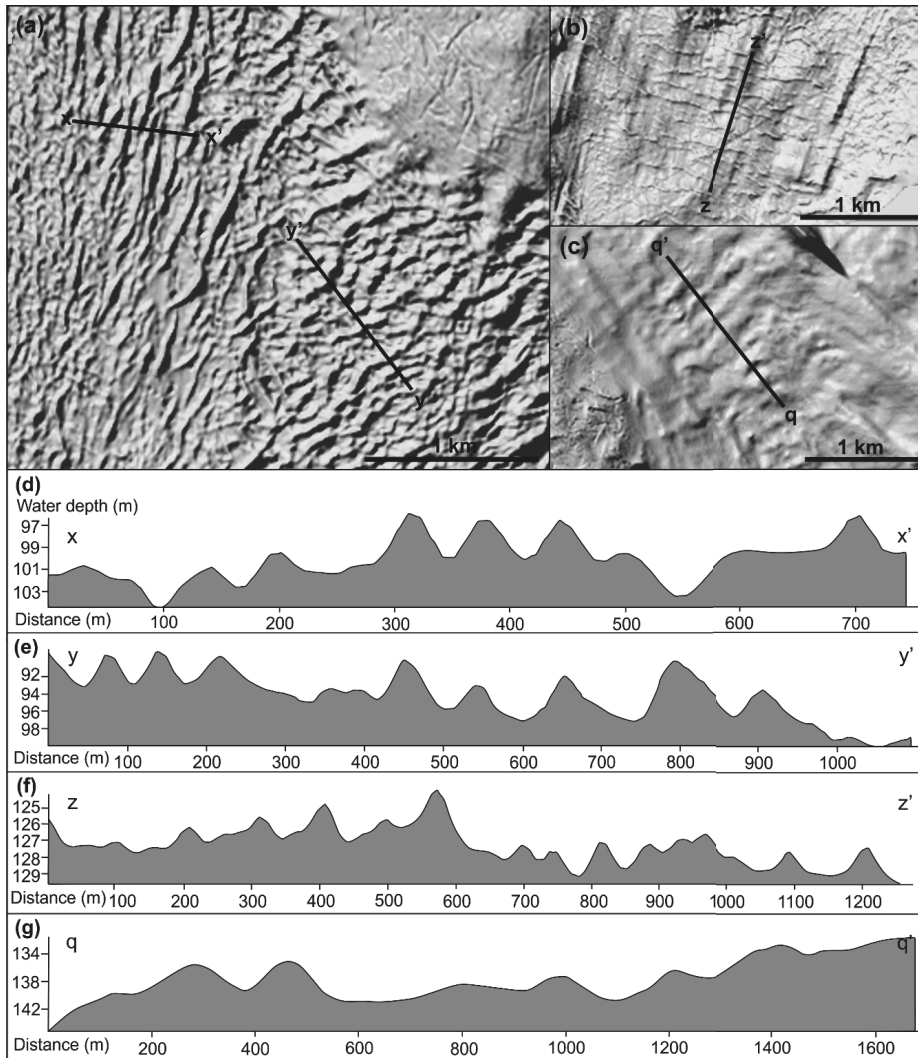


Fig. 7. (a) Crevasse-squeeze ridges in the south basin. (b) Crevasse-squeeze or possible annual retreat moraines in the inner south basin. (c) De Geer moraines in the north basin. (d) Cross-profile of the longitudinal crevasse-squeeze ridges. (e) Cross-profile of the oblique crevasse-squeeze ridges. (f) Cross-profile of the transverse crevasse-squeeze ridges. (g) Cross-profile of the De Geer moraines. For location of figures see Fig. 3.

5.4. Geometric ridge networks: crevasse-squeeze ridges

5.4.1. Description

A prominent geometric ridge network is present in the south basin (Figs 3 and 7a). The ridges are sharp-crested, have varied orientations and intersect each other. They are symmetric in cross-profile and overprint pre-existing bedforms, such as glacial lineations. The ridges in the outer south basin have both transverse, longitudinal- and oblique orientations in relation to inferred ice flow (Fig. 7a). The longitudinal and some of the oblique ridges are significantly larger than the transversely oriented ridges. They are up to 900 m long, 9 m high and 100 m wide (Fig. 7d). The majority of the oblique and the transverse ridges are a couple of hundred m long, 1-3 m high and 50 m wide (Fig. 7e). A geometric ridge network can be observed between the crests of the R-1 ridge (Fig. 6a). In the inner south basin the ridges are mainly transverse to inferred ice flow (Fig. 7b). They are 100-500 m long, 1-3 m high, 60 m wide and have a fairly regular crest-to-crest spacing of 80-120 m. The ridges intersect, but are generally less sharply crested than the ridges in the outer south basin.

5.4.2. Interpretation

The geometric ridge networks are interpreted as crevasse-squeeze ridges, based on their varied orientation, intersecting nature and similarity to previously described crevasse-squeeze ridges (Boulton *et al.* 1996; Rea & Evans 2011; Lovell *et al.* 2015). Crevasse-squeeze ridges form as soft subglacial sediments are squeezed upward into basal crevasses during surge stagnation (Kristensen & Benn 2012; Lovell *et al.* 2015). High basal water pressures, close to ice overburden, coupled with high extensional strain rates in turn enable bottom-up crevasse propagation or hydrofracturing and subsequent sediment squeeze into the basal crevasses (Rea & Evans 2011; Lovell *et al.* 2015). Crevasse-squeeze ridges in a landform assemblage have been used as a characteristic criteria for identifying surging glacier (Solheim & Pfirman 1985; Evans & Rea 1999; Farnsworth *et al.* 2016).

The crevasse-squeeze ridges in Vaigattbogen (particularly the longitudinal ridges), have larger dimensions compared to typical crevasse-squeeze ridges in Svalbard fjords, which indicates that the glacier front was highly crevassed during their formation (Boulton *et al.* 1996; Ottesen *et al.* 2008; Lovell *et al.* 2015). The submarine crevasse pattern and the large size of the ridges might suggest top-down full-depth crevasse penetration, which in turn would indicate high strain rates and a thin glacier front (cf. Rea & Evans 2011). The multi-lobate shape of the R.1 ridge supports this interpretation, suggesting that the terminus was subjected to high extensional strain rates and possibly experienced rapid thinning as a result of rapidly stagnating ice flow at the end of a surge. The predominantly transverse orientation of the crevasse-squeeze ridges in the inner south basin indicate that these ridges could consist both, De Geer/annual retreat moraines and crevasse-squeeze ridges. Since the ridges occur as short sections and locally intersect each other they have been mapped as crevasse-squeeze ridges, despite of their dominantly transverse orientation. Similar, dominantly transverse crevasse-squeeze ridges have been described earlier from terrestrial settings (Lovell *et al.* 2015).

6. Sediment cores

6.1. Description

Four sediment cores were recovered from Vaigattbogen. Core HH16-01 was 295 cm long and recovered from a water depth of 198 m, from an area dominated by glacial lineations (Fig. 2). The HH16-02 core was 360 cm long and recovered from a water depth of 170 m. The HH16-03 core was 222 cm long and recovered from the crest of the R.1 ridge at a water depth of 67 m (Fig. 3). The HH16-04 core was 138 cm long at and was recovered from an area dominated by crevasse-squeeze ridges, at a water depth of 107 m (Fig. 3). The top 170 cm of the HH16-01 core consist of massive olive grey mud (Fm(d)) with occasional

outsized clasts, shells and shell fragments (Fig. 8a). Sand lenses are present in the lower section of the unit. The Fm(d) unit is followed by a laminated unit (Fl) between 170-235 cm. The laminations are well defined by both color and grain size changes. They are 2-10 mm thick, alternating between pink and grey colors and silty clay to silt. They are accompanied by a decrease in shear strength and grain size. Three sand layers are present in the Fl unit. The layers consist of massive, fine- to medium sand. The lowermost sand layer contains outsized clast of pebble size. From 235-295 the core consists of massive diamict with sub-angular to sub-rounded clasts. The diamict is less compact with a higher water content in its upper part. The top 0-262 cm of the HH16-02 core consist of a similar massive olive grey mud with a few outsized clasts, shells and gravel lenses (Fig. 8b). A layer of coarse sand is present at 106 cm. The Fm(d) unit is followed by a Fl(d) unit with occasional outsized clasts and a gravel lense. The laminations are similar to the Fl unit in the HH16-01 core and are predominantly defined by color changes between pink to grey. At 320 cm, the Fl(d) unit is followed by massive sand with outsized clasts (Smd). The proportion of coarser grains increases towards the base of the Smd unit.

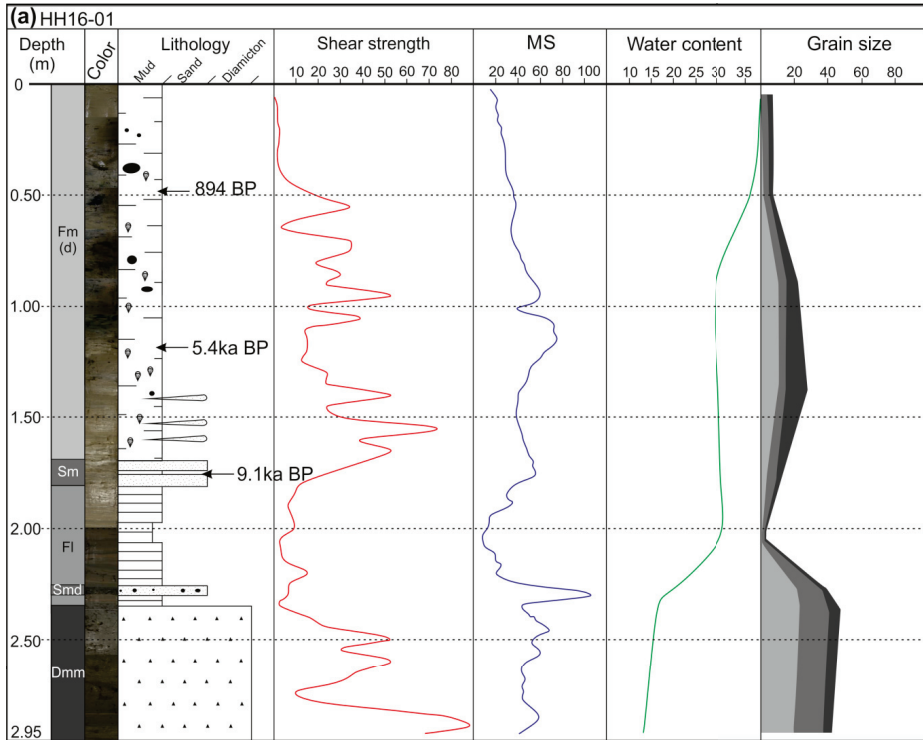
Table. 1. Lithofacies in the HH16 cores. Lithological codes were adopted from Eyles *et al.* (1983)

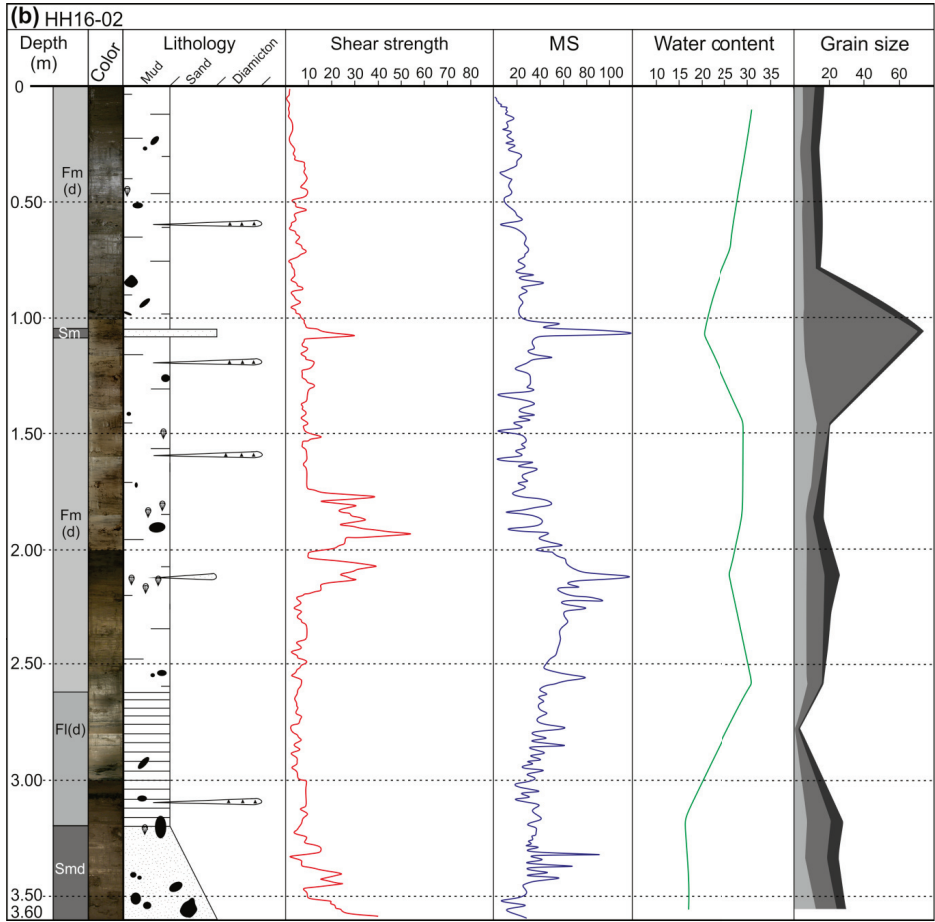
Lithofacies	Description
<i>Mud</i>	
Fm(d)	Mud, massive, with rare clasts
Fmd	Mud, massive, with abundant clasts
Fl(d)	Mud, laminated, with rare clasts (lamination are parallel, 1-10 mm thick)
Flw(d)	Mud, weakly laminated, with rare clasts
<i>Sand</i>	
Smd	Sand, massive, with abundant clasts
<i>Diamict</i>	
Dmm	Diamict, massive, matrix-supported, with randomly oriented clasts

The HH16-03 core displays a complex sedimentology with several different units (Fig. 8c). The uppermost unit consists of olive grey mud with occasional outsized clasts and a sand lense. Between 55-85 cm the core consists of weakly laminated mud Flw(d). The laminations are diffuse, 2-5 mm thick and alternate between clayey silt and sandy silt. Unlike the laminations in HH16-01 and HH16-02 cores, they are defined based on grain size changes rather than alternating colors. The laminations in the lower section of the unit are generally thicker; contain a higher amount of sand and occasional gravel sized clasts. The Flw(d) unit is followed by a clast rich mud unit Fmd, which gradually becomes sandier between 90-115 cm and displays a distinct color change to dark greyish-brown at 114 cm. The color change is accompanied by an increase in shear strength values from 20 to 80 kPa. The Smd unit consists of massive sand, a high number of outsized clasts and a gravel lense. At 155 cm occurs a sharp change to a silty mud unit with outsized clasts, a gravel lense, shells and shell fragments. The Fmd unit has high and variable shear strength values. It is followed by a unit of massive sand (Smd) with outsized, predominantly sub-angular clasts and a lens with diamictic material. The boundary between the units is gradational.

The top 0-65 cm of the HH16-04 core consists of massive mud with occasional outsized clasts. Unlike the other cores, foraminifera were extremely rare and shells were absent in the HH16-04 core. The Fm(d) unit is followed by a layer of coarse sand with gravel sized clasts. The boundary between the Fm(d) unit and the sand layer is sharp and conformable. The sand layer is followed by a massive diamict with a clayey-silty matrix and sub-angular to sub-rounded clasts. The diamict has been divided into two different units based on their distinctly different color. At 110 cm, the matrix displays a sharp color change from brown to grey. Both Dmm units are poorly-consolidated and have relatively low shear

strength values. The Dmm1 unit has shear strength values below 20 kPa, while shear strength values in the Dmm2 are slightly higher and more variable (Fig. 8d).





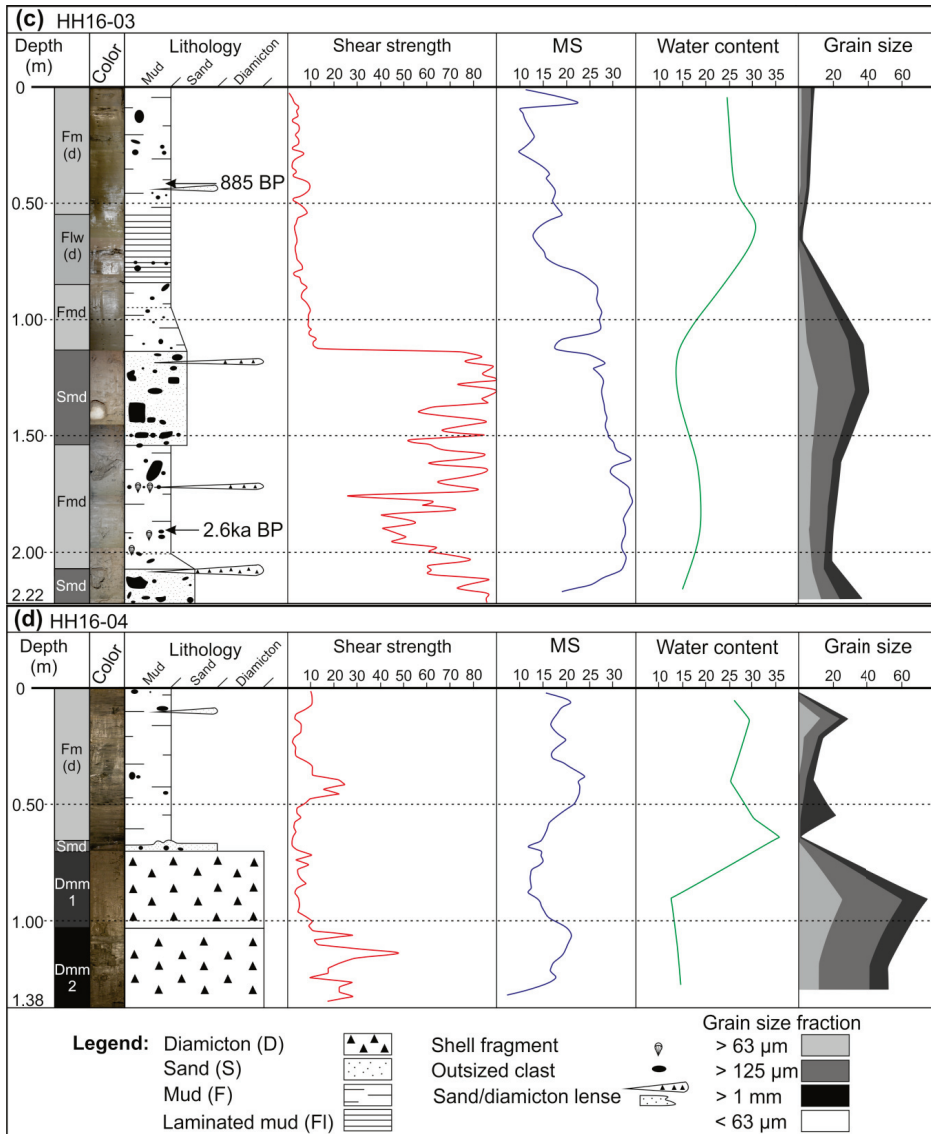


Fig. 8. Composite logs for the HH16 cores showing lithology, undrained shear strength (kPa), magnetic susceptibility (SI units), water content as a percentage of total sample weight and grain-size distribution as a percentage of total dry weight. Arrows point to ^{14}C sample depths. (a) HH16-01, (b) HH16-02, (c) HH16-03 and (d) HH16-04.

6.2. Interpretation

The Fm(d) unit, which comprises the topmost part in all cores represents fine-grained mud accumulated in a distal glacial marine environment. The glacial marine mud has been described previously from the northern Barents Sea (Elverhøy *et al.* 1989; Hogan *et al.* 2010a, b). Radiocarbon ages confirm that the Fm(d) unit is of Holocene age (Fig. 8 and Table. 2). The oversized clasts are interpreted as iceberg rafted debris. The sand and gravel lenses could have formed from iceberg dumping. The glacial marine mud in core HH16-02 contains sand layers and gravel lenses, which could be a result of iceberg dumping or mass flows. The glacial marine mud in cores HH16-01 and 02 contain multiple shells and shell fragments, suggesting that the environment was favorable for shells during the deposition of the sediments. The laminated units in the HH16-01 and 02 cores are interpreted as a proximal glacial marine unit, formed as a result of rhythmically changing sedimentation near a tidewater glacier front in the absence of bioturbation. It is possible that the laminae represent changes in seasonal deposition, where subglacial meltwater-driven processes have played a role. An early Holocene age from the HH16-01 core, from the top of the Fl unit indicates that the laminated unit represents the deglaciation phase (Fig. 8 and Table. 2).

Table. 2. Uncalibrated and calibrated radiocarbon ages from the HH16-01 and HH16-03 cores.

Sample name	Depth (cm)	C ¹⁴ age BP	Uncertainty ±	Cal. age BP Two sigma error	Cal. age BP mean
HH16-01	48-49	1468	28	794-993	894
HH16-01	118-119	5194	37	5320-5560	5440
HH16-01	175-176	8550	45	8941-9234	9088
HH16-03	42-43	1456	36	778-992	885
HH16-03	190-191	2948	33	2463-2719	2591

The relatively soft basal diamict in HH16-01 is interpreted as a subglacial till based on its lithology and succession in the core. The distinctly different diamict units in the HH16-04 core have formed as a result of two different processes. The core was recovered from the slope of a crevasse-squeeze ridge and the soft Dmm1 unit could thus represent sediments which were squeezed into the basal crevasse during the final stages of the surge. The Dmm2 is also a soft diamict and although it has extremely low shear strength values and differs from typical subglacial tills that are commonly over-consolidated it is interpreted as a subglacial till based on its succession below the Dmm1 unit. Subglacial tills from the troughs in eastern Svalbard have however been described as extremely soft and poorly consolidated, indicating that they have formed as a result of subglacial deformation (Hogan *et al.* 2010b). This suggests that the Dmm2 and the till in HH16-01 both represent deformation tills and have formed through subglacial deformation below relatively fast moving ice.

The basal Smd unit in HH16-02 core is interpreted as a glacial proximal unit based on its lithology and succession in the core. Similar units have previously been interpreted as mass-flow deposit originating from the base of a retreating ice margin (Hogan *et al.* 2010a, b). Therefore the sediments in cores HH16-01- and 02 display a classic deglacial succession with a subglacial or glacial-proximal deposit at the base followed by laminated deglacial sediments and covered by distal glacial marine sediments, which accumulated in open water conditions. The HH16-03 core contains a complex sedimentary sequence, which can be attributed to the core being recovered from the distal slope of the R.1 ridge. Multiple iceberg ploughmarks on the ridge crest and debris-flow lobes suggest that these processes contributed to the complex sedimentology of the core. The Fm(d) unit between 155-210 cm is similar to the Fm(d) unit in cores HH16-01 and HH16-02 suggesting that it formed in open marine conditions (Fig. 8). The Fm(d) unit has a mid-Holocene age indicating that the Smd unit above it could have formed as a result of a glacial surge which affected the core site after 2.6 ka BP (Fig. 8c).

7. Sub-bottom data

Sub-bottom data were collected along a north-south transects in Vaigattbogen (Fig. 9a). Additional transects were acquired from the south basin (Fig. 9b). The sub-bottom data indicates that the seafloor in the study area is covered by a relatively thin cover of marine sediments. The sediments in Vaigattbogen can be divided into five acoustic facies, described and interpreted in detail in Table. 3.

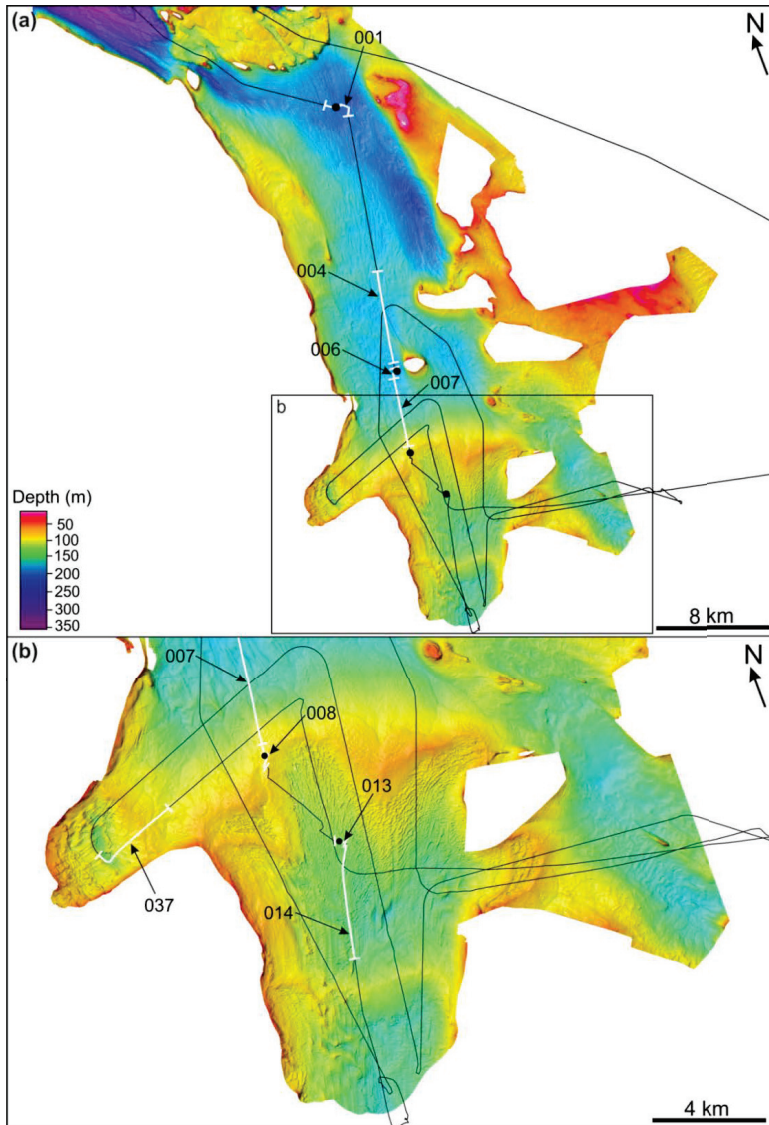


Fig. 9. (a) Acquired chirp data in Vaigattbogen. (b) Zoom-in on the south and NW basins. White lines mark chirp lines shown in Figs 10 and 11.

Table 3. Acoustic facies identified from the sub-bottom (chirp) data in Vaigattbogen

Acoustic facies	Description	Interpretation	Examples
F.1	Acoustically transparent, homogenous facies with moderate to high amplitude upper reflector forming small mounds, often associated with slopes. 5-15 m thick.	Mass-flow deposits. Correlate to the debris-flow lobes on the distal flanks of large moraine ridges.	Fig. 11b
F.2	Acoustically transparent, homogenous facies with a high-amplitude upper reflector and locally discontinuous bottom reflector. 1-5 m thick, forming a drape covering the seafloor.	Holocene glacimarine mud, formed in a distal open marine setting. Correlates with lithological unit Fmd.	Fig. 10a, Fig. 11a
F.3	Multiple parallel or sub-parallel reflectors with total thickness between 1-5 m. Commonly found below the F.2 facies, but is locally exposed on the seafloor adjacent to slopes or as infill in depressions.	Laminated muds with two possible formation processes: 1) in an ice-proximal setting through rhythmic suspension settling driven by seasonal variations. Correlates to the F1 unit and represents deglacial sediments. 2) Formed as a combination of open marine sedimentation and mass flows. Correlates to unit Fmd in core HH16-02.	Fig. 10a, b, Fig. 11d
F.4	Acoustically transparent facies without internal structures. 2-8 m thick and occurs locally in the north basin. Present below the F.1, F.2 or F.3 facies	Homogenous sediments. Correlate with the Smd unit in core HH16-02, suggesting that the facies consist of glacimarine sediments with high sand content, formed in a glacial proximal setting.	Fig. 10b, Fig. 11b
F.5	Acoustically featureless facies with high-amplitude upper reflector. Little to no penetration of the acoustic signal below the upper reflector. Present across the entire study area. Commonly covered by the F.1 to F.4 facies.	Acoustic basement comprised of hard substrate such as bedrock or diamict. Correlates with the Dmm unit in core HH16-01. Glacial landforms have formed in the F.5 facies suggesting that it represents a subglacial till across most of the area.	Fig. 10c, d

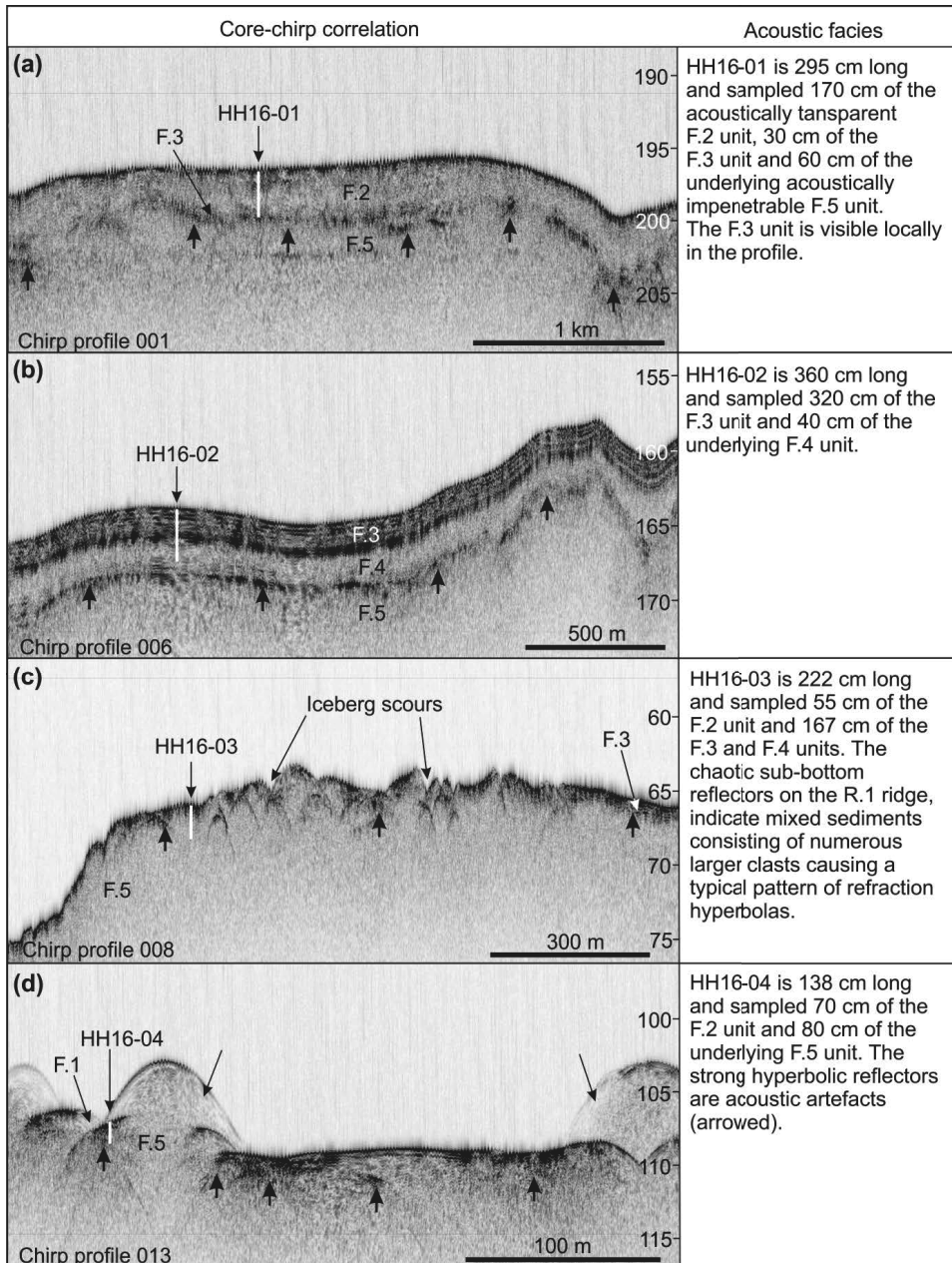


Fig. 10. Core locations and sub-bottom profiles with acoustic facies indicated. Basal reflectors arrowed. White bars show the approximate penetration depth of the cores. (a) HH16-01 (b) HH16-02 (c) HH16-03 and (d) HH16-04. Vertical scale is in meters below sea level. Locations of the profiles are shown in Fig. 9.

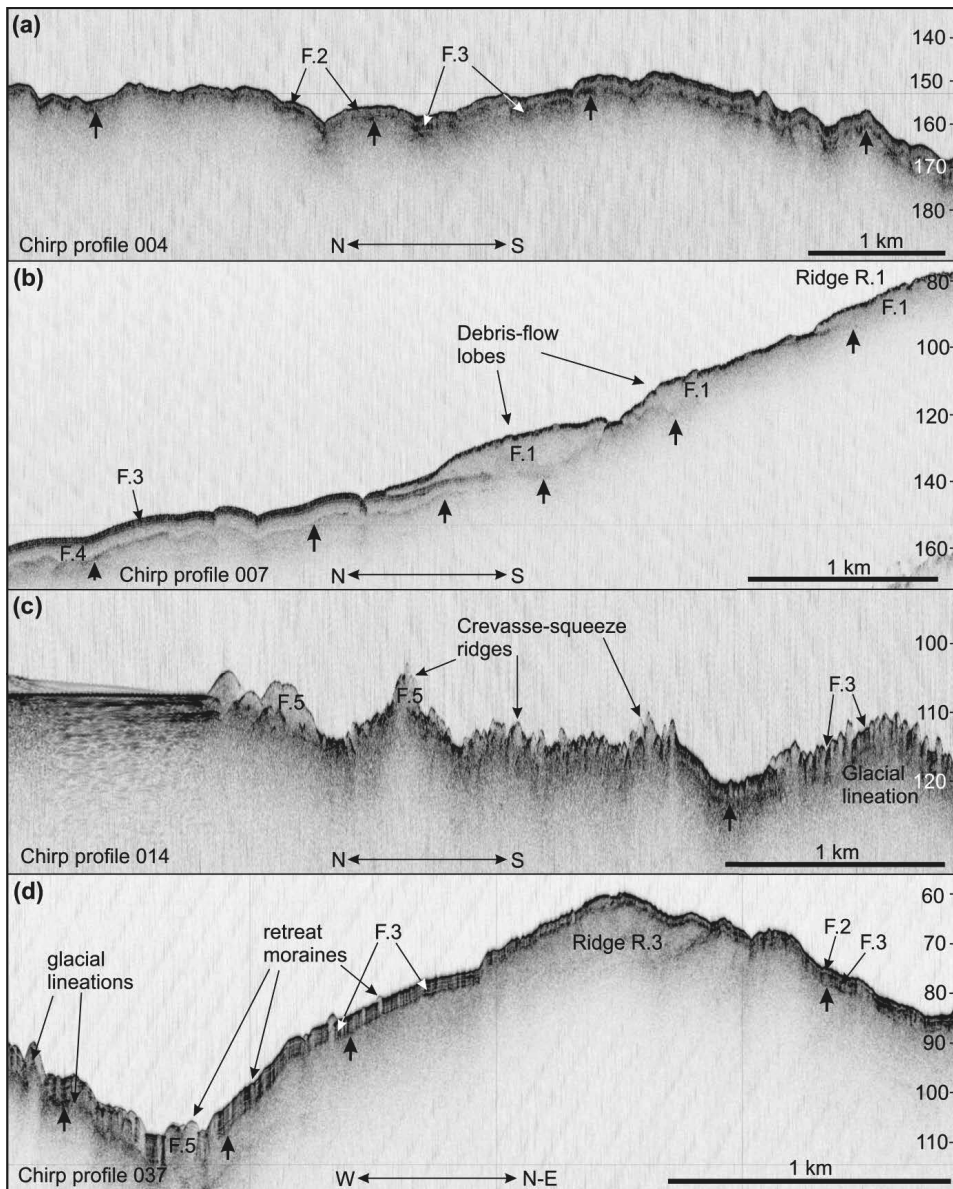


Fig. 11. Examples of sub-bottom profiles from Vaigattbogen. (a) Holocene sediment drape in the north basin. (b) The distal slope of the R.1 ridge with debris-flow lobes. (c) Crevasse-squeeze ridges overprinting glacial lineations. (d) The landform assemblage of Chydeniusbreen. Note the almost buried retreat moraines proximal to the ridge. Small arrows outline basal reflectors. Vertical scale is in meters below sea level. Locations of the profiles are shown in Fig. 9.

8. Discussion

8.1. Last glacial ice sheet dynamics in northeastern Spitsbergen and western Nordaustlandet

The landform assemblage together with the high elongation ratios of the longitudinal landforms suggest relatively fast ice flow in Vaigattbogen during the Last glacial. Crag-and-tails indicate a northward ice flow direction (Figs 2 and 12) towards the Hinlopen Trough and the shelf edge. The geomorphological record of the Hinlopen Trough with progressively longer subglacial landforms and higher elongation ratios from the inner- towards the outer-shelf suggests progressively faster ice flow towards the shelf edge (Batchelor *et al.* 2011). This is consistent with our study where longer lineations at the mouth of the north basin suggest faster ice flow. Similarly, it has been proposed that ice flow speeds increased towards the mouth of Wahlenbergfjorden, east of the Hinlopen Strait (Flink *et al.* 2017). The landform assemblage in Vaigattbogen is similar to that of Wahlenbergfjorden with predominantly crag-and-tails in the inner fjord and longer glacial lineations at the fjord mouth (Flink *et al.* 2017). Lower elongation ratios in the inner fjord and in the vicinity of the dolerite islands (Fig. 1) could also relate to changes in bedrock geology. As ice flows over a hard bed the abrasion rate increases (Roberts & Long 2005) suggesting that the complex bedrock geology in Vaigattbogen played a role in landform development.

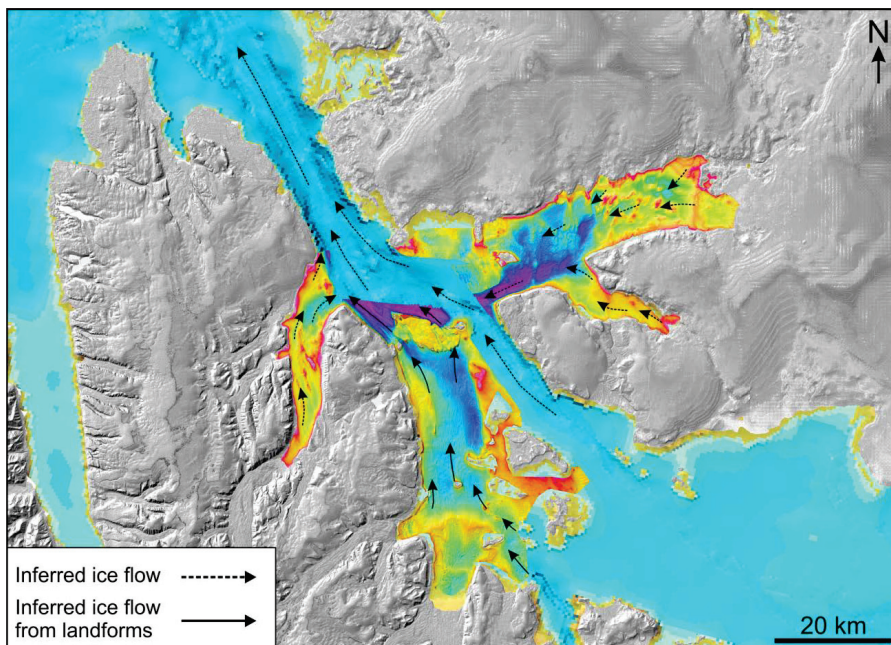


Fig. 12. Regional ice flow in north-eastern Spitsbergen and western Nordaustlandet. Solid arrows show reconstructed ice flow based on this study. Dashed arrows show ice flow based on Dowdeswell *et al.* 2010; Flink *et al.* 2017 and Streuff *et al.* (in review). Background shows the IBCAO, Version 3.0, (Jakobsson *et al.* 2012).

8.2. Deglacial ice sheet dynamics in northeastern Spitsbergen and western Nordaustlandet

Hinlopen Trough deglaciated rapidly with no major still-stands of the ice front (Dowdeswell *et al.* 2008; Ó Cofaigh *et al.* 2008; Batchelor *et al.* 2011). The lack of ice-transverse landforms, such as grounding-zone wedges and transverse moraine ridges in the trough suggest that the ice front detached from the bed and retreated rapidly by calving (Ottesen *et al.* 2007; Dowdeswell *et al.* 2008). The ice sheet begun to retreat from the shelf edge between 19-16.5 ka BP (Chauhan *et al.* 2015; Hogan *et al.* In press). Open marine conditions prevailed at the HH16-01 core location prior to 9.1 ka BP. Summer sea ice was largely absent from the Hinlopen Strait region by 10.8 ka BP (Koc *et al.* 2002). It is likely that the ice sheet had retreated from outer Vaigattbogen latest around 11 ka BP, indicating relatively rapid ice retreat from the shelf edge. Inner Wahlenbergfjorden was ice free prior to 11.3 ka BP (Flink *et al.* 2017), lending further support to rapid ice sheet retreat in the Hinlopen area. An absence of ice transverse landforms in both, outer Wahlenbergfjorden and Vaigattbogen suggests that the terminus of the ice sheet became floating during the deglaciation and disintegrated by rapid calving (Flink *et al.* 2017).

The rapid deglaciation of the area coincide with a period of rapid sea level rise between 16-12.5 ka BP (Lambeck *et al.* 2002) suggesting that sea level rise could have been driving or at least contributing to the rapid deglaciation. De Geer moraines in Vaigattbogen indicate that the ice sheet locally experienced episodic retreat with minor re-advances, most likely due to the shallower seafloor and narrow geometry of the Hinlopen Strait. It is likely that the morphology of the strait exerted lateral drag on the retreating ice sheet terminus, while the Islands in Vaigattbogen induced pinning points to stabilize the ice front. The direction of the De Geer moraines in the shallow areas around the islands suggests that ice was present on the islands after the outer basin was deglaciated.

Sedimentation rates from the HH16-01 and HH16-03 cores indicate a similar sedimentary environment in Vaigattbogen and Wahlenbergfjorden. In Vaigattbogen sedimentation rates were relatively high in early Holocene, estimated to 48 cm/ka⁻¹ and decreasing to 26 cm/ka⁻¹ during mid-Holocene. Sedimentation rates increased to 47-54 cm/ka⁻¹ from 900 BP to the present. These values are similar to inner Wahlenbergfjorden where late Holocene sedimentation rates were 54 cm/ka⁻¹ (Flink *et al.* 2017). The higher sedimentation rate could be attributed to abundant availability of sediments due to sedimentary bedrock and higher glacial activity in Vaigattbogen during the earlier part of the Holocene. The sedimentation rates in the lower part of the HH16-03 core are significantly higher, up to 111 cm/ka⁻¹ between 2.6 ka BP- 890 BP which could result from surge activity.

8.3. Ice-sheet configuration during the Late glacial and deglaciation

The highest marine limits on Svalbard were measured at Kongs- and Svenskøya suggesting that the SBSIS was centered on Kong Karls Land or just to the south of the Islands during the Late Weichselian (Ingólfsson *et al.* 1995; Lambeck 1995; Landvik *et al.* 1998; Forman *et al.* 2004). Streamlined landforms with a W-E direction in the Erik Eriksen and Olga Straits suggest that a local ice dome was located in the southern Hinlopen Strait area (Dowdeswell *et al.* 2010; Hogan *et al.* 2010b). The landform record in Vaigattbogen suggesting northwards ice flow does not contradict the location of a dome in the southern Hinlopen Strait area. It is possible that the ice dome location suggested by (Hogan *et al.* 2010b; Dowdeswell *et al.* 2010) records a late Weichselian flow event, which occurred sometime during the early deglaciation, when the central part of the SBSIS, around the Storbanken area had already begun to deglaciate. If so, it is possible that the center of the SBSIS migrated towards the northwest, suggesting eastern Svalbard was covered by multi-domed ice sheet during the late glacial and early deglaciation (Ottesen *et al.* 2007; Dowdeswell *et al.* 2010; Hormes *et al.* 2013; Ingólfsson & Landvik 2013). During the deglaciation of Hinlopen Strait, Vaigattbogen and Wahlenbergfjorden, the land areas and most likely also the Islands in the Hinlopen Strait remained glaciated longer than the adjacent seafloor. The early

deglaciation of Wahlenbergfjorden suggests a possible double-domed ice sheet over Nordaustlandet during the deglaciation with the domes located approximately at the present positions of Vest- and Austfonna. This agrees with the reconstruction by Hormes *et al.* (2013) who suggested that Nordaustlandet was covered by locally cold-based ice domes during MIS2.

8.4. Holocene glacier dynamics in Vaigattbogen

The submarine landform assemblage in inner Vaigattbogen indicates that the Hinlopen/Oslobreen glacier system experienced at least three surge-type advances during the Holocene. Both, the 1901 and 1971 terminal positions are located near the R.2 ridge (Fig. 4). The match between the ridge and the mapped LIA position (De Geer 1923) could indicate that the R.2 ridge formed partly during the LIA and was only modified by the 1971 surge. It is, however, possible that the Hinlopenbreen terminus reached farther out during the LIA maximum, which occurred prior to 1901. Radiocarbon dates from the HH16-03 core on the R.1 ridge yield a minimum age of 2.6 ka BP demonstrating that the R.1 ridge formed prior to the LIA. It is possible that the R.1 ridge formed as early as in Early Holocene since the HH16-03 core did not sample subglacial diamict and the time of deglaciation at that location is not known. Crevasse-squeeze ridges between the double ridge crests indicate that the glacier front reached the position of the R.1 ridge at least during two consecutive surges.

Pre-LIA advances have been suggested for several other Svalbard glaciers (Salvigsen *et al.* 1990; Ronnert & Landvik 1993; Werner 1993; Andersson *et al.* 2000; Hald *et al.* 2001; Kristensen *et al.* 2009; Reusche *et al.* 2014; Flink *et al.* in prep). Flink *et al.* (in prep) suggested that a surge-type advance occurred in Mohnbukta in early Holocene prior to 7.7 ka BP. The surge reached the outer moraine ridge in Mohnbukta, which is high and steep-sided, similarly to the R.1 ridge in Vaigattbogen. The size of the ridge suggests that a large amount of sediment was brought to the glacier front in order to form the ridge. Large, steep-sided push-ridges have been suggested to form when well consolidated sediments with low water content are pushed up by the glacier front (Evans *et al.* 2006). The similarity between the ridges in Mohnbukta and Vaigattbogen could imply that both formed in similar conditions in the early Holocene. The early Holocene surge-type advance in Mohnbukta has been attributed to rapid climatic and environmental change after the deglaciation, which induced a climatically controlled jump into surge-mode (Sevestre *et al.* 2015; Sevestre & Benn 2015; Flink *et al.* in prep). It is possible that the Hinlopenbreen basin experienced a similar jump into surge-mode during early Holocene.

After 1901, Hinlopenbreen retreated until the early 1970s when it surged (Fig. 4). The surge front reached further out on the east side of the fjord and has generally the same configuration as the submarine R.2 ridge (Fig. 4). The shape of the R. 2 ridge, with gentle flanks and debris-flow lobes on both sides suggests that it formed by ice pushing up soft sediments with high water content. It is likely that the eastern part of the glacier front became floating at the end of the surge, which permitted highly liquefied, low shear strength sediments to flow down the proximal slope and bury crevasse-squeeze ridges. Since 1971, the glacier front has retreated approximately 156 m yr^{-1} along its center line. This is a high retreat rate compared to previous estimates of $30\text{--}150 \text{ m yr}^{-1}$ for east coast glaciers (Błaszczuk *et al.* 2009; Flink *et al.* in prep). The retreat rates have increased since the 1980s from 64 m yr^{-1} between 1971-1986, to 259 m yr^{-1} between 1986-1999, and decreased to 159 m yr^{-1} between 1999-2014.

Similarity between the Chydenius- and Hinlopenbreen landform records suggests that the Chydeniusbreen landsystem might have formed by a surge-type advance during the end of the LIA. Sub-bottom acoustic data indicates thick glacial marine sediments which have locally buried retreat moraines or crevasse-squeeze ridges (Fig. 11d). In the 1901 map, the joint fronts of Chydenius- and Polarisbreen

reach the position of the R.3 moraine ridge suggesting that the ridge formed during the advance of these glaciers (De Geer 1923). All the glaciers in Vaigattbogen have retreated since 1901 except for the 1970s Hinlopenbreen surge and a minor re-advance of Chydeniusbreen in 2002 (Fig. 4). Increased retreat rates are observed since the late 1990s and early 2000s for most of the glaciers. Since 1999, Kosterbreen and Allfarvegen have retreated 600 and 1330 m, respectively from approximately their LIA maxima. Vaigattbreen has retreated 500 m since 2002 (Fig. 4). The recent speed-up of retreat rates seems to be in accordance with other studies from the east coast, for example, the retreat rates in Mohnbukta have increased to 200 m yr⁻¹ since 2002 (Flink *et al.* In prep). It is likely that the increase in retreat rates is climatically induced and correlates to generally warmer temperatures and loss of sea ice in east Svalbard.

9. Conclusions

- Vaigattbogen, as most of Svalbard, was covered by the SBSIS during the last glacial. The ice sheet flowed northwards through Vaigattbogen and merged with the Hinlopen Strait ice stream. Elongation ratios of glacial lineations suggest higher flow velocities in the northern than in the southern part of Vaigattbogen.
- Absence of ice-flow transverse landforms in the deeper north basin of Vaigattbogen implies lift-off and relatively rapid disintegration of the ice sheet, most likely through calving. De Geer moraines on the western slope of the fjord suggest that the terminus was at least a partly grounded and experienced slower retreat with minor re-advances.
- Open marine sedimentation at the HH16-01 core site indicates that the north basin deglaciated prior to 9.1 ka BP.
- Although the landform record in Vaigattbogen suggests ice flow towards the Hinlopen Strait, it does not contradict the location of an ice dome in the southern Hinlopen Strait area sometime during the late glacial or early deglaciation.
- Two large terminal moraine ridges with crevasse-squeeze ridges in front of Hinlopenbreen suggest that at least two surge-type advances have occurred in the Hinlopen-Oslobreen basin.
- The R.1 ridge formed prior to 2.6 ka BP and marks the Holocene maximum extent of the Hinlopen-Oslobreen glacier systems. Radiocarbon data yields a minimum age of 2.6 ka BP for the ridge although it could have formed much earlier. Crevasse-squeeze ridges between the double-crests of the R.1 ridge suggest that Hinlopen/Oslobreen have experienced at least two pre-LIA surges.
- During the 1970s surge, the Hinlopenbreen glacier front reached the innermost, R.2 ridge and has since then been retreating. The retreat rates of the glaciers in Vaigattbogen have increased since the early 2000s most likely driven by warmer climate and less sea ice in the east Spitsbergen fjords.

Acknowledgements

We would like to thank Berit Jakobsen, Head Librarian at the University Centre in Svalbard for her help with historic maps and documents. The bathymetric data were provided by the Norwegian

Hydrographic Service (permission nr. 13/G706). Aerial/satellite images and maps were used and presented by the courtesy of the Norwegian Polar Institute (NPI). We acknowledge the U.S Geological Survey and NASA for access to Landsat satellite data.

Reference list

Andersson, T., Forman, S., Ingólfsson, Ó, & Manley, W., 2000. Stratigraphic and morphologic constraints on the Weichselian glacial history of northern Prins Karls Forland, western Svalbard. *Geografiska Annaler*. Vol. 82. p. 455-470

Andreassen, K., Winsborrow, M.C.M., Bjarnadóttir, L.R., & Rüther, D.C., 2014. Ice stream retreat dynamics inferred from an assemblage of landforms in the northern Barents Sea. *Quaternary Science Reviews*. Vol. 92. p. 246-257

Batchelor, C.L., Dowdeswell, J.A., & Hogan, K.A., 2011. Late Quaternary ice flow and sediment delivery through Hinlopen Trough, Northern Svalbard margin: Submarine landforms and depositional fan. *Marine Geology*. Vol. 284. p. 13-27

Beadry, L.M., & Prichonnet, G., 1991. Late glacial De Geer moraines with glaciofluvial sediment in the Chapais area, Quebec, Canada. *Boreas*. Vol. 20. p. 377-394

Blake, K.P., 2000. Common origin for De Geer moraines of variable composition in Raudvassdalen, northern Norway. *Journal of Quaternary Science*. Vol. 15. Nr. 6. p. 633-644

Błaszczuk, M., Jania, J.A., Hagen, J.O., 2009. Tidewater glaciers in Svalbard: Recent changes and estimates of calving fluxes. *Polish Polar Research*. Vol. 30. No. 2. p. 85-142.

Boulton, G.S., 1976. Origin of glacially fluted surfaces. *Journal of glaciology*. Vol. 17. p. 287-301

Boulton, G.S., 1986. Push-moraines and glacier-contact fans in marine and terrestrial environments. *Sedimentology*. Vol. 33. p. 667-698

Boulton, G.S., van Der Meer, J.J.M., Hart, J., Beets, D.J., Ruegg, G.H.J., Van Der Wateren, F.M., & Jarvis, J., 1996. Till and moraine emplacement in a deforming bed surge—An example from a marine environment. *Quaternary Science Reviews*. Vol. 15. p. 961–987.

Boulton, G.S., van der Meer, J.J.M., Beets, D.J., Hart, J.K., & Ruegg, G.H.J., 1999. The sedimentary and structural evolution of a recent push moraine complex: Holmstrømbreen, Spitsbergen. *Quaternary Science Reviews*. Vol. 18. p. 339-371

Burton, D., Dowdeswell, J.A., Hogan, K. & Noormets, R., 2015. Marginal fluctuations of a Svalbard surge-type tidewater glacier, Blomstrandbreen, since the Little Ice Age: a record of three surges. *Arctic Antarctic and Alpine Research*. Vol. 48. p. 411-426.

Chauhan, T., Rasmussen, T.L., & Noormets, R., 2015. Paleoceanography of the Barents Sea continental margin, north of Nordaustlandet, Svalbard during the last 74 ka. *Boreas*. Vol. 45. p. 76-99.

Dallmann, W.K., Ohta, Y., Elvevold, S., & Blomeier, D., 2002. Bedrock map of Svalbard and Jan Mayen. *Norsk Polarinstitutt Temakart*. (Norwegian polarinstitute) No. 33.

De Geer, G., 1923. Missions Scientifiques pour la mesure d'un arc de Méridien au Spitsberg entreprises en 1899-1902 sous les auspices des gouvernements Russe et Suédoise. Mission Suédoise. Tome II. Topographie. Geologie. *Aktiebolaget Centraltryckeriet, Stockholm*. 1923

De Geer, G., 1940. *Geochronologia suecica* principes. Vol. 18. Almqvist & Wiksells. Sweden

Dowdeswell, J.A., & Forsberg, C.F., 1992. The size and frequency of icebergs and bergy bits derived from tidewater glaciers in Kongsfjorden, northwest Spitsbergen. *Polar Research*. Vol. 11. Nr.2. p. 81-91.

Dowdeswell, J.A., Ottesen, D., Evans, J., Ó Cofaigh, C. & Anderson, J.B., 2008, Submarine glacial landforms and rates of ice-stream collapse. *Geology*. Vol. 36. p. 819-822.

Dowdeswell, J.A., Hogan, K.A., Evans, J., Noormets, R., Ó Cofaigh, C., & Ottesen, D., 2010. Past ice-sheet flow east of Svalbard inferred from streamlined subglacial landforms. *Geology*. Vol. 38. p. 163-166.

Dowdeswell, J.A., & Ottesen, D., 2013. Buried iceberg ploughmarks in the early Quaternary sediments of the central North Sea: A two million year record of glacial influence from 3D seismic data. *Marine Geology*. Vol. 344. p. 1-9

Elverhøy, A., Pfirman, S.L., Solheim, A., & Larssen, B.B., 1989. Glaciomarine sedimentation in epicontinental seas exemplified by the Norwegian Barents Sea. *Marine Geology*. Vol. 85. p. 225-250

Evans, D.J.A., & Rea, B.R., 1999. The geomorphology and sedimentology of surging glaciers: A land-system approach. *Annals of glaciology*. Vol. 28. p. 75-82.

Evans, D.J.A., Dowdeswell, J.A., & Ó Cofaigh, C., 2004. Late Quaternary submarine bedforms and ice-sheet flow in Gerlache Strait and on the adjacent continental shelf, Antarctic Peninsula. *Journal of Quaternary Science*. Vol. 19. p. 397-407

Evans, D.J.A., Phillips, E.R., Hiemstra, J.F., & Auton, C.A., 2006. Subglacial till. Formation, sedimentary characteristics and classification. *Earth Science Reviews*. Vol. 78. p. 115-176

Farnsworth, W.R., Ingólfsson, Ó., Retelle, M., & Schomacker, A., 2016. Over 400 previously undocumented Svalbard surge-type glaciers identified. *Geomorphology*. Vol. 264. p. 52-60

Flink, A.E., Noormets, R., Kirchner, N., Benn, D.I., Luckman, A., & Lovell, H., 2015. The evolution of a submarine landform record following recent and multiple surges of Tunabreen glacier, Svalbard. *Quaternary Science Reviews*. Vol. 108. p. 37-50

Flink, A.E., Noormets, R., Fransner, O., Hogan, A.K., Ó Regan, M., & Jakobsson, M., 2017. Past ice flow in Wahlenbergfjorden and its implications for late Quaternary ice sheet dynamics in northeastern Svalbard. *Quaternary Science Reviews*. Vol. 163. p. 162-179

Flink, A.E., Hill, P., Noormets, R., & Kirchner, N., Evidence of a pre-LIA advance in Mohnbukta, east Spitsbergen; inferred from submarine morphology and marine sediment cores. *Boreas*. In review

Fransner, O., Noormets, R., Flink, A.E., & Hogan, K.A., 2016. Glacial landforms and their implications for glacial dynamics in Rijpfjord and Dufvefjord, northern Nordaustlandet Svalbard. *Journal of Quaternary Science*. Vol. 32(3). p. 437-455

Hagen, J.O., Liestøl, O., Roland, E., & Jørgensen, T., 1993. Glacier Atlas of Svalbard and Jan Mayen. *Meddelelser 129*, Norwegian Polar Institute, Oslo.

Hald, M., Dahlgren, T., Olsen, T.E., & Lebesbyen, E., 2001. Late Holocene palaeoceanography in Van Mijenfjorden, Svalbard. *Polar Research*. Vol. 20. p. 23-35

Hogan, K.A., Dowdeswell, J.A., Noormets, R., Evans, J., Ó Cofaigh, C., & Jakobsson, M., 2010a. Submarine landforms and ice-sheet flow in the Kvitøya Trough, northwestern Barents Sea. *Quaternary Science Reviews*. Vol. 29. p. 3545-3562.

Hogan, K.A., Dowdeswell, J.A., Noormets, R., Evans, J., & Ó Cofaigh, C., 2010b. Evidence for full-glacial flow and retreat of the Late Weichselian Ice Sheet from the waters around Kong Karls Land, eastern Svalbard. *Quaternary Science Reviews*. Vol. 29. p. 3563-3582.

Hogan, K.A., Dowdeswell, J.A., Hillenbrand, C-D., Ehrmann, W., Noormets, R., & Wacker, L. (In press). Subglacial sediment pathways and deglacial chronology of the northern Barents Sea Ice Sheet. *Boreas*.

Hormes, A., Gjermundsen, E F., & Rasmussen, T.L., 2013. From mountain top to deep sea- Deglaciation in 4D of the northwestern Barents Sea ice sheet. *Quaternary Science Reviews*. Vol. 75. p. 78-99

Ingólfsson, Ó., Rögnvaldsson, F., Bergsten, H., Hedenäs, L., Lemdahl, G., Lirio, J.H., & Sejrup, H.P., 1995. Late Quaternary glacial and environmental history of Kongsaya, Svalbard. *Polar Research*. Vol. 14. p. 123-139

Ingólfsson, Ó., & Landvik, J.Y., 2013. The Svalbard Barents Sea ice-sheet e Historical, current and future Perspectives. *Quaternary Science Reviews*. Vol. 64. p 33-60

IPCC., 2014. *Synthesis Report. Contribution of Working Groups I, II and III to the Fifth Assessment Report of the Intergovernmental Panel on Climate Change* [Core Writing Team, R.K. Pachauri and L.A. Meyer (eds.)]. IPCC, Geneva, Switzerland.

Jakobsson, M., Mayer, L.A., Coakley, B., Dowdeswell, J.A., Forbes, S., Fridman, B., Hodnesdal, H., Noormets, R., Pedersen, R., Rebesco, M., Schenke, W-H., Zarayskaya, Y., Accettella, A.D., Armstrong, A., Anderson, R.M., Bienhoff, P., Camerlenghi, A., Church, I., Edwards, M., Gardner, J.V., Hall, J.K., Hell, B., Hestvik, O.B., Kristoffersen, Y., Marcussen, C., Mohammad, R., Mosher, D., Nghiem, S.V., Pedrosa, M.T., Travaglini, P.G., & Weatherall, P., 2012. The International Bathymetric Chart of the Arctic Ocean (IBCAO) Version 3.0. *Geophysical Research Letters*. Vol. 39. doi: [10.1029/2012GL052219](https://doi.org/10.1029/2012GL052219)

Joughin, I., Smith, B.E., & Medley, B., 2014. Marine ice sheet collapse potentially under way for the Thwaites Glacier Basin, West Antarctica. *Science*. Vol. 34. p. 735-738

King, E.C., Hindmarsh, R.C.A., & Stokes, C.R., 2009. Formation of mega-scale glacial lineations observed beneath a West Antarctic ice stream. *Nature Geoscience*. Vol. 2. p. 585-588

Koç, N., Klitgaard-Kristensen, D., Hasle, K., Forsberg, K.F., & Solheim, A., 2002. Late glacial palaeoceanography of Hinlopen Strait, northern Svalbard. *Polar Research*. Vol. 21. p. 307-314

Kristensen, L., Benn, D.I., Hormes, A., & Ottesen, D., 2009. Mud aprons in front of Svalbard surge moraines: Evidence of subglacial deforming layers or proglacial glaciotectonics? *Geomorphology*. Vol. 111. p. 206-221

Kristensen, L., & Benn, D.I., 2012. A surge of the glaciers Skobreen-Paulabreen, Svalbard, observed by time-lapse photographs and remote sensing data. *Polar Research*. Vol. 3. 11106, doi.org/10.3402/polar.v31i0.11106.

Lambeck, K., 1995. Constraints on the late Weichselian ice sheet over the Barents Sea from observations of raised shorelines. *Quaternary Science Reviews*. Vol. 14. p. 1-16

Lambeck, K., Yokoyama, Y., & Purcell, T., 2002. Into and out of the Last Glacial Maximum: sea-level change during Oxygen isotope stage 3 and 2. *Quaternary Science Reviews*. Vol. 21. p. 343-360

Landvik, J.Y., Bondevik, S., Elverhøi, A., Fjeldskaar, W., Mangerud, J., Salvigsen, O., Siegert, M.J., Svendsen, J.-I., & Vorren, T.O., 1998. The last glacial maximum of Svalbard and the Barents Sea area: ice sheet extent and configuration: *Quaternary Science Reviews*. Vol. 17. p. 43-75.

Lefauconnier, B., & Hagen, J.O., 1991. Surging and calving glaciers in eastern Svalbard. *Nor. Polarinst. Medd (Norwegian polarinstitute)*. Vol. 116. p.1-130

Linden, M., & Möller, P., 2005. Marginal formation of De Geer moraines and their implications to the dynamics of grounding-line recession. *Journal of Quaternary Science*. Vol. 20. p. 113-133

Lovell, H., Fleming, E.J., Benn, D.I., Hubbard, B., Lukas, S., Rea, B.R., Noormets, R., & Flink, A.E., 2015. Debris entrainment and landform genesis during tidewater glacier surges. *Journal of Geophysical Research*. Vol. 120. No. 8. p. 1574-1595

Noormets, R., Kirchner, N., & Flink, A.E., 2016a. Medial moraines in Hambergbukta, south-eastern Spitsbergen. Atlas of Submarine glacial landforms: Modern, Quaternary and Ancient. *Geological Society, London, Memoirs*, 46. p. 986

Noormets, R., Kirchner, N., Flink, A.E., & Dowdeswell, J.A., 2016b. Possible iceberg-produced terraces in Hambergbukta, Spitsbergen Atlas of Submarine glacial landforms: Modern, Quaternary and Ancient. *Geological Society, London, Memoirs*, 46. p. 985

Ó Cofaigh, C., Pudsey, C.J., Dowdeswell, J.A., & Morris, P., 2002. Evolution of subglacial bedforms along a paleo-ice stream, Antarctic Peninsula continental shelf. *Geophysical Research Letters*. Vol. 29. p. 41.1-41.4

Ó Cofaigh, C., Dowdeswell, J.A., Evans, J., & Larter, R.D., 2008. Geological constraints on Arctic paleo-ice stream retreat rates. *Earth Surface Processes and Landforms*. Vol. 33. p. 513-525

Ottesen, D., Dowdeswell, J.A., & Rise, L., 2005. Submarine landforms and the reconstruction of fast-flowing ice streams within a large Quaternary ice sheet: The 2500-km-long Norwegian Svalbard margin

(57°-80°N). *Geological Society of America Bulletin*. Vol. 7. p. 1033-1050

Ottesen, D., & Dowdeswell, J.A., 2006. Assemblages of submarine landforms produced by tidewater glaciers in Svalbard. *Journal of Geophysical Research, Earth Surface*. Vol. 111. p. 1-16

Ottesen, D., Dowdeswell, J.A., Landvik, J.Y., & Mienert, J. 2007. Dynamics of the Late Weichselian ice sheet on Svalbard inferred from high-resolution sea-floor morphology. *Boreas*. Vol. 36. p. 286-306

Ottesen, D., Dowdeswell, J.A., Benn, D.I., Kristensen, L., Christiansen, H.H., Christensen, O., Hansen, L., Lebesbye, E., Forwick, M., & Vorren, T.O., 2008. Submarine landforms characteristic of glacier surges in two Spitsbergen fjords. *Quaternary Science Reviews*. Vol. 27. no. 15-16. p. 1583-1599

Ottesen, D., & Dowdeswell, J.A., 2009. An inter-ice-stream glaciated margin: Submarine landforms and a geomorphic model based on marine-geophysical data from Svalbard. *Geological Society of America Bulletin*. no. 11-12. p. 1647-1665.

Plassen, L., Vorren, T. O., & Forwick, M., 2004. Integrated acoustic and coring investigation of glacial deposits in Spitsbergen fjords. *Polar Research*. Vol. 23. p. 89-110.

Rea, B.R., & Evans, J.A., 2011. An assessment of surge-induced crevasse and the formation of crevasse squeeze ridges. *Journal of Geophysical Research*. Vol. 116. p. 1-17

Reusche, M., Winsor, K., Carlson, A. E., Marcott, S.A., Rood, D.H., Novak, A., Roof, S., Retelle, M., Werner, A., Caffee, M., & Clark, P.U., 2014. ¹⁰Be surface exposure ages on the Late-Pleistocene and Holocene history of Linnebreen on Svalbard. *Quaternary Science Reviews*. Vol. 89. p. 5-12,

Roberts, D.H., & Long, A.J., 2005. Streamlined bedrock terrain and fast ice flow, Jakobshavn Isbrae, West Greenland: implications for ice stream and ice sheet dynamics. *Boreas*. Vol. 34. p. 25-42

Ronnert, L., & Landvik, J.Y., 1993. Holocene glacial advances and moraine formation at Albrechtbreen, Edgeøya, Svalbard. *Polar Research*. Vol. 12. p. 57-63

Salvigsen, O., Elgersma, A., Hjort, C., Lagerlund, E., Liestøl, & Svensson, N-O., 1990. Glacial history and shoreline displacement on Erdmannflya and Bohemanflya, Spitsbergen, Svalbard. *Polar Research*. Vol. 8. p. 261-273

Sharp, M., 1984. Annual moraine ridges at Skalafellsjökull, south-east Iceland. *Journal of glaciology*. Vol. 30. p. No. 104. p. 82-93

Sevestre, H., & Benn, D.I., 2015. Climatic and geometric controls on the global distribution of surge-type glaciers: implications for a unifying model of surging. *Journal of Glaciology*. Vol. 61. p. 646-662

Sevestre, H., Benn, D.I., Hulton, N.R.J. & Bælum, K., 2015. Thermal Structure of Svalbard Glaciers and implications for thermal switch models of glacier surging. *Journal of Geophysical Research*. Vol. 110. p. 2220-2236

Sobota, I., Weckwerth, P., & Nowak, M., 2016. Surge dynamics of Aavatsmarkbreen, Svalbard, inferred from the geomorphological record. *Boreas*. Vol. 45. p. 360-376

Solheim, A., & Pfirman, S.L., 1985. Sea-floor morphology outside a grounded, surging glacier; Bråsvellbreen, Svalbard. *Marine Geology*. Vol. 65. p. 127-143

Stokes, C., & Clark, C.D., 2002. Are long subglacial bedforms indicative of fast ice flow? *Boreas*. Vol. 31. p. 239-249

Streuff, K., Forwick, M., Szczucinski, W., Andreassen, K., & Ó Cofaigh, C. 2015. Submarine landform assemblages and sedimentary processes related to glacier surging in Kongsfjorden, Svalbard. *Arktos*. Vol. 1:14. p.1-19

Streuff, K., Ó Cofaigh, C. & Noormets, R. In review. Submarine landforms and glacial marine sedimentary processes in Lomfjorden, East Spitsbergen. *Marine Geology*.

Stuiver, M., Reimer, P.J., & Reimer, R.W. 2017. CALIB 7.1 [WWW program] at <http://calib.org>, accessed 2017-4-4

Vassiliev, 1907. Missions Scientifiques pour la Mesure d'un arc de Méridien au Spitsberg entreprises en 1899-1901 sous les auspices des gouvernements Russe et Suédois. Mission Russe. In. Backlund., H. 1907. Observation géologique du Spitsberg Central. *Imprimerie de l'Académie Impériale des Sciences. St. Petersbourg*.

Vieli, A., Jania, J., & Kolondra, L., 2002. The retreat of a tidewater glacier: observations and model calculations on Hansbreen, Spitsbergen. *Journal of Glaciology*. Vol. 48. No. 163. p. 592-600

Werner, A., 1993. Holocene moraine chronology, Spitsbergen, Svalbard: lichenometric evidence for multiple Neoglacial advances in the Arctic. *The Holocene*. Vol. 3. p. 128-137

Zilliacus, H., 1989. Genesis of De Geer moraines in Finland. *Sedimentary Geology*. Vol. 62. p. 309-317

Appendix

Table 1. Maps, aerial and satellite images used to map the glacier terminal positions in Vaigattbogen.

Data type and detail	Year	Source
Historical maps	1901	De Geer 1923, Vassiliev 1907
Oblique aerial images. ID: 1666-98, 1770-93, 1793-1806	1938	NPI
Map	1956	Lefauconnier & Hagen
Map and aerial images. ID: 2134-35, 3484, 2145-46	1970	NPI
Aerial images. ID: 7553-54, 56	1971	NPI
Map	1986	Lefauconnier & Hagen
Landsat image. ID: L71218003_00319990710	1999	USGS
Landsat image ID: LE72170032002192EDC00	2002	USGS
Landsat image ID: L5216003_00320060723	2006	USGS
Aerial image ID: 25161	2011	NPI
Satellite image, TopoSvalbard	2013	NPI
Satellite image, TopoSvalbard	2014	NPI

V

Glacial landforms and their implications for glacier dynamics in Rijpfjorden and Duvefjorden, northern Nordaustlandet, Svalbard

O. FRANSNER,^{1*} R. NOORMETS,¹ A. E. FLINK,¹ K. A. HOGAN,² M. O'REGAN³ and M. JAKOBSSON³

¹Department of Arctic Geology, University Centre in Svalbard, Longyearbyen 9171, Norway

²British Antarctic Survey, Cambridge CB3 0ET, UK

³Department of Geological Sciences, Stockholm University, Stockholm 10691, Sweden

Received 11 April 2016; Revised 24 October 2016; Accepted 26 January 2017

ABSTRACT: Observations of subglacial landforms yielding the configuration and dynamics of former ice-flows have for the first time been made in Rijpfjorden and Duvefjorden, Nordaustlandet, Svalbard, using sub-bottom acoustic, swath-bathymetric data and sediment cores. Five acoustic-stratigraphic units were distinguished suggesting the presence of a complete glacial–postglacial succession in the central fjord basins. ¹⁴C ages from the sediments indicate that the inner Rijpfjorden and central Duvefjorden were deglaciated before ca. 10.6 cal ka BP and 11.0 cal ka BP, respectively. Maximum sediment thickness in Rijpfjorden and Duvefjorden is 26 m, resulting in sediment accumulation rates of ca. 66 cm ka⁻¹. The landform record suggests that the ice streaming in both fjords was topographically controlled. The considerably deeper basin and higher elongation ratios of the crag-and-tails in Duvefjorden are linked to the faulted bedrock and possibly to somewhat larger ice stream and/or more focused ice-flow compared to that in Rijpfjorden. De Geer moraines suggest slower retreat of a grounded ice margin from shallow areas of Rijpfjorden. In deeper areas of the fjords, the glaciers were probably floating, resulting in the lack of ice-marginal transverse landforms. The ice margin retreat from these areas was probably relatively rapid and dominated by calving. Copyright © 2017 John Wiley & Sons, Ltd.

KEYWORDS: Late Weichselian; glacial landforms; deglaciation; ¹⁴C ages; Nordaustlandet.

Introduction

Ice sheets are important for the global climate system (e.g. NAD Science Committee, 1992). Particularly important are the marine-based ice sheets that are resting below sea level as they are most exposed and vulnerable to the sea level rise associated with climate warming (Patton *et al.*, 2015; Stokes *et al.*, 2015). Most of the mass-loss from the marine-based ice sheets occurs through calving at the margins of marine-terminating ice streams that rapidly transport ice from the interior of the ice sheet to its margins (Rignot and Kanagaratnam, 2006). Ice streams are therefore important for relatively fast changes in ice sheet mass-balance and associated oceanographic changes at high latitudes (Bond and Lotti, 1995).

The Svalbard-Barents Sea Ice Sheet (SBIS) was marine-based during the Late Weichselian and was drained through numerous ice streams flowing in the cross-shelf troughs of the Barents Sea during the Last Glacial Maximum (LGM) (Siebert *et al.*, 2001; Andreassen *et al.*, 2004; Ottesen *et al.*, 2005; Robinson and Dowdeswell, 2011). These ice streams were often sourced in the major fjord valleys where the underlying topography resulted in the confluence of glaciers. On the western Svalbard shelf, all cross-shelf troughs are linked to major fjord systems (Ottesen *et al.*, 2005).

The drainage patterns and deglaciation history in cross-shelf troughs along the western margin of the former SBIS are relatively well established due to numerous expeditions there (e.g. Andreassen *et al.*, 2004, 2008; Landvik *et al.*, 2005; Ottesen *et al.*, 2005, 2007; Winsborrow *et al.*, 2010; Rüter *et al.*, 2011; Bjarnadóttir *et al.*, 2013; Rebesco *et al.*, 2014). Off eastern and northern Svalbard, the drainage patterns and deglaciation history are known only in general terms (e.g.

Ottesen *et al.*, 2007; Dowdeswell *et al.*, 2010; Hogan *et al.*, 2010a,b). This is mainly due to the remoteness of these areas from the nearest ports and generally harsh sea ice conditions. However, decreasing sea ice extent has given easier access to surface vessels, which has resulted in several studies over the recent years from these areas (e.g. Hogan *et al.*, 2010a,b; Batchelor *et al.*, 2011; Chauhan *et al.*, 2014, 2016a,b).

It has been established that the ice sheet reached the shelf edge north of Svalbard during the LGM (Knies *et al.*, 2001; Chauhan *et al.*, 2016a) and that fast-flowing ice reached there mainly through Hinlopen, Albertini and Kvitøya Troughs (Hogan *et al.*, 2010b; Batchelor *et al.*, 2011; Noormets *et al.*, 2012). Retreat of the ice sheet from the shelf edge in this area begun ca. 18.5 ka (Knies *et al.*, 2001; Chauhan *et al.*, 2016a).

The aim of this paper is to improve our understanding of and further constrain the configuration and dynamics of the marine-based BSIS along its relatively poorly known northern Barents Sea margin. This includes better constraining the character and timing of deglaciation of the inner shelf and the fjords of Rijpfjorden and Duvefjorden in northern Nordaustlandet, using new high-resolution swath-bathymetric and sub-bottom acoustic data together with sediment core analyses.

Geological and glaciological setting

The Svalbard Archipelago is located at the north-western margin of the Barents Sea (Fig. 1a). The Barents Sea shelf and the Svalbard Archipelago formed because of tectonic uplift after the Eocene rifting, break up and opening of the Norwegian–Greenland Sea (Faleide *et al.*, 1996). After the uplift, the region was shaped by the Plio-Pleistocene glacial–interglacial processes (Mangerud *et al.*, 1998; Knies *et al.*, 1998). Major morphological imprints of the glacial cycles on the Barents Sea shelf and the Svalbard Archipelago are the

*Correspondence to: O. Fransner, as above.
E-mail: osarjacob.fransner@unis.no

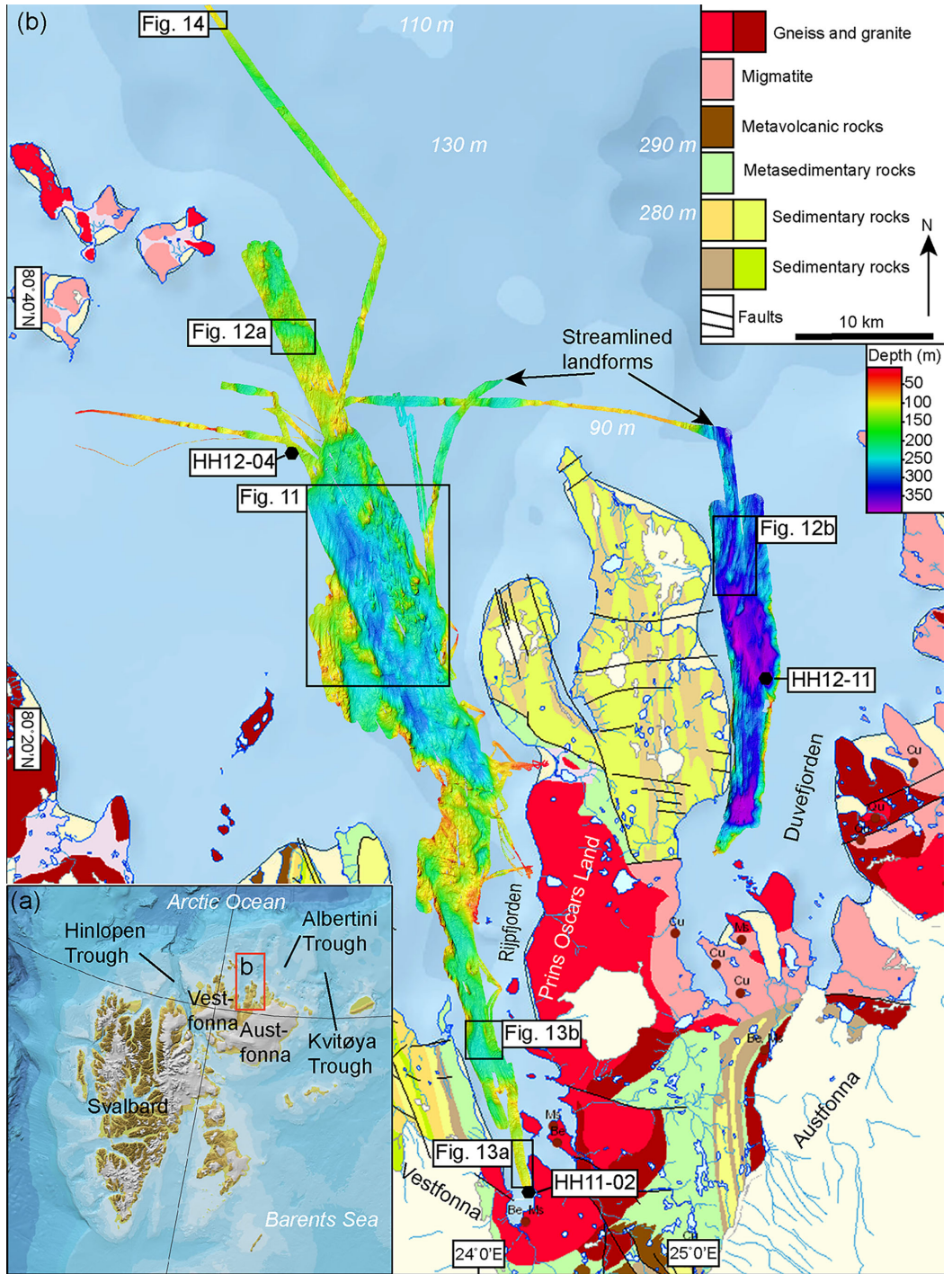


Figure 1. (a) IBCAO map showing the location of the study area and place names mentioned in the text. (b) Swath-bathymetric coverage of the study area. The three gravity core locations (HH11-02, HH12-04 and HH12-11) are marked with black hexagons. Streamlined landforms north of Rijpfjorden and Duvefjorden are arrowed. The study area is relatively faulted, especially Prins Oscars Land, where both E-W- and NW-NE-trending faults are present. The geological map of ice-free land areas is modified from online Svalbardkartet by Norsk Polarinstitutt. Background bathymetry data are from IBCAO version 3.0 (Jakobsson *et al.*, 2012).

cross-shelf troughs and fjords eroded by streaming glacier ice draining the ice sheet (Ottesen *et al.*, 2007; Batchelor and Dowdeswell, 2014). Hinlopen and Kvitøya Troughs are two major cross-shelf troughs on the northern Svalbard margin that were occupied by streaming ice during the LGM (Koc, *et al.*, 2002; Hogan *et al.*, 2010b; Batchelor *et al.*, 2011). These troughs have a S–N orientation and reach the continental shelf edge (Hogan *et al.*, 2010b; Batchelor *et al.*, 2011).

Nordauslandet is the second largest island of the Svalbard Archipelago situated in its north-eastern part between the Hinlopen and Kvitøya Troughs to the east and west of it, respectively (Fig. 1a). Rijpfjorden and Duvefjorden are two major fjords shaping the landscape of the northern Nordauslandet, west and east of Prins Oscars Land, respectively (Fig. 1b). Both fjords have a S–N orientation and are open to the Arctic Ocean in the north (Fig. 1b). According to the coarse bathymetry map IBCAO, the respective maximum water depth north of Rijpfjorden and Duvefjorden is 130 and 290 m, respectively (Fig. 1b).

The geology of the ice-free parts of northern Nordauslandet is dominated by Caledonian Rijpfjorden granite and migmatite (Flood *et al.*, 1969; Dallmann *et al.*, 2002; Johansson *et al.*, 2005). Sedimentary and metasedimentary rock types are present as well (Fig. 1b). Bedrock off the northern Nordauslandet is dominated by the Hecla Hoek formation of Late Precambrian crystalline rocks (Elverhøi and Lauritzen, 1984). Unconsolidated sediments deposited during and after the last glacial are often found on top of the bedrock in the northern Barents Sea region and comprise three lithofacies (from bottom to top): (i) diamicton, (ii) pebbly mud and (iii) massive Holocene mud (Elverhøi *et al.*, 1989). Sediments older than the last glacial are preserved on the continental slope (Knies *et al.*, 2001; Chauhan *et al.*, 2016a, b). These sediments are influenced by mass-flow processes, contour currents as well as sediment deposition from sea ice and icebergs (Chauhan *et al.*, 2016b). During the LGM, the ice sheet margin reached the continental shelf edge north of Nordauslandet ca. 23–22 cal ka BP and its retreat from the shelf edge started ca. 18.5 cal ka BP (Chauhan *et al.*, 2016a). The two ice caps, Vestfonna and Austfonna, are presently covering most of Nordauslandet (Hagen *et al.*, 1993).

Data acquisition and methods

The data used here were acquired during UNIS cruises on R/V *Helmer Hanssen* during 2011 and 2012. The multibeam bathymetric and acoustic sub-bottom data were acquired using a hull-mounted Kongsberg EM300, 30-kHz multibeam

echo sounder system and Edge Tech 3300 chirp sub-bottom profiler.

The multibeam bathymetric data were gridded with 5–10-m isometric grid size and visualized using QPS Fledermaus software. The gridded data were exported to Arc Map (version 10.1) where the maps of glacial landforms were produced.

The sub-bottom data were processed and analysed in Kingdom Suite (version 8.8). A sound velocity of 1500 m s⁻¹ was used for converting the two-way travel-time (TWT) to depth which has been used earlier (e.g. Hogan *et al.*, 2011; Hjelstuen *et al.*, 2013). The digitized acoustic horizons were gridded in the Kingdom suite. The acoustic facies distinguished on the chirp data were correlated with sedimentological data based on three gravity cores which were analysed in the Department of Geological Sciences at Stockholm University, Sweden. A GeoTek multi-sensor core logger was used to measure P-wave velocity, bulk density and magnetic susceptibility in 1-cm intervals. The quality of the density measurements is dependent on the amplitude of the P-wave velocity. Therefore, densities related to P-wave velocities with amplitudes lower than 70% were removed. Clear spikes in magnetic susceptibility were also removed. The cores were also analysed in the ITRAX core scanner for acquiring radiographic images. The radiographic images were acquired with a resolution of 0.2 mm. Shear strength was measured in 5-cm intervals using a Controls group liquid limit penetrometer. A Malvern Master Sizer 3000 laser particle size analyser was used to measure the grain size distribution of the fine fraction (<1 mm) for sediment samples taken in 10-cm intervals. In sections with rapid variations (e.g. thin layers) samples were taken in up to 1-cm intervals. Sixty-five samples were wet-sieved for extracting the organic matter for ¹⁴C dating. Tests of foraminifera, shells and shell fragments were picked from the >125-µm fraction, and from the >63-µm fraction in samples where the organic material was scarce. Seven samples were dated using single stage accelerator mass spectrometry (SSAMS) in the radiocarbon dating laboratory at Lund University, Sweden. Two ages were based on mixed benthic foraminifera, three on shell fragments and two on a *Buccium glaciale* and a paired *Thyasira flexulosa*, respectively (Table 1).

The ¹⁴C ages were calibrated to calendar years using Calib 7.1 with the Marine13 calibration curve, which has a default marine reservoir correction of 405 years (Reimer *et al.*, 2013). This marine reservoir correction was applied for direct comparison with Chauhan *et al.* (2016a). The calibrated ages are shown in 1sigma and 2sigma (Table 1). The sedimentation

Table 1. SSAMS ¹⁴C dates and sedimentation rates for cores HH11-02 and HH12-11. The sedimentation rates are based on mean 1sigma ages.

HH11-02 Inner Rijpfjorden					
Depth (cm)	Material used	¹⁴ C age	Cal. age BP 1 sigma	Cal. age BP 2sigma	Sed. rate (cm/ka)
184-185	<i>Buccinum glaciate</i>	8695-8785	9376-9470	9299-9499	20
225-226	Shell fragments	9645-9745	10531-10658	10464-10738	35
HH12-11 Central Duvefjorden					
Depth (cm)	Material used	¹⁴ C age	Cal. age BP 1sigma	Cal. age BP 2sigma	Sed. rate (cm/ka)
11-12	Paired bivalve (<i>Thyasira flexulosa</i>)	755-895	393-518	297-551	26
47-48	Shell fragments	1665-1775	1224-1298	1174-1336	45
220-221	Shell fragment	5900-5980	6300-6390	6270-6441	34
359-363	Mixed benthic foraminiferas	8865-8965	9503-9621	9463-9704	44
447-453	Mixed benthic foraminiferas	9890-10000	10813-11023	10727-11095	66

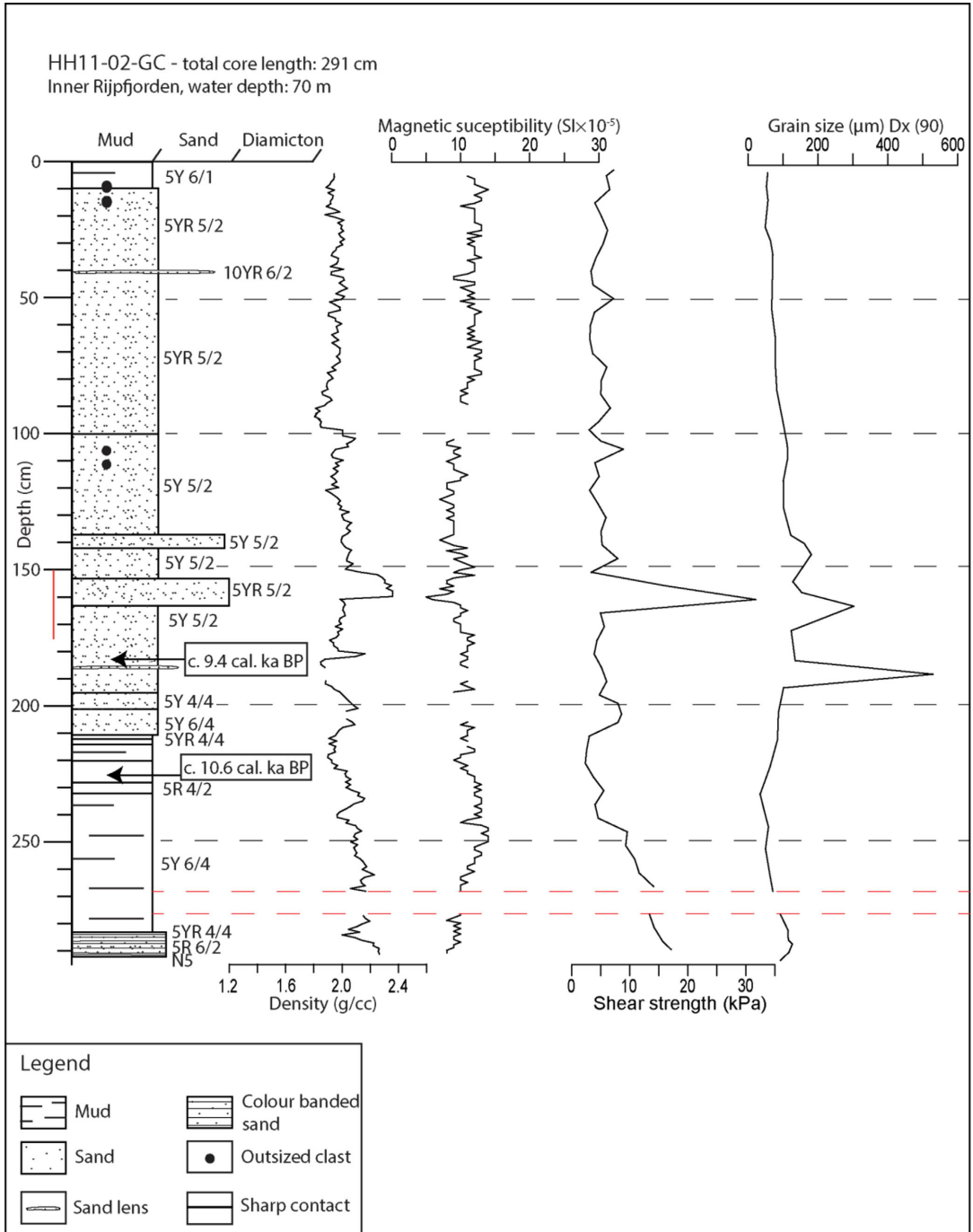


Figure 2. Lithological log with Munsell colour codes and calibrated ¹⁴C ages of the gravity core HH11-02 from the inner Rijpfjorden. The graphs show physical properties (density, magnetic susceptibility, shear strength and grain size) of the core. Note that the sand layer at 41 cm core depth was considered too coarse to be analysed in the Malvern mastersizer 3000. The dashed red lines show areas of major physical disturbance which gives unreliable results of the physical properties. The red line along the scale bar at 150–175-cm indicates the location of Fig. 3a. The lithological units are described in detail in the text. The location of the core is shown in Fig. 1b.

rates were calculated by linear interpolation between the mean 1sigma values of each sample. The respective mean 1sigma values are used throughout the text where ages are mentioned.

Sedimentological data

HH11-02

Description

The 291-cm-long HH11-02 core was acquired from the inner Rjippfjorden (Fig. 1b). From the core, two samples were radiocarbon dated (Table 1). The upper 10 cm of the core consists of light olive grey (5Y 6/1 in Munsell colour chart) massive mud with a small amount of oversized clasts (Fig. 2). This section is followed by a pale brown to pale yellowish brown (5YR 5/2 to 10YR 6/2) 200-cm-thick, relatively mica-rich silty sand layer with four coarse sand layers embedded in it. The top coarse sand layer is found at 41.5–42.5 cm and has the colour 10YR 6/2. This layer has sharp transitions to the surrounding silty sand (Fig. 2). The following sand layers are found at 137–142, 153–163 and 186–186.5 cm, respectively. The four sand layers are characterized by sharp contacts and a relatively high grade of compaction. The thickest coarse sand layer is pale brown (5YR 5/2) and contains a brighter coloured (5R 6/2) deformed layer which is < 1 cm thick. The deformed layer has the same grade of compaction and grain size as the surrounding sand (Fig. 2). A radiographic image illustrates the embedded coarse sand layer at 153–163 cm and its sharp transitions to the silty sand (Fig. 3a). At 184–185 cm core depth, the silty sand is dated to ca. 10.6 cal ka BP using an intact gastropod (*Buccinum glaciale*) (Table 1).

The silty sand is followed by a light olive grey (5Y 6/4) mud that contains diffuse, 1–6-cm-thick reddish bands (5YR 4/4 to 5R 4/2). The mica concentration in the mud is somewhat lower compared to in the silty sand. The grain size of the mud is slightly finer than the mud lithofacies in the top layer of the core. At 225–226 cm core depth, the mud is dated to ca. 9.4 cal a BP using shell fragments (Table 1). At 281–291 cm core depth, the lithology consists of a fine-grained sand unit with colour bands (0.5 cm thick) where brown, pale red and light grey (5YR 4/4, 5R 6/2, N5) units alternate. Foraminifera and shell fragments are rare throughout the core.

The density of the sediment in HH11-02 core is 1.8–2.4 g ml⁻¹. The highest values are characteristic to the coarse sand units in the middle of the core, whereas the lowest values are found in the upper 95 cm of the core (Fig. 2). The magnetic susceptibility shows relatively little variation in its values, which are 5–15 SI × 10⁻⁵ Author: please confirm the units for magnetic susceptibility. The lowest values are found in the coarse-grained layers of the core (Fig. 2). The shear strength shows values from 2.5 to 32 kPa (Fig. 2). However, the maximum value of 32 kPa is not representative as the fall cone method is not adequate for sand. The lowermost 25 cm of the core shows a gradual increase in shear strength from 10 to 17 kPa (Fig. 2). The Dx(90) grain sizes vary from 34 to 560 μm with the highest values recorded in the two sand layers in the middle of the core and a sand lens at 187 cm (Fig. 2). Density, shear strength and grain size are positively correlated, which is particularly clear in the coarser-grained layers, whereas magnetic susceptibility shows an inverse correlation to these parameters (Fig. 2).

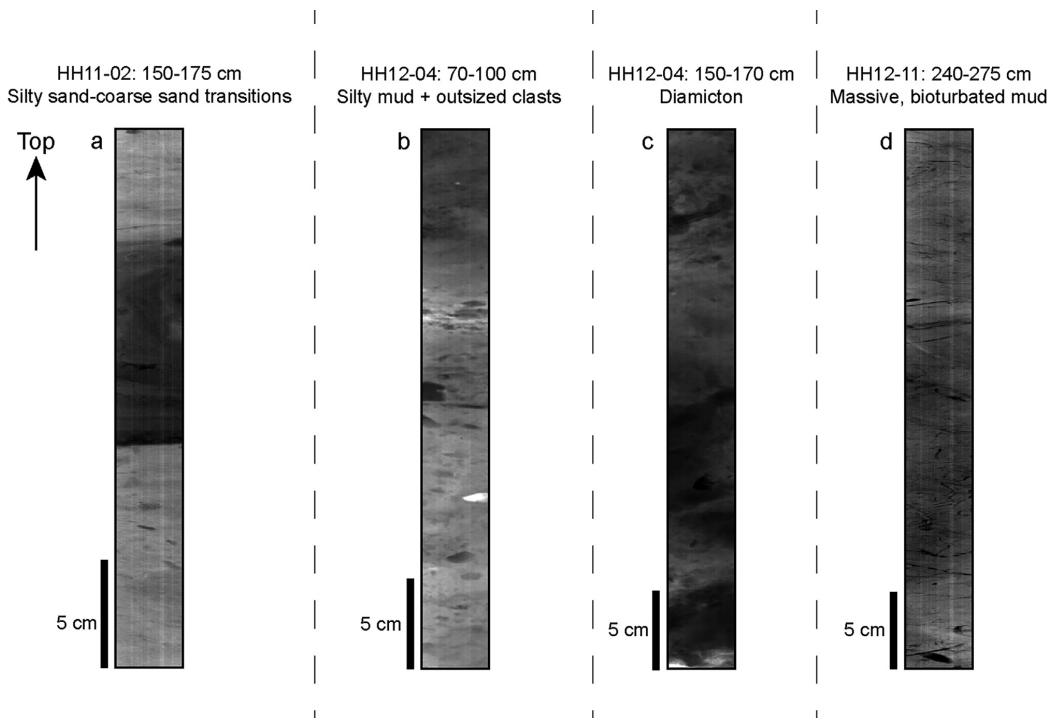


Figure 3. Radiographic images of the major lithofacies from cores HH11-02, HH12-04 and HH12-11. (a) Sharp transitions from silty sand to coarse sand and back to silty sand. (b) Mud rich in oversized clasts. (c) Diamicton with mud lenses. (d) Massive, bioturbated mud.

Interpretation

The massive mud at 0–10 and 210–281 cm is interpreted as marine mud. This is based on its homogeneous fine-grained composition indicating a low-energy depositional environment through suspension settling (Elverhøi and Solheim, 1983). This sediment type is common in the northern Barents Sea (Elverhøi and Solheim, 1983). Rare outsized clasts further indicate little ice-rafted debris (IRD) production (Plassen *et al.*, 2004). The similar colour and composition of the massive mud in the top and bottom of the core further indicate a similar source for these sediments.

The silty sand (10–210 cm) indicates a depositional environment highly influenced by increased meltwater input. This is based on the coarser grain size of the silty sand as well as on its higher mica concentration, which normally indicate changed lithology of the sediment source (Plassen *et al.*, 2004). IRD can be excluded due to the lack of outsized clasts (Elverhøi and Solheim, 1983). The four coarse sand layers embedded in the silty sand are interpreted as mass-flow events. This is based on

their coarser and more angular grains and sharp contacts to the above and underlying mud layers, implying a short transportation and fast deposition of these layers. Changed lithology is also supported by the significant difference in magnetic susceptibility of the coarse sand layer at 153–163 cm. Similar mass flows as envisaged here have been described in the fjords of Svalbard (Ottesen and Dowdeswell, 2006), and resulting sand layers with correlated changes in magnetic susceptibility are, for example, found in Fensfjorden and Austfjorden, Norway (Hjelstuen *et al.*, 2013). The fine-grained sand layer without outsized clasts at 281–291 cm suggests a similar depositional environment as for the silty sand. However, the sharp colour variations are interpreted as variations in lithology of the sediment source (Plassen *et al.*, 2004).

HH12-04

Description

The 173-cm-long HH12-04 core was acquired on the inner shelf off Rippfjorden (Fig. 1b). Three lithofacies were

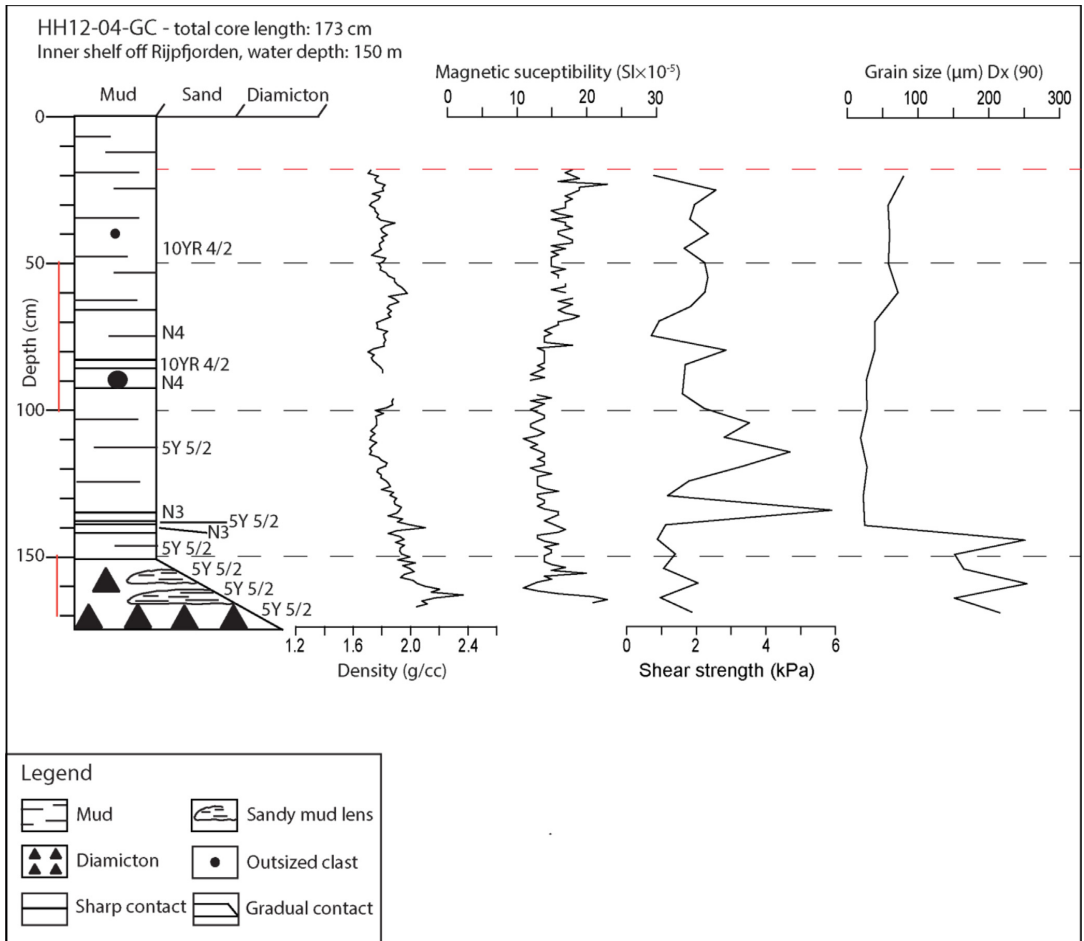


Figure 4. Lithological log with Munsell colour codes and physical properties (density, magnetic susceptibility, shear strength and grain size) of the gravity core HH12-04 from the inner shelf north of Rippfjorden. The core is dominated by two lithofacies of mud (massive and outsized clast-rich) and a fining-upwards diamicton facies at the base. The values of the physical properties corresponding to the first 19 cm of the core were considered unreliable due to physical disturbance of the sediments indicated by the dashed red line at 19 cm. The physical properties above this line have been omitted. The red lines along the scale bar indicate the location of Fig. 3b and c, respectively. The lithological units are described in detail in the text. The location of the core is shown in Fig. 1b.

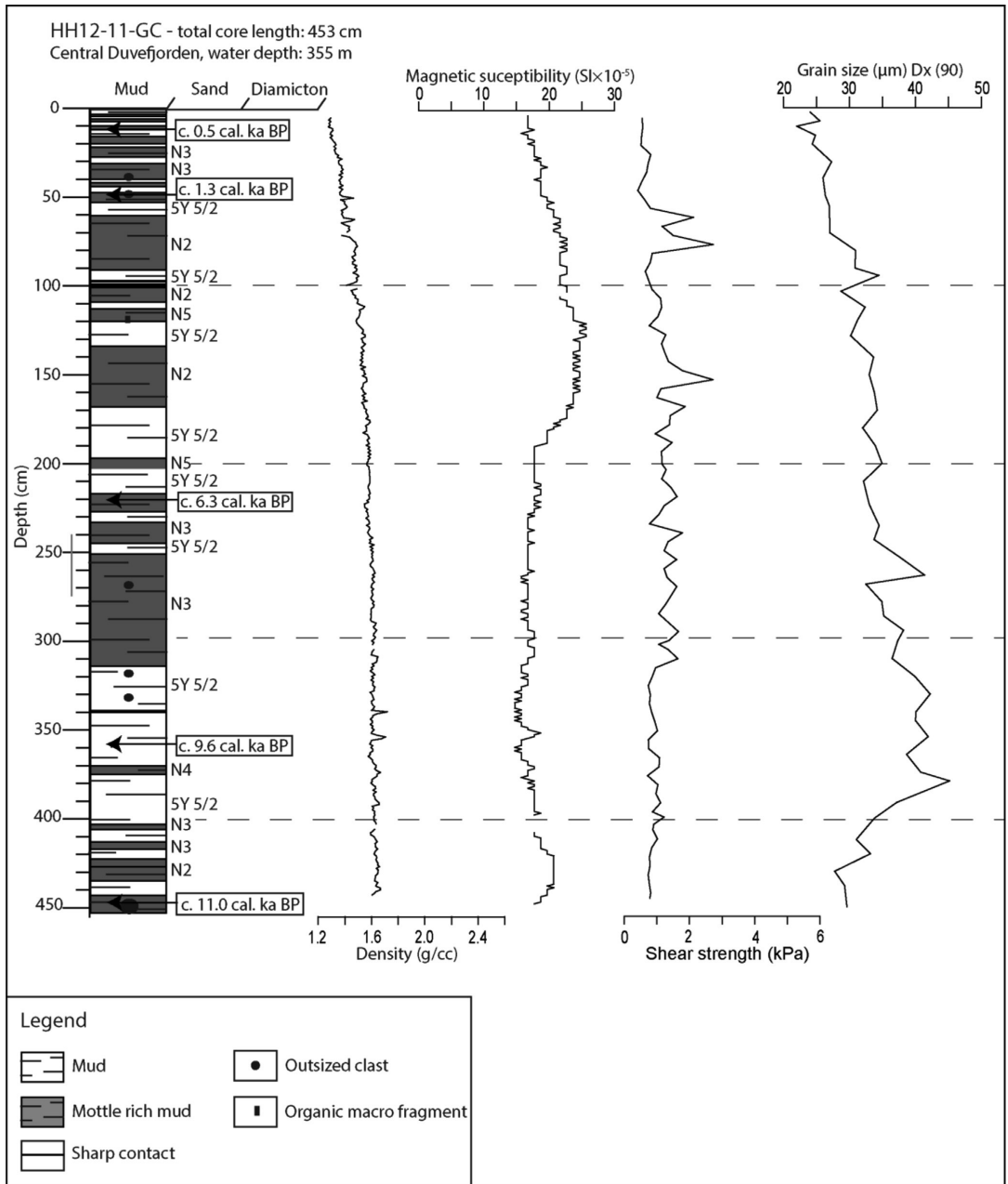


Figure 5. Lithological log with Munsell color codes, calibrated ¹⁴C ages and physical properties (density, magnetic susceptibility, shear strength and grain size) of the gravity core HH12-11 acquired from the central Duvefjorden. The red line along the scale bar at 240–275-cm indicates the location of Fig. 3d. The lithological units are described in detail in the text. The location of the core is shown in Fig. 1b.

distinguished: (i) massive silty mud, (ii) silty mud rich in outsized clasts and (iii) diamicton (Fig. 4). Silty muds, both massive and with a relatively high ratio of outsized clasts (estimated to 10–20%), are the dominating lithofacies types in the HH12-04 core. The massive mud comprises 0–66 cm of the core, but changes to mud with a higher content of outsized clasts (<20 mm in diameter) between 66 and 149 cm (Fig. 4). The radiographic image of the core interval

70–100 cm reveals outsized clasts visible as relatively dark spots (Fig. 3b). The colour of the mud generally varies from dark yellowish brown to medium grey (10YR 4/2 to N4) with sharp transitions in between. Locally, olive grey (5Y 5/2) intervals are also present. The thickness of the differently coloured mud layers varies from 60 to 1–2 cm. Foraminifera are rare in the mud. From 151 to 173 cm, the core is dominated by coarse sand that changes gradually to

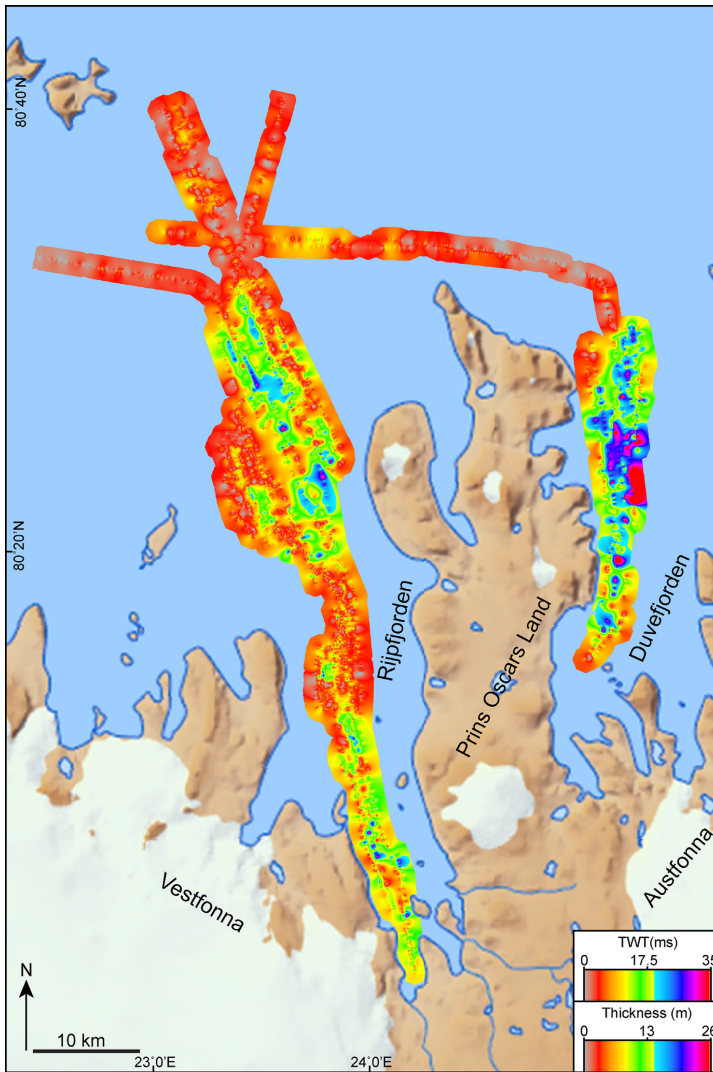


Figure 6. Total thickness of deglacial and postglacial sediments in Rijpfjorden and Duvefjorden and on the inner shelf north of the fjords. The thickness in metres is based on a sound velocity of 1500 m s^{-1} .

diamicton with subangular clasts with up to 20-mm-long a -axes (Fig. 4). The diamicton contains two olive grey (5Y 5/2) sandy mud lenses. In the radiographic image, the diamicton appears darker than the mud lenses (Fig. 3c).

The density of the sediments in HH12-04 core varies from 1.7 to 2.4 g ml^{-1} , higher values being typically at the lower part of the core, corresponding to the diamicton (Fig. 4). Magnetic susceptibility varies from 11 to $23 \text{ SI} \times 10^{-5}$ and shows a significant anomaly at 75 cm , where the magnetic susceptibility first drops and then gradually increases down-core. This gradual increase correlates with the top of the silty mud rich in outsized clasts. Shear strength varies from 0.7 to 6 kPa and shows highest variations at the depths correlated with the silty mud rich in outsized clasts. The $\text{Dx}(90)$ grain size varies from 19 to $272 \mu\text{m}$ (Fig. 4). Grain size decreases downwards until 141-cm core depth. The highest grain size values are found in the diamicton. The variation of the grain size in the lower part of the core corresponds to the sandy mud lenses in the diamicton (Fig. 4). Magnetic susceptibility is negatively correlated with shear strength except for in the

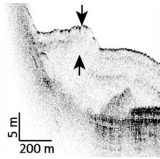
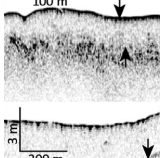
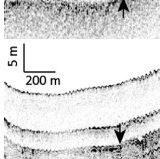
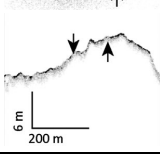
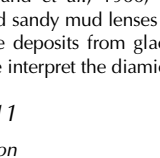
diamicton (Fig. 4). The top 19 cm is not presented on the physical properties logs due to physical disturbance in the core (Fig. 4).

Interpretation

The massive mud in the uppermost 66 cm of the core was probably deposited in a similar environment as the massive mud in HH11-02. This is based on the similar grain size and physical properties of these sediments (Fig. 2 and 4). The high concentration of outsized clasts in the relatively fine-grained mud between 66 and 149 cm indicates a glaciomarine depositional environment highly influenced by IRD. Similar pebbly mud from the central and northern Barents Sea is described by Elverhøi and Solheim (1983) and in Kvitøya Trough (Hogan *et al.*, 2010b).

The low shear strength of the upwards-fining diamicton at the base of HH12-04 suggests the diamicton to be either subglacial deformation till (e.g. Alley *et al.*, 1987; Hogan *et al.*, 2010b), or dropstone diamicton (possibly basal meltout-till)

Table 2. Description and interpretation of the acoustic units identified from the chirp data from Rijpfjorden and Duvefjorden. Each unit is arrowed in the chirp example column.

Acoustic unit	Chirp example	Description	Interpretation
5		Acoustically transparent or chaotic lobes. The upper bounding reflector is of moderate to high amplitude and medium continuity. Unit 5 is present at the foot of steep slopes (Fig. 7d).	The acoustic characteristics of unit 5, its lobate geometry and particularly the location at the foot of steep slopes are common for mass-flow deposits (e.g. Hogan et al., 2011).
4		Acoustically transparent unit. Locally semi-transparent in the inner fjords. The upper bounding reflector is of high amplitude and high continuity. Normally unit 4 is the topmost unit but is covered by unit 5 when present (Fig. 7c).	Unit 4 was found in all three gravity cores (Figs 8-10). The 14C dates from HH11-02 and HH12-11 cores infer a Holocene age of this unit. Interpreted as marine mud with a higher content of sand in the inner Rijpfjorden compared to the inner shelf and in the central Duvefjorden.
3		Acoustically transparent unit. Locally semi-transparent in the inner fjords. The amplitude of the upper bounding reflector is usually low and of moderate continuity.	The transparent reflection signature infers a homogenous composition. Interpreted as glaci-marine, uniform mud that probably has a high sand content in inner Rijpfjorden based on the fine sand-rich mud recovered in the lowermost 10 cm of HH11-02 (Fig. 2).
2		The reflection geometry contains multiple reflectors of medium to high amplitude and moderate continuity. The reflectors are semi-parallel to parallel to each other and to the acoustic basement. Locally, disturbed areas with chaotic acoustic signature occur. The upper bounding reflector is of moderate to high amplitude and high continuity.	The parallel to semi-parallel conformal reflection geometry of unit 2 infers a semi-rhythmically varying sediment composition or structure. This is characteristic for glaci-marine laminated mud formed due to seasonal variations in glacial melt-out deposits. Similar sediments have been reported in several Spitsbergen fjords (Plassen et al., 2004).
1		High amplitude and high continuity top reflector. Little to no penetration of acoustic signal below this reflector. This unit represents the acoustic basement and is either subcropping on the sea floor or is covered with a thin layer of unit 2 or 4 deposits.	Sampled by HH 12-04 and therefore identified as diamicton. However, different moraine types and bedrock cannot be distinguished based on their acoustic character alone. Therefore, U1 may consist of bedrock in other areas.

(e.g. Harland et al., 1966; Dreimanis, 1979). Based on the embedded sandy mud lenses in diamicton, probably representing plume deposits from glacial meltwater discharge (Powell, 1984), we interpret the diamicton to be a basal meltout.

HH12-11

Description

The 453-cm-long HH12-11 core was acquired from a basin of 355 m water depth in the central Duvefjorden (Fig. 1b). Massive mud dominates throughout the core (Fig. 5). This mud displays a mottle-rich, medium dark grey to dark grey (N3–N2) and light olive grey (5Y 5/2) units (Fig. 5). Bioturbation is present throughout the core, particularly between 100 and 300 cm. Bioturbation is shown as black, thread-like microburrows on the radiographic images of the core (Fig. 3d). Microburrows are easily distinguished in radiographic images when they are pyritized (Löwemark et al., 2006). Foraminifera are rare throughout the core. The most common species are *Nonionella labradorica*, *Elphidium excavatum* and *Epistominella exigua*. Outsized clasts are rare, but when present they are subangular with diameters of 1–5 mm. The base of the core contains one subrounded granitic clast with the dimensions of 65 × 50 × 25 mm.

The density of sediments in the HH12-11 core varies from 1.3 to 1.7 g ml⁻¹. The lowest values are found at the top,

increasing gradually towards the bottom of the core (Fig. 5). Magnetic susceptibility varies between 15 and 26 SI × 10⁻⁵ and increases downwards in the core until 160 cm from where it is relatively constant until 350 cm followed by another increase to 440 cm (Fig. 5). Shear strength varies from 0.4 to 2.7 kPa and has the highest values between 50 and 310 cm of the core (Fig. 5). Grain size varies from 22 to 46 μm coarsening downwards until 380 cm core depth, from where it decreases until the base of the core (Fig. 5). Five radiocarbon dates were acquired from HH12-11 (Table 1). These dates reach from ca. 0.46 to 11 ca ka BP.

Interpretation

Based on the ¹⁴C dates, the massive and often bioturbated mud present throughout HH12-11 is Holocene marine mud, deposited under similar conditions as the massive mud of HH11-02 and HH12-04. The mottles in the mud are monosulphides, which are relatively common in this type of mud (Elverhøi et al., 1989). The outsized clasts in the core are interpreted as IRD, which is supported by their subrounded geometries and their scattered distribution, suggesting glacial erosion and transportation. IRD is common in the northern Barents Sea (Elverhøi and Solheim, 1983; Hogan et al., 2010b). The wide range of rock types of northern Nordaustlandet makes provenance interpretations difficult (Fig. 1b).

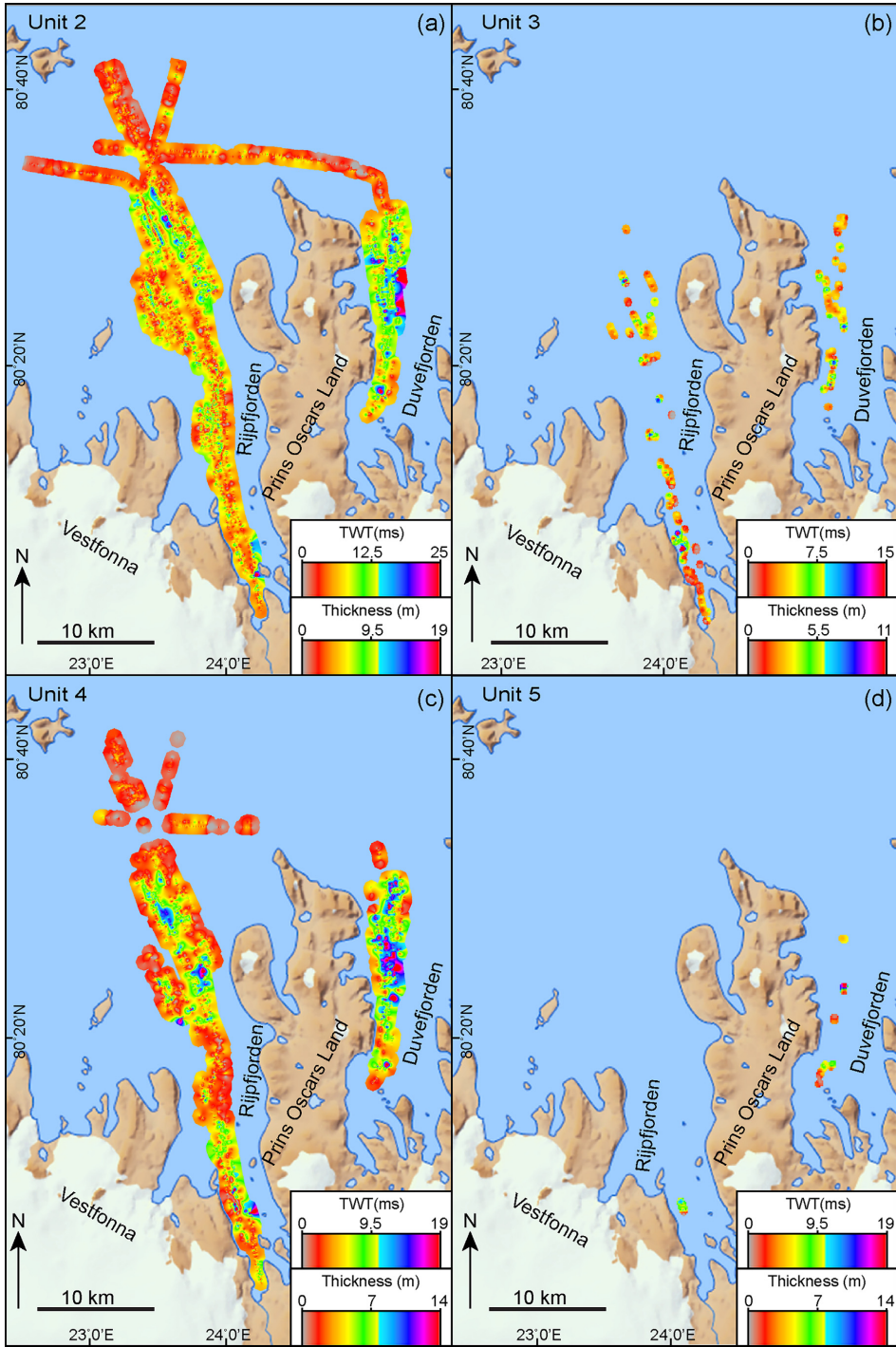


Figure 7. Thickness and distribution of acoustic units 2 (a), 3 (b), 4 (c) and 5 (d). The thickness scale bars in metres are based on sound velocity of 1500 m s^{-1} .

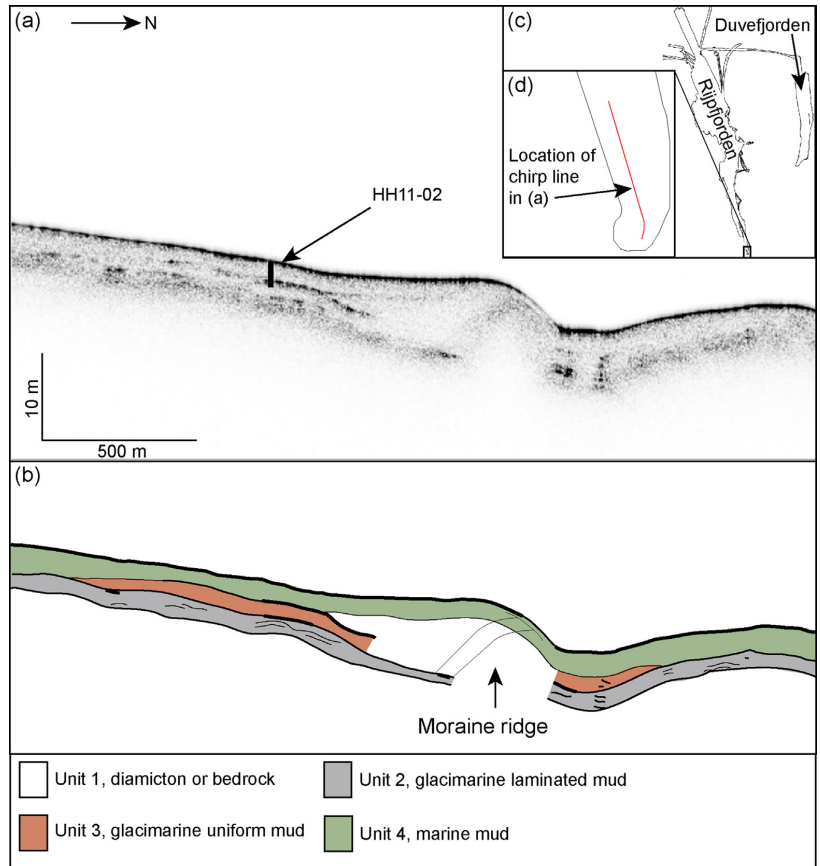


Figure 8. (a) Chirp profile showing the location and approximate penetration depth of core HH11-02 (arrowed). (b) Interpretation of the chirp profile in (a) based on the acoustic facies analysis and the lithology of HH11-02. (c,d) The location of the chirp profile, which is marked with a red line in (d).

However, the IRD in HH12-11 probably originated from the onshore bedrock surrounding Duvefjorden. The significant increase in sedimentation rate at ca. 1.3 cal ka BP and the higher values in magnetic susceptibility indicate increased sediment input of different lithology, probably due to increased meltwater input (Plassen *et al.*, 2004).

Chirp sub-bottom data

The total sediment thickness of deglacial and postglacial sediments in Rijpfjorden and Duvefjorden varies from 0 to 35 ms TWT (or 0–26 m based on a sound velocity of 1500 ms^{-1}) (Fig. 6). Thickest sediment successions are found in the deepest areas of the fjords, whereas the inner shelf and the relatively shallow areas of the fjords are characterized by relatively thin or absent sediment cover (Fig. 6). Based on acoustic characteristics, five units were distinguished in the acoustic stratigraphy (U1–U5, from base to top). The acoustic characteristics and interpretations of the units are presented in Table 2. Isopach maps are presented for each unit (Fig. 7).

Interpretation of the acoustic units and correlation with sediment cores

Inner Rijpfjorden – HH11-02

A buried ridge-shaped feature consisting of the acoustic unit U1 is present at the core location of HH11-02 (Fig. 8).

Although the acoustic characteristics of U1 alone are not sufficient to distinguish diamicton and bedrock, the ridge shape of the buried feature indicates a buried moraine similar to findings in Isfjorden (Plassen *et al.*, 2004). The conformal draping of U2 indicates an ice-proximal glaci-marine environment of inner Rijpfjorden during deposition (cf. Hogan *et al.*, 2011) (Fig. 8). The base of HH11-02 correlates with U3, indicating a glaci-marine mud with relatively high sand content, indicating influence of meltwater input during deglaciation (cf. Plassen *et al.*, 2004) (Fig. 8). U4 is conformably overlying U3 (Fig. 8). The overall acoustic transparency of U4 and its fine grain size together with ^{14}C ages in HH11-02 indicate deposition through suspension settling during the Holocene (cf. Hogan *et al.*, 2011).

Inner shelf – HH12-04

U1 was sampled by HH12-04 which locally indicates the presence of diamicton (Fig. 9). The deglacial–postglacial sediment stratigraphy of the inner shelf is, however, poorly developed, with < 3 m of U4 locally draped over U1 (Fig. 9). U4 was sampled by HH12-04, which indicates finer grain size of the mud matrix compared to in inner Rijpfjorden, but with a downcore increase in IRD (Fig. 4). This indicates less influence of meltwater but greater presence of drifting ice on the inner shelf compared to inner Rijpfjorden (cf. Plassen *et al.*, 2004; Hogan *et al.*, 2010b).

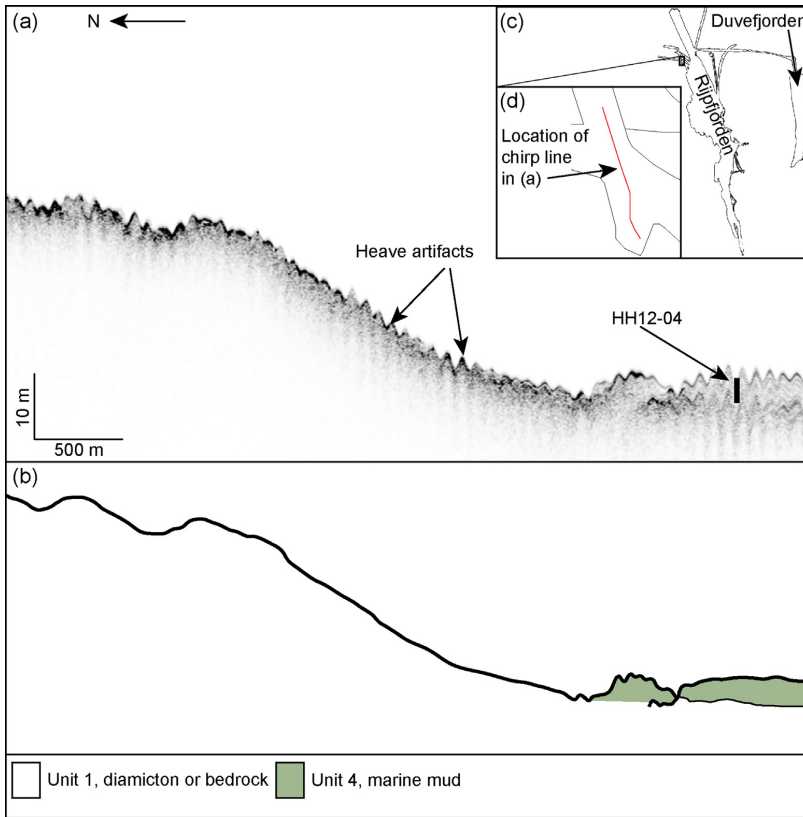


Figure 9. (a) Chirp profile showing the location and approximate penetration depth of core HH12-04 (arrowed). (b) Interpretation of the chirp profile in (a) based on the acoustic facies analysis of the chirp data and the lithology of HH12-04. (c,d) The location of the chirp profile, which is marked with a red line in (d).

Central Duvefjorden – HH11-12

Central Duvefjorden is dominated by a sediment accumulation basin for deglacial–postglacial sediments reaching 26 m in thickness (Figs 6 and 10). The base of HH11-12 sampled U3, indicating a distal glacial marine environment with the presence of drifting ice (Fig. 5). The fine grain size and the ^{14}C ages of U4 indicate Holocene deposition through suspension settling (cf. Hogan *et al.*, 2011). Mass-flow deposits are present in and on top of the glacial marine laminated mud as well as within the marine mud, indicating mass-flows during the deglaciation (Fig. 10). The mass-flow deposit interpretations are supported by their location next to steep slopes in the bathymetry (Fig. 10) (Hogan *et al.*, 2011). Gas in sediment often gives similar acoustic characteristics to mass-flow deposits, but gas is considered unlikely because more chimney-like geometries could be expected (e.g. Roy *et al.*, 2014).

Bathymetric data

Longitudinal landforms

Description

Crudely streamlined longitudinal landforms are common on submarine elevations in Rijpfjorden, Duvefjorden and on the adjacent inner continental shelf (Figs 11 and 12). These landforms are characteristic to the areas with scarce sediment cover (Figs 6, 11 and 12). In the inner Rijpfjorden, the crudely streamlined landforms have a S–N orientation that gradually changes to SSW–NNE in its central and outer parts (Fig. 11).

At water depths of 100–210 m on the inner shelf off Rijpfjorden, the crudely streamlined longitudinal landforms transform into a series of parallel landforms with blunt and wide southern parts and narrowing northern parts (Fig. 12a). These landforms have a SSW–NNE orientation and reach dimensions of $1100 \times 160 \times 30$ m (length/width/height). Maximum elongation ratio of the individual landforms on the shelf is 7:1 (Fig. 12c). The distance between the landforms of the same cluster varies from 30 to 200 m.

The crudely streamlined landforms in Duvefjorden are found in depths from 250 to 375 m and are characterized by their blunt southern and narrower northern parts (Fig. 12b). The lengths and widths of these landforms vary (from 2400 to 4400 m and 100–400 m, respectively). Their heights are between 30 and 50 m (Fig. 12b). The elongation ratios vary from 9:1 to 20:1. The long axis orientation varies from S–N in the inner to central fjord to SW–NE in the outer fjord. The spacing between the landforms in Duvefjorden varies from 150 to 800 m. One of the most prominent individual landforms in Duvefjorden is shown in Fig. 12d.

Streamlined fjord-parallel landforms are also observed on the inner shelf north of both Rijpfjorden and Duvefjorden. These landforms are ca. 100–200 m wide and 10 m high. Their lengths are > 1 km but reach beyond the limits of the dataset (Fig. 1b).

Interpretation

The crudely streamlined landforms in inner and outer Rijpfjorden are interpreted as bedrock-lineations that have been polished by streaming glacier-ice (Fig. 11)

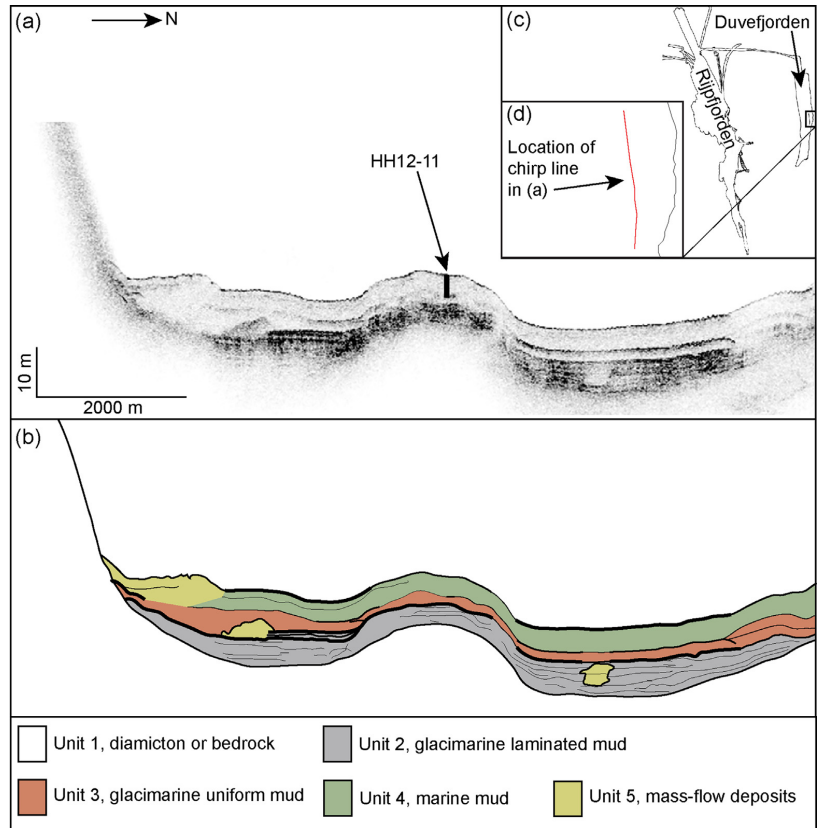


Figure 10. (a) Chirp profile showing the location and approximate penetration depth of core HH12-11 (arrowed). (b) Interpretation of the same chirp profile based on the acoustic facies analysis and the lithology of HH12-11. (c,d) The location of the chirp profile, which is marked with a red line in (d).

(Stroeve and Swift, 2008). Sub-cropping bedrock is supported by the scarce sediment cover in the chirp data (Fig. 6). The longitudinal landforms with blunt proximal and narrowing distal parts in Duvefjorden and on the inner shelf north of Rjippfjorden are interpreted as crag-and-tails, which is based on their characteristic shape and dimensions (e.g. Benn and Evans, 2010). The location of these landforms on elevated seafloor areas with sub-cropping bedrock (Fig. 6) is typical for crag-and-tails (Ottesen *et al.*, 2005; Smith *et al.*, 2006). The crag-and-tails formed at the base of streaming ice, where the long axis orientation is in the direction of palaeo-ice flow (Hogan *et al.*, 2010b). The streamlined landforms north of both Rjippfjorden and Duvefjorden are interpreted as glacial lineations that also formed at the base of streaming ice (Fig. 1b) (e.g. Stokes and Clark, 2002). The location of the glacial lineations implies that ice-flow from both Rjippfjorden and Duvefjorden continued out on the shelf (Fig. 1b).

Transverse ridges

Description

Sets of parallel ridges, roughly perpendicular to the fjord axis, occur in water depths < 210 m in Rjippfjorden and on the adjacent shelf (Figs 11b,c and 13). The ridges have maximum length/width/height of 750 × 100 × 5 m, and the distance between the ridges varies from 40 to 200 m (Fig. 13). The ridges generally display symmetrical cross-profiles with slope angles of 4–12° (Fig. 11c). The ridges in

inner Rjippfjorden are covered by marine mud (Fig. 8), whereas the ridges in the central to outer Rjippfjorden are superimposed on streamlined bedrock and have a thinner sediment cover (Fig. 11c). In the deeper parts of Rjippfjorden as well as throughout the mapped area of Duvefjorden, transverse ridges are absent.

Interpretation

The transverse ridges are interpreted as De Geer moraines formed during relatively short-term still-stands or readvances of the glacier margin during the deglaciation. This is supported by the local superimposition on streamlined bedrock (Fig. 11c). The local drape of marine mud supports that the ridges formed by glacial marginal processes and later were covered by sediments deposited in a marine environment (Fig. 8). The dimensions and distances between the individual ridges are similar to the De Geer moraines described earlier from other areas by, for example, Lindén and Möller (2005) and Flink *et al.* (2015).

Grooves

Description

Grooves with V-shaped cross-sections were identified at 50–100 m water depth on the inner shelf north of Rjippfjorden (Fig. 14). These grooves have varying orientations, dimensions and cross-cutting relationships. Common widths of the grooves are 70–100 m. Their depth is usually 2–3 m (Fig. 14).

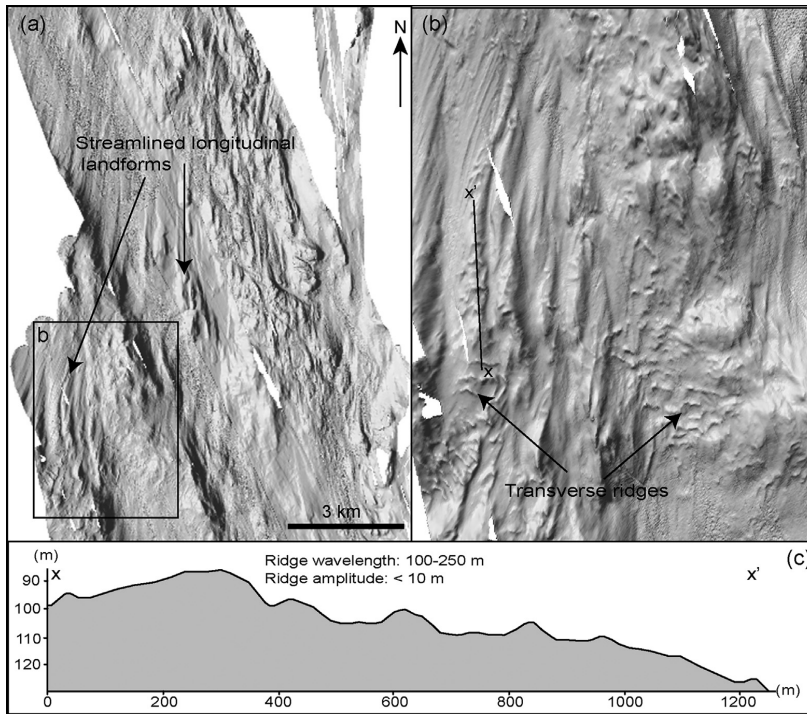


Figure 11. Central and outer Rijpfjorden are dominated by sets of streamlined longitudinal landforms (arrowed in a). (b) Prominent streamlined features are locally superimposed by parallel transverse ridges. (c) Along-profile of these transverse ridges shows their relatively symmetrical profile. Location of the area is shown in Fig. 1b.

Interpretation

The grooves on the inner shelf are commonly found on high-latitude continental margins and are interpreted as iceberg ploughmarks. Iceberg ploughmarks are formed because of seafloor scouring by floating icebergs, which originate from calving glacier fronts (e.g. Dowdeswell *et al.*, 1992).

Discussion

Ice-sheet dynamics

The submarine landform record shows that both Rijpfjorden and Duvefjorden accommodated ice streams that flowed in northerly to north-easterly directions out onto the shelf (Fig. 15). The locally deeper bathymetry northwards from the fjords (Fig. 1b) as well as the landform record in Albertini Trough and the dated sediment record at its trough mouth confirm that ice-flow continued there before it reached the continental shelf edge north of Nordaustlandet (Noormets *et al.*, 2012; Chauhan *et al.*, 2016a,b) (Fig. 1). The deeper basin and higher elongation ratios of streamlined subglacial landforms in Duvefjorden suggest that a larger and/or more focused ice-stream flowed there compared to in Rijpfjorden (Fig. 15). The comparatively well-developed trough extending out onto the inner shelf from Duvefjorden (Fig. 1b) suggests that the ice-flow from Duvefjorden reached further out onto the shelf than the ice-flow from Rijpfjorden (cf. Wellner *et al.*, 2001).

The varied depth of the Rijpfjorden basin shows relatively good correlation to the variation in coastal geology (Fig. 1b). The deeper inner and central fjord basins probably consist of the surrounding sedimentary bedrock types (Fig. 1b). The relatively low resistance to glacial erosion of such bedrock probably made it possible for ice-flow to focus there,

consequently forming the deeper basins (Fig. 1b). The crudely streamlined bedrock in the central to outer Rijpfjorden and crag-and-tails on the inner continental shelf show proximity to crystalline bedrock, which is more resistant to erosion (cf. Wellner *et al.*, 2001). These areas are suggested to have been important for obstructing and slowing down the ice-flow in Rijpfjorden and on the inner continental shelf and preventing trough development (Fig. 1b).

The deeper and narrower basin of Duvefjorden probably consists of similar sedimentary bedrock as found on the adjacent Prins Oscars Land (Fig. 1b). The relatively easily erodible sedimentary bedrock facilitated the focusing of the ice-flow in the narrower trough, potentially resulting in a build-up of a larger and faster ice stream due to easier passage compared to Rijpfjorden (cf. Wellner *et al.*, 2001). In addition, the E–W-trending faults on the eastern part of Prins Oscars Land probably extend into the basin of Duvefjorden, which is suggested to have facilitated ice-flow there (Fig. 1b). Based on the IBCAO (Jakobsson *et al.*, 2012), it is likely that the ice stream in Duvefjorden flowed out onto the continental shelf and eroded a distinct trough there that continues over 30 km north of the fjord (Figs 1b and 15). This supports our interpretation that Duvefjorden accommodated a somewhat larger ice stream than Rijpfjorden, although both were probably significant outlets draining the SBIS (Fig. 1b).

Deglaciation

The presence of De Geer moraines in areas shallower than 210 m on the inner continental shelf and in Rijpfjorden indicate a relatively slow and punctuated retreat of the ice margin there (Fig. 15). The timing of the formation of the De Geer moraines is uncertain. However, if assuming annual formation, the retreat of the ice margin is estimated to

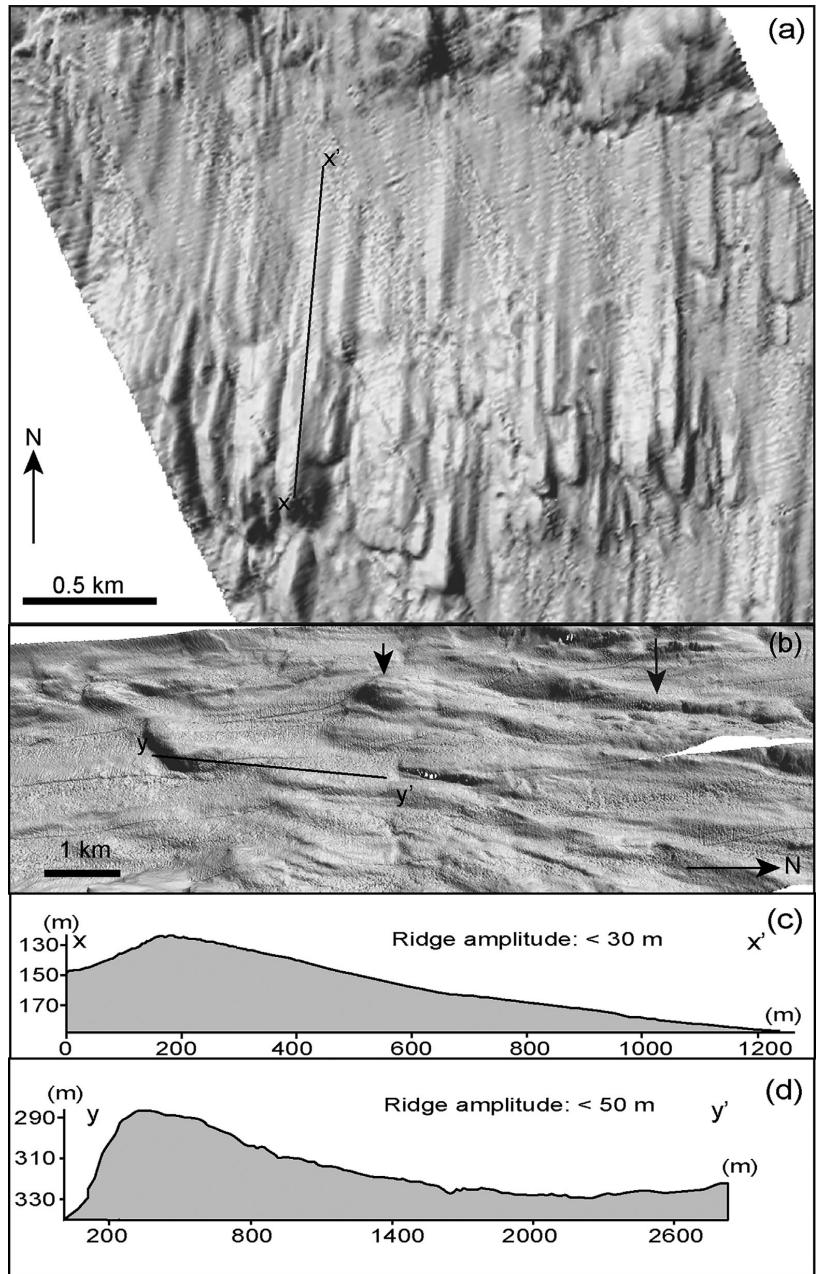


Figure 12. (a) The inner shelf off Rijpfjorden is dominated by parallel elongated landforms with blunt proximal and narrower distal parts with SSW–NNE orientation. (b) Duvefjorden is dominated by elongated landforms (arrowed) with blunt proximal and narrower distal sides. Their elongation ratios vary from 9: 1 to 20: 1. (c) Along-profile of one of the most prominent elongated landforms on the inner shelf off Rijpfjorden. (d) Along-profile of one of the most prominent elongated landforms found in the central Duvefjorden. Locations of the areas are shown in Fig. 1b.

100–250 ma^{-1} in the areas where De Geer moraines are present (Fig. 15). Annual formation of De Geer moraines has earlier been suggested based on relatively even spacing between moraines in Borebukta and Tempelfjorden (Ottesen and Dowdeswell, 2006; Flink *et al.*, 2015). Deeper areas of Rijpfjorden and Duvefjorden lack retreat-related landforms in both the bathymetric and the chirp data, which suggest that those areas featured floating ice margins during the deglaciation (Fig. 15). The iceberg ploughmarks on the inner shelf north of Rijpfjorden and Duvefjorden suggest that the floating margins disintegrated mainly through calving (Fig. 15). In

particular, the deep fjord basin of Duvefjorden was probably of importance for iceberg production and transportation out to the continental shelf north of Nordaustlandet (Fig. 1b) where a high abundance of iceberg ploughmarks has been reported (Noormets *et al.*, 2012). Also at modern times, calving has been suggested as the dominating mechanism of retreat of the Austfonna ice cap margin (Moholdt *et al.*, 2010).

Samples obtained from glacial marine mud in the inner Rijpfjorden and central Duvefjorden yielded the oldest ^{14}C ages (Table 1). These ages indicate that the innermost part of Rijpfjorden and the central Duvefjorden were

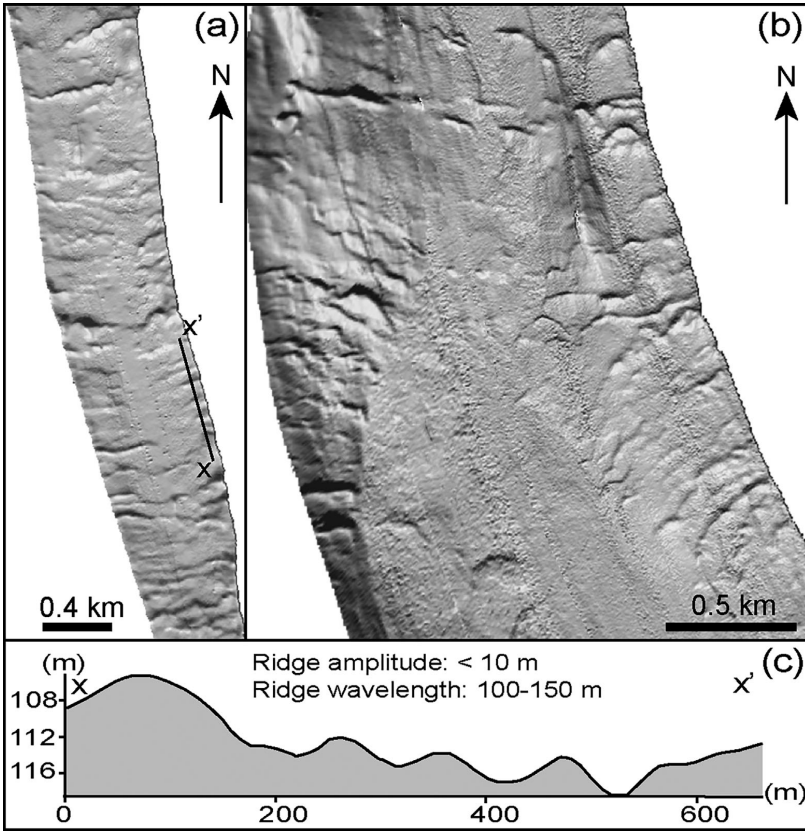


Figure 13. (a,b) The inner Rijpfjorden is dominated by semi-parallel, transverse ridges with maximum length/width/height of 750 × 100 × 10 m. The ridges occur in water depths of <210 m. (c) Distance between the transverse ridges is between 100 and 150 m. For location, see Fig. 1b.

deglaciated ca. 10.6 and 11.0 cal a BP, respectively (Table 1). The somewhat earlier deglaciation of Duvefjorden could be attributed to its deeper central basin facilitating faster retreat of the ice margin through calving (Fig. 1b).

The basal meltout-till with embedded plume deposits at the base of core HH12-04 indicate basal melting during retreat over the inner shelf (cf. Powell, 1984). The gradual decrease of IRD from the base to top in HH12-04 suggests a decreased

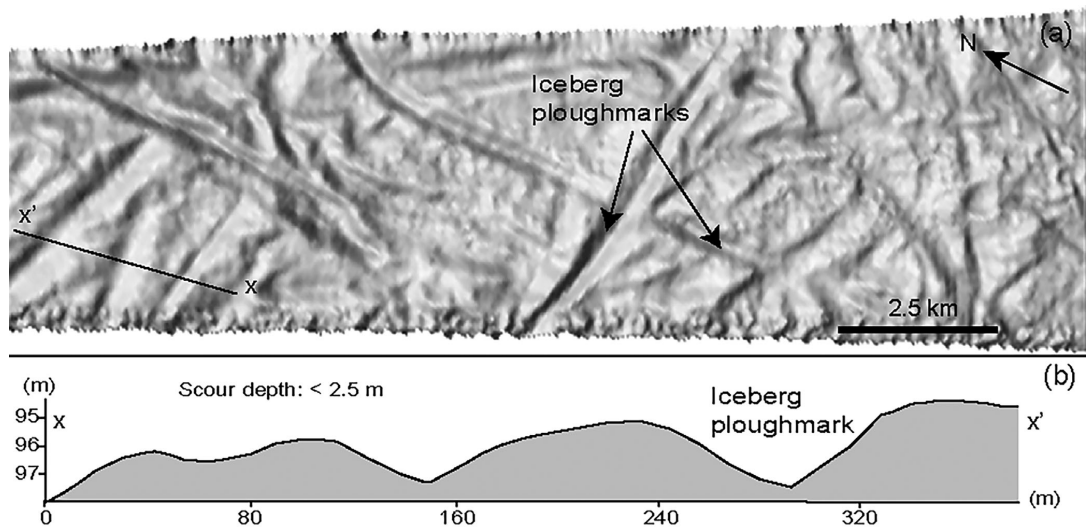


Figure 14. (a) Grooves are found on the inner shelf north of Rijpfjorden. (b) V-shaped cross-sections of the grooves are up to 2.5 m deep. For location of the area, see Fig. 1b.

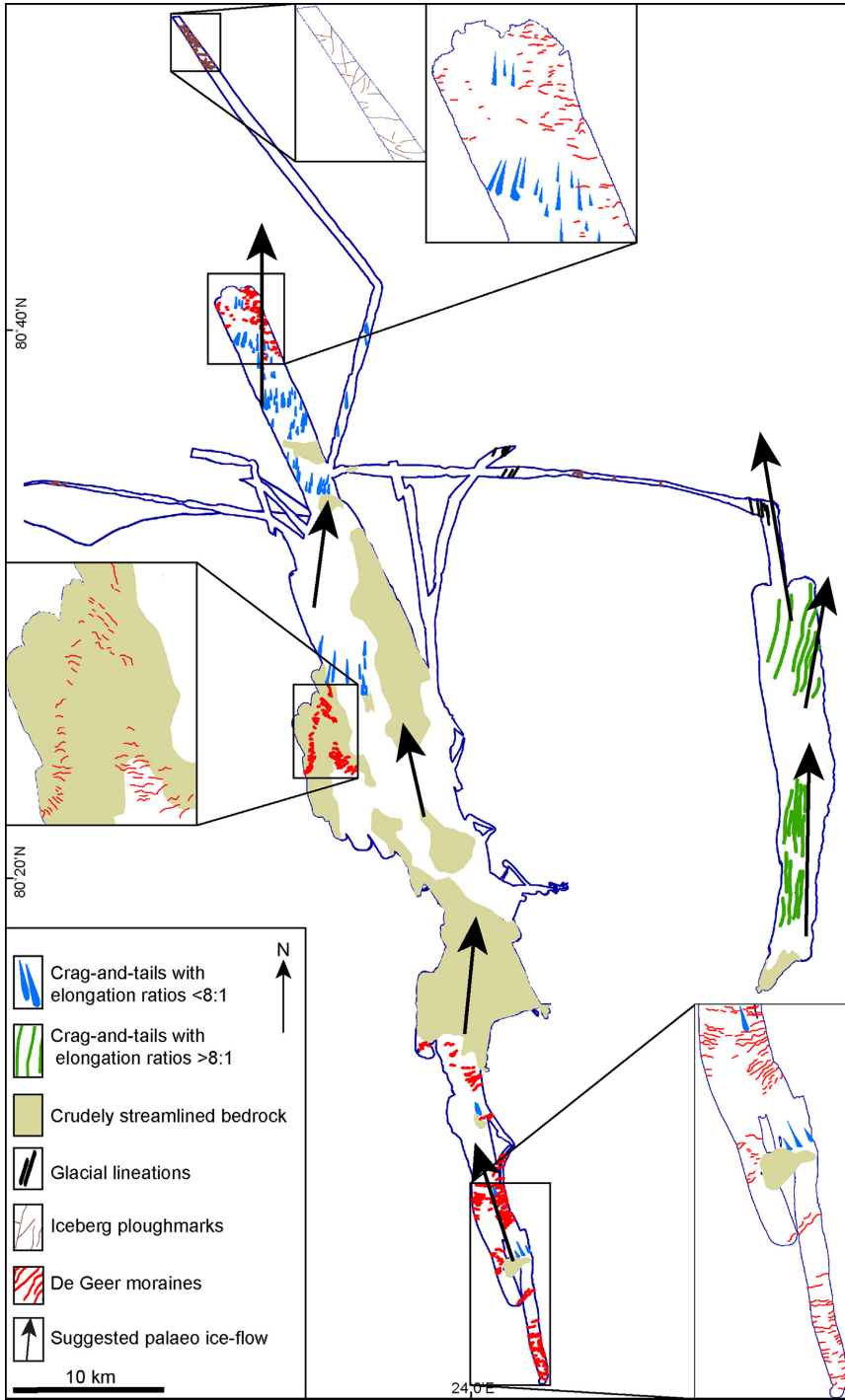


Figure 15. Distribution of major glacial landforms in Rijpfjorden and Duvefjorden. Palaeo ice-flow directions are indicated with arrows.

calving rate of the glacier front and a gradual transition from glacialmarine to a marine environment (cf. Elverhøi and Solheim, 1983). The thickest postglacial sediment sequences correspond to deeper bathymetry in Rippfjorden and Duvefjorden (Fig. 6). This shows that the areas of greatest glacial erosion became sediment accumulation basins after the deglaciation (Fig. 6). Mass-flow deposits are mainly recorded in the deep basin of Duvefjorden (Fig. 6), indicating that the steep basin walls facilitated gravity-driven mass-flows (cf. Syvitski *et al.*, 1987). The upward decrease in sedimentation rates in core HH11-02 suggests a gradually increasing distance to the glacier front into a marine environment during the Holocene (Table 1). However, the four mass-flow deposits in the core indicate mass-flow events throughout the Holocene probably influenced by increased meltwater input, which is supported by the relatively coarse matrix surrounding the mass-flow deposits (Fig. 2). Increased meltwater input could be explained by the proximity of the coring site to the coastline, resulting in direct input from glacially fed rivers (Fig. 1b). However, the relatively low variations in magnetic susceptibility in HH11-02 may indicate a relatively stable drainage area of the glacially fed rivers that reached Rippfjorden (Fig. 2).

The decreased sedimentation rate from the deglaciation until the mid-Holocene and the general fining of sediments upwards in core HH12-11 suggest a gradual change from a higher-energy glacialmarine to lower-energy marine environment (Table 1). The following increase in sedimentation rate correlates with increased magnetic susceptibility values for the top 170 cm of core HH12-11 (Fig. 5; Table 1), which suggests increased melt-off, changed lithology and potentially changed sediment source (Robinson *et al.*, 1995; Plassen *et al.*, 2004). This could indicate somewhat more dynamic drainage patterns for Austfonna compared to Vestfonna if they were separated during the mid- to late Holocene.

Conclusions

Based on analysis of the distribution and geometry of submarine landforms and the lithology and stratigraphy of the sediments, the ice sheet dynamics and deglacial history of Rippfjorden, Duvefjorden and their adjacent shelf have been reconstructed.

- Submarine landform patterns suggest streaming ice which was topographically controlled in Rippfjorden and Duvefjorden. Ice-flow was S–N in the inner Rippfjorden changing to SSW–NNE in the outer fjord. In Duvefjorden ice-flow was S–N in the inner fjord, spreading laterally from S–N to SW–NE in the outer fjord.
- Duvefjorden probably accommodated a somewhat larger ice stream and/or more focused ice-flow compared to that in Rippfjorden. This has been attributed to the bedrock geology and its structures.
- The deglaciation of Rippfjorden and Duvefjorden was relatively slow and punctuated in areas shallower than ca. 210 m. The retreat rate of the ice margin there is estimated to 100–250 m a⁻¹ based on the spacing between the De Geer moraines. Floating ice margin conditions probably existed in deeper parts of the fjords where the ice margin disintegrated through calving. The calving process produced large icebergs that generated the numerous ploughmarks across the shelf.
- The deglaciation of the inner Rippfjorden was complete by ca. 10.6 cal a BP, whereas the central Duvefjorden was glacier ice-free by ca. 11.0 cal a BP. The timing of the

deglaciation of the northern Svalbard shelf is therefore estimated to ca. 8 ka.

- The areas of Rippfjorden and Duvefjorden that were most heavily eroded by streaming ice became sediment accumulation basins after the deglaciation. Sediment mass-flows were promoted there during the Holocene due to the steep slopes of the eroded basins.

Acknowledgements. This research received funding from the People's Programme (Marie Curie Actions) of the European Union's Seventh Framework Programme FP7/2007-2013/ under REA grant agreement no. 317217. The research is a contribution to the GLANAM (GLACiated North Atlantic Margins) Initial Training Network.

Abbreviations. IRD, ice-rafted debris; LGM, Last Glacial Maximum; SBIS, Svalbard–Barents Sea Ice Sheet; SSAMS, single stage accelerator mass spectrometry; TWT, two-way travel time.

References

- Alley RB, Blankenship DD, Bentley CR *et al.* 1987. Till beneath ice stream B: 3. Till deformation: evidence and implications. *Journal of Geophysical Research* **92**: 8921–8929.
- Andreassen K, Laberg JS, Vorren TO. 2008. Seafloor geomorphology of the SW Barents Sea and its glaci-dynamic implications. *Geomorphology* **97**: 157–177.
- Andreassen K, Nilssen LC, Rafaelson B *et al.* 2004. Three-dimensional seismic data from the Barents Sea margin reveal evidence of past ice streams and their dynamics. *Geology* **32**: 729–732.
- Batchelor CL, Dowdeswell JA. 2014. The physiography of high Arctic cross-shelf troughs. *Quaternary Science Reviews* **92**: 68–96.
- Batchelor CL, Dowdeswell JA, Hogan KA. 2011. Late Quaternary ice flow and sediment delivery through Hinlopen Trough, Northern Svalbard margin: submarine landforms and depositional fan. *Marine Geology* **284**: 13–27.
- Benn DI, Evans DJA. 2010. *Glaciers and Glaciation, 2nd edn.* Routledge: New York.
- Bjarnadóttir LR, Rüther DC, Winsborrow MCM *et al.* 2013. Grounding-line dynamics during the last deglaciation of Kveithola, W Barents Sea, as revealed by seabed geomorphology and shallow seismic stratigraphy. *Boreas* **42**: 84–107.
- Bond GC, Lotti R. 1995. Iceberg discharges into the North Atlantic on millennial time scales during the last glaciation. *Science* **267**: 1005–1010.
- Chauhan T, Noormets R, Rasmussen TL. 2016b. Glacialmarine sedimentation and bottom current activity on the north-western and northern continental margins of Svalbard during the late Quaternary. *Geo-Marine Letters* **36**: 81–99.
- Chauhan T, Rasmussen TL, Noormets R *et al.* 2014. Glacial history and paleoceanography of the southern Yermak Plateau since 132 ka BP. *Quaternary Science Reviews* **92**: 155–169.
- Chauhan T, Rasmussen TL, Noormets R. 2016a. Palaeoceanography of the Barents Sea continental margin, north of Nordaustlandet, Svalbard, during the last 74 ka. *Boreas* **45**: 76–99.
- Dallmann WK, Ohta Y, Elvevold S *et al.*, eds. 2002. Bedrock map of Svalbard and Jan Mayen. *Norsk Polarinstittutt Temakart* No. 33.
- Dowdeswell JA, Jakobsson M, Hogan KA *et al.* 2010. High-resolution geophysical observations of the Yermak Plateau and northern Svalbard margin: implications for ice-sheet grounding and deep-keeled icebergs. *Quaternary Science Reviews* **29**: 3518–3531.
- Dowdeswell JA, Whittington RJ, Hodgkins R. 1992. The sizes, frequencies, and freeboards of East Greenland icebergs observed using ship radar and sextant. *Journal of Geophysical Research* **97**: 3515–3528.
- Dreimanis A. 1979. The problems of waterlain tills. In *Moraines and Varves*, Schlüchter, C (eds). Balkema: Rotterdam; 167–177.
- Elverhøi A, Lauritzen O. 1984. Bedrock geology of the northern Barents Sea (west of 35° E) as inferred from the overlying Quaternary deposits. *Norsk Polarinstittutt Skrifter* **180**: 5–16.
- Elverhøi A, Pfirman SL, Solheim A *et al.* 1989. Glacialmarine sedimentation in epicontinental seas exemplified by the northern Barents Sea. *Marine Geology* **85**: 225–250.

- Elverhøi A, Solheim A. 1983. The Barents Sea ice sheet – a sedimentological discussion. *Polar Research* **1**: 23–42.
- Faleide JJ, Solheim A, Fiedler A *et al.* 1996. Late Cenozoic evolution of the western Barents Sea-Svalbard continental margin. *Global and Planetary Change* **12**: 53–74.
- Flink AE, Noormets R, Kirchner N *et al.* 2015. The evolution of a submarine landform record following recent and multiple surges of Tunabreen glacier, Svalbard. *Quaternary Science Reviews* **108**: 37–50.
- Flood B, Gee DG, Hjellev A *et al.* 1969. The geology of Nordaustlandet, northern and central parts. *Norsk Polarinstittutt Skrifter* **146**.
- Hagen JO, Liestøl O, Roland E *et al.* 1993. Glacier atlas of Svalbard and Jan Mayen. *Norwegian Polar Institute Meddelelser* **129**. Oslo.
- Harland WB, Herod KN, Krinsley DH. 1966. The definition and identification of tills and tillites. *Earth-Science Reviews* **2**: 225–256.
- Hjellev BO, Kjennbakken H, Bleiklie V *et al.* 2013. Fjord stratigraphy and processes – evidence from the NE Atlantic Fensfjorden system. *Journal of Quaternary Science* **28**: 421–432.
- Hogan KA, Dix JK, Lloyd JM *et al.* 2011. Seismic stratigraphy records the deglacial history of Jakobshavn Isbræ, West Greenland. *Journal of Quaternary Science* **26**: 757–766.
- Hogan KA, Dowdeswell JA, Noormets R *et al.* 2010a. Evidence for full-glacial flow and retreat of the Late Weichselian Ice Sheet from the waters around Kong Karls Land, eastern Svalbard. *Quaternary Science Reviews* **29**: 3563–3582.
- Hogan KA, Dowdeswell JA, Noormets R *et al.* 2010b. Submarine landforms and ice-sheet flow in the Kvitøya Trough, northwestern Barents Sea. *Quaternary Science Reviews* **29**: 3345–3362.
- Jakobsson M, Mayer L, Coakley B *et al.* 2012. The international bathymetric chart of the Arctic Ocean (IBCAO) Version 3.0. *Geophysical Research Letters* **39**.
- Johansson A, Gee DG, Larionov AN *et al.* 2005. Grenvillian and Caledonian evolution of eastern Svalbard – a tale of two orogenies. *Terra Nova* **17**: 317–325.
- Knies J, Kleiber HP, Matthiessen J *et al.* 2001. Marine ice-rafted debris records constrain maximum extent of Saalian and Weichselian ice-sheets along the northern Eurasian margin. *Global and Planetary Change* **31**: 45–64.
- Knies J, Vogt C, Stein R. 1998. Late Quaternary growth and decay of the Svalbard/Barents Sea ice sheet and paleoceanographic evolution in the adjacent Arctic Ocean. *Geo-Marine Letters* **18**: 195–202.
- Koc N, Klitgaard-Kristensen D, Hasle K *et al.* 2002. Late glacial palaeoceanography of Hinlopen Strait, northern Svalbard. *Polar Research* **21**: 307–314.
- Landvik JY, Ingólfsson Ó, Mienert J *et al.* 2005. Rethinking Late Weichselian ice-sheet dynamics in coastal NW Svalbard. *Boreas* **34**: 7–24.
- Lindén M, Möller P. 2005. Marginal formation of De Geer moraines and their implications to the dynamics of grounding-line recession. *Journal of Quaternary Science* **20**: 113–133.
- Löwemark L, Schönfeld J, Schäfer P. 2006. Deformation of pyritized burrows: a novel technique for the detection and estimation of core shortening in gravity cores. *Marine Geology* **233**: 37–48.
- Mangerud J, Dokken T, Hebbeln D *et al.* 1998. Fluctuations of the Svalbard-Barents Sea ice sheet during the last 150000 years. *Quaternary Science Reviews* **17**: 11–42.
- Moholdt G, Hagen JO, Eiken T *et al.* 2010. Geometric changes and mass balance of the Austfonna ice cap, Svalbard. *The Cryosphere* **4**: 21–34.
- NAD Science Committee. 1992. The Arctic Ocean record: key to global change – initial science plan of the Nansen Arctic Drilling Program. *Polarforschung* **161**.
- Noormets R, Hogan K, Austin W *et al.* 2012. Submarine glacial landform assemblages on the outer continental shelf north of Nordaustlandet, Svalbard. In *The 6th Arctic Paleoclimate and its Extremes (APEX) Meeting, Program and Abstracts*, Oulu University, 15–18 May. Oululanka Research Station, Finland; 70.
- Ottesen D, Dowdeswell JA. 2006. Assemblages of submarine landforms produced by tidewater glaciers in Svalbard. *Journal of Geophysical Research* **111**: F1.
- Ottesen D, Dowdeswell JA, Landvik JY *et al.* 2007. Dynamics of the Late Weichselian ice sheet on Svalbard inferred from high-resolution seafloor morphology. *Boreas* **36**: 287–306.
- Ottesen D, Dowdeswell JA, Rise L. 2005. Submarine landforms and the reconstruction of fast-flowing ice streams within a large Quaternary ice sheet: the 2500-km-long Norwegian-Svalbard margin (57°–80°N). *Geological Society of America Bulletin* **117**: 1033–1050.
- Patton H, Andreassen K, Bjarnadóttir LR *et al.* 2015. Geophysical constraints on the dynamics and retreat of the Barents Sea ice sheet as a paleobenchmark for models of marine ice sheet deglaciation. *Reviews of Geophysics* **53**: 1051–1098.
- Plassen L, Voren TO, Forwick M. 2004. Integrated acoustic and coring investigation of glacial deposits in Spitsbergen fjords. *Polar Research* **23**: 89–110.
- Powell RD. 1984. Glacimarine processes and inductive lithofacies modelling of ice shelf and tidewater glacier sediments based on Quaternary examples. *Marine Geology* **57**: 1–52.
- Rebesco M, Laberg JS, Pedrosa MT *et al.* 2014. Onset and growth of trough-mouth fans on the north-western Barents Sea margin – implications for the evolution of the Barents Sea/Svalbard Ice Sheet. *Quaternary Science Reviews* **92**: 227–234.
- Reimer PJ, Bard E, Bayliss A *et al.* 2013. IntCal13 and Marine13 radiocarbon age calibration curves 0–50, 000 years cal BP. *Radiocarbon* **55**: 1869–1887.
- Rignot E, Kanagaratnam P. 2006. Changes in the velocity structure of the Greenland ice sheet. *Science* **311**: 986–990.
- Robinson P, Dowdeswell JA. 2011. Submarine landforms and the behavior of a surging ice cap since the last glacial maximum: the open-marine setting of eastern Austfonna, Svalbard. *Marine Geology* **286**: 82–94.
- Robinson SG, Maslin MA, McCave IN. 1995. Magnetic susceptibility variations in Upper Pleistocene deep-sea sediments of the NE Atlantic: implications for ice rafting and paleocirculation at the last glacial maximum. *Paleoceanography* **10**: 221–250.
- Roy S, Senger K, Braathen A *et al.* 2014. Fluid migration pathways to seafloor seepage in inner Isfjorden and Adventfjorden, Svalbard. *Norwegian Journal of Geology* **99**: 1–19.
- Rüther DC, Mattingsdal R, Andreassen K *et al.* 2011. Seismic architecture and sedimentology of a major grounding zone system deposited by the Bjørnøyrenna Ice Stream during Late Weichselian deglaciation. *Quaternary Science Reviews* **19**: 2776–2792.
- Siegert MJ, Dowdeswell JA, Hald M *et al.* 2001. Modelling the Eurasian Ice Sheet through a full (Weichselian) glacial cycle. *Global and Planetary Change* **31**: 367–385.
- Smith MJ, Rose J, Booth S. 2006. Geomorphological mapping of glacial landforms from remotely sensed data: an evaluation of the principal data sources and an assessment of their quality. *Geomorphology* **76**: 148–165.
- Stokes CR, Clark CD. 2002. Are long subglacial bedforms indicative of fast ice flow? *Boreas* **31**: 239–249.
- Stokes CR, Tarasov L, Blomdin RL *et al.* 2015. On the reconstruction of palaeo-ice sheets: recent advances and future challenges. *Quaternary Science Reviews* **125**: 15–49.
- Stroeven AP, Swift DA. 2008. Glacial landscape evolution – implications for glacial processes, patterns and reconstructions. *Geomorphology* **97**: 1–4.
- Syvitski JPM, Burrell DC, Skei JM. 1987. *Fjords – Processes and Products*. Springer Verlag: New York.
- Wellner JS, Lowe AL, Shipp SS *et al.* 2001. Distribution of glacial geomorphic features on the Antarctic continental shelf and correlation with substrate: implications for ice behavior. *Journal of Glaciology* **47**: 397–411.
- Winsborrow MCM, Andreassen K, Corner GD *et al.* 2010. Deglaciation of a marine-based ice sheet: Late Weichselian palaeo-ice dynamics and retreat in the southern Barents Sea reconstructed from onshore and offshore glacial geomorphology. *Quaternary Science Reviews* **29**: 424–442.

